1990

Diffusivity Estimation for Counterdiffusing Reactants in Catalytic Solids.

Chauchyun Chang
Louisiana State University and Agricultural & Mechanical College

INFORMATION TO USERS

This manuscript has been reproduced from the microfilm master. UMI films the text directly from the original or copy submitted. Thus, some thesis and dissertation copies are in typewriter face, while others may be from any type of computer printer.

The quality of this reproduction is dependent upon the quality of the copy submitted. Broken or indistinct print, colored or poor quality illustrations and photographs, print bleedthrough, substandard margins, and improper alignment can adversely affect reproduction.

In the unlikely event that the author did not send UMI a complete manuscript and there are missing pages, these will be noted. Also, if unauthorized copyright material had to be removed, a note will indicate the deletion.

Oversize materials (e.g., maps, drawings, charts) are reproduced by sectioning the original, beginning at the upper left-hand corner and continuing from left to right in equal sections with small overlaps. Each original is also photographed in one exposure and is included in reduced form at the back of the book.

Photographs included in the original manuscript have been reproduced xerographically in this copy. Higher quality 6" x 9" black and white photographic prints are available for any photographs or illustrations appearing in this copy for an additional charge. Contact UMI directly to order.

U·M·I

University Microfilms International
A Bell & Howell Information Company
300 North Zeeb Road, Ann Arbor, MI 48106-1346 USA
313/761-4700 800/521-0600

Order Number 9123183

Diffusivity estimation for counterdiffusing reactants in catalytic solids

Chang, Chauchyun, Ph.D.

The Louisiana State University and Agricultural and Mechanical Col., 1990

U·M·I
300 N. Zeeb Rd.
Ann Arbor, MI 48106

Diffusivity Estimation for Counterdiffusing Reactants in Catalytic Solids

A Dissertation

Submitted to the Graduate Faculty of the
Louisiana State University and
Agricultural and Mechanical College
in partial fulfillment of the
requirements for the degree of
Doctor of Philosophy

in

The Department of Chemical Engineering

by
Chauchyun Chang
B.S. Tatung Institute of Technology, Taiwan, 1981
M.S. Louisiana State University, 1988
December 1990

To my parents
for
their love and support

Acknowledgements

I would like to express my sincere gratitude to my major professor, Dr. Kerry M. Dooley, who initiated me into this research and guided me with patience, encourgement, and understanding throughout this study. Thanks are due to Dr. F. Carl Knopf, Dr. Robert F. O'Connell, Dr. Geoffrey L. Price, Dr. Paul S. Russo, and Dr. David M. Wetzel for their time and cooperation in serving on my graduate committee.

The fincial support provided by National Science Foundation and Chemical Engineering Department of LSU during my graduate study in here was deeply appreciated.

I would also like to thank all the graduate students who I have met while attending LSU who have help me maintain my sanity as well as challenged my intelligence. Thanks are due to Paul Rodriquez and his staff for their many hours of help and suggestions.

Special Thanks are due my parents, my brother, and my dear daugther for their undying support of me in my quest to become a Ph.D. They have given me so much and never ask for return from me.

Table of Contents

List of Tables

List of Figures

Abstract

The diffusivities of molecules whose sizes approach the intracrystalline pore sizes of zeolites have been studied at and near conditions prevailing during catalysis, by both desorption and kinetics techniques.

For the desorption approach, a series of unary isothermal desorption experiments (following an almost instantaneous initial temperature rise) were conducted for toluene or benzene with five different zeolites. Diffusion and readsorption are shown to control the process. The intracrystalline diffusivities (D_e) were derived by fitting the desorption curves with four models of varying complexity; only models which take into account readsorption (either at equilibrium or not) can both fit the data adequately and give reasonable estimations of D_e. A nonequilibrium readsorption model is probably superior to an equilibrium readsorption model, because: (1) it can fit both the rising and falling portions of isothermal desorption curves and (2) the D_e's predicted by such a model are comparable to those reported in the literature by other techniques (chromatographic, adsorptive uptake) under similar conditions. But these D_e's are still at least three orders of magnitude smaller than those predicted by the Pulse Field Gradient (NMR) technique.

For the kinetics apporach, the disproportionation of toluene, a well understand reaction, was studied using the same zeolites at intraparticle-diffusion-limited conditions in order to estimate the product of effectiveness factors and rate constants. The D_e for

toluene in counterdiffusion was estimated by fitting the rate data to generalized effectiveness factor expressions, using literature results for the rate expression. The rate constants obtained in this study are comparable to the second-order intrinsic rate constants for zeolite catalysts obtained from the literature; however, the effective binary D_e 's for toluene computed from this approach are at least two to three orders of magnitude smaller than the D_e's derived from the desorption curves. This result suggests a reduction of molecular mobility resulting from restricted passage of counterdiffusing reactants in zeolite windows during catalysis.

CHAPTER 1

INTRODUCTION AND LITERATURE REVIEW

1.1 Introduction

Diffusion in porous catalysts plays an important role in predicting the performance of catalytic processes, and in operating these processes optimally. If all mass transfer phenomena can be mathematically modeled, it would be helpful in the design of a new catalyst's pore size and active site distributions.

At present, many of the catalysts used industrially are formed by tabletting, extruding or compressing microporous particles. This method of catalyst preparation gives rise to pellets with a bimodal pore-size distribution, with large, long pores between microparticles (macropores), and small, short pores (pore diameters less than $\simeq 30$ Å) within microparticles (micropores). The large pores communicate with each other by an interconnecting pore network with the smallest pores having sizes in the range of molecular dimensions. Diffusion in these two sets of pores may occur by different mechanisms depending upon the pore size, the electronic properties of the pore surface, and the relative sizes of the diffusing molecule and pore (as commonly quantified in the parameter λ, critical molecular diameter divided by pore diameter).

For large pores (pore size > molecular mean free path), the pore diffusion coefficient equals the bulk value. For smaller pore sizes (pore size $\simeq$ mean free path), transport is by Knudsen diffusion, with a diffusivity proportional to the pore diameter. For $\lambda > \simeq 0.1$, the

transport is often called "configurational diffusion", because of the close approach of molecular dimensions to pore size. Also, for molecules which adsorb appreciably, the migration of adsorbed molecules ("surface diffusion") is important in characterizing transport within porous catalysts.

The relative significance of surface vs. configurational diffusion is the least understood phenomenon in microporous transport. It has been questioned whether in fact these are two distinct phenomena, but merely differ in the magnitude of molecule-surface interaction energies (Prasher and Ma, 1977; Gelbin and Fiedler, 1980; Haag et al., 1982). Attempts to extract "surface fluxes" from transient sorption experiments in large pores and to relate surface to configurational diffusion are often in error, because the analysis involves subtraction of a Knudsen flux in the micropore from the total flux, and the Knudsen flux itself is difficult to estimate (Thakur et al.,1980; Shindo et al.,1983).

Previous studies have attempted to describe simultaneous reaction and molecular transport by theories based on parallel bulk and Knudsen mechanisms. These theories are seriously in error as pore sizes shrink and molecules are subject to surface potentials (Barrer, 1971; Gilliand et al., 1974; Ruthven, 1977). The predicted diffusivities are generally orders of magnitude larger than measured values. For example, for methane diffusing through 4A molecular sieve (a zeolite, which is a crystalline aluminosilicate more fully described in Section 1.3.1) at 323 , the predicted pre-exponential diffusivity (D_χ) is 1.67 x 10^{-11} (cm^2/s) compared with the experimental D_χ of 5.7 x 10^{-13} (cm^2/s). Also, the assumption of a single-size "average" pore

in the analysis of reaction kinetics or transient sorption data leads to incorrect diffusivity estimates if the pore structure is bidisperse (Ruckenstein et al., 1971; Hashimoto and Smith, 1974). Several sophisticated models for transient diffusion in bidisperse porous solids have appeared (Wakao and Smith, 1962; Ruckenstein et al., 1971; Neogi and Ruckenstein, 1980), but owing to the dependence of the transport mechanism on pore dimension and surface properties, the simplifications of these models, especially the assumption of concentration-independent diffusivities, are unproven.

Most previous diffusion studies were conducted away from practical reaction conditions using structurally and chemically simple materials, such as single crystal zeolites or large-pore metal oxides. The "solvent" in such experiments is typically a light component smaller than the diffusing component, and therefore solvent-solute interactions within the micropores are less important than is the case in catalysis. In this thesis the following systems are studied: (1) unidirectional diffusion of molecules at temperatures slightly below those typical of catalytic reactions, but in typical zeolite catalysts which strongly interact with the diffusing molecules; and (2) counterdiffusion of two similarly sized molecules in the same catalysts, but at reaction conditions.

Under these conditions, accurate estimation of configurational diffusivities proves the major obstacle in describing pore transport. The alteration of surface electronic properties with the slight perturbations of surface compositions, and the experimental difficulties involved in transient (unidirectional) diffusion experiments, are two factors retarding progress in this area.

An example of the problem is diffusion in small-pore metal-loaded zeolites. Different metal cations occupy different sites inside the small pores and exhibit different mobilities. Therefore, varying the type and number of ion-exchanged metal cations affects both intrinsic catalytic activities and diffusivities by orders of magnitude (Ruthven, 1977; Lee and Ma, 1977; Ruthven, 1983).

When a reaction occurs as well, the situation is even more complex. Several investigators have assumed uniform point-sink microparticles in order to derive the effectiveness factors (η, related to both diffusivity and rate constant) for simple reactions in bidisperse catalysts (Mingle and Smith, 1961; Carberry, 1962; Jayaraman et al., 1983), e.g., most zeolites; general formulations of the simultaneous diffusion-reaction equation for this situation have also appeared (Ors and Dogu, 1979; Park and Kim, 1984). However, it is not yet possible to analytically predict η for the realistic case, in which micropore diffusion is strongly dependent on surface properties, pore geometry and interactions between counterdiffusing molecules. This situation persists because the defining relations for microporous transport are uncertain, especially for ionic solids such as zeolites or when $\lambda > 0.1$.

With these problems, micropore diffusivities in structually complex catalysts are obtainable only through experiments which take into account the effects of concentration, micropore size and distribution, and surface electronic properties. Although a comprehensive set of experiments is probably impossible to design, in this thesis a beginning is made as follows.

Kinetics were obtained for a simple reaction (toluene disproportionation to benzene and xylenes) involving 3-5 molecules with $\lambda > 0.1$, using zeolite catalysts. This reaction was chosen because of its relative lack of complicating side reactions, because there exist kinetics data for zeolite catalysts to indicate the form of the rate expression, and because it involves a reactant and products with critical diameters approaching the micropore sizes of typical zeolite catalysts. The toluene disproportionation reaction was run at intraparticle diffusion-limited conditions to determine values of η which were used to compute the effective diffusion coefficient for two counterdiffusing large molecules (for example toluene and p-xylene). The diffusivities derived here were compared with the values obtained by other methods, such as transient sorption and pulse chromatography. These experiments typically involve only one diffusing molecule of interest and therefore the diffusivities so obtained are free from the effects of molecular interactions in pores.

Several investigators have estimated the counterdffusivities of hydrocarbons in zeolites by adsorptive or desorptive counterdiffusion techniques (Satterfield and Katzer, 1971; Satterfield et al., 1971; Moore and Katzer, 1972), or from kinetics data (Haag et al., 1982; Post et al., 1983; Kolaczkowski and Ullah, 1989), or by Monde Carlo simulation (Rajadhyaksha et al., 1990). They found that the counterdiffusivities of hydrocarbons in zeolites depend upon the size of the diffusing molecules, the strength of the interaction between the diffusing molecules and zeolites, and the pore geometry of the zeolites. Generally the counterdiffusivities are 1 to 2 orders of magnitude smaller than the corresponding unidirectional diffusivities

in zeolites with three dimensional pore structrues such as faujasite, under similar conditions. The discrepancy between the two types of diffusivities increases to 3 to 4 orders of magnitude for zeolites with a one dimensional pore network, such as mordenite. This phenomenon can be explained as follows: there are interconnecting pore apertures in a three dimensional pore structure which offer sufficient space for free counterdiffusion, while in one dimensional tubular pores the molecules either not pass each other at all or by diffusion along the surface.

In addition, a series of unary, isothermal desorption (ID) experiments for toluene and benzene were performed on the same catalysts at similar adsorbate loadings. The component's unidirectional effective diffusivity, D_e, and equilibrium constant at the external surface, K, are the quantities extracted from the ID experiments. It is shown that: (1) ID experiments at elevated temperatures are possible; (2) readsorption of desorbed gas phase material complicates the mathematical analysis and must be taken into account; and (3) D_e values from ID experiments in general correspond to accurate values measured by other long-time scale techniques. The diffusivities derived here were compared with the values obtained from the kinetics experiments. The discrepancies between these two sets of data indicate the effects of interactions between diffusing molecules.

1.2 Overview of Diffusion in Porous Catalysts

1.2.1 Diffusion in Macropores

If a diffusing solute is small compared to the pore size, its effective diffusivity is related to its bulk diffusivity as follows:

$$D_p = \frac{\varepsilon D_b}{\tau} \qquad (1-1)$$

where D_p is effective diffusivity, D_b is bulk diffusivity, ε is porosity, and τ is tortuosity. Since τ is essentially a geometric factor, it should be independent of temperature and the nature of the diffusing species. No reliable expression for τ has been obtained (Mitani,1984). Theoretical predictions of τ may be made, but this requires measurement of both pore shape and size distributions; it is generally simpler to treat τ as an empirical constant which is determined experimentally for any particular adsorbent. Experimental tortuosity factors generally fall within the range 2-6.

For short mean free path, transport within a macropore occurs only by molecular diffusion; the diffusivity of an individval component in an ideal gas mixture may be estimated from a relationship based on the Stefan-Maxwell equation (Froment and Bischoff, 1979, Ch. 3):

$$\frac{1}{D_{jm}} = \frac{\sum_{k=1}^{N} \frac{1}{D_{jk}} \left(Y_k - Y_j \frac{N_k}{N_j}\right)}{1 - Y_j \sum_{k=1}^{N} \frac{N_k}{N_j}} \qquad (1-2)$$

where D_{jm} is the diffusivity for species j in the mixture, D_{jk} is the binary diffusivity for species j and k, N_j is the molar flux for reacting component j, and Y_j is the mole fraction for species j. Eq. (1-2) is often used to compute D_{jm} in reacting systems. For a single chemical reaction,

$$\frac{N_j}{\alpha_j} = \text{Constant} \qquad (1-3)$$

where α_j is the stoichiometric coefficient of component j in a single reaction. And so eq. (1-2) becomes

$$\frac{1}{D_{jm}} = \frac{\sum_{k=1}^{N} \frac{1}{D_{jk}} \left(Y_k - Y_j \frac{\alpha_k}{\alpha_j}\right)}{1 - Y_j \sum_{k=1}^{N} \frac{\alpha_k}{\alpha_j}} \qquad (1-4)$$

For long mean free path, the Knudsen diffusivity of a gas molecule in a straight round pore may be estimated using the wall collision rate from kinetic theory, resulting in

$$D_K = \frac{4}{3} r \left(\frac{2}{\pi} \frac{RT}{M}\right)^{\frac{1}{2}} \qquad (1-5)$$

where D_K is the Knudsen diffusivity, r is pore radius, M is the molecular weight of the diffusing species, T is temperature, and R is the gas constant. It is possible for molecular diffusion to be dominant in the large pores while Knudsen diffusion is dominant in the smaller pores. Because of the dependence of mean free path on pressure, for any given adsorbent and adsorbate there will be a transition from molecular diffusion at high pressure to Knudsen diffusion at low pressure.

For a binary gas mixture in a porous solid at constant pressure, the combined diffusivity is given by (Evans et al., 1961; Scott and Dullien, 1962)

$$\frac{1}{D_{e_j}} = \frac{1 - Y_j \left(1 + \frac{N_k}{N_j}\right)}{D_{e_{jk}}} + \frac{1}{D_{e_{K_j}}} \qquad (1-6)$$

For multicomponent ideal gas systems, we can use the D_{jm} in eq. (1-4) to find the effective multicomponent diffusivity at constant total pressure, if we neglect the nonzero bulk flow in the catalyst. This assumption is justified by the fact that most of the reactions we are studying are such that $\sum_{i=1}^{N} \alpha_i = 0$ anyway.

$$\frac{1}{D_{e_{jm}}} = \sum_{k=1}^{N} \frac{1}{D_{e_{jk}}} \left(Y_k - \frac{\alpha_k}{\alpha_j} Y_j\right) + \frac{1}{D_{e_{K_j}}} \qquad (1-7)$$

There is the possibility of a direct contribution to the macropore flux by transport of adsorbed molecules, referred to as surface diffusion. Direct measurement of a surface flux is not feasible. In order to study surface diffusion, it is necessary to substract the gas-phase contribution from the total flux. The normal procedure, illustrated by the work of Schneider and Smith (1968), involves measuring fluxes over a range of temperatures. The gas-phase flux is determined from high temperature measurements, because under these conditions the surface flux can be neglected. The gas-phase flux at a lower temperature is then found by extrapolation and subtracted from the measured flux. Surface diffusion is significant only in pores of small diameter in which gas-phase flux can be attributed entirely to Knudsen diffusion; this considerably simplifies the extrapolation.

Theories of surface diffusion typically relate the phenomenon to the statistical mechanics of two-dimensional random walks; they are

discussed elsewhere (Cunningham and Williams, 1980, Ch. 1; Smith and Metzner, 1964; Gilliland et al., 1974; Okazaki et al., 1981). These models suffer from a lack of understanding of adsorbed molecule-surface interactions.

1.2.2 Diffusion in Micropores

Uptake rate measurement is a conventional method to estimate micropore diffusivity; it is applicable only if the rate of micropore diffusion is slow relative to other serial mass transfer rates or if the catalyst crystals are large. Otherwise, it is difficult to minimize the contributions of external heat transfer and the bed diffusional resistance to the overall transport process. Therefore, it is not uncommon to see differences of several orders of magnitude between the diffusivity data reported by this measurement and other methods (Ruthven, 1977, Table IV; Barrer, 1980, Table I; Ruthven, 1983; Karger and Ruthven, 1989). Ruthven (1980) found that erroneously low values of diffusivities were obtained for fast diffusing molecules or with small crystals, due to the breakdown of the isothermal assumption typically imposed on sorption systems. He obtained diffusivities that were in order of magnitude agreement with those measured by other techniques, if a nonisothermal model was used to fit the sorption data. Tracer exchange is a modified uptake rate experiment, measuring the self-diffusivity by exposing the adsorbent to a change in the concentration of an isotopically labeled tracer at constant total sorbate concentration.

Chromatography (response of a packed bed of adsorbent to a pulse input) is an alternative to uptake rate measurements. The inherent difficulty of this method is that the response peak is broadened by dispersion as well as diffusion, making it difficult to use such broadening to estimate micropore diffusivities. Recently, Eic and Ruthven (1988) have proposed a "zero-length column (ZLC) chromatography" technique, in which the effects of dispersion were minimized by using only 1-2 mg of adsorbent in a desorption vessel. Their diffusivity data for o-xylene in 50- and 100-μm NaX crystals derived by the ZLC technique were within 10% of the values obtained by uptake rate and tracer exchange techniques.

Nuclear Magnetic Resonance (NMR) techniques provide another widely used experimental method for measuring intracrystalline self-diffusivities. There are three different NMR techniques (Karger et al., 1978a; Karger et al., 1978b; Karger et al., 1980; Caro et al., 1985; Ruthven, 1984, Ch. 5; Karger and Ruthven, 1989) : (1) Relaxation method, which measures the spin lattice relaxation time; (2) Pulse Field Gradient (PFG) method, which measures the rms displacement of molecules by marking the phase differences of the nuclear spin of protons that are excited by two rf pulses (with a 90° phase difference) during a short period of time (several milliseconds); (3) Fast-Tracer Desorption, a modified PFG method, which measures the exchange rate of spin-tagged molecules between the crystal and its surroundings.

The relaxation method measures the average time between molecular jumps directly. Then the self-diffusivity is calculated indirectly based on an assumed jump distance. Therefore, it is an indirect method for estimating microdiffusivity. By contrast, the PFG method allows

the "direct" determination of the probability distribution of the lengths of the diffusion path during a known time interval. In a homogeneous system the measured rms displacements are related to the self-diffusivity, D_s, by Einstein's equation

$$\langle r^2(\Delta)\rangle = 6D_s\Delta \qquad (1-8)$$

where $\langle r^2(\Delta)\rangle$ and Δ denote, respectively, the mean square jump distance and the mean lifetime between two jumps. Hence, the diffusivity data obtained by the PFG method are believed to be more accurate than those derived by Relaxation measurements.

From eq. (1-8) one can estimate the range of intracrystalline diffusivities accessible in PFG-NMR experiments as follows:

1. The lower limit depends on the spatial resolution of the technique. In the present state of development, the technique guarantees a resolution down to about 0.5 μm.

2. The upper limit for the observation is given by the crystallite sizes of zeolites available. The largest crystallites which have been used for diffusion studies are roughly 100 μm.

Therefore, with lower and upper limits of 0.5 and 100 μm for the rms displacements and a typical observation time of 10 ms, one obtains from eq. (1-8) values from 4×10^{-8} to 2×10^{-3} cm^2/s for the range of intracrystalline self-diffusivities accessible in PFG-NMR experiments (Karger et al., 1978a; Karger et al., 1980; Ruthven, 1984, chp. 5; Karger and Ruthven, 1989).

For the fast-tracer desorption technique, the isotopic spin-tagged molecule is moving under the influence of applied magnetic-field gradient pulses. The decay of the NMR signal (the "spin echo") is given by:

$$\Psi(\gamma, \delta, g) = \Psi(0) \exp\{-\gamma^2\delta^2g^2D_st\} \qquad (1-9)$$

where γ, δ and g are, respectively, the gyromagnetic ratio, the width and the intensity of the gradient pulse. D_s may be conveniently determined from the slope of the semilogarithmic plot of echo amplitude vs $(\gamma g)^2$, but the bounds on D_s are still given by eq. (1-8).

From the above discussion, it is apparent that the PFG NMR technique is applicable to rapidly diffusing ($D > 10^{-8}$ cm^2/s) species and large crystals. For each PFG experiment, temperature and concentration gradients are absent. The system is in equilibrium and the self-diffusivity is measured. From simple thermodynamic considerations it may be shown that the D_s derived from a PFG experiment should be comparable to the corrected diffusivity (D_0), calculated from the uptake diffusivity (D) according to Darken's equation:

$$D = D_0 \frac{\partial \ln a}{\partial \ln C} \qquad (1-10)$$

in which the nonlinear correction factor $\partial \ln a/\partial \ln C$ is obtained directly from the equilibrium isotherm.

Comparison of diffusivity data reported by Uptake and NMR methods have shown differences of several orders of magnitude, but the trends of temperature and concentration dependence are generally the same. The discrepancies between the results of these two methods are hard

to explain, but several investigators suggested the following possibilities: (1) the effect of temperature changes due to the heat of adsorption (Doelle and Riekert, 1977); (2) the sorption rate being controlled by a process other than intracrystalline diffusion; this process could be intercrystalline flow, transmission through a surface skin, or intercrystalline heat transfer (Ruthven, 1977; Barrer, 1980; Ruthven and Eic, 1988; Karger and Ruthven, 1989); (3) differences in the zeolite samples arising from either the pre-treatment processes or the syntheses (Ruthven, 1980). Recently, Karger and Ruthven (1989) showed that all the above postulates could not be true sources for the discrepancy. They argued that the only rational explanation for this phenomenon is a slow reversible exchange between mobile and relatively immobile molecules within the crystal. This hypothesis was based on the difference in time scales between NMR and uptake rate experiments, the former being on the order of a few milliseconds, whereas the latter are on the order of minutes, or even hours. Therefore, NMR measurements are made on time scales that may be short compared to the half-times of immobilization; the measurement may observe only the mobile intracrystalline state. The intracrystalline transport on this time scale could be described by a normal Fickian diffusion model. For a measurement with a long time scale, equilibrium would be established between the mobile and immobile molecules, and molecules would exchange between these two groups several times, so that one would again see Fickian diffusion but with a diffusivity reduced in proportion to the ratio of mobile and immobile molecules.

Tentative evidence in support of this hypothesis was provided by frequency response measurements (i.e. measuring the pressure response

of a sorption system to sinusoidal volume variation) carried out over a wide range of time scales (Yasuda, 1982; Yasuda and Yamamoto, 1985); however, the observed intensities of the PFG-NMR signals suggest that all the molecules are "seen" in the NMR experiment and this result does not support the mobile-immobile hypothesis (Karger et al., 1980).

The limited attempts to predict microporous diffusivities have focused on correcting the bulk diffusivity. A restriction factor, $F(\lambda)$, is sometimes multiplied by D_p in this case. This phenomenon of "restricted" or "configurational" diffusion was first observed for diffusion of liquids through membranes. The prevalent explanation for restricted diffusion is of fluid dynamic origin and involves the following two phenomena. First, there is partitioning of solute at the pore mouth, typically expressed as a linear isotherm:

$$\varkappa_p = \frac{C_\mu}{C_M} \qquad (1-11)$$

where $\varkappa_p$ is equilibrium partition coefficient. The mean concentration of solute molecules just inside the pore (C_μ) is based on the total pore cross-section, as is C_M , the fluid phase concentration in a connecting macropore. Ferry (1936) proposed that restricted diffusion occurs because of the exclusion of molecules due to statistical effects related to the size of molecules relative to that of the pore; in this case the equilibrium partition coefficient is given by:

$$\varkappa_p = (1-\lambda)^2 \qquad (1-12)$$

Since the center of mass of the molecule cannot be closer to the pore wall than the distance of the molecular radius, only the fraction

$(1 - \lambda)^2$ of the pore cross-section is accessible to the molecule. Using similar reasoning, Satterfield et al. (1973) suggested

$$\kappa_p = \frac{(1 - \lambda_{solute})^2}{(1 - \lambda_{solvent})^2} \qquad (1 - 13)$$

assuming the size of the solvent molecule also approaches that of the pore diameter.

One drawback of the geometric exclusion hypothesis is the neglect of adsorption or repulsion of molecules by the pore wall. In fact, some experimental data (Satterfield et al., 1973; Prasher and Ma, 1977; Prasher et al., 1978) indicate that the partition coefficient, at least in the case of molecules with $\lambda < 0.3$, depends more on interactions between molecules and the pore surface than on λ itself. Thus κ_p values between 1.0 and 4.0 have been reported.

The second phenomenon associated with configurational diffusion is the increase in frictional drag on the diffusing molecule when constrained by the cylindrical pore wall. κ_r is used to represent the resulting fractional reduction in D_p. Pappenheimer (1953) and Renkin (1954) derived a κ_r presumably valid for λ up to about 0.5:

$$\kappa_r = 1 - 2.014\,\lambda + 2.089\,\lambda^2 - 0.948\lambda^3 \qquad (1 - 14)$$

where κ_r is drag coefficient. Baltus and Anderson (1983) have shown that for $\lambda < 0.5$, eq. (1-14) is approximated by

$$\kappa_r = \exp(-4.6\,\lambda) \qquad (1 - 15)$$

which is comparable to Satterfield's (1973) empirical result for nonadsorbed solutes with $\lambda < 0.3$,

$$\varkappa_r = \exp\,(-2.0\,\lambda) \qquad (1-16)$$

eq. (1-16) was found to successfully correlate liquid-phase effective diffusivity data for small liquid molecules with $\varkappa_p = 1$, but it was found that diffusivities for liquid molecules with $\varkappa_p$ values greater than 1 or of macromolecules are several times smaller than values predicted using eqs. (1-14) and (1-16).

From the above discussion we can relate a liquid's effective diffusivity in micropores (D_e) to an "unrestricted" diffusivity (D_b):

$$D_e = \frac{D_b\,\varepsilon\,\varkappa_p\,\varkappa_r}{\tau} \qquad (1-17)$$

Note that the "unrestricted" diffusivity for liquids corresponds to the bulk diffusivity; most micropore diffusion data have been obtained for liquid systems. For a gas it is not clear what value D_b would take on, because of the breakdown of the assumptions behind Knudsen diffusion for $\lambda > \simeq 0.1$.

Surface diffusion was reported to significantly contribute to intraparticle transport of aromatic compounds in microporous activated carbons (Neretnieks, 1976; Sudo et al., 1978). When both surface and pore diffusion contribute to the total flux, and the adsorption rate is infinitely fast, the effective diffusivity can be expressed as (Chantong and Massoth, 1983)

$$D_e = \frac{D_b\,\varepsilon\,\varkappa_p\,\varkappa_r}{\tau} + \rho\,D_s\left(\frac{\partial q}{\partial C_\mu}\right) \qquad (1-18)$$

where $\frac{\partial q}{\partial C_\mu}$ is the slope of the equilibrium adsorption isotherm, and ρ is the particle density.

1.3 Zeolite Structures and Kinetics

1.3.1 General Properties and Framework Structure

Zeolites are crystalline aluminosilicates which upon dehydration develop a uniform pore structure consisting of almost cylindrical channels and (sometimes) large, almost spherical cages. The structure consists of a three-dimensional framework of SiO_4 and AlO_4 tetrahedra, each of which contains a silicon or aluminum atom in the center. The structural formula of a zeolite is best expressed for the crystallographic unit cell as:

$$M_{x/n}[(AlO_2)_x (SiO_2)_y] \cdot ZH_2O \qquad (1 - 19)$$

where M is the cation of valence n, and y/x has values of 1-5 depending on the crystallographic structure (Satterfield, 1970, Ch. 7).

The well-defined pore structure and the high internal surface areas of zeolites result in high adsorption capacities and permit adsorption separations to be carried out on the basis of molecular size and shape, the so-called molecular sieving, as in the separation of n-paraffins from isoparaffins. Various cations are present in zeolites to produce electrical neutrality, because for each aluminium tetrahedron in the lattice there is an overall charge of -1. These cations create strong electrostatic fields which can result either in adsorbate interactions with specific cations or strong acidity. The acid site densities of exchanged zeolites can be 10 to 100 times

greater than those of silica-alumina, a typical amorphous solid acid catalyst. These acid sites are relatively uniform, which during catalysis can result in less poisoning and higher selectivity to desired products.

Another reason for the widespread use of zeolites as catalysts is that the unique structures of zeolites can determine product selectivities. The size and shape of zeolite pores can affect a reaction's selectivity in two ways. One mechanism for enhanced selectivity is due to differences in the intracrystalline diffusivities of molecules of different size (Derouane, 1982; Haag et al., 1982). In this "reactant" or "product" selectivity, catalysis within crystals is restricted to small molecules. For example, diffusional discrimination between xylene isomers is illustrated by the relative rates of isomerization of the three xylene isomers catalyzed by P-ZSM-5 catalyst (a phosphorus-modified pentasil). The rates were:

$$p\text{-xylene}:m\text{-xylene}:o\text{-xylene} = 5:2.5:1. \qquad (1-20)$$

The para-selectivity is consistent with the more rapid diffusion of the smaller para isomer in the zeolite, in conjuction with isomer interconversion (Young, et al., 1982).

The second mechanism for selectivity is due to differences in size and structure of transition-state complexes. Some reactions involve transition states which cannot be accommodated in an intracrystalline pore, even though the products can diffuse through the pores. An example of this "transition-state" selectivity is again the isomerization of xylenes catalyzed by ZSM-5. The superior selectivity

for isomerization is achieved because the bimolecular xylene disproportionation reaction has a transition state that cannot be accomodated by the intracrystalline pores (Haag, et al., 1982).

The unique properties of zeolites mentioned above make them the most widely used solid acid catalysts. The major industrial catalytic applications of zeolites are as follows (Chen et al., 1988):

1. Petroleum refining, for example fluidized-bed cracking, hydrocracking, reforming, and dewaxing.

2. Synfuels production, for example conversion of methanol and ethanol to gasoline or gasoline additives.

3. Petrochemical manufacture, for example xylene isomerization, toluene disproportionation, ethylbenzene synthesis, and toluene alkylation with methanol.

4. NO_x abatement.

The five types of zeolites used in this study are HY, HΩ, HL, and pentasil MFI, all obtained from Linde Molecular Sieves, and a self-synthesized large crystal pentasil (denoted P1). The structure (Figure 1.1). of Y zeolite is generated by linking sodalite units, which contain 24 silica and alumina tetrahedra that join together to form a cuboctahedron. Y zeolite has three-dimensional intersecting channels in which the minimum free diameter is the same in each direction. It consists of an array of supercages having internal diameters of about 12 Å. Access to each supercage is through six equispaced necks of

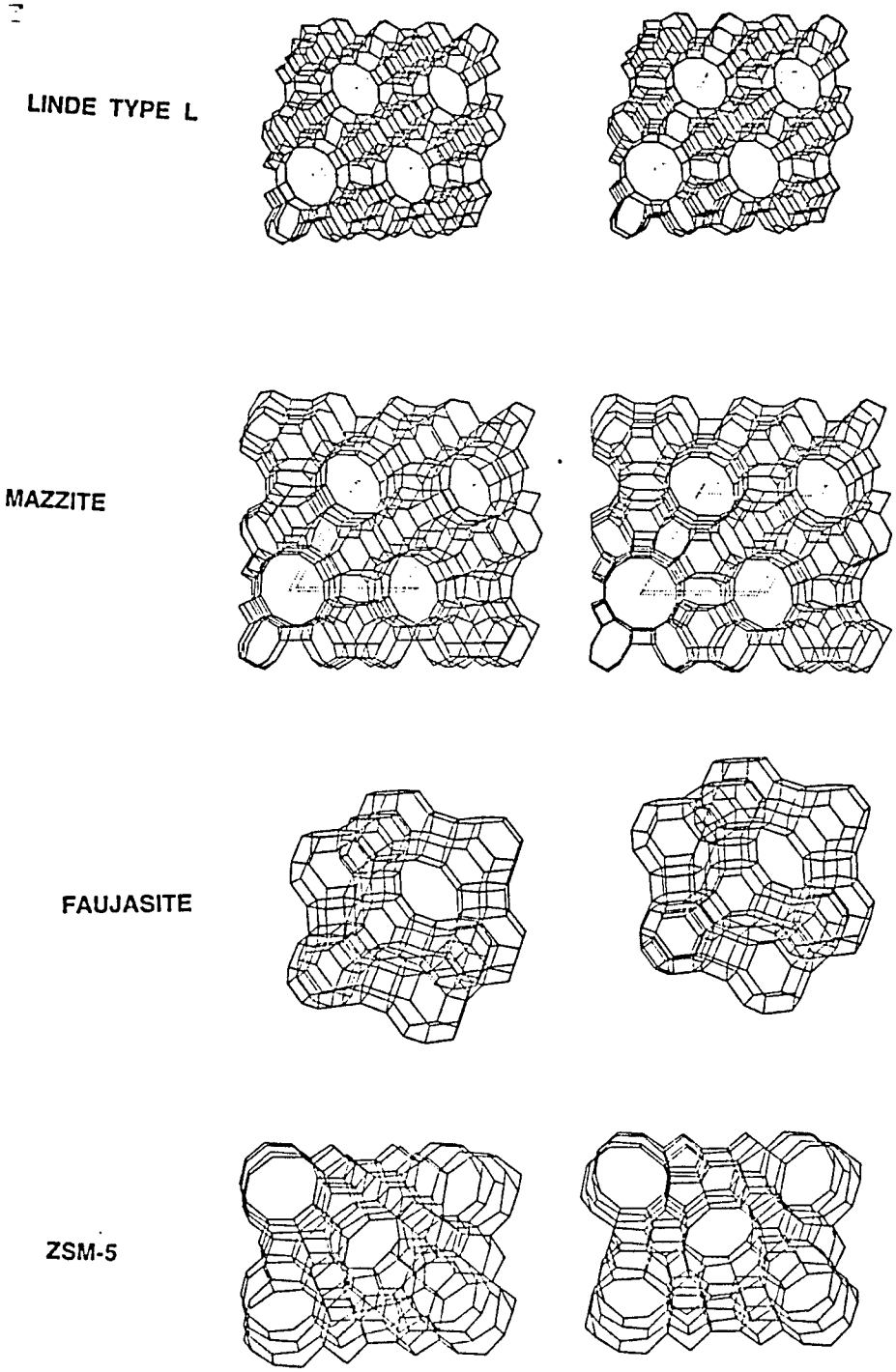

Figure 1.1 Structures of Linde Zeolites Used in This Study

diameter ≈ 7.4 Å. The Y zeolite has one of the largest minimum apertures sizes of any zeolite, and the highest void fraction (0.48).

The framework structure of Ω zeolite is characterized by 12-sided, nearly cylindrical channels that traverse one axis of the zeolite crystal. After dehydration, molecules with a kinetic diameter of about 10 Å will fit into the channel. There is a second channel system composed of distorted 8-membered rings which does not intersect the main channel system. Unlike Y zeolites, diffusion between adjacent main channels is not possible.

The structure of zeolite L consists of cancrinite-type cages linked by double six-ring oxygen bridges. The cancrinite structure is characterized by planar 12-ring (12 oxygen atoms in ring) pores aligned to produce one-dimensional channels. The pore opening is 7.1 Å. These main channels are linked through small pore openings which will not admit H_2O molecules. A minor two-dimensional pore system, parallel to the main channel system, is created by the linked cancrinite cages.

The MFI pentasil has a two-dimensional intersecting channel system. There are near-circular zig-zag channels of 5.0 Å, and elliptical straight channels 5.8 x 5.1 Å in size. The framework of pentasils contains linked tetrahedra. These units join through edges to form chains. These chains are connected to form sheets, and the linking of these sheets forms the 3-dimensional structure of pentasils.

1.3.2 Toluene Disproportionation

Disproportionation of toluene can be carried out in the vapor phase using a variety of acidic catalysts, but zeolites are preferred. Typical side reactions include the disproportionation of xylene to benzene and trimethyl or methylethylbenzene, and the hydrodealkylation of toluene to benzene and methane in the presence of H_2 (Matsumoto and Morita, 1967; Aneke et al., 1979b; Davidova et al., 1979; Olson and Haag, 1984; Chang et al., 1987). To maintain activity and prevent side reactions or coke formation on a catalyst, the presence of hydrogen is effective (Iwamura et al., 1971).

Very little of the information on the disproportionation of toluene deals with the reaction kinetics. Yashima's studies (Yashima et al., 1970), using an H-mordenite catalyst, took the pronounced catalyst deactivation into account by extrapolating the reaction rate to zero time on stream. The rates obtained in this manner were high and it is therefore not surprising that above 350° C pore diffusion was rate-determining; above this temperature, the apparent activation energy decreased to 11.8 from 18.8 kcal/mol. Yashima found a zero-order dependence of the rate on toluene concentration at P = 1 atm, when the N_2/toluene ratio was 5/1.

Aneke et al. (1979b) studied the same reaction catalyzed by Cu/β - AlF_3/HY. Their apparent activation energies appeared to vary with total pressure (2 to 9 atm) as well as toluene partial pressure (0.113 to 0.509 atm), and were about 19-25 kcal/mol. This pressure dependence suggests that at least one of the adsorption terms in the rate equation was significant. Langmuir-Hinshelwood-Hougen-Watson (LHHW) rate models were used and the data were adequately described by three LHHW models of the form:

$$r = \frac{k P_T}{1 + K_{H_2} P_{H_2}^n + K_T P_T P_{H_2}^m} \qquad (1-21)$$

where n is either 1/2 or 1 and m can take on values of 0, 1/2 or 1, r is the reaction rate for toluene disproportionation, k is the reaction rate constant, K_{H_2} and K_T are adsorption equilibrium constants for hydrogen and toluene, respectively, and P_{H_2} and P_T are partial pressures for hydrogen and toluene, respectively. For model 1 (n=1, m=0) and model 2 (n=1/2, m=1/2) the adsorption of toluene was assumed to be rate-limiting, while the formation of the active surface species was the rate-limiting step in model 3 (n=1, m=1). An F test revealed that the difference between the three models is not significant at the 95% confidence level, and therefore it is difficult to say which model best fits the data.

Brignac (1984) studied the toluene disproportionation reaction catalyzed by nickel-modified Y zeolites. The observed rates also followed LHHW kinetics, consistent with the reaction of an adsorbed species with a gas phase toluene molecule,

$$r = \frac{k K_T P_T^2}{1 + K_T P_T} \qquad (1-22)$$

The activation energies were about 18-25 kcal/mol. Note that this expression predicts, as a limiting case, second order behavior at low toluene partial pressure (less than 0.1 atm) and first order behavior at high toluene partial pressures (higher than 1 atm).

Dooley et al. (1990) have reexamined these and some 13 other kinetics studies on catalytic toluene disproportionation. For the

isothermal data, they estimated the microparticle and macroparticle η's by first calculating the observable (Weisz) modulus (Froment and Bischoff, 1979, chp. 3):

$$\Phi = \eta \varphi^2 = \frac{\rho\, r_{obs}\, L^2\, g(C_s)}{\left[2\int_{C_{eq}}^{C_s} D_e\, g(C)\, dC\right]} \qquad (1-23)$$

$$g(C) = r(C)\rho/k_v \qquad (1-24)$$

where Φ is the Weisz modulus, φ the Thiele modulus, ρ apparent catalyst density, r_{obs} the observed reaction rate, L the characteristic diffusional half-width, C_s the external surface concentration, C_{eq} the equilibrium concentration, and k_v the volume-based reaction rate constant. They found that only data from four of these studies (Aneke et al., 1979b; Brignac, 1984; Nayak and Riekert, 1986; Chang et al., 1987) are adequate for the determination of intrinsic kinetics. All four sets of data were fitted with LHHW rate expressions, and all could be successfully correlated by rate equations with kinetics falling into two categories: (1) first order in toluene with toluene inhibition and H_2 dissociation and inhibition; and (2) second order in toluene with toluene and possibly H_2 inhibition. The data of Aneke et al. (1979b) are of type (1) and all other data are apparently of type (2). The distinctness of type (1) can be explained by the differences between the catalysts used by Aneke et al. (1979a) and the other catalysts; the type (1) catalyst had a high metal loading and a separate AlF_3 phase, and was strongly inhibited by H_2.

Dooley et al. (1990) concluded that when purely acidic catalysts were used for toluene disproportionation, the reaction follows a

second-order rate expression, which is consistent with the alkyl transfer mechanism (Pukanic and Massoth, 1973; Poutsma, 1976) shown in Table 1.1. However, the rate expression is also consistent with certain limiting forms of the biphenylalkane (benzylic cation) mechanism also shown in Table 1.1 (Poutsma, 1976; Aneke et al., 1979a; Kaeding et al., 1981a, b). Several investigators (Streitwieser and Reif, 1960; Amelse, 1988) have tried to determine the dominant carbenium ion intermediate that would account for the transalkylation reaction, but no definite conclusion regarding alkyl transfer vs. biphenylalkane mechanisms for zeolites can be drawn. Dooley et al. (1990) also found that a biphenylalkane mechanism is consistent with the kinetics of the type (1) catalysts, because it can predict eq. (1-21). Therefore, the differences between the kinetics of the two types of catalysts are possibly related to a difference in rate determining steps.

1.4 Diffusivity Estimation from Kinetics Data

1.4.1 Computation of Effectiveness Factors

In porous catalysts one is frequently required to solve coupled nonlinear differential equations in order to regress a numerical value of D_e from kinetics data. The nonlinearities of these equations can be found in the reaction rate, in the derivative term (e.g., when density changes exist), in the coefficients of the governing equations (e.g., concentration and temperature dependences of transport parameters), or in the boundary conditions. For most cases of physical

1. Alkyl transfer (Pukanic and Massoth, 1973; Poutsma, 1976)

$$T + S \rightleftarrows TS$$

$$TS + T \rightleftarrows B + XS$$

$$X + S \rightleftarrows XS$$

2. Benzylic Cation (Poutsma, 1976; Aneke et al., 1979b; Keading et al., 1981a, b)

$$T + H^{+}S^{-} \rightleftarrows T \cdot {}^{+}S^{-} + H_2$$

$$T \cdot {}^{+}S^{-} + T \rightleftarrows D \cdot {}^{+}S^{-}$$

$$D \cdot {}^{+}S^{-} \rightleftarrows B + X \cdot {}^{+}S^{-}$$

$$X + H^{+}S^{-} \rightleftarrows X \cdot {}^{+}S^{-}\ H_2$$

T=toluene, B=benzene, X=xylene, S=an unspecified surface site.

Table 1.1. Mechanisms of Toluene Disproportionation

interest, no analytical solution can be found and one has to resort to numerical analysis.

For a porous catalyst, the species mass balance equation in dimensionless form is

$$\frac{1}{X^a}\ \frac{d}{dX}\ (D_e X^a\ \frac{dC}{dX}) = r(C) \qquad (1-25)$$

with boundary conditions

$$C = C_s \qquad \text{at } X = 1 \qquad (1-26.a)$$

$$\frac{dC}{dx} = 0 \qquad \text{at } X = 0 \qquad (1-26.b)$$

For a catalyst of slab geometry, Bischoff (1965) has derived the generalized effectiveness factor as

$$\eta = \frac{\sqrt{2}}{Lr(C_s)}\left[\int_{C_L}^{C_s} D_e(\alpha)\, r(\alpha)\, d\alpha\right]^{0.5} \qquad (1-27)$$

where

$$L = \int_{C_L}^{C_s} \frac{D_e(\beta)\, d\beta}{\left[2\int_{C_L}^{\beta} D_e(\alpha)\, r(\alpha)\, d\alpha\right]^{0.5}} \qquad (1-28)$$

The integral in eq. (1-27) can often be evaluated (especially for constant D_e), but the integration of eq. (1-28) is difficult. Thus, although in principle eqs. (1-27) and (1-28) constitute a solution for the general finite particle problem, numerical values are often difficult to compute.

Therefore, it is necessary to discuss "rational approximation" methods to predict η. These methods avoid numerical integration of

the mass and energy balance equations for inside the catalyst particle, and require at most the solution of a nonlinear algebraic equation.

In order to find the approximate η by perturbation methods, eq. (1-25) is rewritten as:

$$\frac{1}{X^a}\ \frac{d}{dX}\ (X^a D_e(C)\ \frac{dC}{dX}\ ) = \varphi^2 R(C) \qquad (1-29)$$

If R(C) is nonlinear with respect to C, eq. (1-29) does not have an analytical solution; the expression for η becomes

$$\eta = (a + 1) \int_0^1 R(C)\, X^{a+1}\, dX \qquad (1-30)$$

and since C(X) is not known, η cannot be found directly. However, eq. (1-29) can be solved approximately by perturbation techniques when the first order Thiele modulus $\varphi << 1$ or $\varphi >> 1$ (Gonzo and Gottifredi, 1983; Gottifredi et al., 1983 a, b; Haynes, 1986).

When $\varphi << 1$, the approximate solution for η is:

$$\eta = 1 - \sigma_1 \varphi^2 + \sigma_2 \varphi^4 + O(\varphi^6) \qquad (1-31)$$

where σ_1 and σ_2 are integral functions of R and X. When $\varphi^2 \to \infty$, the asymptotic expression for η is

$$\eta = \frac{\rho_1}{\varphi} + \frac{\rho_2}{\varphi^2} + O(\varphi^2) \qquad (1-32)$$

where ρ_1 and ρ_2 are integral functions of R and X. Wedel and Luss (1980) have given expressions for ρ_1 and ρ_2 for some cases of practical interest. Equations (1-31) and (1-32) need to be matched over the

whole range of intermediate φ values. Several investigators have attempted this; for example, Churchill (1977), Wedel and Luss (1980), and Gottifredi et al. (1983a), have proposed one, two and five parameter expressions, respectively.

Collocation methods are also used to approximate η. Villadsen and Michelsen (1978, Ch. 3, 4 and 7) have applied the orthogonal collocation method to eq. (1-29). The solution can be written as:

$$\eta \simeq \eta_N = \sum_{i=1}^{N} W_i J_i \qquad (1-33)$$

where J_i is a Jacobi polynomial trial function and W_i is a weight of the Jacobi polynomial, as given by Villadsen and Stewart (1967; Tables 2-4). They found that collocation approximations are good for small values of φ, but the procedure breaks down if φ exeeds 75 to 100 (due to the large concentration gradient). In order to improve the solution for large φ, Villadsen and Michelsen (1978) used global spline collocation with different choices of the one spline point. They have used the penetration solutions of Aris (1975, p109) at X=0 to determine the spline collocation points. The results of the global spline collocation are presented in their Tables 7.6-7.8 and are accurate to within 0.05%

1.4.2 Effectiveness Factor for Catalysts with Complex Pore Structures

The procedure for calculation of macroeffectiveness factors (η_M) in bimodal porous catalysts is to first obtain a microeffectiveness factor (η_μ) that must then be used at various positions in the pellet

(Henri et al., 1961; Mingle and Smith, 1961; Carberry, 1962). For catalysts with a bidisperse pore size distribution one can derive the general isothermal model equations based on the following assumptions (Wakao and Smith, 1964; Ors and Dogu, 1979; Dooley, 1982):

1. Each microparticle is a separate catalytic aggregate.

2. Significant reaction occurs only within the microparticles, with the rate expression expressed as:

$$r(C) = \frac{k\, g(C)}{h(C)} \qquad (1-34)$$

where k is the rate constant and h(C) is dimensionless.

3. The chemisorption equilibrium at the microparticle external surface is:

$$C_\mu = K\, C_M \qquad (1-35)$$

where μ represents microparticle and M macropore.

4. Diffusion occurs through the macropores surrounding the microparticles and in series fashion into the microparticles.

5. At steady state, the transport rate of the limiting reactant into the microparticles ($R(C_M)$) equals the observed microparticle reaction rate ($r(C_\mu)$). This rate is:

$$R(C_M) = \eta_\mu\, (1 - \varepsilon_M)\, r(C_\mu^s) \qquad (1-36)$$

Then the conservation equations in dimensionless form can be written as (α is the micro to macrodiffusivity ratio):

$$\frac{1}{\zeta^a}\ \frac{d}{d\zeta}\left[\bar{D}_\mu\ \frac{d\psi_\mu}{d\zeta}\right] - \Phi_\mu^2\ \frac{g(\psi_\mu)}{h(\psi_\mu)} = 0 \qquad (1-37)$$

$$\frac{1}{\xi^b}\ \frac{d}{d\xi}\left[\bar{D}_M\,\varepsilon_M\,\xi^b\ \frac{d\psi_M}{d\xi}\right] - \alpha\left[\bar{D}_\mu\ \frac{d\psi_\mu}{d\xi}\right]_{\zeta=a+1} = 0 \qquad (1-38)$$

subject to the following boundary conditions:

$$\frac{d\psi_\mu}{d\zeta} = 0 \qquad \text{at } \zeta = 0 \qquad (1-39a)$$

$$\psi_\mu = \frac{C_\mu^s}{C_M^s} \qquad \text{at } \zeta = a+1 \qquad (1-39b)$$

$$\frac{d\psi_M}{d\xi} = 0 \qquad \text{at } \xi = 0 \qquad (1-39c)$$

$$\psi_M = 1 \qquad \text{at } \xi = 1 \qquad (1-39d)$$

where ψ is the dimensionless concentration and ζ and ξ are the dimensionless coordinates in the microparticle and pellet, respectively.

For the general case of concentration-dependent D_μ and D_M, and an unspecified $r(C_\mu)$, eqs. (1-37) and (1-38) have been solved [Ors and Dogu (1979); a similar solution for spherical geometry is given by Mingle and Smith (1961)] for slab geometry to yield:

$$\eta_\mu = \frac{\left[2 \int_{\psi_\mu^0}^{\psi_\mu^s} \bar{D}_\mu \left[\frac{g(\psi_\mu)}{h(\psi_\mu)} \right] d\gamma \right]^{\frac{1}{2}}}{\Phi_\mu \left[\frac{g(\psi_\mu^s)}{h(\psi_\mu^s)} \right]} \qquad (1-40)$$

and

$$\eta_M = \frac{\left[2 \int_{\psi_M^0}^{1} \bar{D}_M \varepsilon_M \left[\frac{g(\psi_\mu)}{h(\psi_\mu)} \right] d\gamma \right]^{\frac{1}{2}}}{\alpha^{0.5} \Phi_\mu \left[\frac{g(\psi_\mu^{ss})}{h(\psi_\mu^{ss})} \right]} \qquad (1-41)$$

where α is the ratio of diffusion times and ψ_μ^0 and ψ_M^0 are centerline dimensionless concentrations in microparticle and pellet, respectively. The numerical values for ψ_M^0 and ψ_μ^0 can be found from equations analogous to eq. (1-28), if one knows the characteristic lengths for the microparticle and pellet.

The integrals are from centerline to surface concentrations. It is instructive to analyze an idealized limiting case of the model. Consider an irreversible first-order reaction, $g(\psi_\mu) = \psi_\mu$, and constant diffusivity, $\bar{D}_M = 1$ and $\bar{D}_\mu = 1$. The overall reaction-diffusion modulus is (Ors and Dogu, 1979):

$$\Phi = \left(\frac{1}{\eta_M} \right)_{C_M^0 = C_\mu^0 = 0} = \left(\frac{\alpha}{\varepsilon_M} \right)^{\frac{1}{2}} \Phi_\mu^{\frac{3}{2}} = \Phi_M \Phi_\mu^{\frac{1}{2}} \qquad (1-42)$$

Therefore, the present development can allow us, in certain limiting cases, to decouple the microparticle from macropore transport

phenomena, resulting in simple individual mass transfer moduli. Carberry (1962) obtained the same asymptotic solution for reversible first-order reaction at large values of Φ_μ and Φ_M. A large value of Φ_M indicates large concentration gradients in the macropores; a large value of Φ_μ indicates a large microparticle gradient. Because the microparticles are small, only if $D_\mu << D_M$ can Φ_μ be large relative to Φ_M.

1.5 Applicability of Desorption Techniques to Diffusivity Measurement

Temperature programmed desorption (TPD) is a commonly used technique in characterizing adsorbate-catalyst interactions. The TPD experiment consists of the following steps (Cvetanovic and Amenomiya, 1972; Falconer and Schwarz, 1983): (1) catalyst pretreatment, (2) preadsorption of the adsorbate, (3) evacuation to remove physically adsorbed gas, (4) programmed desorption of the chemisorbed gas into the carrier gas, (5) detection of the desorbed gas.

As the catalyst is heated, adsorbed gases desorb, and sometimes react. The desorption rate increases, goes through a maximum, and drops back to zero as the surface is depleted. The result is a desorption spectrum, a record of desorbed gas concentration as a function of temperature. TPD spectra usually have more than one maximum or peak. The shape and position (temperature) of the peak maximum are related to the desorption kinetics, and can provide information on desorption energies (Falconer and Schwarz, 1983).

There are several potential advantages in adapting TPD techniques to diffusivity measurement. These include:

1. The ability to collect data rapidly;
2. The surface coverage as a function of temperature is easily obtained;
3. The order of the desorption kinetics can be evaluated from analysis of curve shapes or from variation of initial coverage;
4. An easy-to-manipulate quantity (carrier gas flow rate) can be used to attain the necessary accuracy in D_e measurement. Increasing this rate improves experimental accuracy by: (1) increasing the heat transfer rate at the interface, and therefore making the adsorbent more isothermal; (2) decreasing the lag time to detection.

However, the detailed analysis of spectra from porous catalysts can be obscured by inappropriate experimental conditions (carrier gas flowrates, catalyst particle sizes, and bed lengths). Under certain conditions the rate-limiting step in the desorption process is shifted, changing the information content of the TPD spectrum. Several investigators have analyzed the problem of TPD from porous samples, with the aim of establishing the influence of readsorption and mass transfer effects on the position and shape of TPD peaks for a first-order desorption process.

Herz et al. (1982) have studied CO desorption from a thin layer of Pt/Al_2O_3, both into a carrier gas and under vaccum. A comparison of the experimental conditions suggests that CO readsorption contributed to the differences between the TPD results. They showed that adsorption equilibrium is closly approached at each point in the sample; this is termed "free readsorption".

Gorte (1982) applied dimensional analysis to the TPD model equations, and was able to characterize the problem in terms of four

dimensionless groups. He concluded that concentration gradients within the sample can be eliminated by appropriate selection of sample weight and carrier gas flow rate. Conversely, appropriate choice of these variables can ensure that such gradients are significant. Readsorption, however, cannot be eliminated for any reasonable combination of conditions. It was also demonstrated that the lag time for sample measurement and the lag time for gas efflux from the pores can be made negligibly small; the presence of intraparticle concentration gradients is controlled by the ratio of the rate of adsorbate removal to the rate of internal diffusion. This ratio is (QL/D_eS), and the intraparticle gradients are negligible if $(QL/D_eS) < 0.1$, while pore diffusion governs TPD when $(QL/D_eS) > 20$.

Demmin and Gorte (1984) and Rieck and Bell (1984) have extended Gorte's work, showing that readsorption and mass transfer effects also complicate TPD curves in a similar manner for desorption from a packed bed. Leary et al. (1988) have shown that subsurface diffusion have similar effects on TPD curves, in extreme cases resulting in the appearance of two peaks in the spectrum for a single adsorbate. They verified their numerical calculations with experiments on H_2 desorbing from a 9% Pd/SiO_2 catalyst.

Huang et al. (1988) also examined the effect of mass transfer during TPD for both first- and second-order desorption from a bed of porous particles. By using an analog to the Weisz-Prater method, they attempted to develop criteria to confirm the absence of intraparticle gradients. They defined the following Weisz-Prater pseudo-modulus for nth-order desorption kinetics:

$$9\eta\varphi_s^2 C_s = \frac{r_{obs}R^2}{VD_e} \qquad (1-43)$$

where φ_s is the Thiele modulus for a spherical particle. However, C_M, the average adsorbate concentration in the particles, is the quantity determined experimentally. Hence, they designate φ_s as a pseudo-modulus. A band of values for the pseudo-modulus was obtained in contour plots of η vs $r_{obs}R^2/VD_e$; their calculations using the pseudo-modulus are consistent with results obtained by applying Demmin and Gorte's (1984) criteria.

Tronconi and Forzatti (1985, 1986) used several TPD spectra of methanol desorbing from a bed of $\gamma - Al_2O_3$ to demonstrate the effects of intraparticle diffusion on TPD. They observed an increase in peak temperature (T_M) and a decrease in the effective desorption rate constsnt (k_{eff}) as the catalyst particle size (R) was increased above a critical value. If the experimental values for T_M and log (k_{eff}), for several runs using particles of different sizes, are plotted vs. log (r), such plots are horizontal lines when diffusional effects are negligible. If the rate-determining step is pore diffusion with equilibrated readsorption, then the same plots were shown to be straight lines with slopes of (3.7q) and (-2), respectively. They concluded that significant concentration gradients in the pores do not affect the TPD curves unless readsorption is fast. Also, the ratio k_{eff}/k_d changes during a TPD experiment, the "worst" situation corresponding to the end of the experiment. In a subsequent paper, Tronconi and Forzatti (1987) have studied the influence of surface heterogeneity on diffusion-limited TPD experiments. They assumed that

the activation energy of desorption is a linear function of coverage, and included it into the TPD model equations developed for the homogeneous case. They found that the same criteria for determining the existence of intraparticle diffusion limitation for TPD experiments for homogeneous surfaces can be extended to the heterogeneous case as well.

Forni and Magni (1988a, b) tested the controlling step of the TPD process by fitting the TPD spectra of ammonia-NaHY systems with different model equations. They found that the desorption process for this system was controlled by intracrystalline diffusion, with D_e values ranging from 4×10^{-18} to 3×10^{-14} cm^2/s for the 423-573 K temperature range. These D_e values were several orders of magnitude smaller than reported D_e values for several aromatics diffusing in Y under similar conditions (Satterfield and Katzer, 1971; Moore and Katzer, 1972). In this model, Forni and Magni divided the TPD spectrum into constant temperature intervals (with 1 K difference), and applied the solution for an isothermal model at each interval. Under these conditions, if the zeolite crystal were large enough, then material desorbing at higher temperature near the external surface will overlap with material desorbing at lower temperature near the centerline. Then the $M_{\Delta t_i}$ used in their model may not represent the actual amount of material desorbed at each specified interval. Hence, the proposed method of analysis for extracting D_e from TPD data and the reported diffusivities are suspect. The difficulties inherent in this method point to the necessity of ID, rather than TPD, experiments to enable accurate D_e measurement in desorption studies.

CHAPTER 2

EXPERIMENTAL METHODS

2.1 Catalyst Preparation

Linde LZ-Y-52 (NaY), ELZ-L (NaKL), ELZ - Ω - 6 (HΩ), ELZ-105-6 (a MFI pentasil), and a large-crystallite MFI pentasil (P1) synthesized according to published procedures (von Ballmoos, 1981) were used as starting materials representative of Y, L, Ω, and pentasil zeolites. The chemical composition and several physical properties of the Linde zeolites, as supplied, are listed in Table 2.1.

The zeolites used as catalysts in this study were all sized to 140-200 mesh and dried in a muffle furnace at 300°C for 12 hours before ion exchange. All the zeolites (except ELZ - Ω - 6) were ion-exchanged by the following method. First, 50 g of zeolite was placed in a 1000-ml round bottom flask with a 10-fold excess (on a volume basis) of 1.0 M $NH_4(NO_3)$ solution. Next, the solution was stirred at reflux for 2 hours. The resulting suspension was filtered, washed with deionized water three times, and the solid dried overnight at 100°C . The catalyst was then stored in capped bottles sealed with Paraffin.

For some kinetics experiments, the zeolites were pressed into pellets, without binder, by a Preco Hydraulic Press (Model PA6) at 3000 psi for 30 minutes. The resulting pellet had a diameter of 1.2 cm and a thickness of 0.4 cm.

	LZ-Y-52	ELZ-L	ELZ-105-6	ELZ-Ω-6
SiO_2 wt. %	63.8	64.86	94.95	78.9
Al_2O_3 wt. %	22.9	18.09	3.73	18.8
Na_2O wt. %	13.0	-	0.03	0.68
Fe_2O_3 wt. %	0.13	-	-	-
K_2O wt. %	-	15.32	-	-
CaO wt. %	0.38	-	-	-
SiO_2/Al_2O_3 Ratio	4.74	6.0	43.3	7.1
Na_2O/Al_2O_3 Ratio	0.93	-	0.01	0.06
K_2O/Al_2O_3 Ratio	-	0.92	-	-
BET Area, m^2/g	900	386	-	300
Unit Cell Size, A	24.68	18.4	-	18.2
Free Aperture, A	7.4	7.1	7.6	7.5
Crystal Density, g/cm^3	1.3	2.0	1.8	1.9

Table 2.1 Chemical Composition and Physical Properties of Linde Zeolites

2.2 Catalyst Characterization

2.2.1 Electron Microscope

The zeolite samples to be examined under the electron microscope were prepared as follows. A 0.1 g sample was ground into fine powder with an agate mortar. The powder was suspended in a thin layer of exopy, which was spread over an aluminum sample mount (15 x 10 mm). The sample and mount were placed in the sputtering chamber of the Hummer VI sputtering system, and pumped down to 6×10^{-3} torr. The sputtering chamber was filled with Ar to 2.5×10^{-2} torr, and a thin layer of gold coating was deposited on the sample at 10 mA and 2700 V for 10 minutes.

Then the sample and mount were loaded to the specimen chamber of the International Scientific Instrument Model ISI-60A scanning electron microscope (SEM), and pumped down to 1.5×10^{-2} torr. At this point the specimen is ready for scanning by the electron beam. The beam was accelerated at 15 KV and produced an emission current of 30 μA for all the experiments. Several micrographs were taken of each sample. The dimensions of the zeolite crystallites, for the powder zeolites used in the kinetics and desorption studies, were on the order of 1 μm for all the Linde zeolites examined.

2.2.2 Pore Geometry of Zeolite Catalyst

The BET surface areas and the pore size distributions of the zeolite catalysts were determined with the Omicron Model Omnisorp-360 analyzer (Figure 2.1). The instrument allows the almost-continuous introduction of adsorbate to a solid sample, while still maintaining equilibrium be-

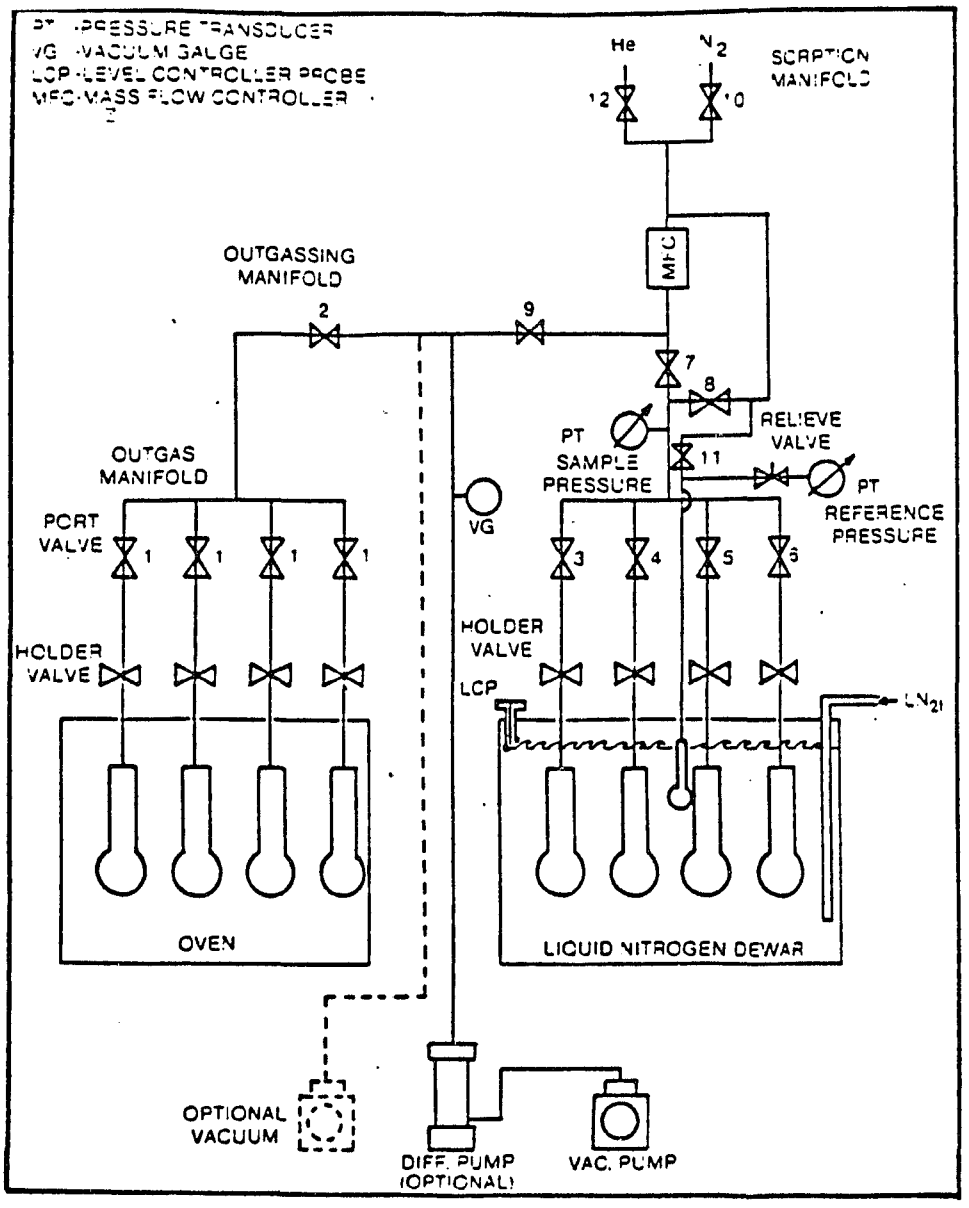

Figure 2.1. Flow Schematic of Omnisorp-360 Analyzer

tween the gas and the adsorbed phases. Equilibrium is achieved by selecting a rate of adsorbate introduction less than the rate of adsorption.

The microparticle surface area was obtained from the N_2 adsorption isotherm at 77.3 K according to BET (Brunaner, Emmett, and Teller, 1938) adsorption theory. Additional information, such as micropore volume, surface area of macropores, and total surface area of the sample, can be extracted from the adsorption isotherm by the t-plot analysis method developed by Lippens and deBoer (1965). This method consists in plotting the adsorption isotherm in terms of the volume of gas adsorbed versus the statistical film thickness, t. Generally, adsorption data presented in the form of a t-plot can form two linear regions, which are seperated by a transition region. Sing (1967) proposed that the first linear region represented both micropore filling and surface coverage of large pores, and the second linear region gave the layer-by-layer adsorption taking place in micropores. The required information on microporous solids can be derived from the slopes and intercepts of these two linear regions.

The pore size distribution is obtained by analysis of the desorption isotherm according to the BJH method (Barrett, Joyner, and Halenda, 1951), which involves using the Kelvin equation to correlate the partial pressure of nitrogen to the size of the pores where capillary condensation takes place. The BET, t-plot, and BJH algorithms are contained within the Omnisorp's instrument control software, and the detailed documentation can be found in the instruction manual for the analyzer.

The Micrometrics Model 1305 helium pycnometer was used to measure the skeletal density of the zeolite catalysts, because the molecular dimensions of helium are small enough (collosion diameter = 2.5 Å) that the gas can fill both the macropores and micropores. Therefore, this exper-

iment measures the total volume, which leads directly to the porosity and skeletal density.

2.2.3 X-Ray Diffraction Analysis

The self-synthesized large crystal and Linde small crystal pentasils were analyzed by X-Ray powder diffraction. These experiments were designed to determine the crystal structure and purity of the former sample, compared with that of the latter.

All X-Ray data were obtained using a Scintag PAD-V Powder X-Ray diffractometer using CuK_{α} radiation. The scan range was from 2.0 - 70.0° (2θ) at 0.01°/s . All diffraction patterns were taken at ambient conditions while exposed to the atmosphere.

2.3 Catalytic Reaction and Desorption Experiments

2.3.1 Apparatus and Procedures for Toluene Disproportionation Reaction

Initial reaction rate data for toluene disproportionation catalyzed by zeolites were determined using a packed-bed flow microreactor (Fig. 2.2), interfaced by means of a Valco 6-port sampling valve to a Varian 2740 gas chromatograph (GC) equipped with dual flame ionization detectors (FID). The liquid reactant was fed into the system by a syringe pump (Sage Model 341A), then vaporized at 250°C and mixed with helium in a 25-cm-long, 1.27-cm-o.d. heated vertical stainless steel tube packed with 4-mm-diameter glass beads.

The reactor was a vertical (upflow) stainless steel tube, 1.27 cm-o.d. and 18 cm long, and was heated by 4 (120V, 300W) electrical heating

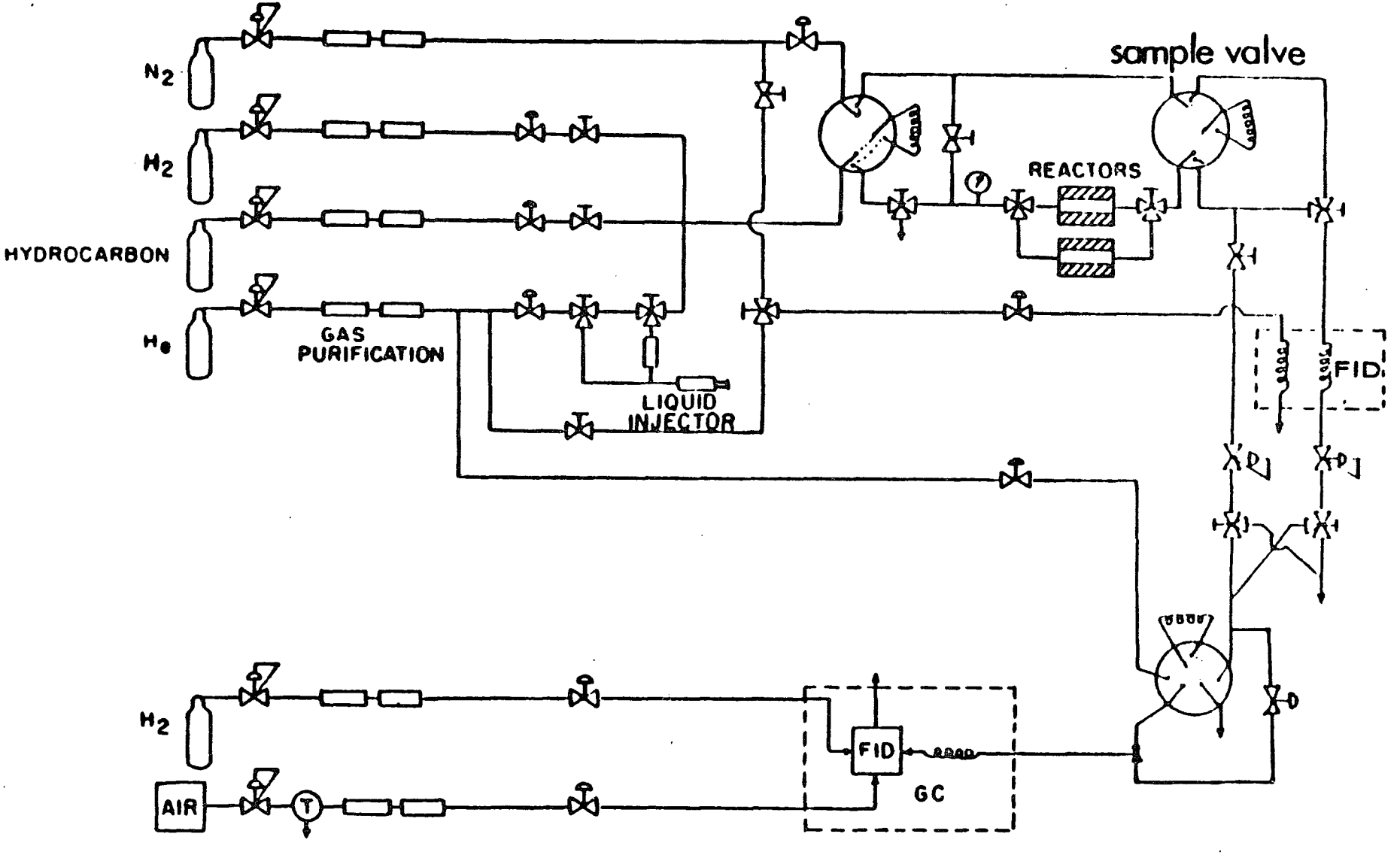

Figure 2.2. Schematic of Apparatus for ID and Catalytic Kinetics Studies.

elements in an 8.2 cm diameter aluminum block, which were controlled by a Valley Forge Model PC 6011 temperature programmer/controller and a Love Model 151 limit controller. The reactor temperature was measured by means of a 2.54-mm iron-constantan thermocouple inserted in the center of the reactor. The lines between the reactor exit and GC as well as the gas sampling valve were also heated (to 150°C) to prevent condensation of product vapors. The temperatures measured by thermocouples attached to these lines were read off a digital temperature indicator (Omega Model 650).

The gas flow rate in the reactor system was controlled by using the Brooks Model 5850 mass flow controller that is accurate to ± 0.5cm^3/ min . A Tescom 26-2300 series back pressure regulator was used to control the outlet pressure of the reactor system, which was maintained at atmospheric pressure for all the kinetics experiments. The reaction products of toluene disproportionation reactions were separated in the GC using a 2.4 m-long, 0.318 cm-o.d., GP 5% SP-1200/1.75% Bentone-34 (Supelco) stainless steel column. The column temperature was held at 75°C. Helium carrier gas flow was 36 cm^3/ min. The FID signal output was integrated by a Hewlett Packard 3392A integrator. The Valco sampling valve and the HP integrator were connected to a ChronTrol Model CD 4-circuit timer, which automatically controlled the sampling valve and activated the integrator.

In a typical experiment, reagent grade toluene (Baker), dried over 5A molecule sieve, was loaded into a 10 - cm^3 syringe that fitted into the pump. The dry catalyst, 0.2-0.8 g of powder, or a single 0.15-0.25 g pellet, was loaded into the center of the reactor between plugs of silanized glass wool surrounded by 20 to 40 mesh glass beads and glass

wool at the reactor top and bottom. The reactor was attached to the rest of flow system by means of two quick-connect fittings.

Prior to use, the catalyst was activated in situ by calcination in a flow of air from room temperature to 500°C, at a heating rate of 2°C/ min, and held at 500°C for 2 hours. Then the catalyst was brought to the reaction temperature. After activation the carrier gas was changed to helium, and the helium flow was adjusted to the desired value using the mass flow controller. The syringe pump delivered toluene to the vaporizer at liquid rate of 0.49 to 1.00 cm^3/hr, where it was mixed with helium. GC samples were taken every 20 minutes while the reactor was in operation.

The reaction products were first identified by their relative retention times, compared to standards. The identifications were later confirmed by GC/MS, using a Finnign 1020 Mass Spectrometer in the electron-impact mode at 70 eV. The molecular weights of parent ions exactly matched those of the assumed products.

2.3.2 Desorption Experiments

Both temperature-programmed desorption (TPD) and isothermal desorption (ID) experiments can be performed in the second reactor unit of Fig. 2.2 using helium as a carrier gas and a linear heating rate. The glass upflow sample tube is 16-cm long, 3.25 cm-o.d., and is heated by a tubular electrical furnace (Heavyduty Electronic Co., type 123-1) with a maximum power output of 422 W. The temperature was controlled by the Eurotherm Type 818 temperature controller/programmer. The input to the temperature controller is from a 2.54 mm-o.d. stainless steel iron-constantan thermocouple inserted in the center of the sample tube. The

furnace temperature is monitored by a 0.794-mm iron-constantan thermocouple placed between the furnace and sample tube at the position of the zeolite bed.

The exit of the glass reactor was directly connected to the FID of the Varian 2740 GC by means of a variable-leak metering valve (Nupro Model S-S1G). This valve controlled the flow rate of desorption stream to the FID; it was fully opened during the desorption experiments, and partially opened during the calibration process. The FID signal output was interfaced to an IBM PC/XT by means of a Data Translation Model 2715/5816 A/D conversion board. The FID output signal was automatically stored on the hard disk of the PC.

In each experiment, from 20 to 30 mg of zeolite were placed upon a fritted disk halfway down the glass tube. Prior to use, the zeolite was activated in situ by calcination in a flow of air from room temperature to 500°C, at a heating rate of 2°C/ min , and held at 500°C for 2 hours. Then the adsorbent was cooled to the desired adsorption temperature, which was determined by the saturation temperature of adsorbate (toluene or benzene) at vapor pressures of 198 and 82 mm Hg, respectively. After activation, the carrier gas was changed to helium. Adsorbate was delivered by the syringe pump to the vaporizer at a liquid rate of 0.74 cm^3/hr, where it was mixed with helium.

Because saturation coverage was desired, the adsorbate mixed with carrier gas was passed through the catalyst bed continuously for 6 hours and then purged with He at the adsorption temperature for 18 to 24 hours. The purge time was determined through a series of experiments by progressively increasing it until the amount of adsorbate desorbed during the subsequent experiment did not change further.

Then the system temperature was raised at a rate of 80 °C/ min from the adsorption temperature to 350°C, which was the highest temperature that no significant extent of reaction been observed. The system was held at 350°C for 30 minutes to ensure that all the adsorbate was desorbed from the system. At several instances, we have raised the system temperature to 500°C, but no adsorbate was observed during this post heating process. Therefore, it was safe to say that all the adsorbate was desorbed during the initial heating and constant temperature holding periods.

The desorption rate was monitored using the online GC. The FID signal was automatically stored on the hard disk of the IBM PC/XT, and was ready to retrieve for future data analysis. The experiment was repeated several times for each adsorbent with the same purge time, to check for reproducibility.

CHAPTER 3

RESULTS

3.1 Properties of Zeolite Catalysts

3.1.1 Surface Area and Pore Size Distribution

The catalyst surface characterization data are summarized in Table 3.1. The specific areas were measured using the N_2 physical adsorption method developed by Brunauer, Emmett, and Teller (1938). The macropore volumes were measured using the BJH analysis developed by Barrett, Joyner, and Halenda (1951). Both methods consist of extracting data from the adsorption or desorption isotherm by plotting the volume adsorbed or desorbed as a function of the relative partial pressure of N_2.

For zeolites the heat of adsorption within the zeolite structure is far greater than for adsorption on the external surfaces of the crystallites. This difference in heat of adsorption results in a characteristic isotherm in which the adsorption substantially takes place at very low partial pressures. These are type I isotherms, typically encountered with microporous powders whose pore sizes do not exceed a few adsorbate molecular diameters. A typical isotherm, for the L-zeolite, is shown in Fig. 3.1. A type I isotherm indicates that the pores are microporous and that the exposed surface resides almost exclusively within the micropores.

The BET specific surface areas listed in Table 3.1 are 16 - 32 % below the values reported by Linde (except for Ω , see Table 2.1), but show a

Catalyst	Geometric Form	BET Specific Area (m^2/g)	Crystal Radius (cm)
L	Powder	324	$1.7x10^{-5}$
Ω - 6	Powder	292	$3.2x10^{-5}$
Y-52	Powder	700	$3.4x10^{-5}$
105-6	Powder	365	$1.9x10^{-5}$
P1	Powder	300	$8.4x10^{-5}$
L	Pellet	40	
Ω - 6	Pellet	74	
Y-52	Pellet	395	
105-6	Pellet	326	
NaY (1)	Powder	546	
HY (1)	Powder	648	
HZSM-5 (2)	Powder	483	
HKL (3)	Powder	453	
NaTMAΩ (4)	Powder	346	
NaΩ (5)	Powder	250	

(1) Aneke et al., (1979b). N_2 adsorption
(2) Choudhary and Akolekar (1989). N_2 adsorption
(3) Parra et al., (1975). N_2 adsopriton
(4) Weeks et al., (19). O_2 adsorption
(5) Chauvin et al., (1990). N_2 adsorption

Table 3.1. Measured Properties of Experimental Zeolites

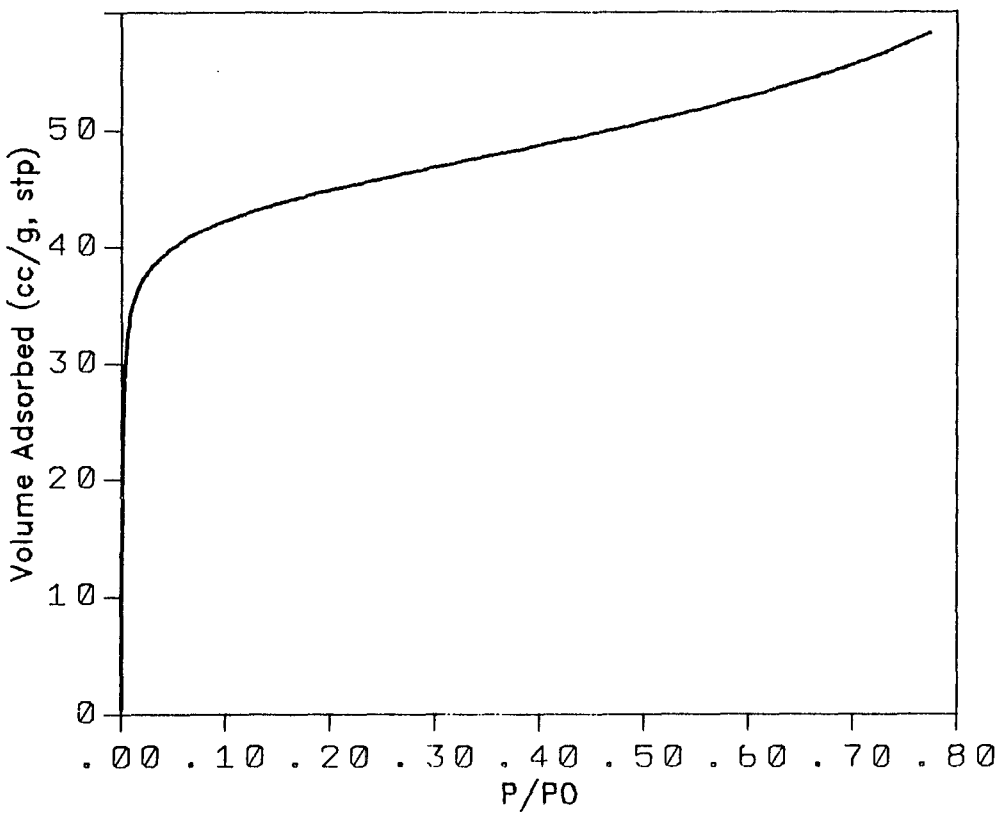

Fig. 3.1, Adsorption Isotherm for Zeolite L

similar trend. All the adsorption experiments were repeated several times to check for reproducibility.

The success of BET estimation of surface area depends upon: (1) determining monolayer coverage, and (2) the cross-sectional area of the molecule (the effective area covered by an adsorbed molecule). The BET surface area is the product of number of molecules in a completed monolayer times the effective cross-sectional area of an adsorbate molecule.

The discrepancies between Linde's and these data are probably due to the following:

1. Different forms of BET theory were used. Linde used the single-point BET method as opposed to the more accurate multipoint BET method employed in this study. The relative error between these two methods is a function of the relative pressure, P/P_{sat}, and the BET parameter C, which is the equilibrium constant for physical adsorption:

$$\text{Single-point Error} = \frac{1 - P/P_{sat}}{1 + (C - 1)P/P_{sat}} \qquad (3 - 1)$$

   Eq. (3-1) discloses that the relative error can be minimized by using a higher relative pressure at fixed C. But the use of relative pressures above 0.3 can lead to other serious errors (for example, due to capillary condensation). Since Linde did not report their C values, there is no way to estimate the relative error by eq. (3-1).

2. Different types of adsorbate, O_2 and N_2, were used by Linde and in this study, respectively. These interact differently with the

zeolite, giving different values of monolayer coverage as well as cross-sectional area. Hence, it is not unusual to have large differences between O_2 and N_2 adsorption data. Some of the literature surface area data obtained by either N_2 or O_2 adsorption are also listed in Table 3.1 for comparison.

Because the macropores of the pellet-form zeolite are formed by compressing zeolite crystals, they can be assumed to satisfy the basic assumptions of the BJH method, which are that the pores are cylindrical with open ends, and that a well-defined network is absent. The macropore size distribution data for pellet-form zeolites are listed in Table 3.2. Only data with pore size larger than 1 nm were reported because: (1) the basic assumption of Kelvin's equation, capillary condensation to fill up the pores, is not valid for pores with size less than 1 nm (these are filled by multilayer adsorption); (2) at smaller sizes there are volumetric contributions from the zeolite micropore volume, which cause the observed deviations from unimodal behavior of some of the pore size distributions. The results show that above 1 nm all the pellets have a unimodal macropore size distribution, with average macropore sizes of 7.0, 14.2, 21.1, and 5.7 nm for L, Ω, Y, and small crystallite pentasil zeolites, respectively. The pore size distribution data listed in Table 3.2 are used in Section 4.2.2 for the estimation of macropore diffusivity.

3.1.2 SEM and Pycnometer Results

The collection of micrographs (Fig. 3.2) illustrates the crystal size distribution of zeolites used in this study. The average crystal sizes for the zeolites are listed in Table 3.1. The average crystal radius was

Pore Radius (nm)	Pore Volume (cm^3/g) L	Ω - 6	Y-52	105-6
1 - 2	0.0020	0.016	0.0057	0.0047
2 - 3	0.0038	0.037	0.0321	0.0040
3 - 4	0.0036	0.041	0.0384	0.0027
4 - 5	0.0035	0.020	0.0191	0.0022
5 - 10	0.0212	0.047	0.0392	0.0100
10 - 20	0.0274	0.129	0.0327	0.0213
20 - 30	0.0038	0.028	0.0067	0.0080
> 30	0.0008	0.014	0.0000	0.0013
Total	0.0661	0.333	0.1740	0.0543

Table 3.2. Pore Size Distribution for Pellet-Form Zeolites

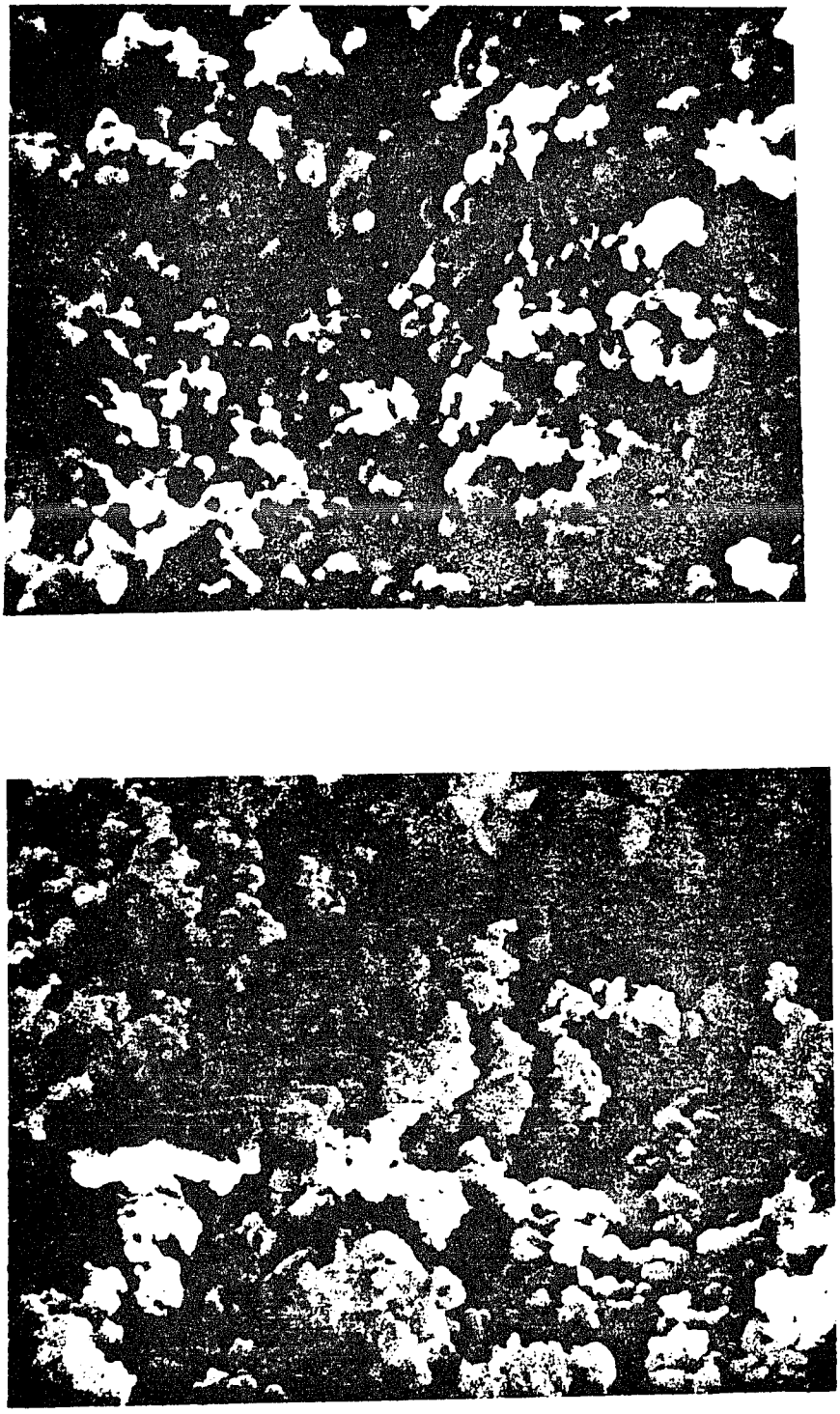

Figure 3.2 SEM Micrographs for Zeolites L andΩ - 6

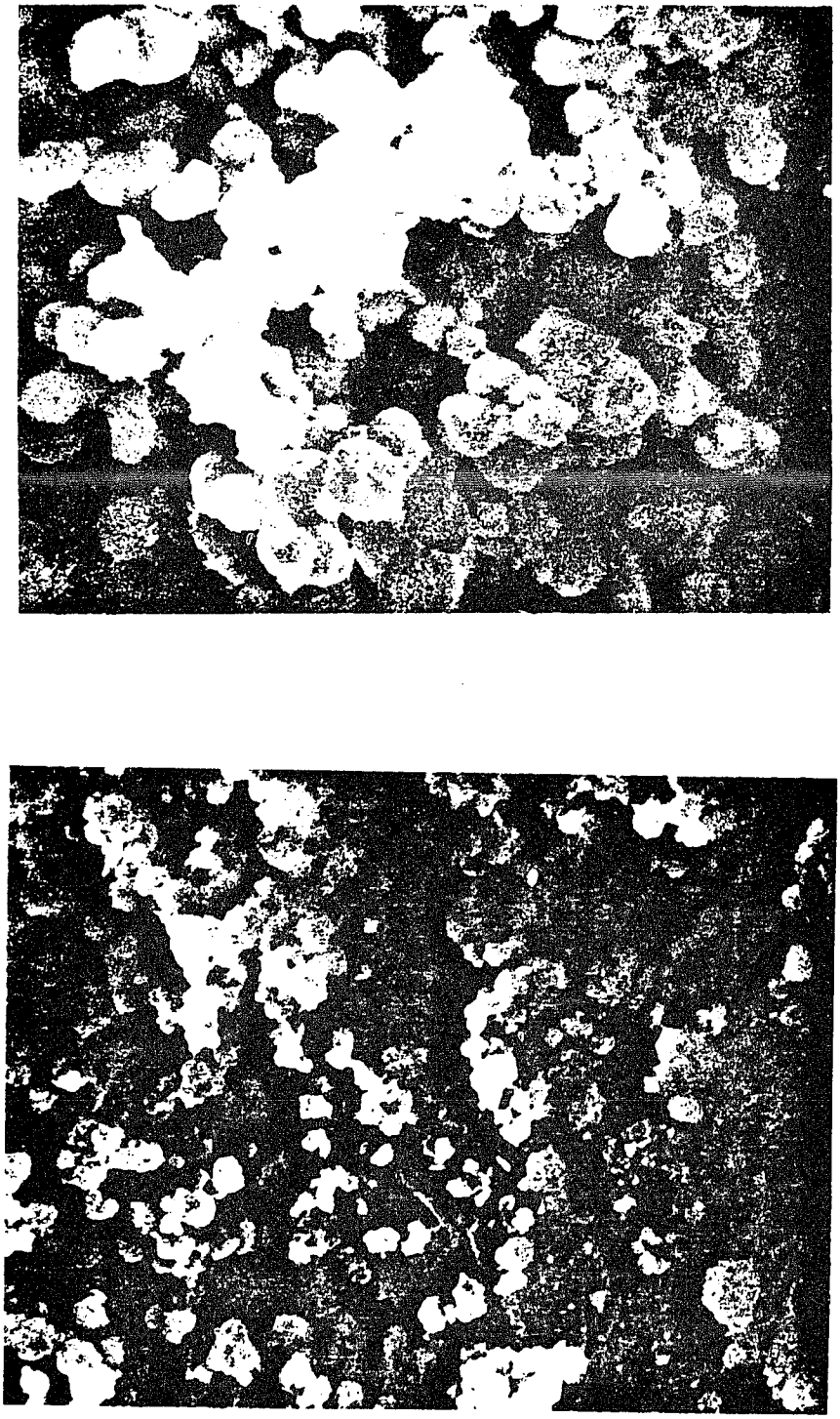

Figure 3.2 (cont.) SEM Micrographs for Zeolites P1 and Y-52

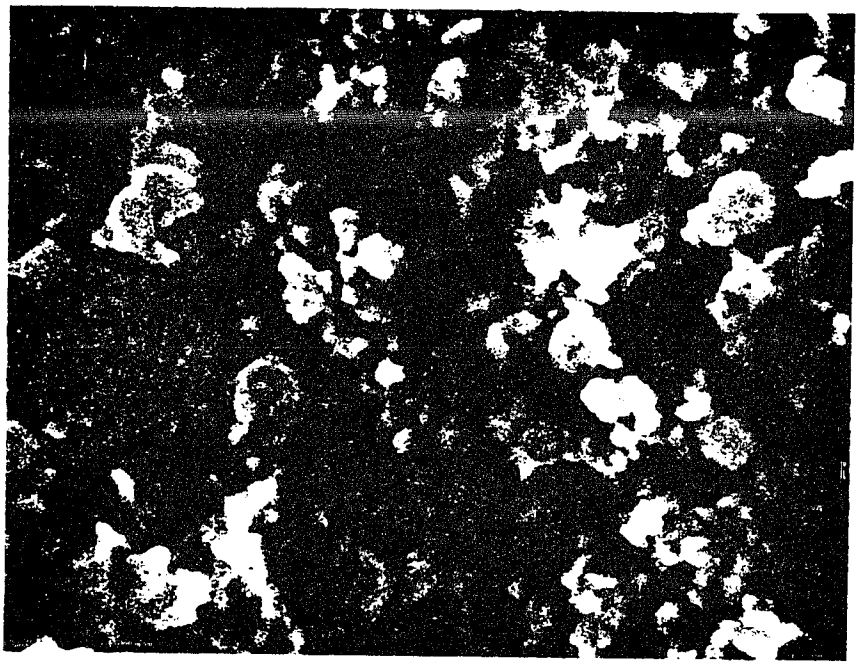

Figure 3.2 (cont.) SEM Micrographs for Zeolite 105-6

determined by measuring the number of crystals at each size and taking the volume average of the measurements. All the zeolites have average crystal sizes on the order of 0.2 to 0.4 μm, except for the large crystallite pentasil, which has an average size of 0.84 μm, which is 4.4 times that of the small crystallite pentasil, 0.19 μm. This difference in crystal size allows one to check the significance of intracrystalline diffusion limitations by performing kinetics experiments on these two zeolites under the same reaction conditions.

The skeletal densities of the zeolites were calculated from framework density data contained in the "Atlas of Zeolite Structure Types" (Meier and Olson, 1978) and the zeolite unit cell compositions provided by Linde. The calculations agreed with reported values (Breck, 1974).

The other important properties related to the zeolites were derived from the properties mentioned above, except that the micropore volumes were obtained from the literature (Breck, 1974). These derived properties are given in Table 3.3; they are calculated as follows:

$$\varepsilon_M = \frac{V_M}{V_M + V_\mu + V_c} \qquad (3-2)$$

$$\varepsilon_\mu = \frac{V_\mu}{V_c + V_\mu} \qquad (3-3)$$

$$\rho_M = \frac{1.0}{V_M + V_\mu + V_c} \qquad (3-4)$$

$$\rho_\mu = \frac{1.0}{V_c + V_\mu} \qquad (3-5)$$

3.1.3 X-Ray Diffraction Results

Properties	L	Ω - 6	Y-52	105-6
ρ_c (g/cm^3)	1.77	1.61	1.35	1.79
V_M (cm^3/g)	0.325	0.333	0.252	0.297
V_μ (cm^3/g)	0.18	0.09	0.35	0.16
V_c (cm^3/g)	0.565	0.621	0.741	0.559
ε_M	0.304	0.319	0.188	0.292
ε_μ	0.242	0.127	0.321	0.224
ρ_M (g/cm^3)	0.935	0.958	0.745	0.984
ρ_μ (g/cm^3)	1.342	1.407	0.917	1.391

Table 3.3. Derived Properties for Pellet-Form Zeolites

Tables 3.4-3.6 give the 25 largest I/I_{max} peaks and the corresponding 2θ (Bragg diffraction angle) values for Linde small crystallite pentasil (105-6), the self-synthesized large crystallite pentasil (P1), and Mobil ZSM-5 (von Ballmoos, 1984) zeolites, respectively. The numerical data include d-spacings, relative intensities, and Miller indices hkl of the contributing reflections.

The types of phases observed during the synthesis of P1 depend on the purity and method of preparation of Al and Si source, the Si/Al ratio, the temperature and time for crystallization, and the type of template used. Generally, amorphous gel, Chabazite, K-M, and Sanidine (poatssium feldspar, $KAlSi_3O_8$) are observed impurity phases. By comparing the powder diffraction data listed in Tables 3.5 and 3.6, it was found that for P1 only the small peaks at 2θ values of 15.84 and 44.97 are not found in Mobil ZSM-5. But these two peaks do not correspond to any peaks characteristic of typical impurity phases. Therefore, one may conclude that there are no observable impurity phases in P1. By comparing the X-Ray Diffraction Patterns shown in Fig. 3.3, one can see that some peaks for P1 are broader than the corresponding peaks for the Linde pentasil. This phenomenon indicates that some amorphous gel remains in the P1 zeolite.

3.2 Kinetics Data for Toluene Disproportionation

3.2.1 Preliminary and Deactivation Experiments

Four different types of zeolites in powder- and pellet-forms were used in the kinetics experiments. The procedure for the preliminary kinetics experiments can be summarized as follows. For each catalyst, the reactant conversion at several temperatures was measured, for discrete

2θ	d	I_{rel}	h	k	l
23.14	3.840	100	0	0	0
7.87	11.224	68	0	0	0
23.81	3.734	47	0	0	0
8.79	10.053	45	0	0	0
24.34	3.655	25	0	0	0
14.86	5.959	17	0	0	0
14.69	6.024	17	0	0	0
20.78	4.270	16	0	0	0
29.87	2.989	14	0	0	0
15.89	5.572	14	0	0	0
29.98	2.978	14	0	0	0
20.69	4.290	14	0	0	0
15.42	5.741	12	0	0	0
45.36	1.998	12	0	0	0
13.86	6.383	12	0	0	0
25.77	3.454	12	0	0	0
17.74	4.996	11	0	0	0
15.60	5.676	11	0	0	0
25.90	3.438	11	0	0	0
17.52	5.059	11	0	0	0
26.91	3.310	11	0	0	0
13.17	6.720	10	0	0	0
26.68	3.338	10	0	0	0
20.29	4.374	10	0	0	0
30.25	2.953	9	0	0	0

Table 3.4. Twenty Five Largest X-Ray Peaks for the Linde 105-6 Zeolite

2θ	d	I_{rel}	h	k	l
23.07	3.852	100	0	0	0
8.79	10.056	54	0	0	0
23.88	3.724	48	0	0	0
24.32	3.658	34	0	0	0
14.74	6.006	17	0	0	0
29.88	2.988	15	0	0	0
15.84	5.591	15	0	0	0
29.20	3.056	14	0	0	0
20.78	4.272	13	0	0	0
44.97	2.014	12	0	0	0
45.39	1.997	12	0	0	0
13.85	6.389	11	0	0	0
26.55	3.355	11	0	0	0
20.27	4.378	11	0	0	0
15.47	5.724	10	0	0	0
26.83	3.321	10	0	0	0
25.82	3.448	10	0	0	0
17.74	4.996	8	0	0	0
30.26	2.951	8	0	0	0
22.13	4.014	7	0	0	0
35.97	2.495	7	0	0	0
13.12	6.741	7	0	0	0
32.70	2.736	6	0	0	0
19.17	4.625	6	0	0	0
25.50	3.490	6	0	0	0

Table 3.5. Twenty Five Largest X-Ray Peaks for Zeolite P1

2θ	d	I_{rel}	h	k	l
23.10	3.850	100	5	0	1
23.26	3.825	78	0	5	1
23.91	3.722	54	3	0	3
7.92	11.165	52	1	0	1
7.94	11.140	48	0	1	1
24.38	3.651	40	1	3	3
23.68	3.757	37	1	5	1
8.87	9.974	35	0	2	0
8.80	10.048	29	2	0	0
9.08	9.743	24	1	1	1
13.91	6.368	17	1	0	2
20.33	4.367	13	0	1	3
25.89	3.442	13	4	3	2
29.25	3.053	12	3	5	2
14.78	5.994	11	3	0	1
15.51	5.713	11	1	3	1
45.47	1.995	9	0	10	0
26.93	3.311	9	1	0	4
30.00	2.978	9	0	5	3
11.90	7.438	9	1	2	1
20.87	4.256	8	4	2	1
22.18	4.009	7	4	3	0
19.24	4.614	7	3	1	2
14.60	6.006	7	1	1	2
13.19	6.714	6	0	0	2

Table 3.6. Twenty Five Largest X-Ray Peaks for Mobil ZSM-5

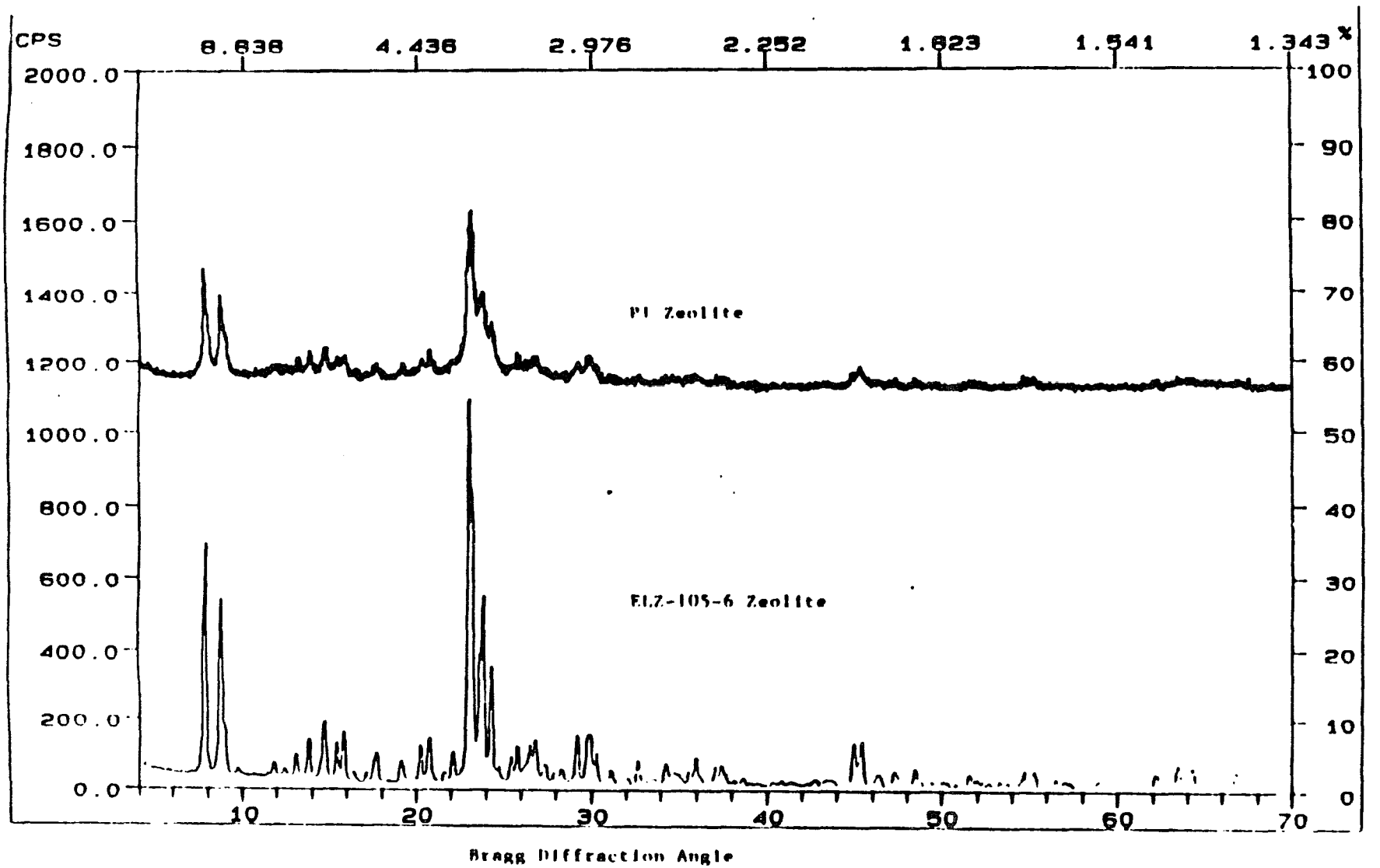

Figure 3.2 Comparsion of X Ray Diffraction Patterns for Pentasils

temperature increases. For example, the chosen temperatures for toluene disproportionation were 673 to 773 K, with 20 K increases every hour. In this manner the optimum temperature for an η in a diffusion-limited range (η = 0.05-0.9) was rapidly identified, and the temperatures resulting in rapid deactivation or side reactions were avoided. The chosen reaction temperature was 673 K for Y zeolite, and 693 K for the other zeolites used in this study.

The next step was to determine the deactivation behavior at the chosen temperature. It was found that for toluene disproportionation catalyzed by Y and pentasil zeolites, the activity is typically constant over a long period of time, after an initial period of transient activity loss that was probably caused by rapid poisoning of very acidic sites. However, for the Ω- and L-type catalysts, the deactivation is continuous. Typical conversion to benzene vs. time graphs for both constant activity and deactivating catalysts are shown in Figs. 3.4 and 3.5, respectively.

3.2.2 Kinetics Experiments

As mentioned in Section 2.3.1, it is possible to conduct extensive kinetics experiments for each catalyst at different space velocities, either changing the amount of catalyst used or the reactant flow rates at the chosen reaction temperature. For example, for powder-form catalysts, 0.2, 0.4, 0.6, and 0.8 g of catalyst were used to vary space velocity, and the toluene liquid flow rate was kept constant at 0.74 cm^3/hr. For pellet-form catalysts, the liquid toluene feed rate was varied from 0.49 to 1.00 cm^3/hr, and the catalyst weight was kept constant at 0.2 g.

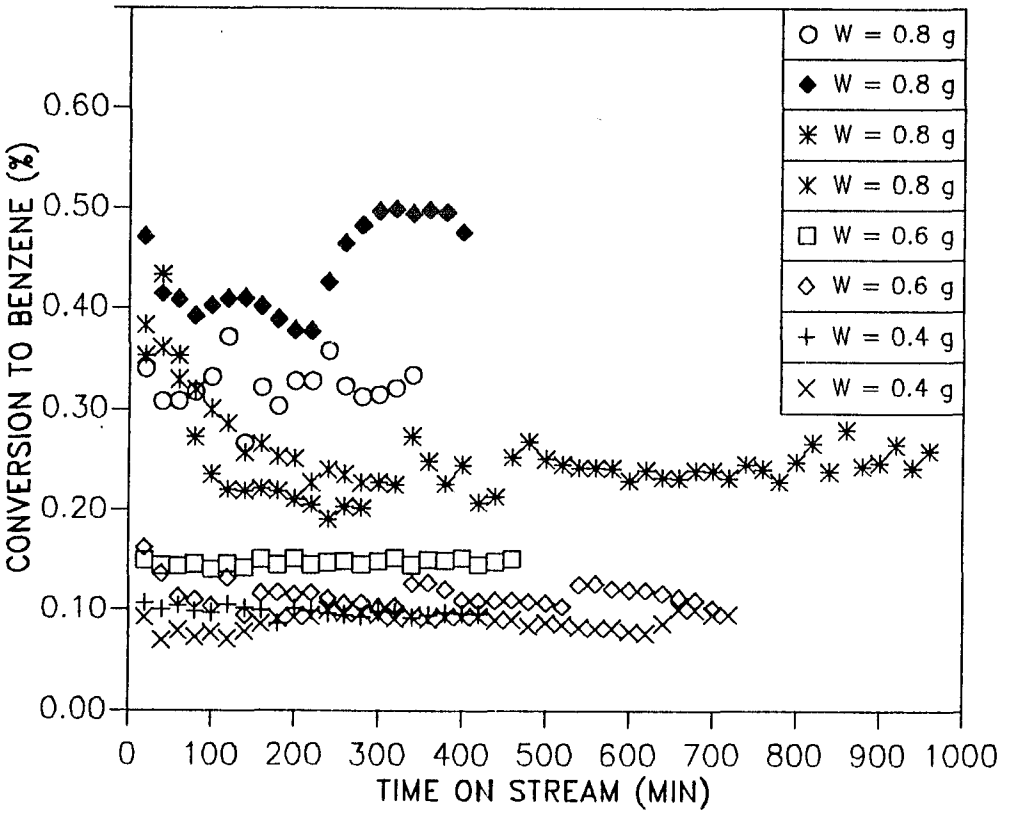

Figure 3.4, Toluene Disproportionation Catalyzed by 105-6 Powder

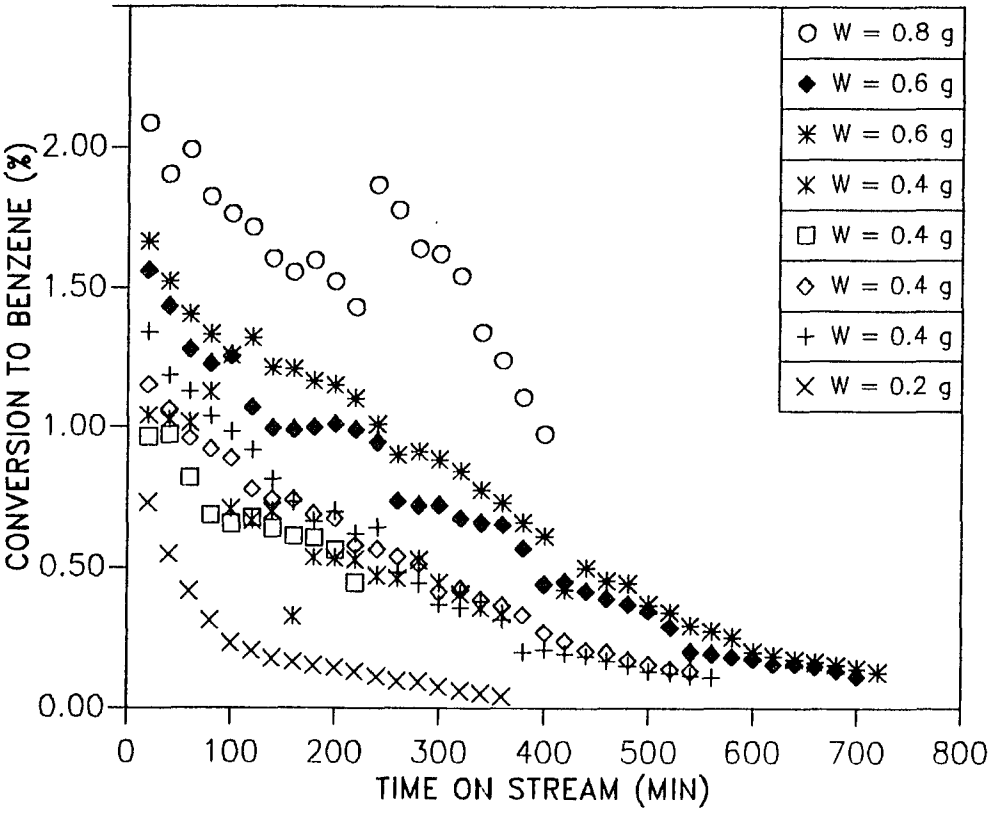

Figure 3.5, Toluene Disproportionation Catalyzed by L Powder

The continuity equation for limiting reactant A in a plug flow reactor is

$$\frac{r_{obs}}{F_A} = \frac{dX_A}{dW} \qquad (3-6)$$

eq. (3-6) shows that a plot of X_A vs. W at constant number of turnovers should be linear with slope r_{obs}/F_A at low conversions.

The conversions based on either benzene or xylenes, for the toluene disproportionation reaction catalyzed by powder-form pentasil and L-type zeolites, are compared in Figs. 3.6 and 3.7, respectively. The toluene disproportionation reaction should produce an equimolar amount of benzene and total xylenes. A comparison of conversions based on benzene to those based on total xylenes indicates that some of the conversions to xylenes exceeded those to benzene (especially for L). However, the GC data produced a sharper, hence better integrated, benzene peak. Therefore, it was decided to use the conversion data based on benzene as a basis for reaction rate calculations. No products other than these were observed.

Raw GC area data were converted to conversions by applying the calibration results shown in Appendix A. Then the conversion information was used to compute the observed rate. For catalysts with constant activity, the average conversion to benzene (X_A) at different weights of catalyst were calculated. Then the slope of X_A vs. W is equal to the initial rate. The X_A vs. W plots at different number of turnovers for the small crystallite pentasil and Y zeolites are shown in Figs. 3.8, and 3.9, respectively. Note that the slopes approach a constant value as the number of turnovers increase.

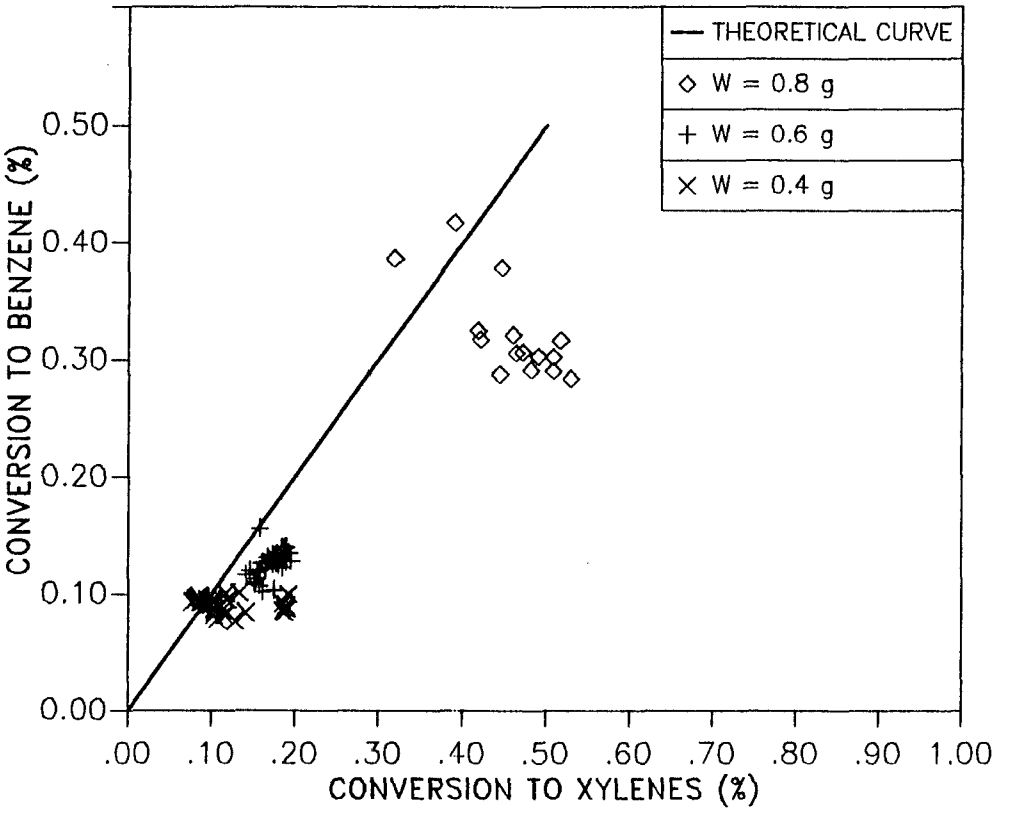

Figure 3.6, Toluene Disproportionation Catalyzed by 105-6 Powder

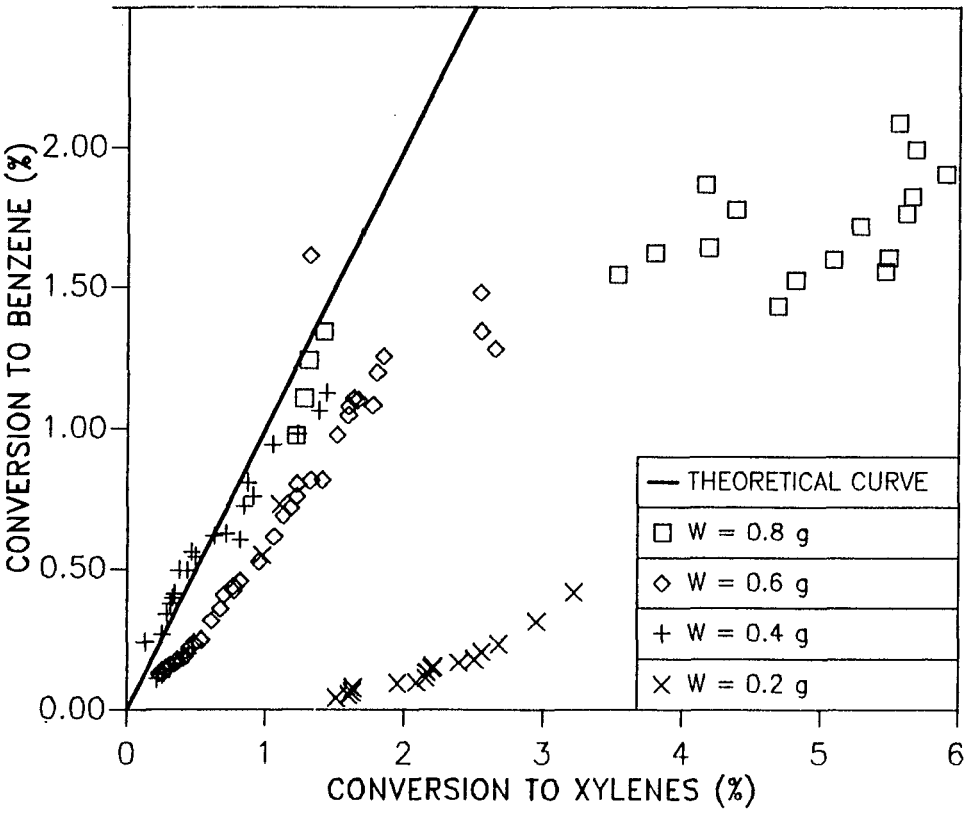

Figure 3.7, Toluene Disproportionation Catalyzed by L Powder

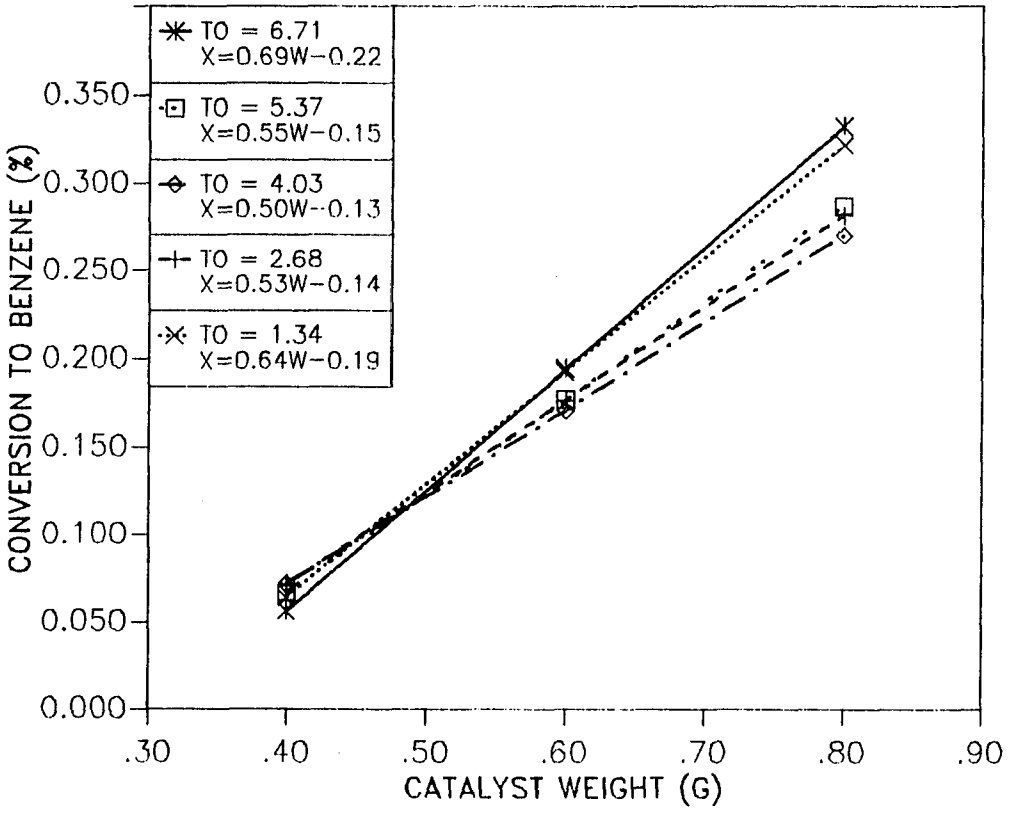

Figure 3.8, Effects of Varying Space Velocities for Toluene Disproportionation Catalyzed by 105-6 Powder

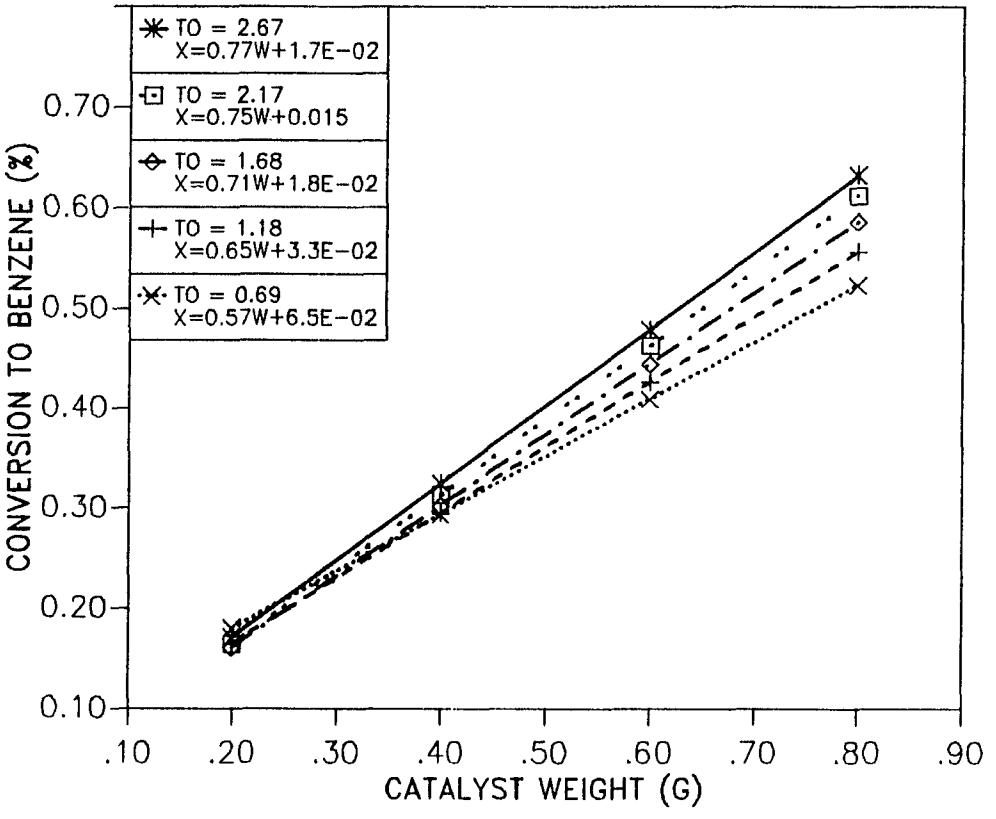

Figure 3.9, Effects of Varying Space Velocities for Toluene Disproportionation Catalyzed by Y-52 Powder

For catalysts characterized by continuous deactivation, one should compare conversion data at a constant number of turnovers (TO). The above argument may be proved as follows:

$$TO = \frac{\text{Wt. Toluene Reacted}}{\text{Catalyst Wt.}} \qquad (3-7)$$

or

$$TO = \int_0^t \frac{(F_A)dt}{W} \qquad (3-8)$$

It is usually found that the rate of deactivation, r_2, is a linear function of r_1, the rate of the primary reaction. Then

$$-\frac{d\theta}{dt} = r_2 = \gamma r_1 \qquad (3-9)$$

The integration of eq. (3-9) gives:

$$\theta_0 - \theta = \gamma \int r_1 dt \qquad (3-10)$$

Using eqs. (3-6) and (3-8) in (3-10) gives the final result:

$$\theta = \theta_0 - \gamma \times (TO) \qquad (3-11)$$

where θ is the fraction of sites still active. Since $r_1 = \theta\, k\, g(C)$, then it is obvious that to compare results from different catalysts at constant r_1, TO must be kept constant.

The X_A vs. W plots at different number of turnovers for the L and Ω zeolites are shown in Figs. 3.10 and 3.11, respectively. The corresponding X_A vs. W plots for pellet-form L, Ω, Y and small crystallite pentasil are listed in Figs. 3.12 to 3.15, respectively.

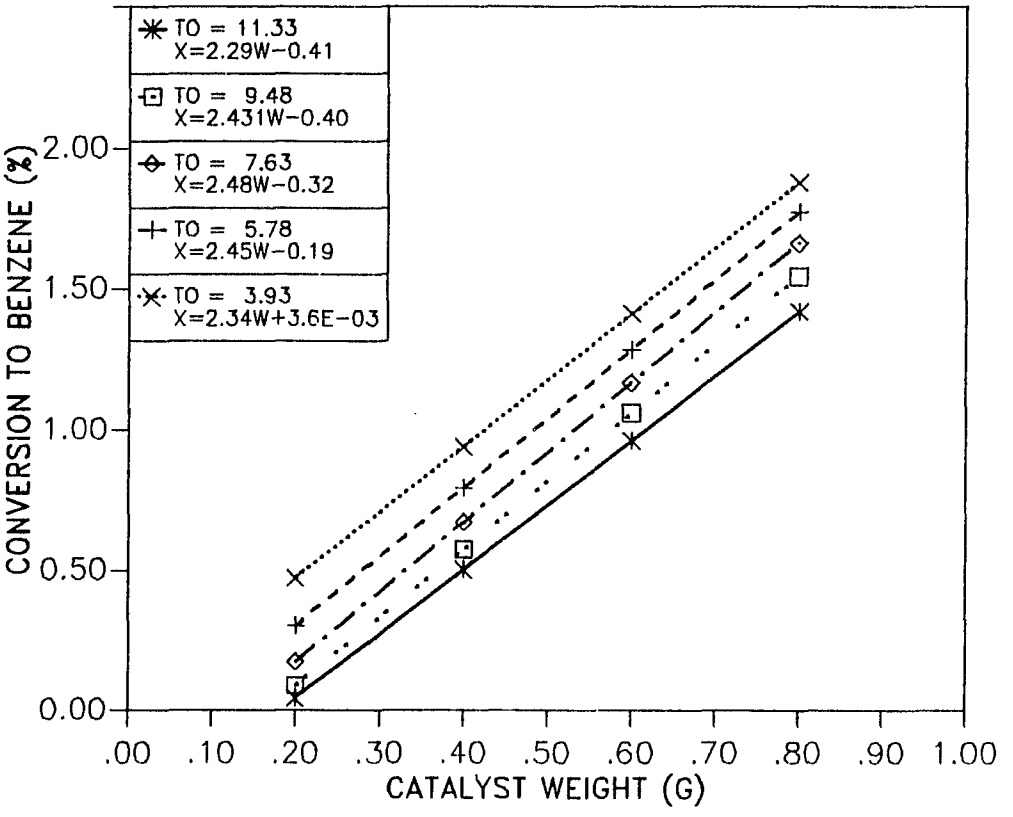

Figure 3.10, Effects of Varying Space Velocities for toluene Disproportionation Catalyzed by L Powder

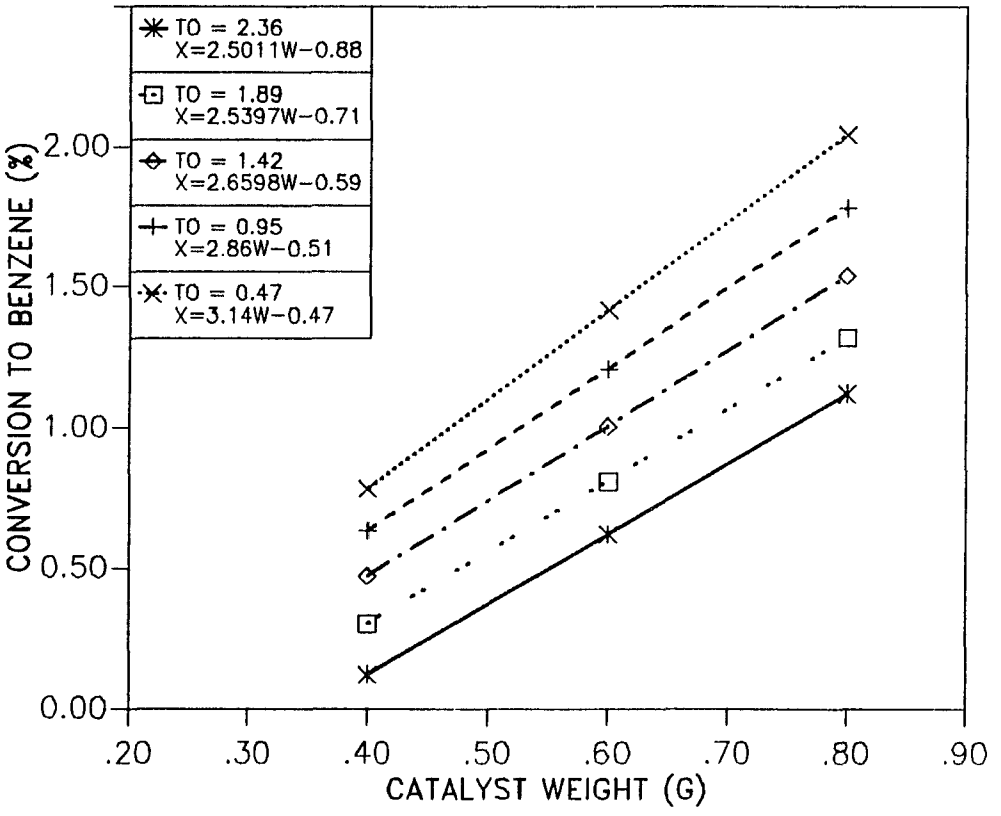

Figure 3.11, Effects of Varying Space Velocities for Toluene Disproportionation Catalyzed by Omega-6 Powder

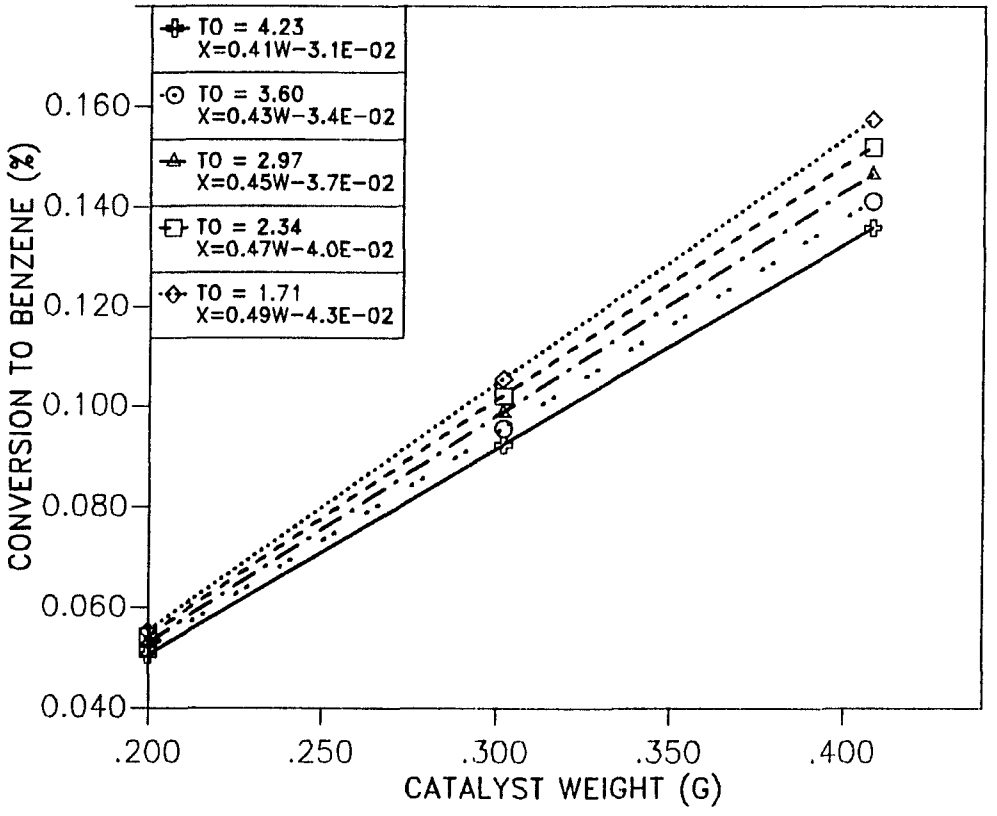

Figure 3.12, Effects of Varying Space Velocities for Toluene Disproportionation by L Pellets

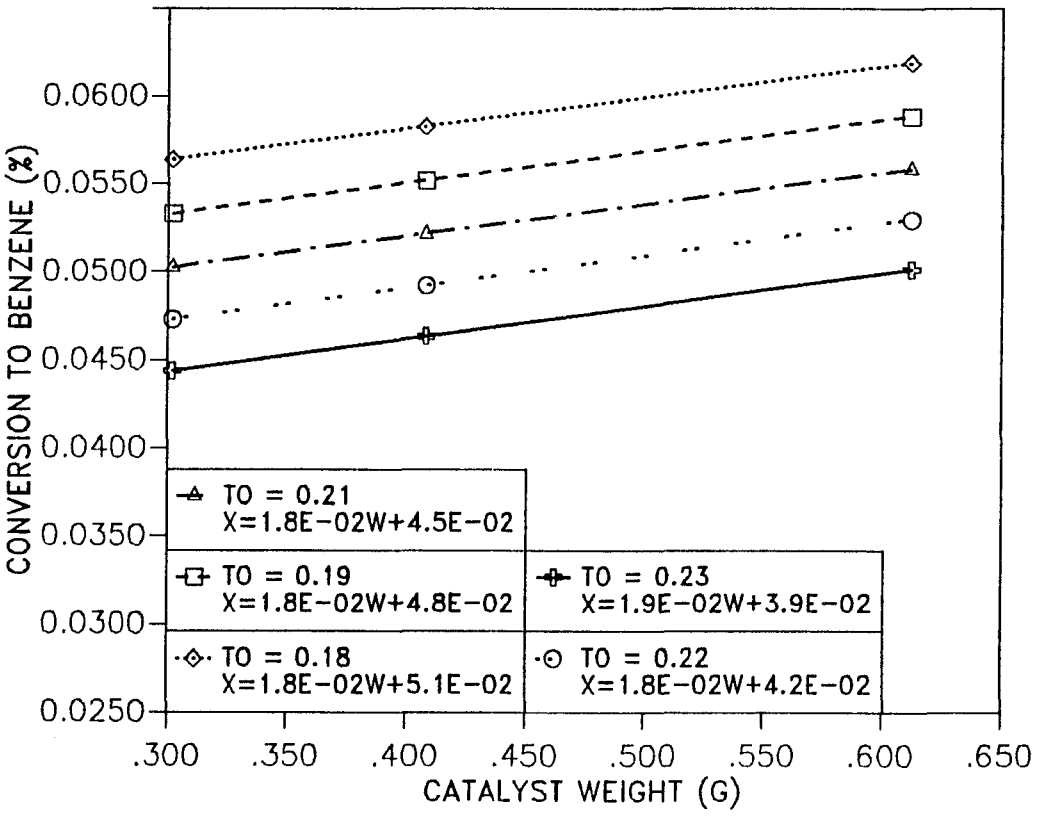

Figure 3.13, Effects of Varying Space Velocities for Toluene Disproportionation by Omega-6 Pellets

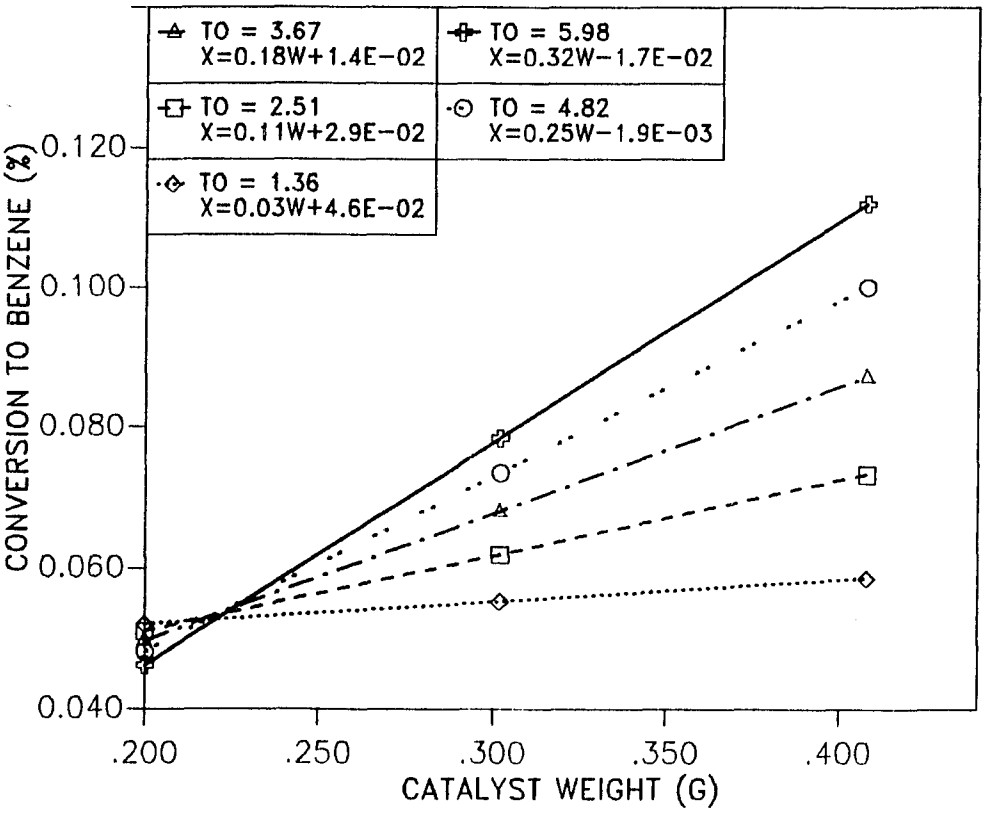

Figure 3.14, Effects of Varying Space Velocities for Toluene Disproportionation by Y-52 Pellets

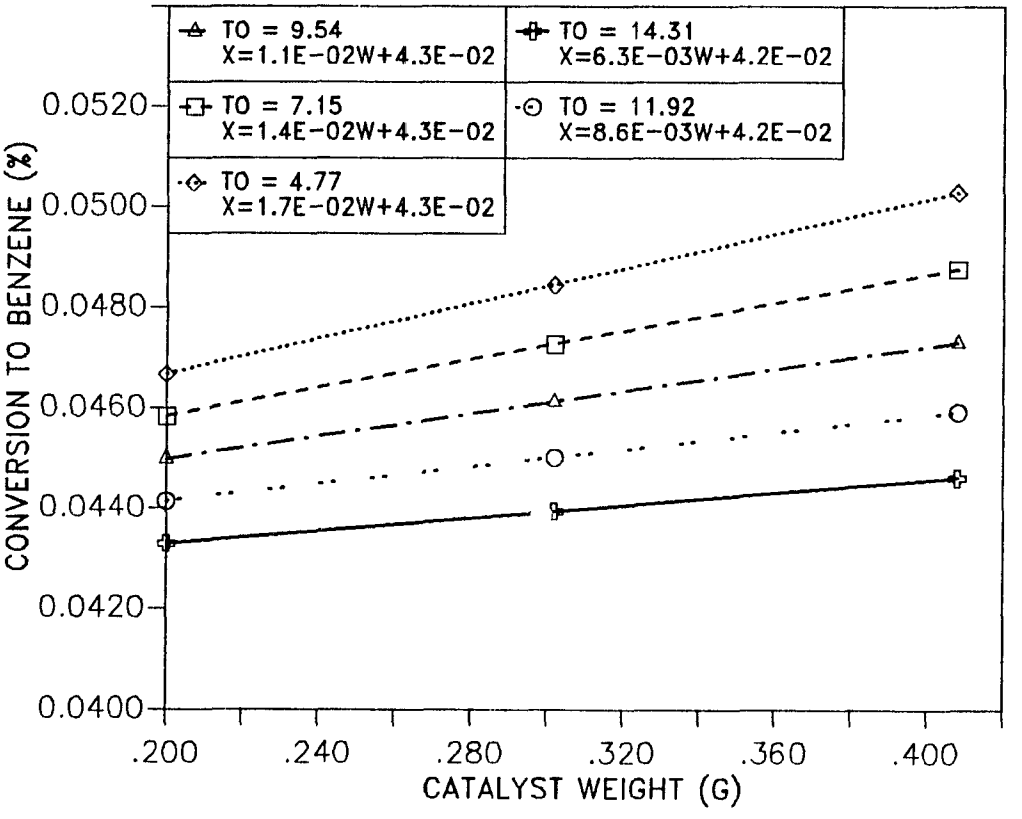

Figure 3.15, Effects of Varying Space Velocities for Toluene Disproportionation by 105–6 Pellets

As can be seen from Figs. 3.8 to 3.15, the slopes of the lines in each plot are not constant. In most cases, these changes appear minor and the slopes approach a constant value as the number of turnovers increases. For Y zeolite (especially Y-pellets), however, there seems to be an activation phenomenon with respect to time on stream as shown in Figs. 3.9 and 3.14. The rate of slope increase does decrease with respect to number of turnovers, implying that if the reaction were run long enough, the slope would approach a constant. Because all the plots for X_A vs. W show some degree of slope change, the average slope value reported in each plot was used in computing the $k\eta$ values. These average $k\eta$ (with σ error) values are listed in Tables 3.7 and 3.8 for powder and pellet form zeolites, respectively.

From the literature review, it is known that the toluene disproportionation reaction exhibits approximately second-order kinetics behavior under the present reaction conditions (673 - 693 K and 10.1 kPa of toluene). The product $k\eta$ at the chosen temperature can be evaluated from the observed reaction rate:

$$r_{obs} = (k_g a_v)(C_b - C_s) = k\eta C_s^2 \qquad (3-12)$$

The C_s value must be estimated from mass transfer equations, using the feed conditions to the reactor to estimate $k_g a_v$ (see Appendix C). For example, for toluene disproportionation catalyzed by the powder-form pentasil at typical reaction conditions, the Reynolds number of the feed is only 10^{-2}. Therefore, the Sherwood number is close to 2.0.

Catalyst	T (K)	P (kPa)	$k\eta \times 10^{-12}$ (kmol/kg - s - kPa^2)	Slope
L	693	10.1	451 ± 13	2.40 ± 0.07
Ω - 6	673	10.1	496 ± 26	2.64 ± 0.14
Y-52	693	10.1	130 ± 12	0.69 ± 0.06
105-6	693	10.1	110 ± 13	0.58 ± 0.07
P1	693	10.1	110 ± 13	2.40 ± 0.07
Y - 62[1]	698	10.1	940	
TEA24 - 2[2]	573	10.1	680	

(1) S.D. Brignac, M.S. Thesis, LSU (1985).
(2) A pentasil used by P. Beltrame et al., (1987).

Table 3.7. Kinetics Results for Toluene Disproportionation, Powder-Form Zeolites

Catalyst	T (K)	P (kPa)	$k\eta \times 10^{-14}$ (kmol/kg - s - kPa^2)	Slope
L	693	10.1	940 ± 60	0.45 ± 0.03
Ω - 6	673	10.1	38 ± 2	0.018 ± 0.001
Y-52	693	10.1	38 ± 2	0.18 ± 0.11
105-6	693	10.1	21 ± 2	0.011 ± 0.004

Table 3.8. Kinetics Results for Toluene Disproportionation, Pellet-Form Zeolites

$$k_g = D_i \times Sh/d_p$$
$$= (1.75\text{x}10^{-3}\ cm^2/s)(2.0)/(4.4\text{x}10^{-3}\ cm) \qquad (3-13)$$
$$= 0.8\ cm/s$$

Substituting this value into eq. (3-12) results in a gradient $C_b - C_s$ for powder-form pentasil of 1.2×10^{-10} mol/cm^3 at a bulk toluene concentration of 1.76×10^{-6} mol/cm^3. The same calculations were performed for powder-form L, Ω, and Y zeolites, respectively. Since all the zeolites used in this study have similar physical properties, the computation showed that it is safe to neglect film mass transfer gradients for all the zeolites used in this study.

A similar computation procedure was applied to the pellet-form zeolites. The results also showed that it is safe to neglect the film resistance for all the pellet-form zeolites used in this study. For example, the gradient $C_b - C_S$ for the pellet-form small crystallite pentasil was 1.99×10^{-8} mol/cm^3 at a bulk toluene concentration of 1.58×10^{-6} mol/cm^3 (the detailed calculation procedures are shown in Appendix C).

3.3 Isothermal Desorption (ID) Experiments

3.3.1 Experimental Conditions

It was pointed out in section 1.5 that a TPD spectrum obtained using a porous catalyst can be strongly affected by the intraparticle diffusion resistance and by readsorption. Therefore, it is necessary to examine the effects of diffusion and readsorption on the quantitative results of

ID experiments. By applying Gorte's (1982) analysis to the ID experimental system discussed in section 2.3, it can be shown that intraparticle mass transfer and readsorption are the controlling steps for the process. The typical experimental values used in this analysis are listed in Table 3.9. The adsorption rate constant was approximated by FS, the product of the collision frequency F, and a sticking coefficient S of 0.5. The intracrystalline diffusivities for benzene, toluene or p-xylene (which are of similar critical diameter) were taken from the literature for Y (Moore and Katzer, 1972; Doelle et al., 1981) and pentasils (Le van Mao et al., 1983; Wu et al., 1983; Forni and Viscardi, 1986).

The numerical values of Gorte's characteristic dimensionless time ratios for the two adsorbates (toluene and benzene), assuming 30 mg (except 20 mg for Ω - 6) of each catalyst, are listed in Table 3.10. The value $\tau_3 > 20$ represents a diffusion time 20 times greater than cell residence time, and therefore the adsorbate concentration at the external surface of the catalyst is near zero. The value $\tau_4 >> 1$ shows that the adsorption time is much smaller than the cell residence time, hence readsorption is significant.

3.3.2 Manipulation of ID Spectra

A series of unary ID experiments were performed for toluene and benzene with different types of zeolites. All the experiments were carried out with 20 (zeolite Ω) - 30 (all others) mg of catalyst, at a carrier gas flow rate of 66 cm^3/min and a temperature of 623 K. The catalyst bed was treated as a single CSTR. The amount of catalyst required for a single

a_v (cm^2/g)	
L	510
Ω - 6	370
Y-52	670
105-6	500
D_e (cm^2/s)	
Benzene	2.3×10^{-9} - 8.5×10^{-11}
Toluene	2.4×10^{-9} - 4.1×10^{-11}
F (1/s)	
Benzene	7.06
Toulene	6.50
Q (cm^3/s)	1.1
r (cm)	4.4×10^{-3}
S (-)	0.5
T (K)	303 - 643
ε (-)	0.5
α (cm^2/g)	
L	3.86×10^6
Ω - 6	3.00×10^6
Y-52	9.00×10^6
105-6	3.98×10^6
ρ_M (cm^3/g)	
L	0.64
Ω - 6	0.41
Y-52	0.64
105-6	0.68
β (K/s)	1.33

Table 3.9. Parameter Values Used to Compute Dimensionless Time Ratios

Catalyst	τ_1	τ_2	τ_3	τ_4
For Benzene with Lower Diffusivity				
L	0.25E-03	0.40E+04	0.59E+08	0.29E+13
Ω - 6	0.39E-03	0.40E+04	0.38E+08	0.14E+13
Y-52	0.25E-03	0.40E+04	0.59E+08	0.68E+13
105-6	0.25E-03	0.40E+04	0.63E+08	0.32E+13
For Toluene with Lower Diffusivity				
L	0.25E-03	0.82E+03	0.12E+08	0.55E+12
Ω - 6	0.39E-03	0.82E+03	0.78E+07	0.27E+12
Y-52	0.25E-03	0.82E+03	0.12E+08	0.13E+13
105-6	0.25E-03	0.82E+03	0.13E+08	0.61E+12
For Benzene with Higher Diffusivity				
L	0.25E-03	0.15E+02	0.22E+06	0.11E+11
Ω - 6	0.39E-03	0.15E+02	0.14E+06	0.53E+10
Y-52	0.25E-03	0.15E+02	0.22E+06	0.25E+11
105-6	0.25E-03	0.15E+02	0.22E+06	0.12E+11
For Toluene with Higher Diffusivity				
L	0.25E-03	0.14E+02	0.21E+06	0.94E+10
Ω - 6	0.39E-03	0.14E+02	0.13E+06	0.47E+10
Y-52	0.25E-03	0.14E+02	0.21E+06	0.22E+11
105-6	0.23E-03	0.14E+02	0.21E+06	0.10E+11

Table 3.10. Numerical Values for Gorte's Dimensionless Time Ratios

CSTR was calculated according to the following empirical expression (Butt, 1980):

$$W = \pi R_b^2 d_p \rho_p (1 - \varepsilon_b)\left(\frac{\Delta Z}{d_p}\right)N \qquad (3-14)$$

and

$$\left(\frac{\Delta Z}{d_p}\right) = \frac{2}{Pe} = \frac{0.6}{ScRe} + \frac{1}{[1 + 3.8/(ScRe)]} \qquad (3-15)$$

where $ScRe = \frac{ud_p}{D_a}$, which equals 0.6 for the ID system.

Three to four isothermal desorption experiments at the same experimental conditions were performed for each combination of adsorbate and adsorbent to check for reproducibility. The desorption spectra for toluene with L, Ω, Y, and small and large crystallite pentasil zeolites are shown in Figs. 3.16 to 3.20, respectively. The corresponding spectra for benzene with the small and large crystallite pentasil zeolites are shown in Figs. 3.21 and 3.22, respectively. The curve for each run has already been corrected with data from a blank (no zeolite) run.

As shown in Figs. 3.16 to 3.22, it was found that only 3 to 5 % of the initially adsorbed toluene had desorbed when the temperature first reached 623 K, as indicated by the legend 'Starting point for ID' in the graphs. Therefore almost all the adsorbate was desorbed at isothermal conditions. This was verified by raising the ID system temperature from 623 K to 793 K after the isothermal desorption process, which did not produce any significant change of the desorption voltage signal from baseline. This result is a fundmental requirement for validity of the

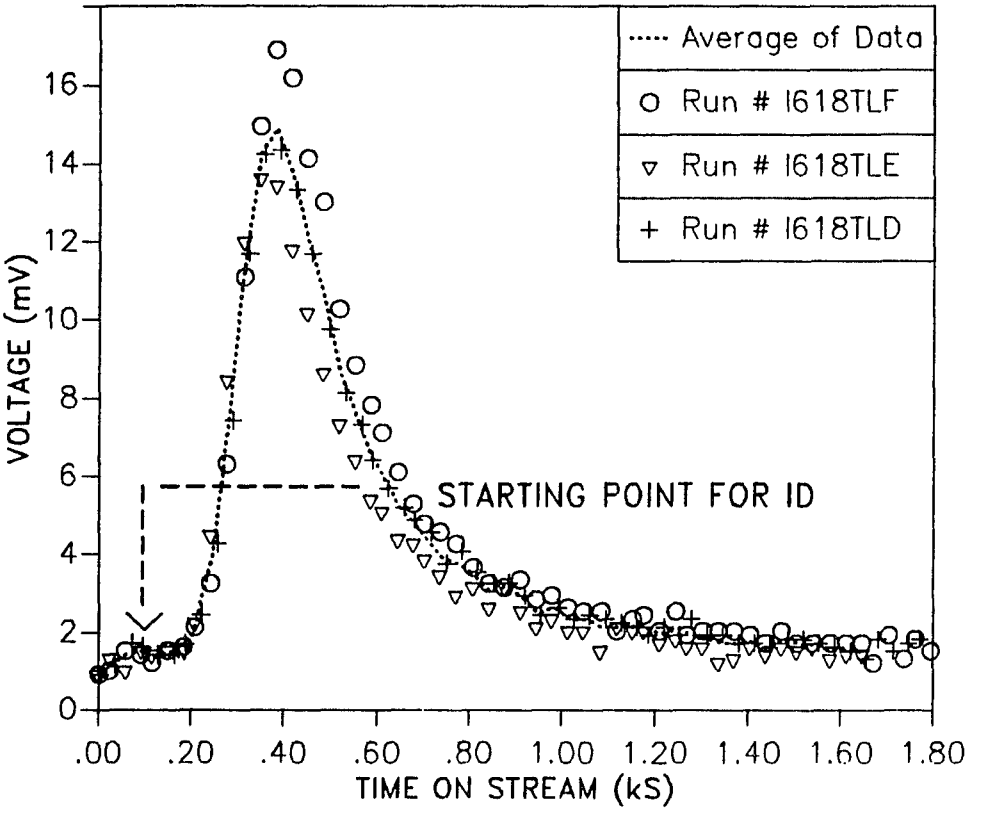

Figure 3.16, Isothermal Desorption of Toluene, Zeolite L.

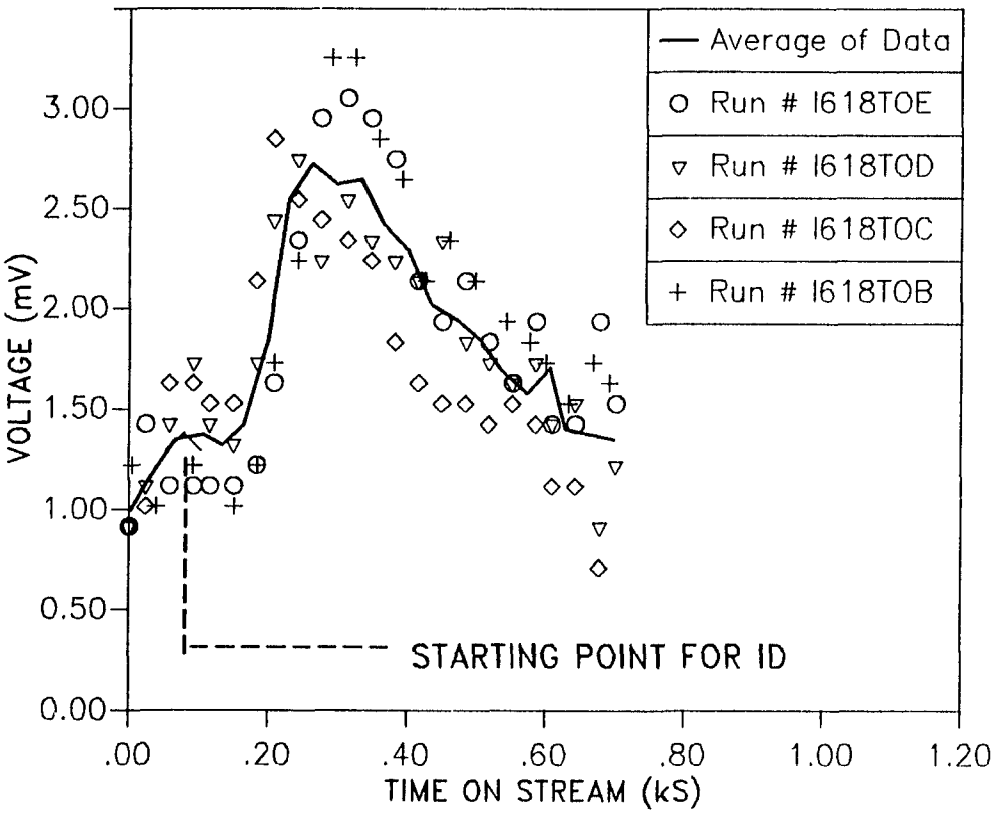

Figure 3.17, Isothermal Desorption of Toluene, Zeolite Omega.

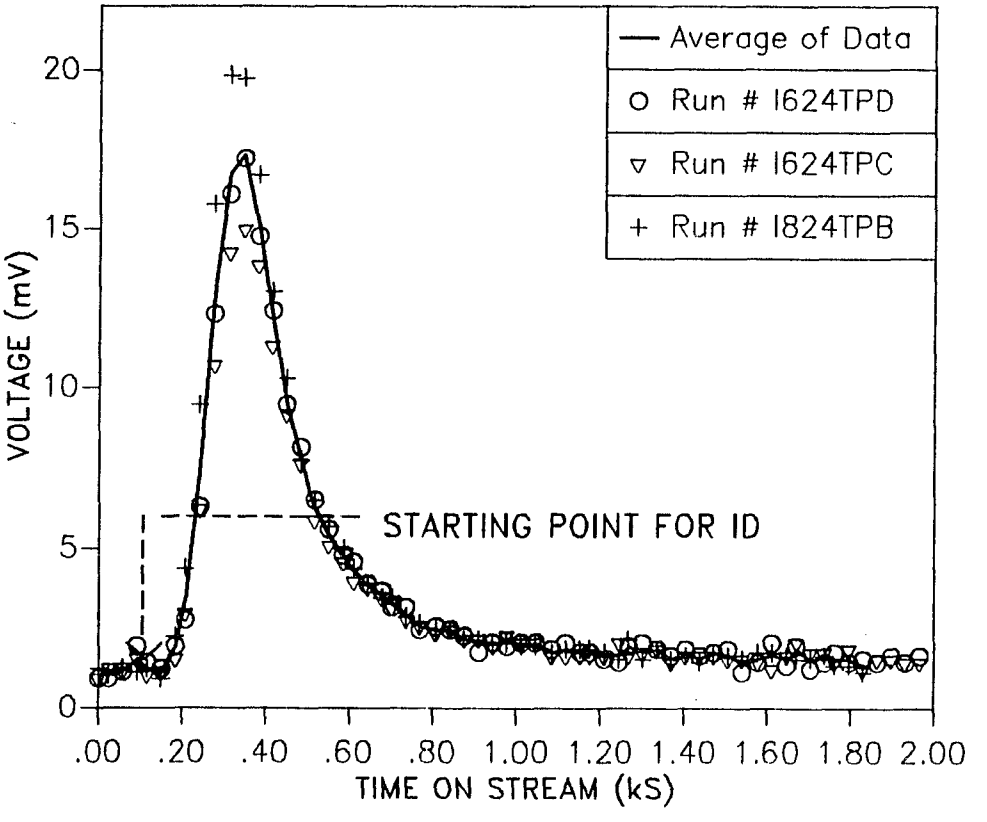

Figure 3.18, Isothermal Desorption of Toluene, Zeolite P1.

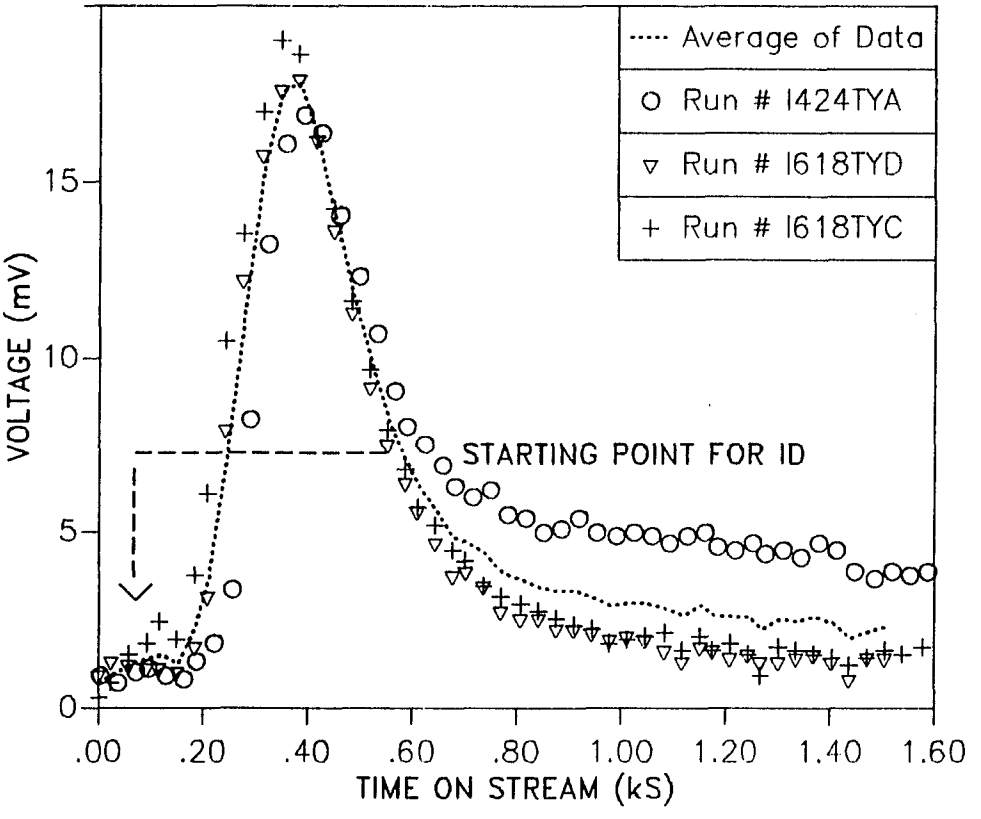

Figure 3.19, Isothermal Desorption of Toluene, Zeolite Y–52.

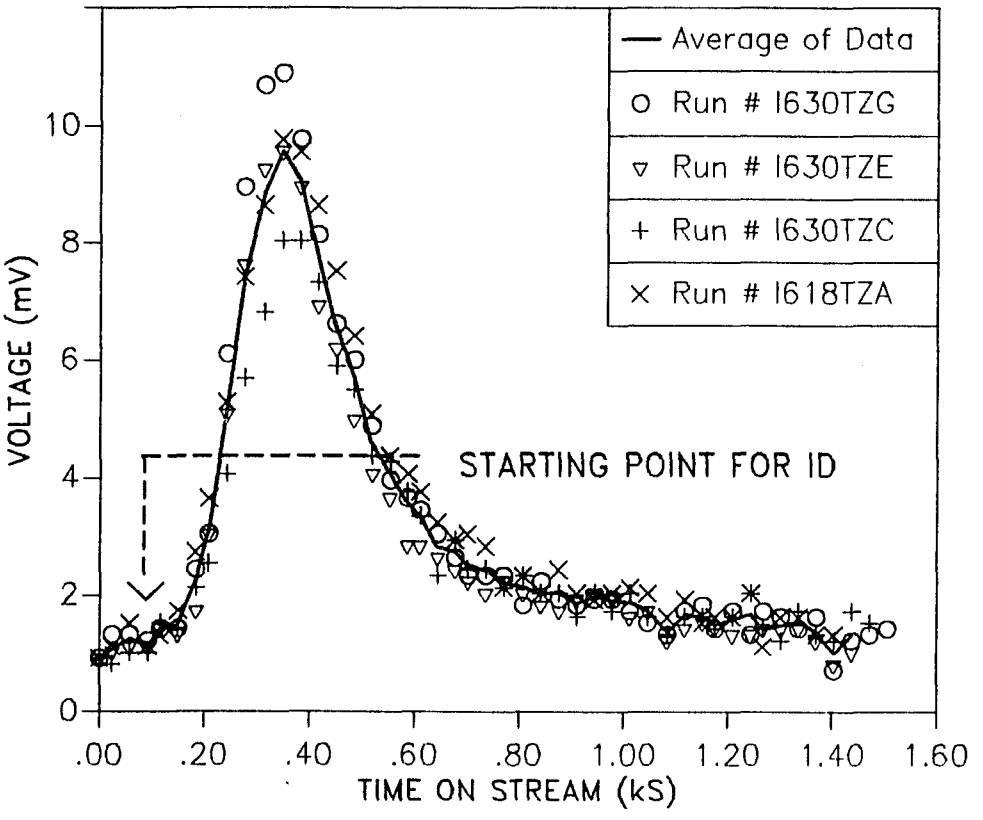

Figure 3.20, Isothermal Desorption of Toluene, Zeolite 105-6.

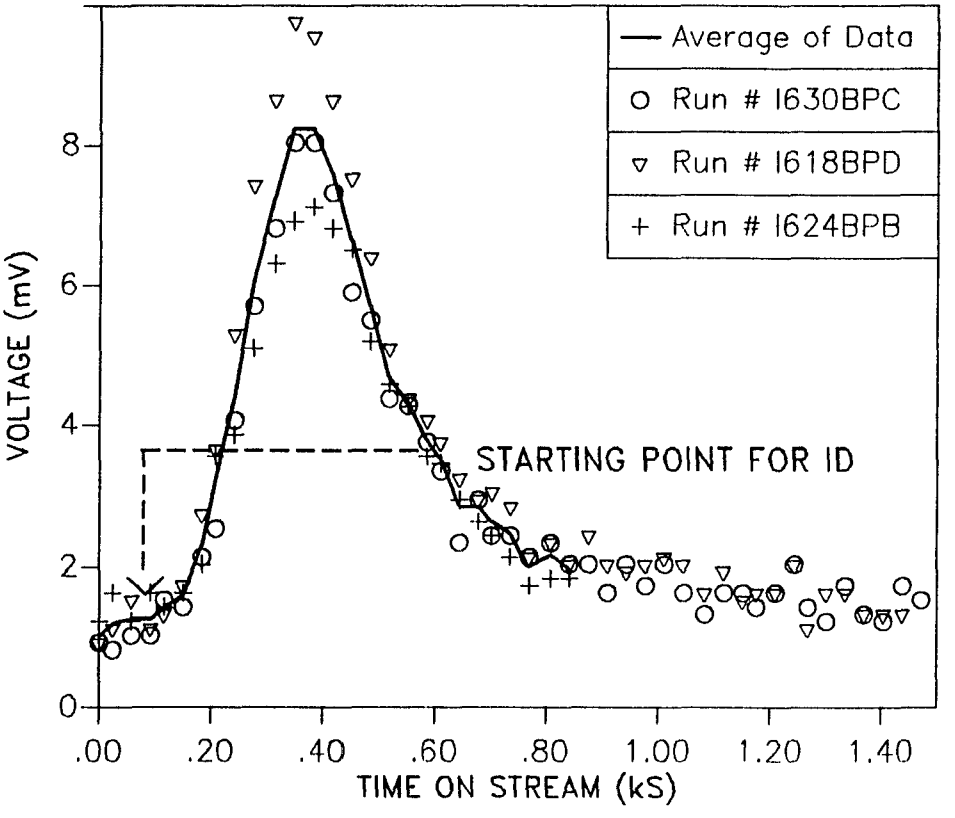

Figure 3.21, Isothermal Desorption of Benzene, Zeolite P1.

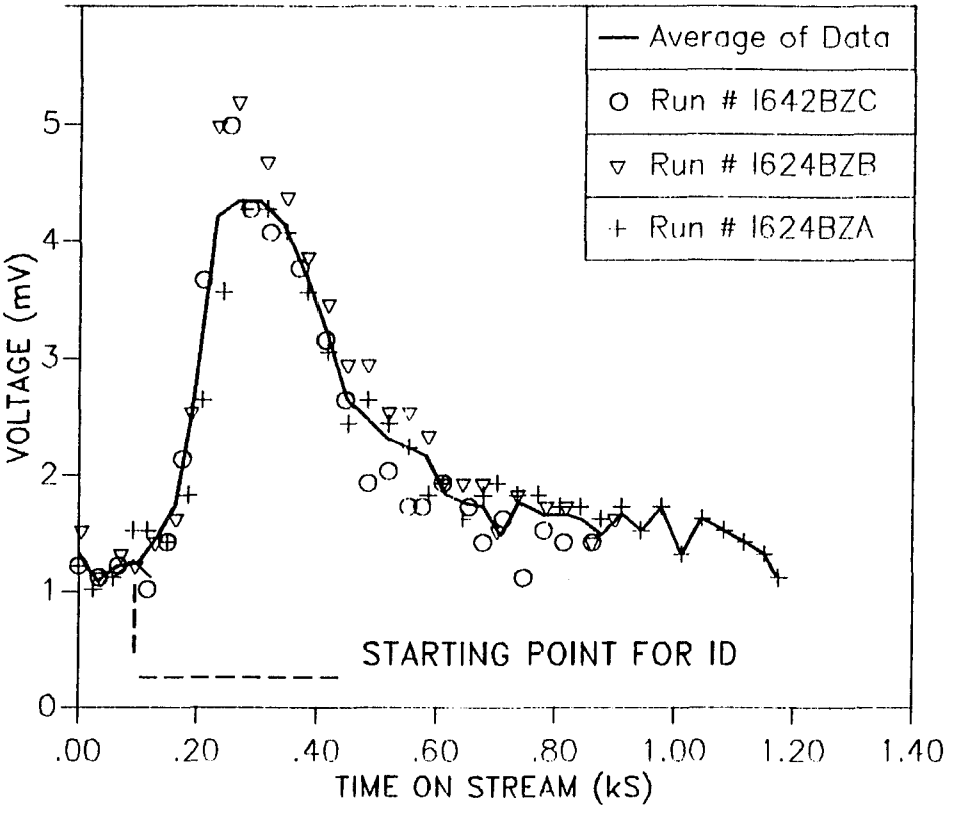

Figure 3.22, Isothermal Desorption of Benzene, Zeolite 105-6.

ID models to be discussed in Section 4.1. The figures also show that it took 0.6 to 1.40 ks for the remaining toluene or benzene to desorb at isothermal conditions.

All the ID spectra exhibited a single desorption peak at approximately the same peak location (with respect to real process time), for the same zeolites with different types of adsorbates. The ratio of the voltage signal at the peak of an ID spectrum to that at the baseline was in the range of 10 - 20 for all the catalysts (except for Ω/toluene and 105-6/benzene) studied. The corresponding ratios for Ω/toluene and 105-6/benzene were 3, which means that lesser amounts of toluene or benzene were adsorbed by the Ω or 105-6 zeolites. For these two adsorbate/adsorbent combinations it was difficult to distinguish the actual desorption signal from the background noise in the regions away from the peak, and therefore the spectra will not generate accurate diffusivity estimates.

The recording of each ID spectrum was suspended when the values of three consecutive voltage signals were equal or less than twice the average signal values of the three initial measurements, i.e., when the desorption signal reached the baseline.

In order to simplify the calculation procedure, the average curve of the several runs for each combination of adsorbate and adsorbent was computed and is shown in Figs. 3.16 to 3.22 by a solid curve. The error associated with each average ID curve was estimated at the halfwidth and peak points. The halfwidth points are the points whose amplitude equals half that of the peak maximum. The standard error (one σ) associated with these points for the different combinations of adsorbate and adsorbent are listed in Table 3.11.

Run ID	$t_{\frac{1}{4}}$ (s)	$V_{\frac{1}{4}}$ (mV)	t_{max} (s)	V_{max} (mV)	$t_{\frac{3}{4}}$ (s)	$V_{\frac{3}{4}}$ (mV)
I618TLD	287	7.1	392	14.3	570	7.1
I618TLE	263	6.7	382	13.4	537	6.7
I618TLF	293	8.5	382	16.9	542	8.5
Average	281	7.4	385	14.8	558	7.4
Std. Error	13	0.8	5	1.5	15	0.8
I618TYC	235	9.5	348	19.0	482	9.5
I618TYD	251	9.0	382	17.9	516	9.0
I424TYA	291	8.4	392	16.8	580	8.4
Average	259	8.9	385	17.8	540	8.9
Std. Error	24	0.5	19	1.0	41	0.5
I618TZA	236	4.9	348	9.8	523	4.9
I618TZC	242	4.0	348	8.0	566	4.0
I618TZE	239	4.8	348	9.5	488	4.8
I618TZG	223	5.4	348	10.8	501	5.4
Average	237	4.8	348	9.5	510	4.8
Std. Error	7	0.5	0	1.0	30	0.5
I624TPB	245	9.9	314	19.8	449	9.9
I624TPC	252	7.5	348	14.9	482	7.5
I624TPD	256	8.6	348	17.2	471	8.6
Average	251	8.7	348	17.3	467	8.7
Std. Error	5	1.0	16	2.0	14	1.0
I624BZA	196	2.1	276	4.2	464	2.1
I624BZB	190	2.6	266	5.1	516	2.6
I624BZC	183	2.5	251	5.0	439	2.5
Average	175	2.2	264	4.3	550	2.2
Std. Error	5	0.2	10	0.4	32	0.2
I624BPB	219	3.6	382	7.1	582	3.6
I618BPD	236	4.9	348	9.7	516	4.9
I630BPG	242	4.0	348	8.0	566	4.0
Average	234	4.1	348	8.2	563	4.1
Std. Error	10	0.5	15	0.9	25	0.5

Table 3.11. Errors for The ID Spectra

A pulse of 1 μl methane gas was injected into the desorption apparatus under the same experimental conditions in order to determine the system's dispersion characteristics and lag time to detection. The E curve obtained from this study showed a 30 s detection lag, which is small compared to the 800 - 1400 s duration of an ID experiment. Therefore, one should expect only a minor dispersion correction to the original ID spectrum. The original and corrected spectra for toluene desorbed from zeolite L is shown in Fig. 3.23 along with the E curve; note the minor differences between the two spectra. The corrected spectra are used to fit the ID models discussed in Section 4.1. The correction was performed using the convolution theorem and the Fast Fourier Transform technique discussed in Section 4.1.4.

Prior to further analysis of the average ID curves, it is necessary to ask whether the magnitude of standard errors shown in Table 3.11 are acceptable or not. In order to answer this question, there is a need to identify the sources of error associated with the ID process:

1. Errors in voltage signal measurements. These are related to the sensitivity of the GC flame ionization detector (FID), and the inherent error associated with this detector as reported by the manufacturer. For a FID GC, an error of ± 10% for the voltage signal is considered normal. For example, the average relative deviation in the toluene calibration curve (Fig. 3.24) was 10.6%.

2. Errors in the conditions under which the experiment was run. These include the desorption temperature, carrier gas flow rate, and GC operating conditions; no matter how sensitively the FID detected the

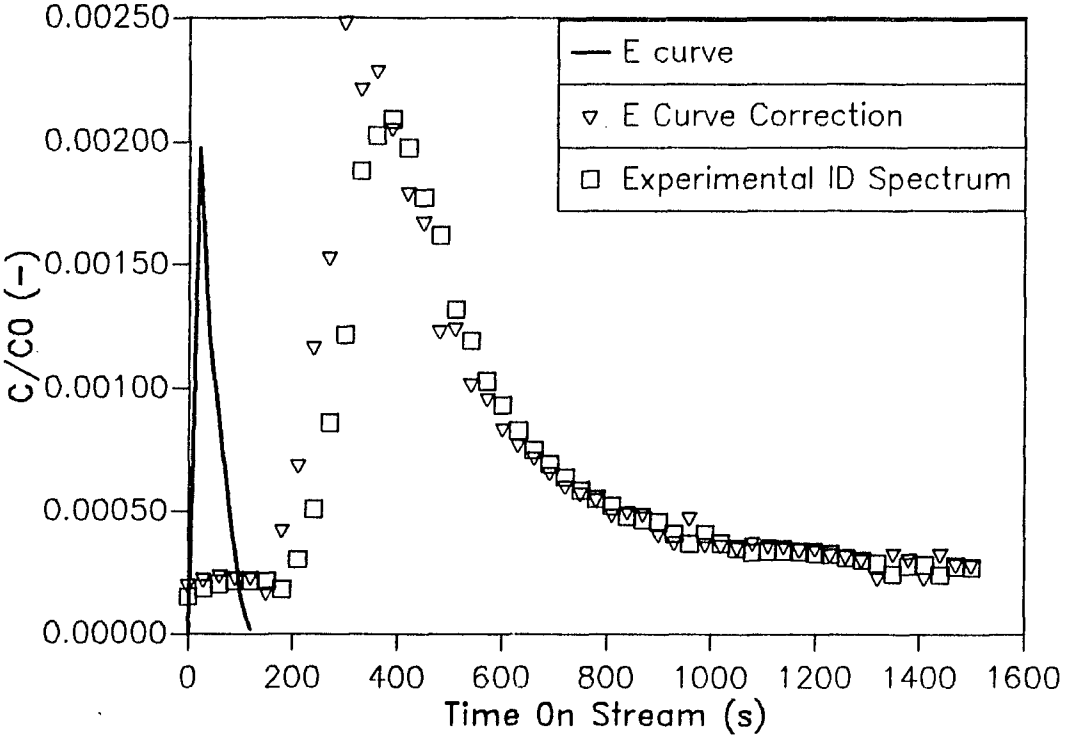

Figure 3.23, E Curve Correction for ID Spectrum of Toluene Desorbed from Zeolite L at 623 K

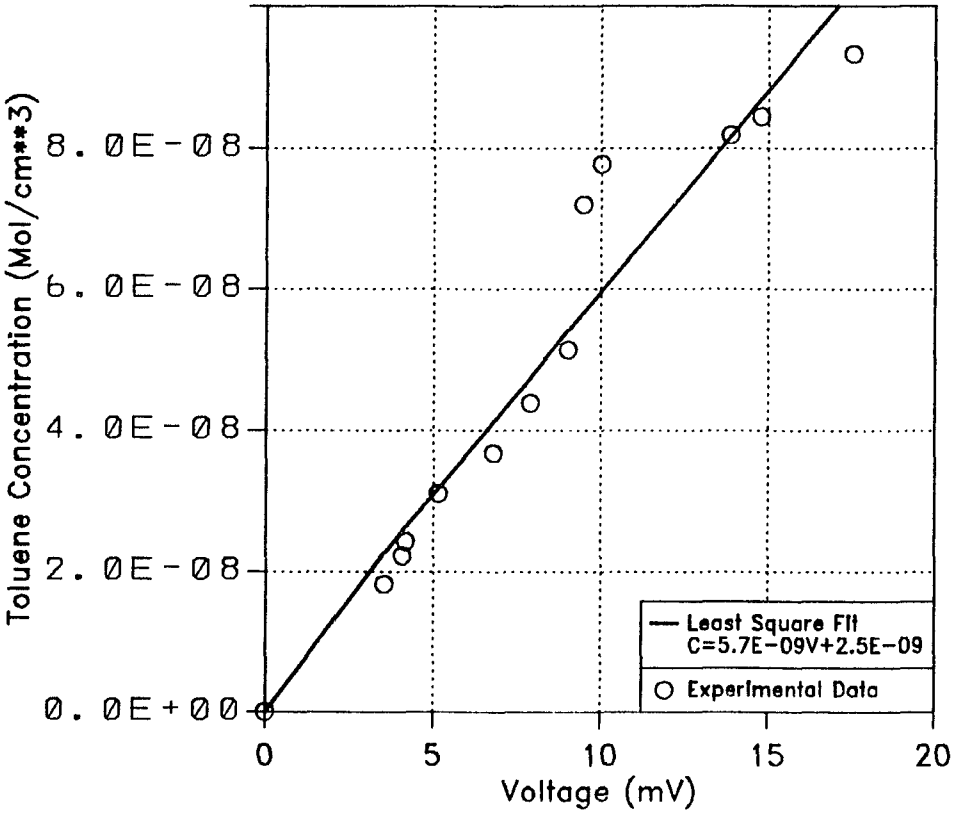

Figure 3.24, Toluene Calibration Curve for ID Experiments at 623 K

signal, there can still be appreciable error associated with a "correct" voltage measurement if these quantities themselves are subject to error.

3. Problems with the experimental setup. This source of error is mainly due to the fact that the desorption stream was fed into the FID continuously. This is not a conventional injection technique and tends to upset the sensitivity of the FID after a long operation time.

The standard errors associated with each ID spectrum, as shown in Table 3.11, were within ± 10% of the corresponding voltage signals. Considering all the types of error discussed above, it could be reasonably concluded that this magnitude of error is associated with item 1, and the data could be employed for further analysis.

By a simple mass balance, it can be shown that the area beneath the entire ID spectrum corresponds to the total amount of adsorbate desorbed. The actual molar amounts of toluene adsorbed were calculated for the different types of zeolites used in this study. The procedures to calculate the sorption concentration in ID experiments are as follows:

1. Convert voltage signal to concentration using a calibration curve as shown in Fig. 3.24.

2. Perform curve integration using the AVINT routine in the ALAMOS (Los Alamos National Laboratory, 1984) package. The area beneath the curve is the product of concentration and time.

3. The amount adsorbed per weight is:

$$M = \frac{Q}{W} \int C dt \qquad (3 - 16)$$

These results were compared to literature values, especially for other types of adsorption measurements (e.g., static volumetric data). The calculated amounts adsorbed and the literature data are listed in Table 3.12. It is seen from the table that the experimental data are in good agreement with literature sorption data, again indicating the validity of the ID method used in this study.

Adsorbate	Adsorbent	T (K)	Sorbate Concentration (mmol/g)	Reference
L	Toluene	393	1.56	This Study
Ω - 6	Toluene	393	0.48	This Study
Y-52	Toluene	393	1.56	This Study
105-6	Toluene	393	1.78	This Study
P1	Toluene	393	1.03	This Study
H-ZSM-5	Toluene	293	1.07	(1)
H-ZSM-5	P-Xylene	293	0.95	(1)
H-ZSM-5	P-Xylene	298	0.97	(2)
Ni-ZSM-5	Toluene	321	0.55	(3)
Silicalite	P-Xylene	293	0.51	(4)
H-ZSM-5	Toluene	323	0.74	(5)
K-Y	Toluene	423	1.78	(6)
K-Y	P-Xylene	423	1.96	(6)
K-Y	P-Xylene	433	1.62	(6)

(1) Anderson et al. (1979).
(2) Derouane and Gabelica (1980).
(3) Hwu and Hightower (1984).
(4) Wu et al. (1983).
(5) Pope (1984)
(6) Paludetto et al. (1987).

Table 3.12. Comparsion of Experimental and Literature Sorption Capacity Data

CHAPTER 4

DISCUSSION

4.1 The ID Models and Method of Analysis

The goal of this section is to estimate the intracrystalline diffusivities from the ID spectra discussed in Section 3.3. The diffusion of benzene or toluene molecules in the intracrystalline micropores plays an important role in the isothermal desorption process. For the case of microporous configurational diffusion, it is assumed (Section 1.2.2) that the adsorption-desorption process takes place on the external surfaces of zeolite crystals. Therefore, one should use the external surface coverage in evaluating the adsorption and desorption rates. Then:

$$r_a = k_a \Psi \bar{C} \qquad (4-1)$$

$$r_d = k_d n \qquad (4-2)$$

where Ψ is some function of surface coverage, usually in the form of $n_{max} - n$, with n_{max} the maximum surface coverage at the external surface.

The ID experiments were analyzed by modifying models currently applied to temperature-programmed desorption (TPD) results. As discussed in Section 3.3.1, the desorption process was controlled by intraparticle diffusion, and readsorption was significant. Under these conditions, the adsorbate mass balance for the material in the pores becomes

$$\frac{1}{t_2}\frac{\partial \theta}{\partial t} = \frac{1}{\bar{r}^2}\frac{\partial}{\partial \bar{r}}\left(\bar{r}^2 \frac{\partial \theta}{\partial \bar{r}}\right) \qquad (4-3)$$

where $t_2 = D_e/\varepsilon R^2$ is the regression parameter for various ID models.

If one assumes the sample cell can be modeled as a CSTR, then the mass balance for the gas phase becomes

$$\frac{\tau_1}{t_2}\frac{d\bar{C}}{dt} = -\bar{C} - \tau_3\left(\frac{\partial\theta}{\partial\bar{r}}\right)_{\bar{r}=1} \qquad (4-4)$$

Eqs. (4-3) and (4-4) have the following initial and boundary conditions:

$$\theta = \theta_0 \text{ and } \bar{C} = 0 \qquad \text{at } t = 0 \qquad (4-5)$$

$$\frac{\partial\theta}{\partial\bar{r}} = 0 \qquad \text{at } \bar{r} = 0 \qquad (4-6)$$

$$\frac{\partial\theta}{\partial\bar{r}} = -\tau_5\theta + \tau_4\bar{\Psi}\bar{C} \qquad \text{at } \bar{r} = 1 \qquad (4-7)$$

Eqs. (4-3) and (4-4) are coupled through eq. (4-7). Exact solutions for θ and $\bar{C}$ require numerical calculations. Therefore, several simplified assumptions about eq. (4-7) were made such that the model can be analyzed analytically.

4.1.1 Model I: Constant Diffusivity Constant Coverage - (CDCC) Model

The simplest assumption one can make about the external surface coverage is to let θ_1 be a constant and let the lag time for detection be negligible. The latter was verified in Ruthven's ZLC experiments (Eic and Ruthven, 1988; $\tau_1 = 7.5 \times 10^{-4}$) and in the ID experiments in this study (an observed cell detection lag time of 30 s as discussed in Section 3.3.1.). Then eq. (4-7) becomes

$$\theta_1 = \frac{1+\tau_4}{\tau_5}\bar{C} = \text{Constant} \qquad \text{at } \bar{r} = 1 \qquad (4-8)$$

The solution for eq. (4-3) with eqs. (4-5), (4-6) and (4-8) at constant diffusivity (Crank, 1975) is

$$\frac{\theta - \theta_0}{\theta_1 - \theta_0} = 1 + \frac{2}{\pi \bar{r}} \sum_{n=1}^{\infty} \frac{(-1)^n}{n} \sin(n\pi\bar{r}) \exp(-n^2\pi^2 t_2 t) \qquad (4-9)$$

If M_t denotes the total amount of adsorbate which has left the catalyst particle at time τ, and M_∞ the corresponding quantity after infinite time, then

$$\frac{M_t}{M_\infty} = \frac{\theta_0 - \bar{\theta}}{\theta_0} = 1 - \frac{6}{\pi^2} \sum_{n=1}^{\infty} \frac{1}{n^2} \exp(-n^2\pi^2 t_2 t) \qquad (4-10)$$

where $\bar{\theta}$ is the average dimensionless surface coverage.

A "desorption rate isotherm" approach was adapted to this technique as follows:

1. $(\frac{M_t}{M_\infty})$ values in the isothermal region were determined from each ID curve by applying a simple curve integration routine (subroutine AVINT, Alamos Scientific Package, 1984). The corresponding percent of mass loss vs. time plots are shown in Figs. 4.1 to 4.5 for different combinations of adsorbate and adsorbent. Then the average surface coverages $\bar{\theta}$ were determined by mass balance.

2. t_2 was determined by regression using eq. (4-10). If the $(\frac{M_t}{M_\infty})$ values do not fall on a smooth curve when plotted against τ, there may be a problem with the assumptions of this analysis. The assumption of a constant θ_1 can be relaxed, as will be shown.

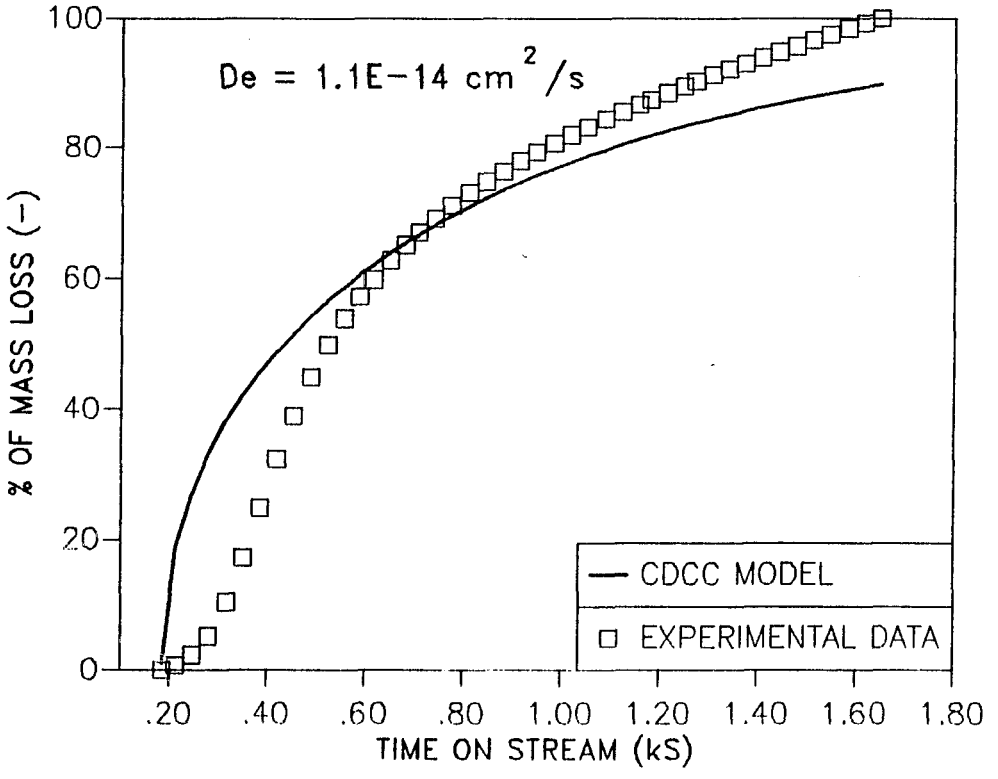

Figure 4.1, Fit of Entire ID Spectrum for Toluene by CDCC Model, Zeolite L.

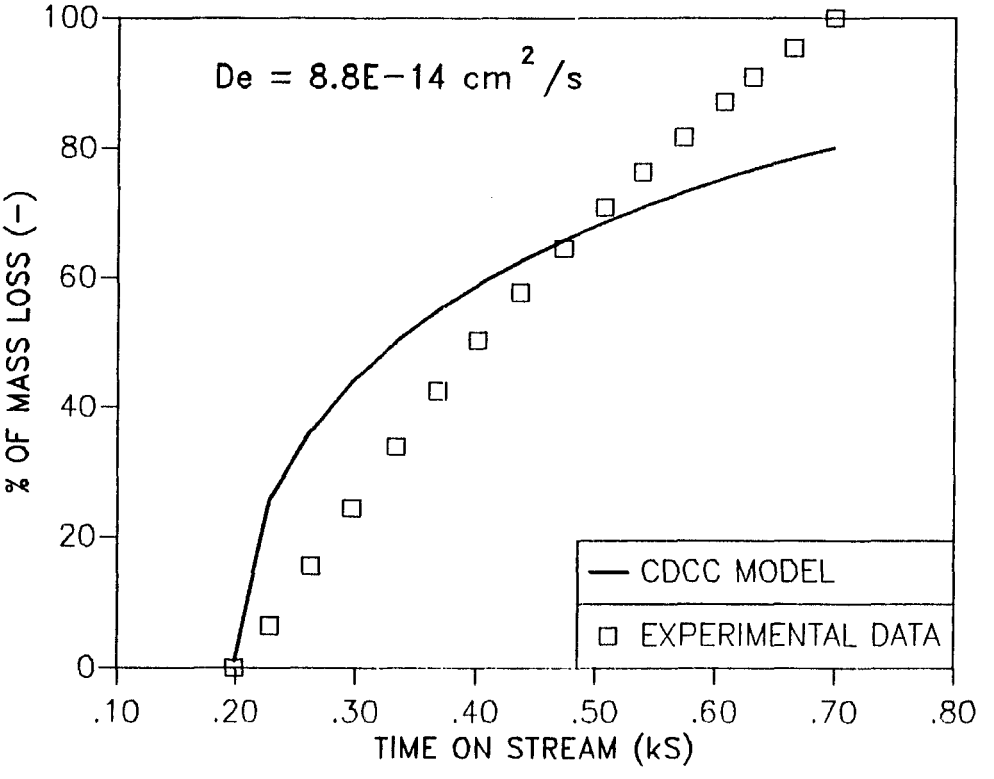

Figure 4.2, Fit of Entire Spectrum for Toluene, by CDCC Model, Zeolite Omega−6.

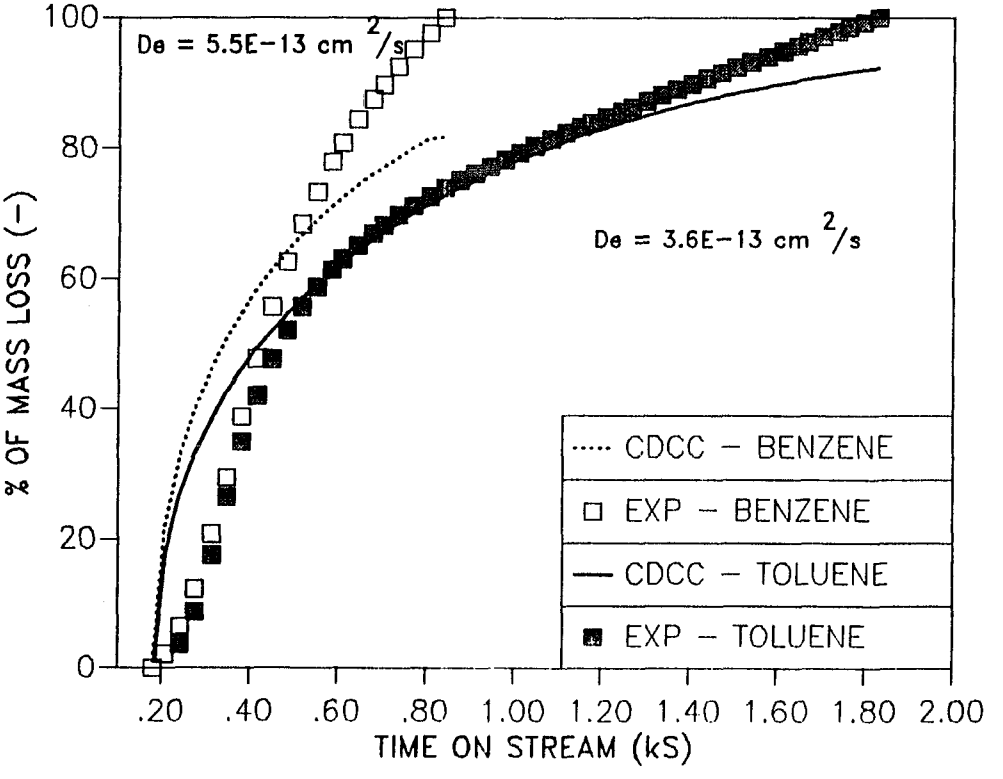

Figure 4.3, Fit of Entire ID Spectrum for Toluene or Benzene by CDCC Model, Zeolite P1.

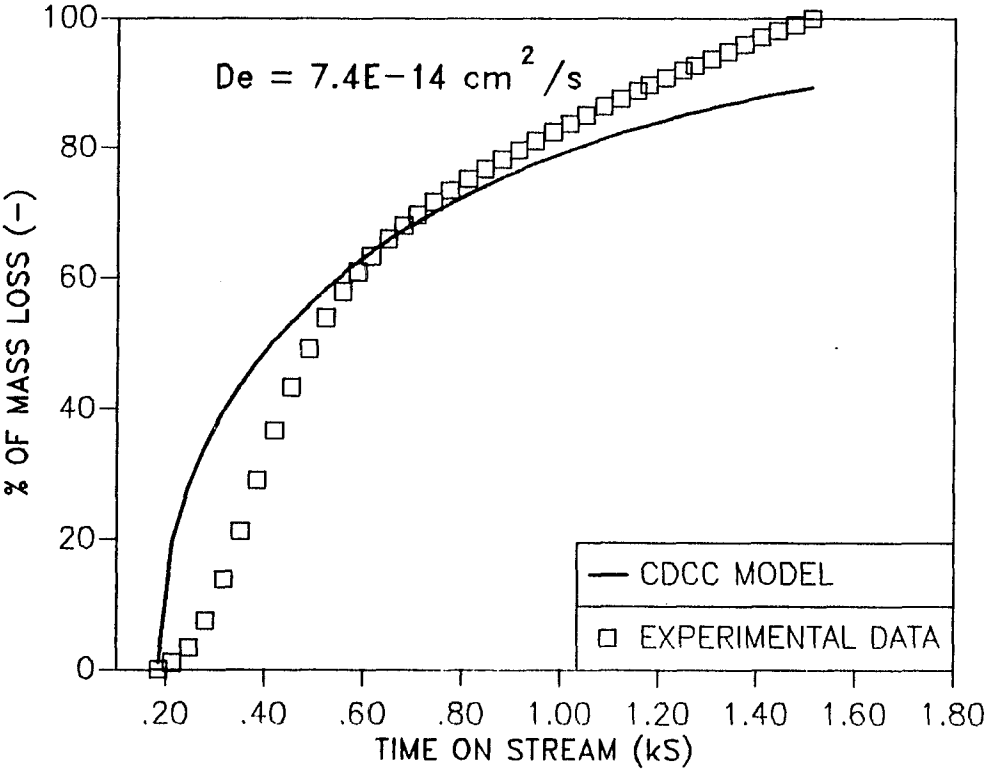

Figure 4.4, Fit of Entire ID Spectrum for Toluene by CDCC Model, Zeolite Y-52.

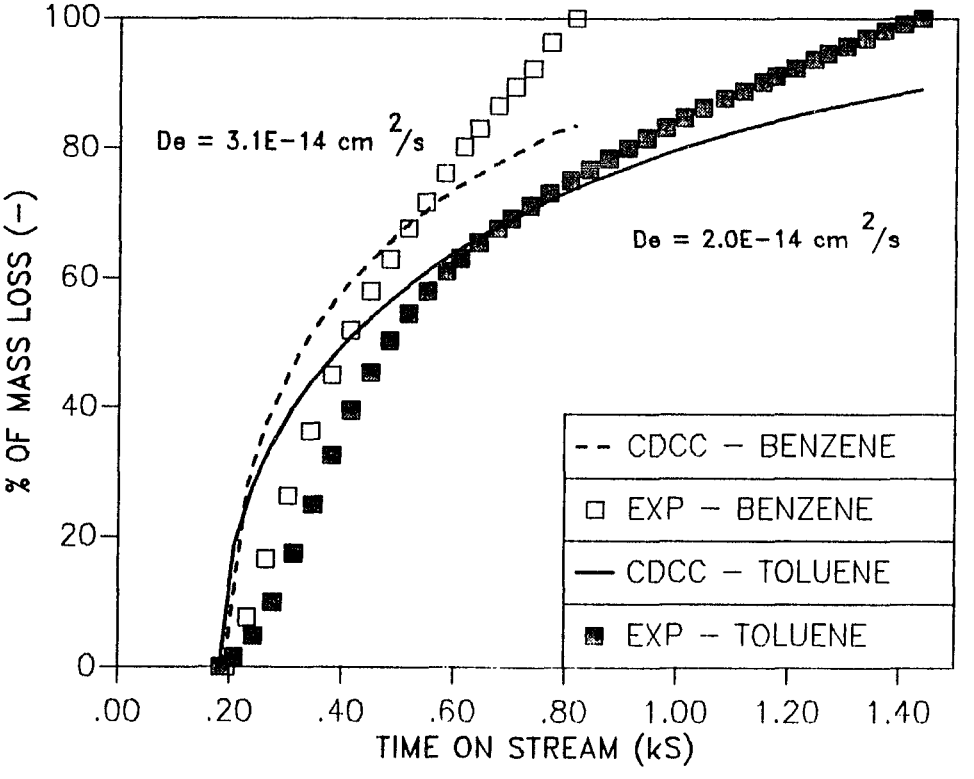

Figure 4.5, Fit of the Entire ID Spectrum of Toluene or Benzene by CDCC Model, Zeolite 105-6.

The $\left(\frac{M_t}{M_\infty}\right)$ data for both the whole spectrum and the falling portion of the spectrum were fitted by the above technique with the constant surface coverage model. Box's (1965) complex method was used as the regression algorithm and the regression results are listed in Tables 4.1 and 4.2 for each case, respectively. The 95% confidence limits of the regressed diffusivities are about 10 - 15% and 6 - 9% (relative deviation) for toluene (except 30 % for $\Omega - 6$, due to the low signal to noise ratio as discussed in Section 3.3.2) for the two cases, respectively. The corresponding limits for the benzene diffusivities are 22% and 26% (relative deviation) for the two cases, respectively. Therefore, the model fits toluene ID curves better than benzene ID curves, a consequence of the lower signal to noise ratio for the benzene ID curves.

Tables 4.1 and 4.2 also give the standard error for each fitted curve. Because the percent of mass loss was scaled between 0 to 100, the standard errors shown in the tables are also relative deviations; they were 8 - 11% and 4 - 7% for toluene for the two cases, respectively, 12 - 16 % and 10 - 11% for benzene for the two cases, respectively. For both toluene and benzene, the falling portion of the ID curve gives smaller standard error. This phemomenon can be explained by the fact that the model can only predict a continuously decreasing desorption rate if there is no lag time for detection and no significant readsorption. Hence, the model should fit the falling portion of the spectrum better than the entire spectrum, for which the desorption rate went through a maximum at short times.

The plots for regressed and experimental percent of mass loss vs. time for the two cases are shown in Figs. 4.1 to 4.5 and Figs. 4.6 to 4.10 for the two cases, respectively. As shown in Figs. 4.1 to 4.10, the model

Adsorbate	Adsorbent	$D_e \times 10^{14}$ cm^2/s	Standard Error	$D_e/R^2 \times 10^5$ s^{-1}
L	Toluene	1.1 ± 0.2	0.110	3.9 ± 0.7
Ω - 6	Toluene	8.8 ± 2.7	0.138	8.6 ± 2.6
P1	Toluene	36.0 ± 4	0.075	5.1 ± 0.5
Y-52	Toluene	7.4 ± 1.2	0.107	6.4 ± 1.0
105-6	Toluene	2.0 ± 0.3	0.100	5.5 ± 0.8
P1	Benzene	55.0 ± 17	0.156	7.8 ± 2.4
105-6	Benzene	3.1 ± 0.8	0.118	8.6 ± 2.2

Table 4.1. Fitted Effective Diffusivities for Whole HD Curve by CDCC Model.

Adsorbate	Adsorbent	$D_e \times 10^{14}$ cm^2/s	Standard Error	$D_e/R^2 \times 10^5$ s^{-1}
L	Toluene	1.4 ± 0.1	0.058	4.8 ± 0.3
Ω - 6	Toluene	10.0 ± 3	0.130	10.2 ± 3.2
P1	Toluene	37.0 ± 2	0.042	5.3 ± 0.3
Y-52	Toluene	8.8 ± 0.8	0.061	7.6 ± 0.7
105-6	Toluene	2.3 ± 0.2	0.068	6.4 ± 0.6
P1	Benzene	87.0 ± 20	0.100	12.3 ± 2.8
105-6	Benzene	3.5 ± 0.8	0.106	9.7 ± 2.2

Table 4.2. Fitted Effective Diffusivities for Falling Portion of the ID Curve by CDCC Model.

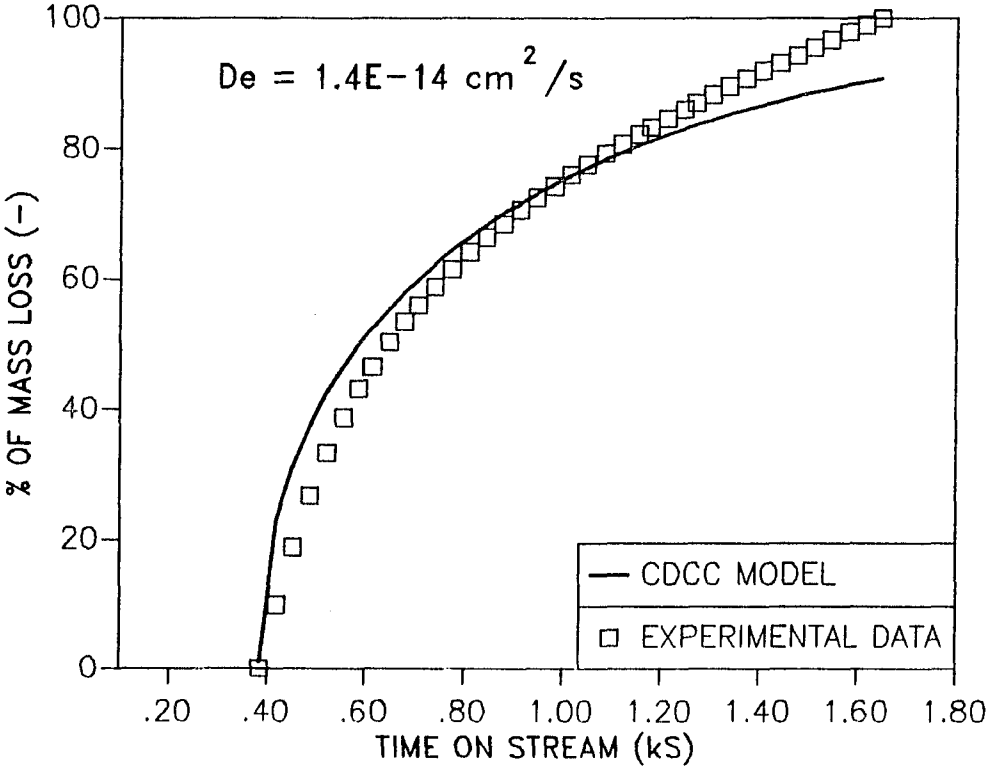

Figure 4.6, Fit of the Falling Portion of the ID Spectrum for Toluene by CDCC Model, Zeolite L.

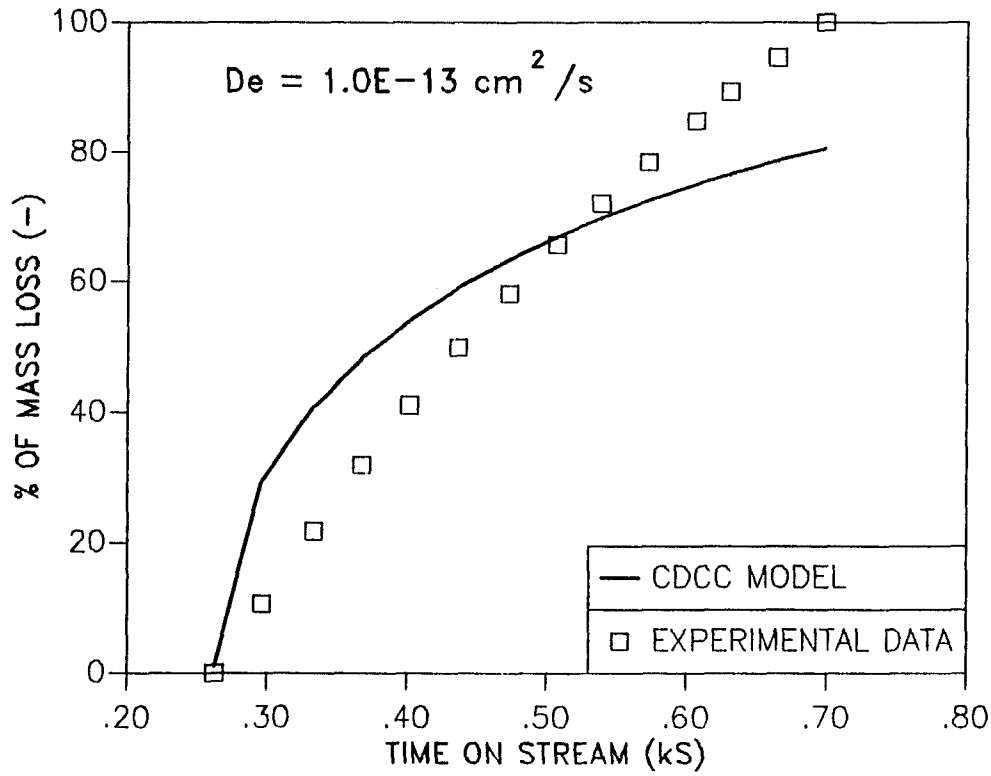

Figure 4.7, Fit of the Falling Portion of the ID Spectrum for Toluene by CDCC Model, Zeolite Omega−6.

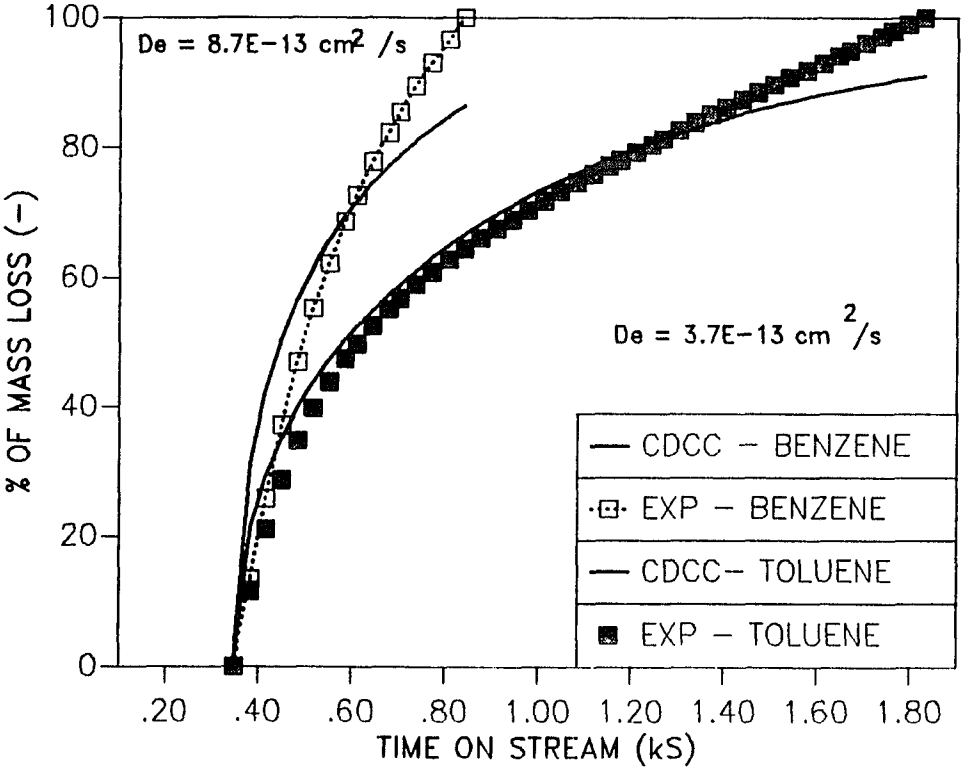

Figure 4.8, Fit of the Falling Portion of the ID Spectrum for Toluene or Benzene by CDCC Model, Zeolite P1.

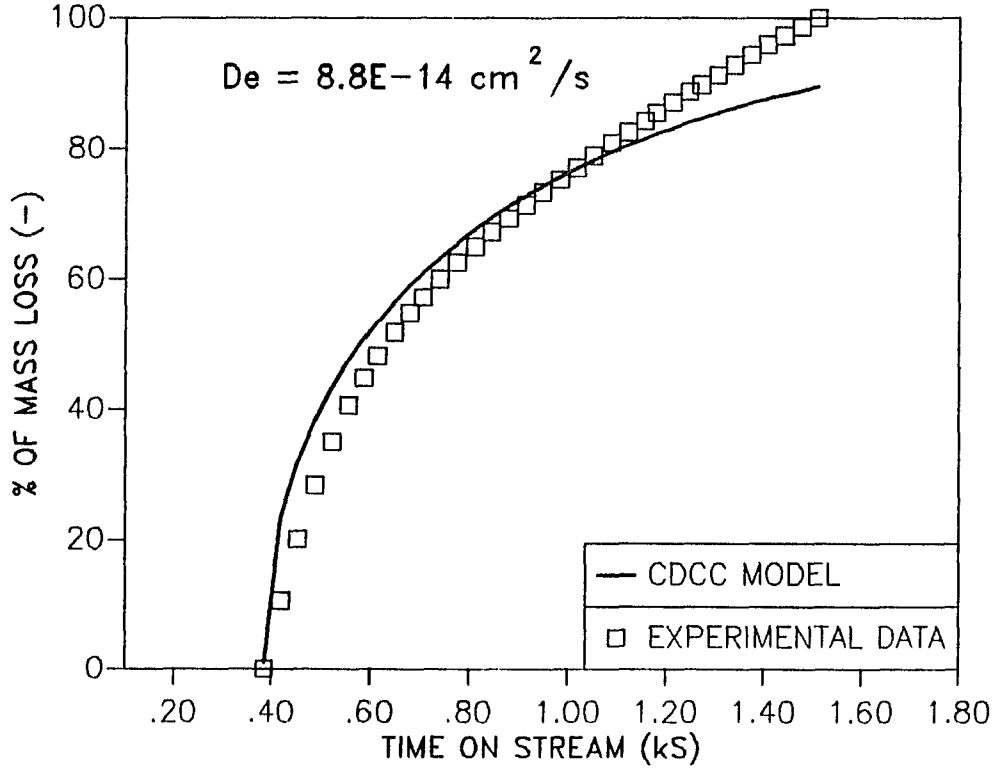

Figure 4.9, Fit of the Falling Portion of the ID Spectrum for Toluene by CDCC Model, Zeolite Y−52.

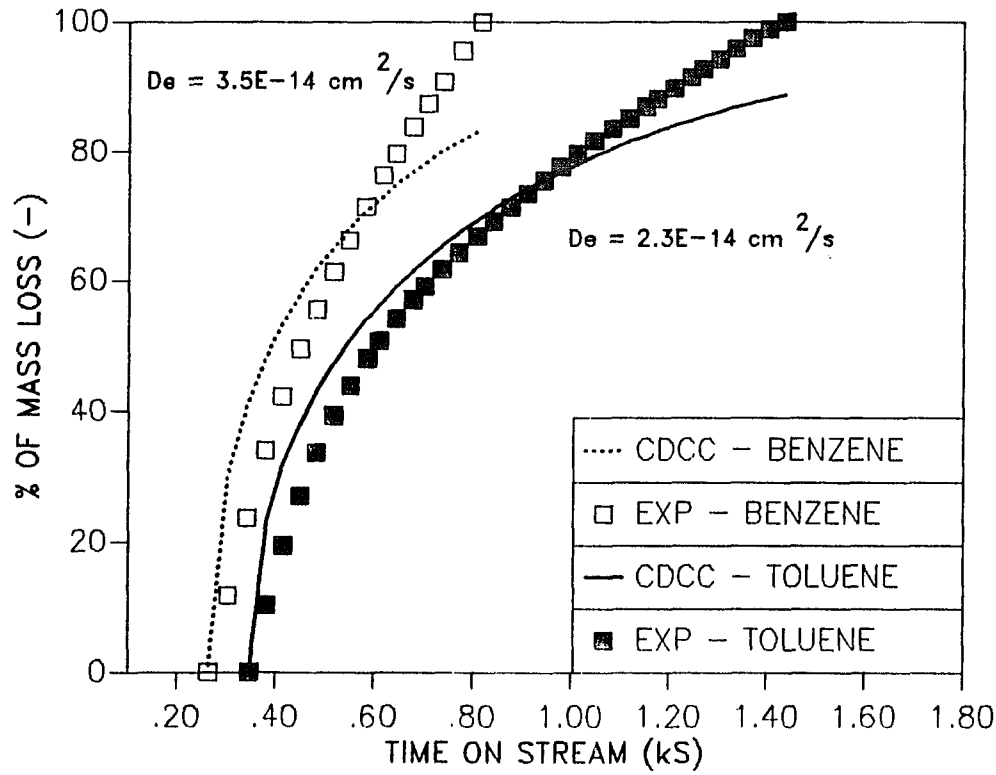

Figure 4.10, Fit of the Falling Portion of the ID Spectrum for Toluene or Benzene by CDCC Model, Zeolite 105-6.

predictions exceed the experimental data in the initial stage of the desorption process and then become smaller than the corresponding experimental values. The transition points where the curves cross are in the range of 0.7 ks for toluene and 0.6 ks for benzene in both cases. The bias in the regression results probably results from the following:

1. The external surface coverage is significantly diffferent from zero in the early stage of the process and becomes relatively constant (zero) at late times. Hence the constant surface coverage assumption is not valid at early stages of the process.

2. A dynamic sorption equilibrium may be established between the fluid phase and the zeolite external surface; desorbed species may be readsorbed onto vacant sites before they can completely diffuse away from the zeolite. This effect would be more pronounced at the later stages of the process, as more of the external surface sites are vacant. If this hypothesis is true, one should expect the overall desorption rate at late times to be controlled both by diffusion and by the sorption equilibrium.

In conclusion, one cannot rule out the possible existence of a rate-controlling process other than intracrystalline diffusion, e.g., readsorption, or the related possibility of non-constant surface coverage.

4.1.2 Model II: Constant Diffusivity Variable Surface Coverage - (CDVC) Model

The assumption of constant θ_1 may be relaxed by approximating the surface coverage of the monotonically decreasing ID curve as

$$\theta_1(t) = \theta_{max} \exp (- \bar{\beta} t_2 t) \qquad (4 - 11)$$

The corresponding solution for (M_t/M_∞) based on the new boundary condition is:

$$\frac{M_t}{M_\infty} = 1 - \frac{6}{\pi^2} \sum_{n=1}^{\infty} \frac{\exp(- n^2\pi^2 t_2 t)}{n^2} + \frac{6\theta_{max}}{\theta_0} \sum_{n=1}^{\infty} \frac{\exp (- \bar{\beta} t_2 t) - \exp(- n^2\pi^2 t_2 t)}{n^2\pi^2 - \bar{\beta} t_2 t} \qquad (4 - 12)$$

The mass ratio derived here is a complex function of $\bar{\beta}$, θ_{max} , and t_2. A similar analysis is possible for a monotonically increasing ID curve, with a mass ratio of:

$$\frac{M_t}{M_\infty} = 1 + \frac{\exp (- \bar{\beta} t_2 t)}{\theta_0 - \theta_{max}} + \frac{6\,\theta_0}{\theta_0 - \theta_{max}} \sum_{n=1}^{\infty} \frac{\exp(- n^2\pi^2 t_2 t)}{n^2\pi^2} - \frac{6\,\theta_{max}\bar{\beta} t_2}{\theta_0 - \theta_{max}} \sum_{n=1}^{\infty} \frac{\exp(- n^2\pi^2 t_2 t) - \exp (- \bar{\beta}\, t_2 t)}{n^2\pi^2 (n^2\pi^2 - \bar{\beta} t_2)} \qquad (4 - 13)$$

For each ID experiment, the $\bar{C}$ vs. τ data can be regressed to find an estimate for $\bar{\beta}$, assuming $\bar{C}$ and θ_1 follow similar ID curves. Since eq. (4-11) predicts a monotonically decreasing external surface coverage, only the falling portion of each ID spectrum was used in the Box regression routine. With this simplification, θ_{max} equals 1 and the rest of the "desorption rate isotherm" procedure is unchanged.

The fitted $\bar{\beta}$ values are in the range 10^{-3} - 10^{-4} (s^{-1}) and the θ_1 values were calculated as < 0.1 for toluene and benzene after 600 and 150 s, respectively. Therefore, the external surface coverage at late stages

of the process should be small, a conclusion supported by the large estimated τ_3 (> 20) values reported in Table 3.10.

The fitted diffusivities for this model are listed in Table 4.3. The diffusivities are several orders of magnitude larger than the corresponding values obtained by the CDCC model. The 95% confidence limits of the regressed diffusivities are about 200 - 800 % and 200% relative deviation for toluene and benzene, respectively.

Although the parameters of CDVC model show much larger confidence limits than those of the CDCC model, the average relative deviation of percent mass loss for the CDVC model is only 2-4 % (except for toluene desorbed from P1, which shows 8% deviation) and 3-4 % for toluene and benzene, respectively.

The corresponding plots for regressed and experimental percent of mass loss vs. time for the CDVC model are shown in Figs. 4.11 to 4.15. As shown in these figures, the model predictions fit the experimental data better, in general not exhibiting the crossover behavior found with the CDCC model.

One problem with the CDVC model was noted by comparing the intracrystalline diffusivities listed in Table 4.3. The toluene has a larger diffusivity than does benzene in the 105-6 zeolite, a consequence of the small $\bar{\beta}$ value fitted for the toluene/105-6 system. Another problem is that the regressed diffusivity for Y-52 is several orders of magnitude larger than the other diffusivities, which can not be explained by any factors associated with the CDVC model.

In order to further check the validity of the CDVC model, the data of Eic and Ruthven (1988; o-xylene desorbed from two Na-X zeolites) have

Adsorbate	Adsorbent	$D_e \times 10^{12}$ cm^2/s	Standard Error	$D_e/R^2 \times 10^2$ s^{-1}	$\bar{\beta} \times 10^3$
L	Toluene	11	0.024	39	2.7
Ω - 6	Toluene	3.9	0.043	3.8	8.4
P1	Toluene	18	0.078	2.5	3.6
Y-52	Toluene	1.0×10^5	0.027	8.7×10^4	2.8
105-6	Toluene	56	0.028	156	2.8
P1	Benzene	29	0.028	7.4	7.5
105-6	Benzene	2.6	0.038	7.1	6.5
NaX (1)	o-xylene	2.7×10^4	0.028	0.43	81.1
NaX (2)	o-xylene	2.5×10^4	0.028	0.10	9.7

(1) 50 μm crystal, data from Eic and Ruthven (1988).
(2) 100 μm crystal, data from Eic and Ruthven (1988).

Table 4.3. Fitted Effective Diffusivities for Falling Portion of the ID Curve by CDVC Model.

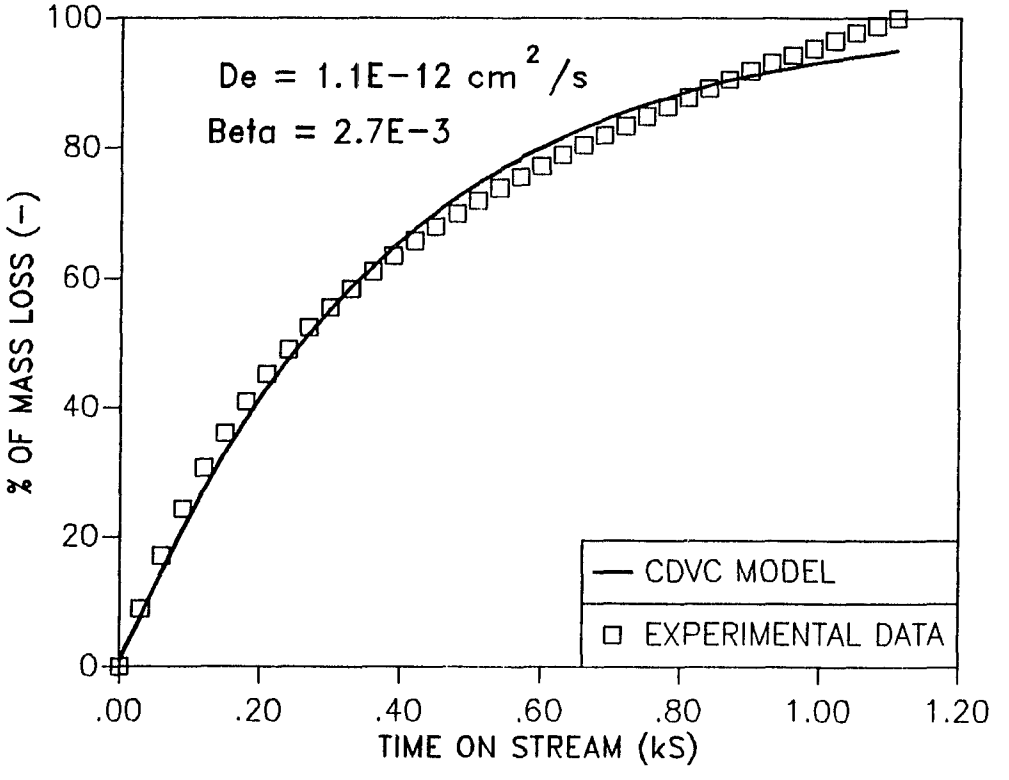

Figure 4.11, Fit of the Falling Portion of the ID Spectrum for Toluene by CDVC Model, Zeolite L.

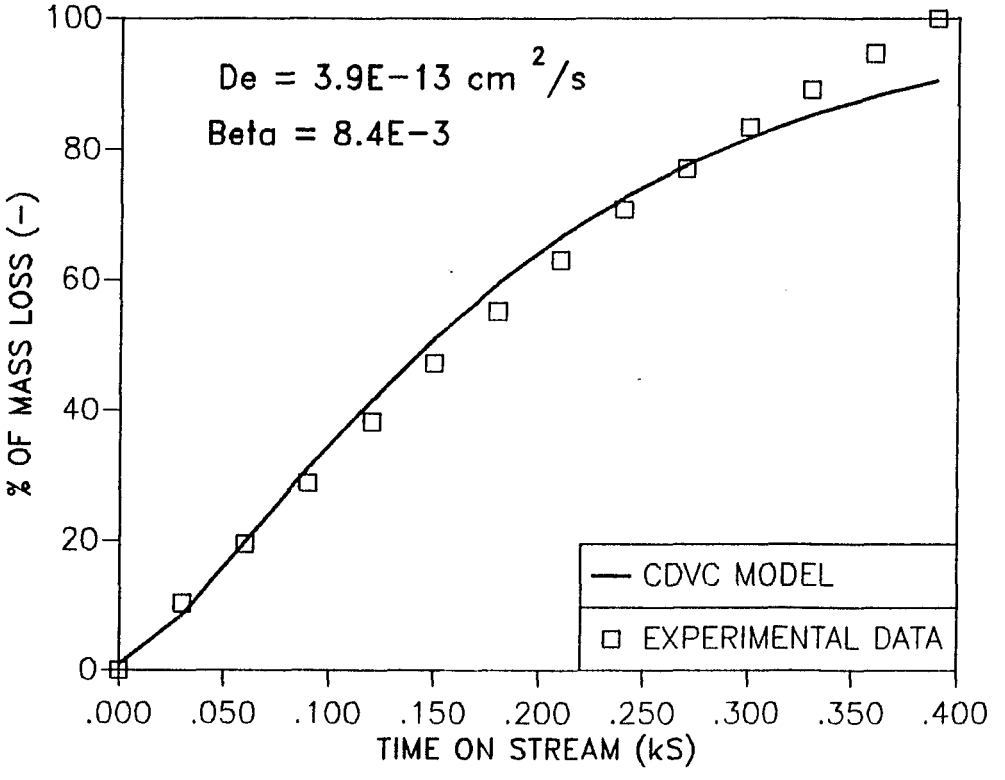

Figure 4.12, Fit of the Falling Portion of the Spectrum of Toluene Desorbed from Zeolite O-6 by CDVC Model.

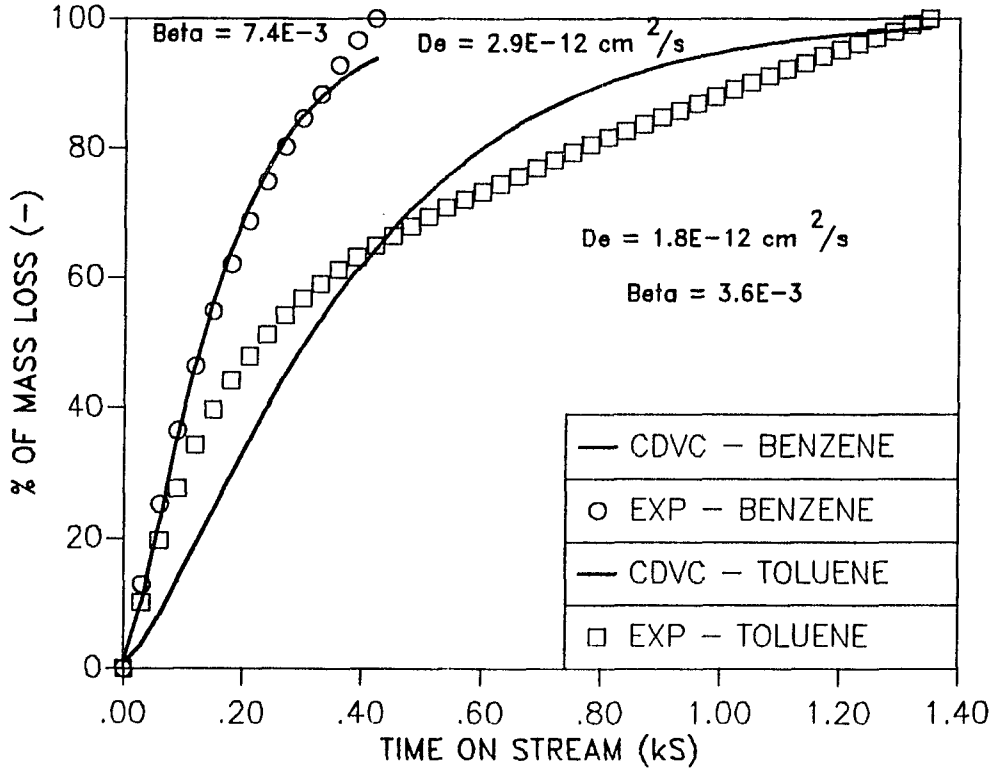

Figure 4.13, Fit of the Falling Portion of the ID Spectrum for Toluene or Benzene by CDVC Model, Zeolite P1.

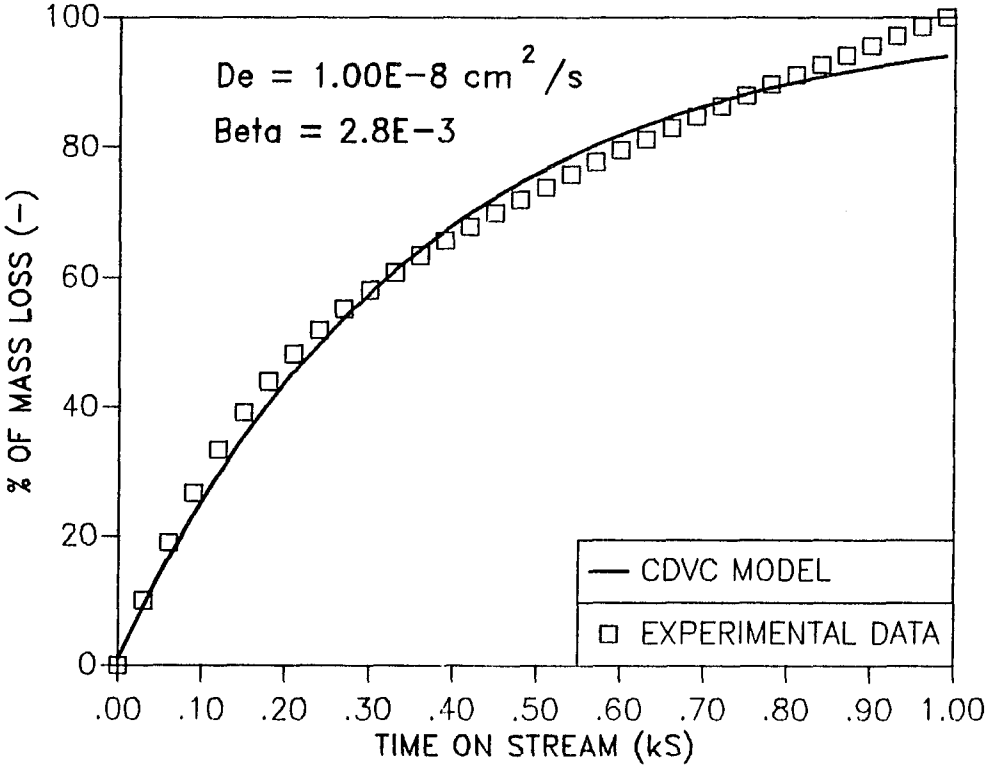

Figure 4.14, Fit of the Falling Portion of the ID Spectrum for Toluene by CDVC Model, Zeolite Y-52.

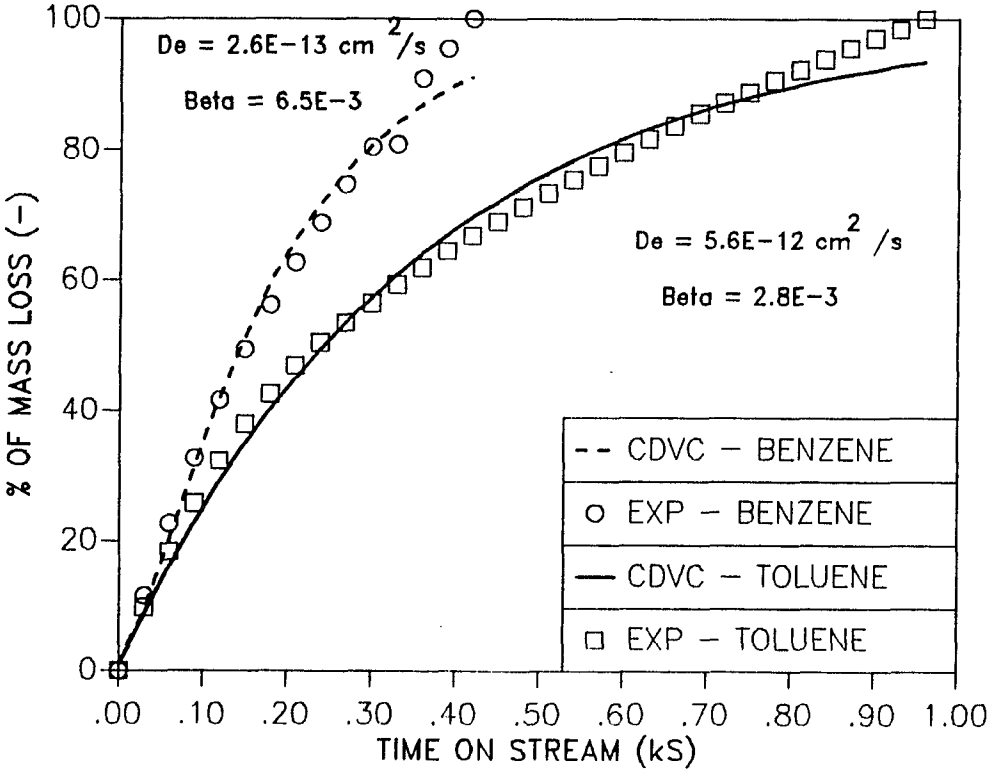

Figure 4.15, Fit of the Falling Portion of the ID Spectrum of Toluene or Benzene by CDVC Model, Zeolite 105-6.

been regressed. The fitting results are also listed in Table 4.7, and the corresponding percent of mass loss vs. time plots are shown in Fig. 4.16. The regressed diffusivities are of the same order of magnitude as the diffusivity data reported by Eic and Ruthven, and the diffusional time constants are inversely proportional to the square of crystal radius. The significance of these results will be explained in Section 4.1.5.

4.1.3 Model III: Zero Length-Column Chromatography (ZLC) Model

Eic and Ruthven (1988) developed a new experimental technique that would allow estimation of the intracrystalline diffusivities of strongly adsorbed species by measuring the desorption curves for a single species at constant temperature but as a function of carrier gas flow rate. The mathematical model they used is essentially the ID model introduced in Section 4.1 except for the following: (1) a sorption equilibrium was assumed between the gas and adsorbed phases; and (2) the accumulation term in the CSTR boundary condition was dropped. Therefore, the ZLC model can be described mathematically as:

$$\frac{1}{t_2}\frac{\partial\theta}{\partial t} = \frac{1}{\bar{r}^2}\frac{\partial}{\partial\bar{r}}\left(\bar{r}^2\frac{\partial\theta}{\partial\bar{r}}\right) \qquad (4-3)$$

with the following initial and boundary conditions:

$$\theta = \theta_0 = K\bar{C}_0 \qquad \text{at } t = 0 \qquad (4-14)$$

$$\frac{\partial\theta}{\partial\bar{r}} = 0 \qquad \text{at } \bar{r} = 0 \qquad (4-6)$$

$$\frac{\partial\theta}{\partial\bar{r}} = -\frac{Q\theta R}{a_v D_e K} \qquad \text{at } \bar{r} = 1 \qquad (4-15)$$

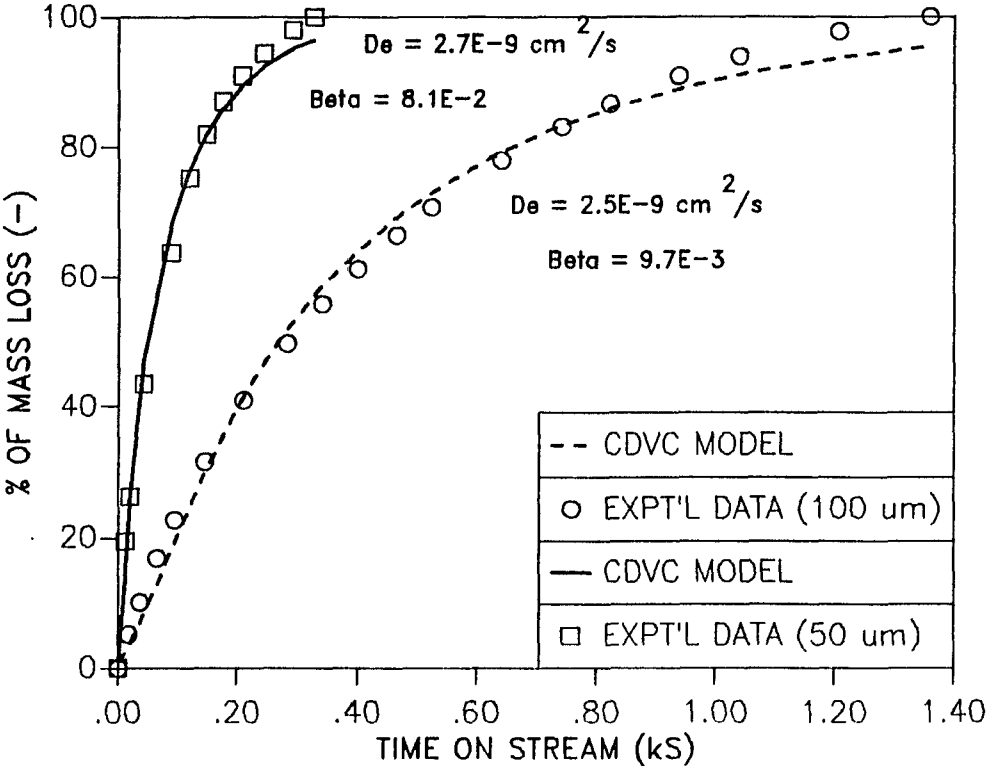

Figure 4.16, Fit of Eic and Ruthven's Data of o-xylene by CDVC Model, 50 um and 100 um NaX Zeolite.

The solution for eq. (4-3) with eqs. (4-14), (4-6), and (4-15) at constant diffusivity (Crank, 1975) is:

$$\frac{\bar{C}}{\bar{C}_0} = 2L \sum_{n=1}^{\infty} \frac{\exp(-\beta_n t_2 t)}{[\beta_n^2 + L(L-1)]} \qquad (4-16)$$

or

$$\frac{M_t}{M_\infty} = 1 - \sum_{n=1}^{\infty} \frac{6L^2 \exp(-\beta_n^2 t_2 t)}{\beta_n^2[\beta_n^2 + L(L-1)]} \qquad (4-17)$$

where $L = \frac{\alpha R}{D_e}$ and $\alpha = \frac{\varepsilon_M v R}{3(1-\varepsilon_M)KZ}$. L may also be expressed as:

$$L = \left(\frac{1}{3}\right)\left(\frac{\text{Purge Flow Rate}}{\text{Crystal Volume}}\right)\left(\frac{R^2}{KD_e}\right) \qquad (4-18)$$

and β_n is given by the roots of the auxiliary equation:

$$\beta_n \cot \beta_n + L - 1 = 0 \qquad (4-19)$$

Eic and Ruthven used eq. (4-16) at two limiting conditions:

1. $L \to 0$ (low flow rate limit), $\beta_1^2 \to 3L$ and

$$\ln\left(\frac{\bar{C}}{\bar{C}_0}\right) = -3Lt_2t \qquad (4-20)$$

2. $L \to \infty$ (high flow rate limit), $\beta_n \to n\pi$ and

$$\left(\frac{\bar{C}}{\bar{C}_0}\right) = \frac{2}{L} \sum_{n=1}^{\infty} \exp(-n^2\pi^2 t_2 t) \qquad (4-21)$$

or

$$\ln\left(\frac{\bar{C}}{C_0}\right) = \ln\left(\frac{2}{L}\right) - \pi^2 t_2 t \qquad (4-22)$$

They performed experiments at these two extreme conditions and obtained D_e and K values from the intercepts and slopes of $\ln\left(\frac{\bar{C}}{C_0}\right)$ vs. t plots. But this approach is not suitable for the ID data of this study, which were obtained at a single purge flow rate. However, there are two different approaches one may employ to fit the ID data to the ZLC model: (1) use K values from the literature (Barthomeuf and Ha, 1973; Eatough et al., 1974; Doelle et al., 1981; Forni and Viscardi, 1986) and regress for D_e using eq. (4-17); (2) perform a two parameter (D_e and K) regression using eq. (4-17).

In order to determine which approach to use, the sensitivity of eq. (4-17) with respect to D_e and K was tested by varying one of them in the feasible range and fixing the other. The K values are obtained from Forni and Viscardi (1986) and Eic and Ruthven (1988) for the ID and ZLC data, respectively. The D_e values are obtained from the CDVC results (Table 4.3) and Eic and Ruthven (1988) for the ID and ZLC data, respectively. The results are shown in Figs. 4.17 and 4.18 for conditions typical of Eic and Ruthven's study.

Fig. 4.17 shows that eq. (4-17) gives almost identical results when K is 1×10^6, R is 2.5×10^{-3} cm, and D_e is varied from 1×10^{-11} to 1×10^{-12} cm^2/s . Therefore the ZLC model is not very sensitive to variation of D_e in a certain range for each set of K and R. Fig. 4.18 shows that the model is sensitive to the variation of K when D_e and R are held at constant. For K values less than 1×10^6, the diffusion rate is much greater than the rate of adsorption. Therefore, all of the initially

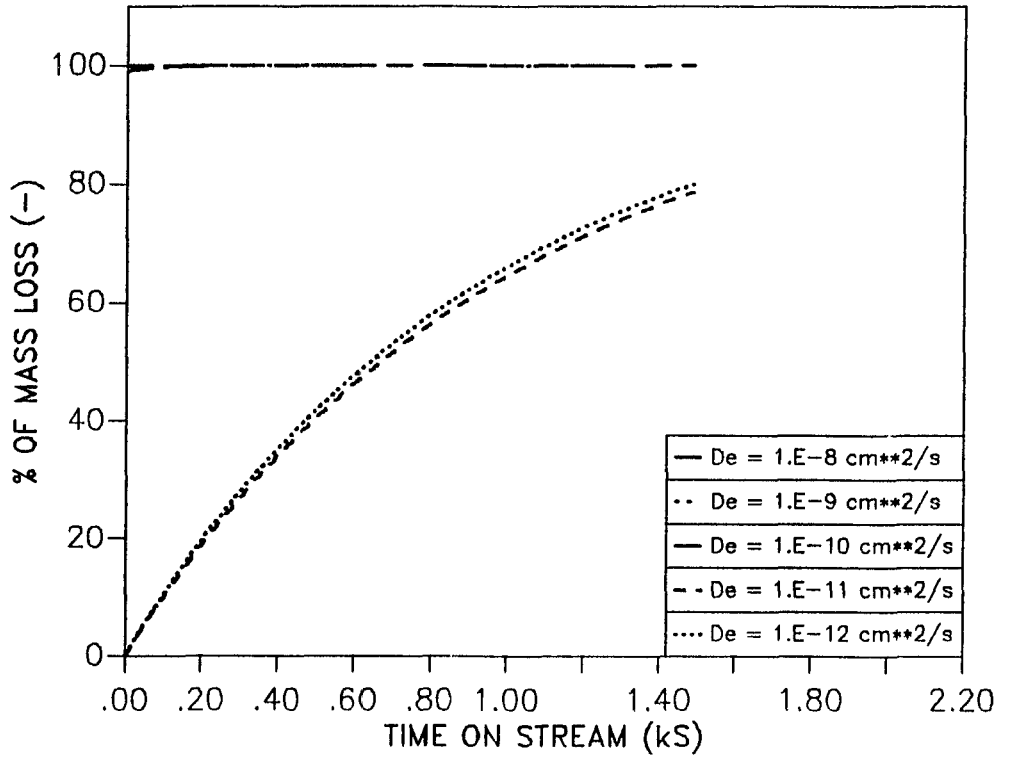

Figure 4.17, % of Mass Loss by ZLC Model with K=1.E6, R=2.5E-3 cm and De varied from 1.E-8 to 1.E-12 cm^2 /s.

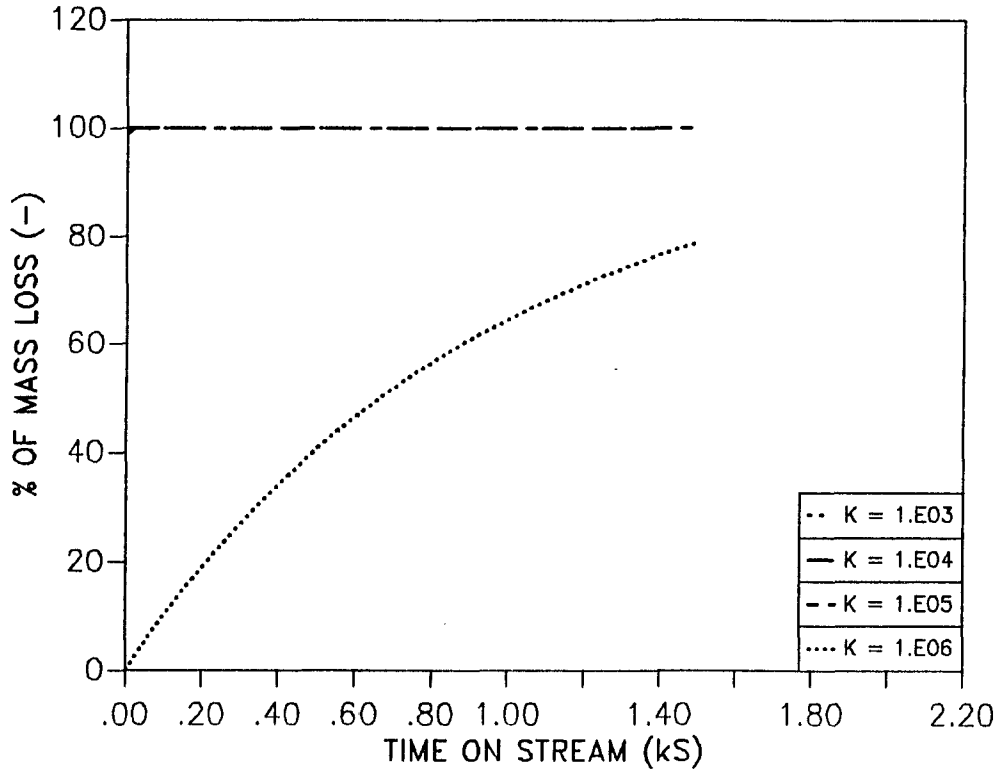

Figure 4.18, % of Mass Loss by ZLC Model with De = 1.E−8 cm^2/s, R = 2.5E−3 cm and K varied from 1.E03 to 1.E06

adsorbed material is rapidly desorbed. But readsorption more significantly affects the ID curves when K values become larger, as Fig. 4.18 shows. Similar conclusions can also be drawn for the ID experimental data. Therefore, the extreme sensitivity to K leads one to conclude that a reasonable fit between eq. (4-17) and ID experimental data can only be obtained by regression of K and D_e simultaneously.

Therefore a two parameter (D_e and K) fitting routine, similar to that used for the CDVC model, was adopted for the ZLC model. Because eq. (4-17) is sensitive to the variation of D_e and K at a fixed R, a random search was performed initially to obtain reasonable estimates of D_e and K. These values were then used as initial guesses in the Box optimization routine to search for the optimum D_e and K values by the "desorption rate isotherm" procedure.

The fitted equilibrium constants for the ZLC model are listed in Table 4.4. The equilibrium constants, which are essentially Henry's law constants, are on the order of 10^4 for toluene and benzene. These predictions for the K values are much larger than the values of 10^2 - 10^3 reported in the literature (Barthomeuf and Ha, 1973; Ruthven and Doetsch, 1976; Doelle et al., 1981; Santacesaria et al., 1982; Forni and Viscardi, 1986) for toluene or benzene desorbed from Y or ZSM-5 zeolites at 623K. It should, however, be noted that all the literature K's (except those of Forni and Viscardi, 1986) were extroplated to 623K from lower temperatures using van't Hoff's equation. The extrapolated K's may be misleading because different modes of adsorption may compete at higher temperatures; when this is the case, extroplated K's always underestimate the true K. The 95% confidence limits of the regressed equilibrium constants are about

Adsorbate	Adsorbent	$D_e \times 10^{12}$ cm^2/s	Standard Error	$D_e/R^2 \times 10^4$ s^{-1}	$Kx10^{-4}$
L	Toluene	6.9 ± 1.6	0.023	2.4 ± 0.1	2.4
Ω - 6	Toluene	21.0 ± 6.0	0.073	1.7 ± 0.2	1.7
P1	Toluene	220 ± 15	0.032	3.1 ± 0.2	3.1
Y-52	Toluene	10.0 ± 2.7	0.033	1.8 ± 0.4	1.8
105-6	Toluene	1.0 ± 0.05	0.029	2.2 ± 0.3	2.2
P1	Benzene	160 ± 20.0	0.044	1.1 ± 0.1	1.2
105-6	Benzene	11.0 ± 1.4	0.055	1.3 ± 0.4	1.3
NaX (1)	o-xylene	$3.0 \pm 0.4x10^4$	0.025	7.5 ± 1.0	7.5
NaX (2)	o-xylene	$2.4 \pm 0.0x10^4$	0.016	3.7 ± 0.0	37

(1) 50 μm crystal, data from Eic and Ruthven (1988).
(2) 100 μm crystal, data from Eic and Ruthven (1988).

Table 4.4. Fitted Effective Diffusivities for Falling Portion of the ID Curve by the ZLC Model.

4 - 26% and 9 - 31% (relative deviation) for toluene and benzene, respectively.

The fitted diffusivities for the ZLC model are also listed in Table 4.4. The fitted diffusivities are one to two orders of magnitude larger than the corresponding values obtained by the CDVC model. The 95% confidence limits of the regressed diffusivities are about 5 - 28% and 13% for toluene and benzene, respectively. The confidence limits are larger than those reported for the CDVC model, which may due to the fact that the ZLC model is very insensitive to large changes of D_e in certain K, R ranges. The average deviation for the ZLC model is only 2 - 3% (except 7%, for Ω) and 4 - 6% for toluene and benzene, respectively. These values are close to the relative deviations for the CDVC model as shown in Table 4.3. This is probably due to the fact that the ZLC model also considers both the variation of external surface coverage and the existence of equilibrium between gas and adsorbed phases.

The corresponding plots for regressed and experimental percent of mass loss vs. time for the ZLC model are shown in Figs. 4.19 to 4.23. As shown in these figures, the model predictions fit the experimental data well except in the later stage of the process, and again do not (in general) exhibit the crossover behavior found with the CDCC model.

One problem with the ZLC model is noted by comparing the intracrystalline diffusivities listed in Table 4.4. For the P1 zeolite, toluene has a larger diffusivity than does benzene in P1 zeolite, which appears unreasonable in view of benzene's smaller critical diameter and smaller elution times to 100% desorption (compares Fig. 4.21). The smaller K values regressed for benzene than for toluene on P1, as listed in Table 4.4, imply a stronger site-molecule attraction for toluene, which in turn

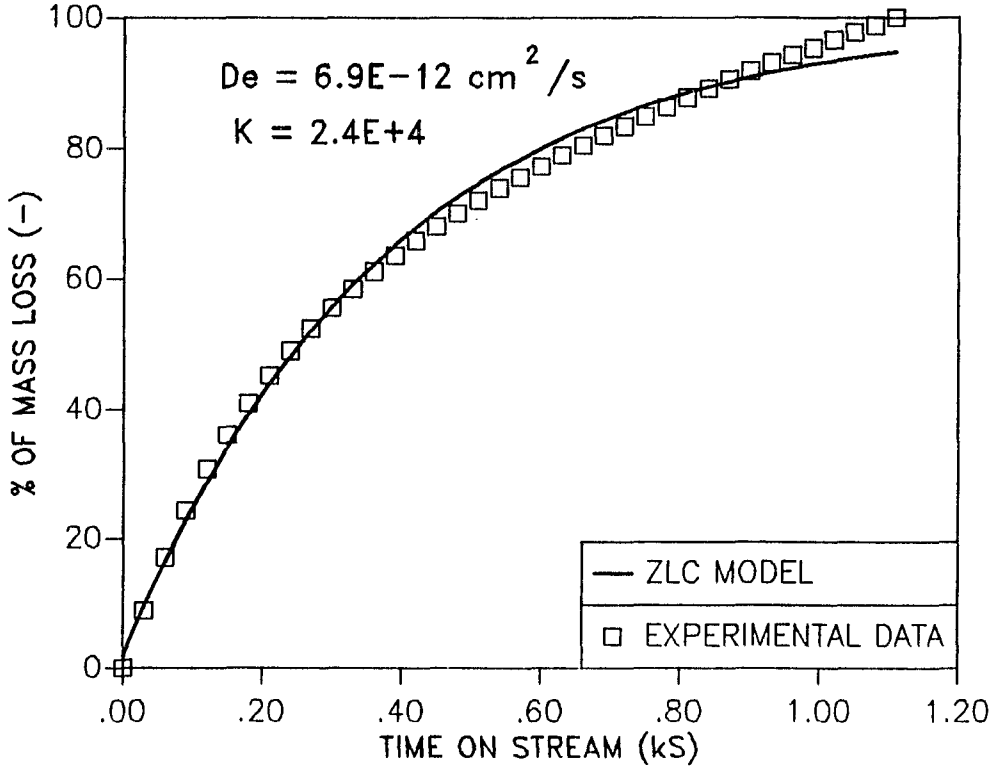

Figure 4.19, Fit of the Falling Portion of the ID Spectrum for Toluene by ZLC Model, Zeolite L.

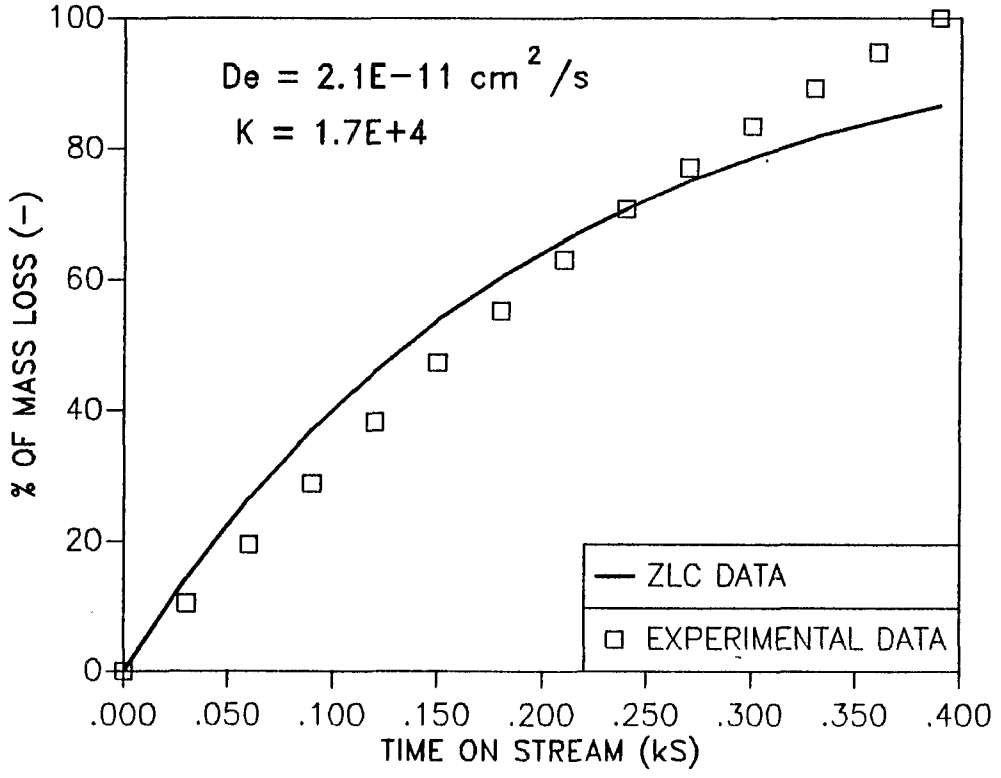

Figure 4.20, Fit of the Falling Portion of the ID Spectrum for Toluene by ZLC Model, Zeolite Omega−6.

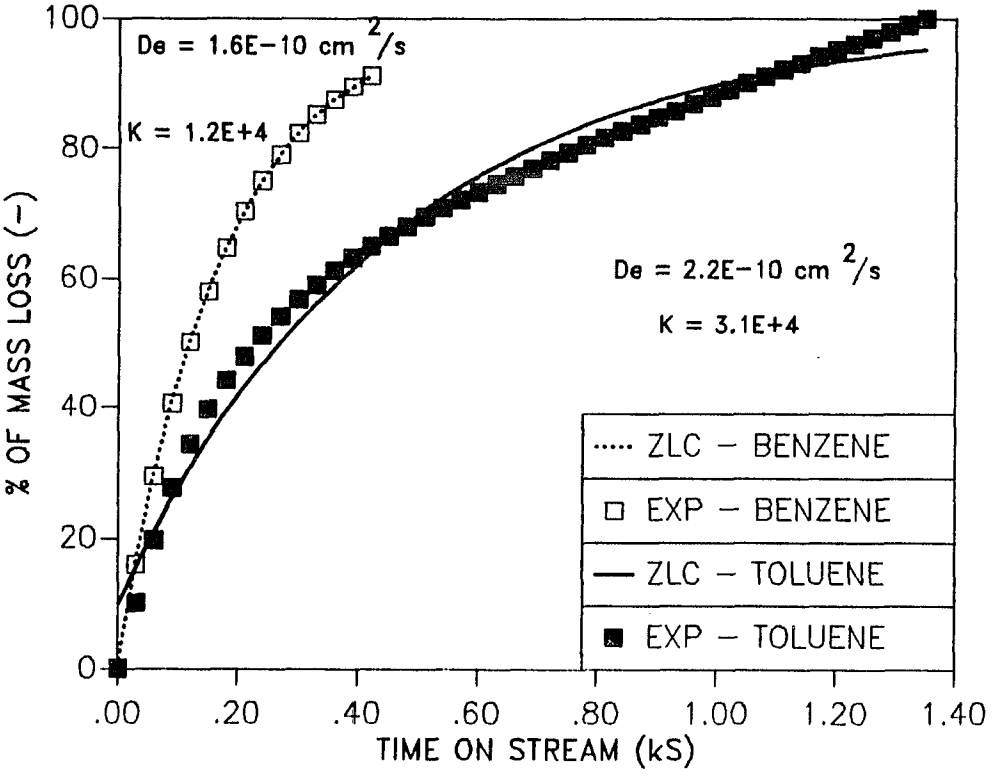

Figure 4.21, Fit of the Falling Portion of the ID Spectrum for Toluene or Benzene by ZLC Model, Zeolite P1.

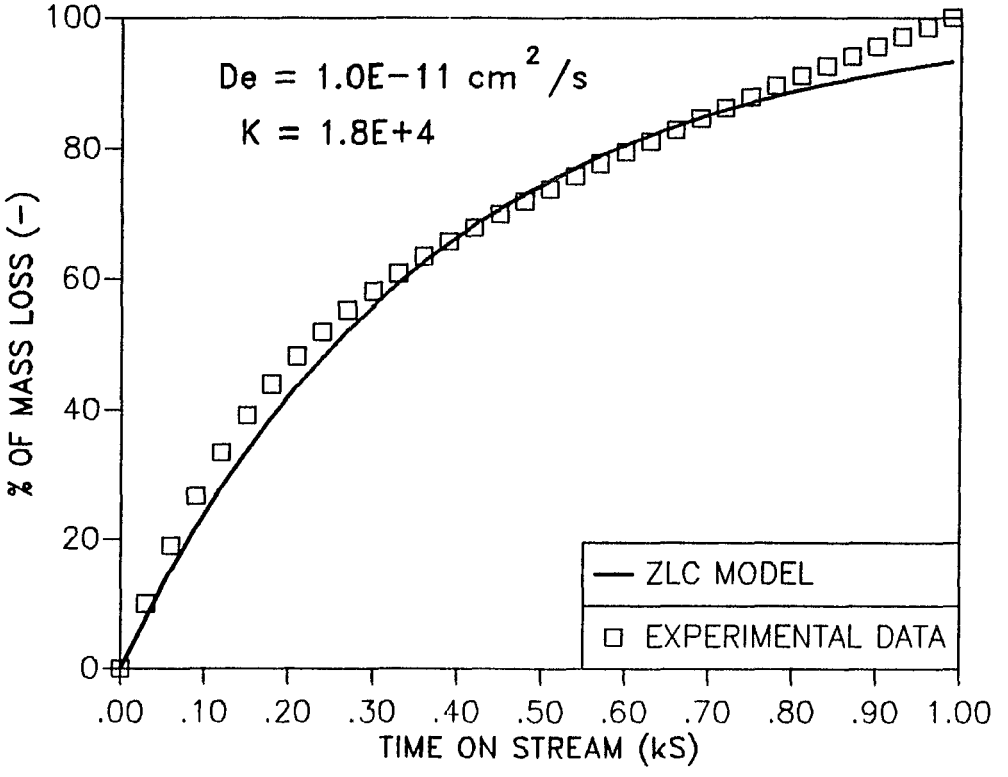

Figure 4.22, Fit of the Falling Portion of the ID Spectrum for Toluene by ZLC Model, Zeolite Y−52.

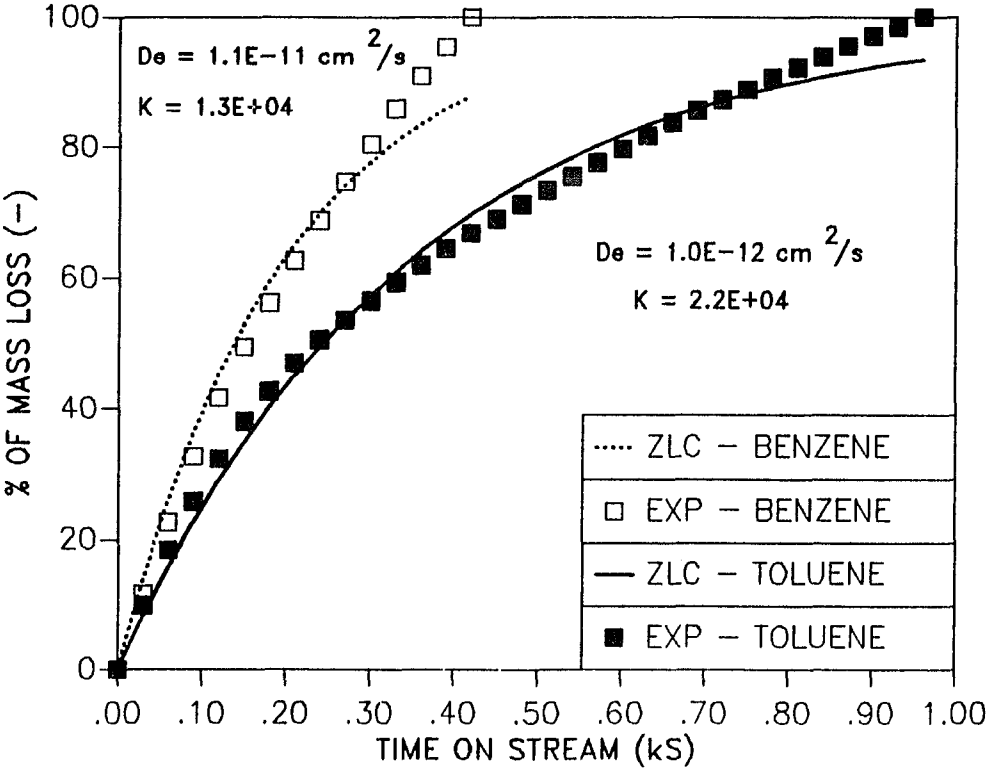

Figure 4.23, Fit of the Falling Portion of the ID Spectrum for Toluene or Benzene by ZLC Model, Zeolite 105–6.

implies a smaller D_e value. Therefore the fitted K-values also contradict the D_e data. The data of Eic and Ruthven (1988; o-xylene desorbed from two NaX zeolites) have also been regressed using the ZLC model. The fitting results are also listed in Table 4.4, and the corresponding percent of mass loss vs. time plots are shown in Figs. 4.24 and 4.25 for 50 μm and 100 μm NaX crystals, respectively. The regressed equilibrium constants are one to two orders of magnitude smaller than the equilibrium constants reported by Eic and Ruthven. The regressed diffusivities are an order of magnitude larger than the diffusivity data reported by Eic and Ruthven, and the diffusional time constants are approximately inversely proportional to the square of crystal radius. The significance of these results will be explained in Section 4.1.5.

The D_e and K values reported by Eic and Ruthven (1988) were substituted into eq. (4-17), and these curves are also shown in Figs. 4.24 and 4.25. As shown in these plots, the Eic and Ruthven parameters imply that the percent of mass loss should reach 100% at very short times, which is obviously incorrect. One possible problem with the Eic and Ruthven estimation technique is the requirement of a high purge rate for certain experiments used to estimate D_e and K. At a high purge rate, the mass transfer rate is too fast to establish equilibrium at the external surface. Therefore, the assumption of equilibrium between fluid phase and external surface concentration as $L \to \infty$ (high flow rates) may not be satisfied at these experimental conditions. Note that Eic and Ruthven used several small L values (e.g., 5.54 and 5.36), compared to the higher L values (159 and 182) calculated using the D_e and K values reported in Table 4.4. However, the D_e values obtained by the present analysis using Eic and Ruthven's data are closer to those obtained by the PFG (NMR)

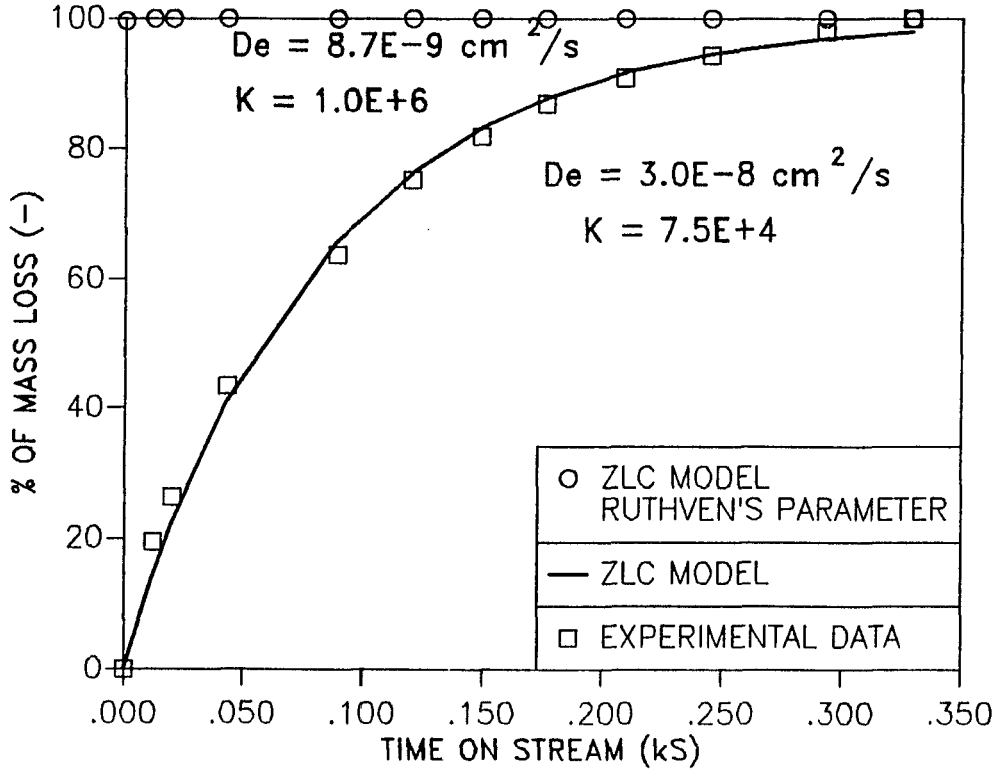

Figure 4.24, Fit of Eic and Ruthven's Data for o−Xylene by ZLC Model, 50 um NaX.

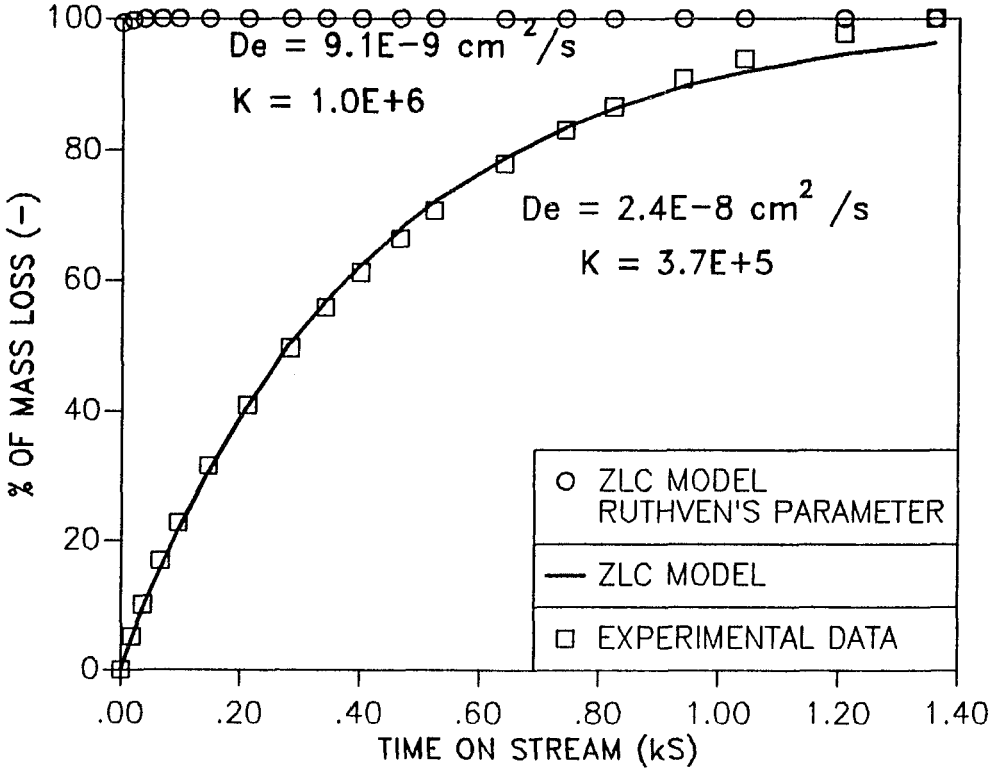

Figure 4.25, Fit of Eic and Ruthven's Data for O-Xylene by ZLC Model, 100 um NaX.

technique. Therefore, the present analysis method, which utilized the medium flow rate data with the ZLC model, may be superior.

Finally, the ZLC model itself is suspect because there is no way to justify the assumption of no accumulation term in the CSTR boundary condition, i.e., eq. (4-15) for the ZLC model. By a simple scaling analysis, the accumulation and the diffusion terms are of order 6×10^{-7} and 2×10^{-7} for the worst case reported in the paper (Eic and Ruthven, 1988). Even for the best case the magnitudes are 4×10^{-6} for accumulation and 1×10^{-5} for diffusion.

4.1.4 Model IV: Linear Model

The drawback of the time dependent surface coverage assumption in the CDVC model is the introduction of two more parameters, θ_{max} and $\bar{\beta}$, which have vague physical meaning and cannot be precisely obtained (only estimated) from theory. A way to solve this problem is to minimize the assumptions and keep the form of eq. (4-7) as much as possible. One way to proceed is to let $\bar{\Psi} = 1$, which gives us the "linear model". This model approaches the exact solution for small n.

Now eqs. (4-3) to (4-7) can be solved analytically in the Laplace domain (denoted by a $\tilde{}$ overbar) by letting $u = \theta\,\bar{r}$, which gives

$$\tilde{\theta}(S,\bar{r}) = \frac{1}{S} + \frac{\left(\frac{\tau_5}{S}\right)(1+\tau_1 S)\sinh[(\tau_2 S)^{0.5}\bar{r}]}{\bar{r}\{[\sigma-(1+\tau_1 S)\tau_5]\sinh[(\tau_2 S)^{0.5}] - \sigma(\tau_2 S)^{0.5}\cosh[(\tau_2 S)^{0.5}]\}} \qquad (4-23)$$

where $\sigma = 1 + \tau_1 S + \tau_3\tau_4$.

The corresponding dimensionless gas phase concentration, $\bar{C}$ is:

$$\tilde{\bar{C}}(S) = \frac{\left(\frac{\tau_5}{S}\right)\tau_3\{\sinh[(\tau_2 S)^{0.5}] - (1+\tau_1 S)\cosh[(\tau_2 S)^{0.5}]\}}{[\sigma-(1+\tau_1 S)\tau_5]\sinh[(\tau_2 S)^{0.5}] - \sigma(\tau_2 S)^{0.5}\cosh[(\tau_2 S)^{0.5}]} \quad (4-24)$$

where τ_1 to τ_5 are the dimensionless parameters defined in the Nomenclature.

Eq. (4-24) can be inverted numerically by direct application of Fast Fourier Transform (FFT) algorithm (Hsu and Dranoff, 1987), which is as follows:

1. Determine all the singularities of $\tilde{\bar{C}}(S)$ and specify a parameter "a" greater than the real parts of all the singularities.

2. Compute the real and imaginary parts of $\tilde{\bar{C}}(S)$ by replacing S with a+jw, $w = \frac{k\pi}{T}$. Here T is the half-period of the function $\tilde{\bar{C}}(a+jw)$ and j is the pure imaginary number.

3. The interval T is chosen as $T < \frac{N}{2}\frac{\pi}{w_{max}}$, where N is the number of data points and w_{max} is the frequency at which $Re\{\tilde{\bar{C}}(a+jw)\}$ and $Im\{\tilde{\bar{C}}(a+jw)\}$ approach zero.

4. The function $\tilde{\bar{C}}(a+jw)$ is periodic over w with period $T/2\pi$, i.e., $\tilde{\bar{C}}(a+jw) = \tilde{\bar{C}}(a+j(w+\frac{2\pi}{T}))$. Then

$$\tilde{\bar{C}}(a+j\frac{\pi k}{T}) = \tilde{\bar{C}}^{\times}(a-j\frac{\pi k}{T}) \quad (4-25)$$

and

$$\tilde{\bar{C}}(a+j\frac{\pi k}{T}) = \tilde{\bar{C}}(a+j\frac{\pi(N-k)}{T}) \quad (4-26)$$

where * denotes (the complex) conjugate. Therefore, only the values of $\tilde{\bar{C}}(a + j\frac{\pi k}{T})$ for k = 0 to N/2 must be computed and the sample points for k = $\frac{N}{2}$ +1 to N can be obtained from eq. (4-26).

5. Finally, the inversion of $\tilde{\bar{C}}(S)$ is

$$\bar{C}(t) = \bar{C}(i\Delta T)$$

$$= \frac{\exp(ia\Delta T)}{2T} \sum_{k=0}^{N-1} \tilde{\bar{C}}(a + j\frac{k\pi}{T}) \exp(j\frac{2\pi ik}{N}) \qquad (4-27)$$

for i = 0, 1, 2....., N - 1

The singularities of eq. (4-24) have been solved for numerically; it was found that the poles lie on the left-hand side of the origin. Therefore, "a" can be set equal to zero, and eq. (4-27) may be simplified to

$$\bar{C}(t) = \bar{C}(i\Delta T)$$

$$= \sum_{k=0}^{N-1} \frac{\bar{C}(j\frac{k\pi}{T})}{2T} \exp(j\frac{2\pi ik}{N}) \qquad (4-28)$$

for i = 0, 1, 2....., N - 1

The corresponding percent of mass loss data were computed by integrating the $\bar{C}(t)$ curve numerically. An experimental ID spectrum was regressed against this numerical solution by employing a two parameter (D_e and K) fitting routine similar to those used for both the CDVC and ZLC models.

The fitted diffusivities for the Linear model in the time domain are also listed in Table 4.5. The fitted diffusivities are two to three orders of magnitude larger than the corresponding values obtained by the ZLC model. The 95% confidence limits of the regressed diffusivities are 18 - 79 % (except 119% for Ω - 6, due to the low signal to noise ratio as

Adsorbate	Adsorbent	$D_e \times 10^9$ cm^2/s	Relative Deviation	D_e/R^2 s^{-1}	$Kx10^{-2}$ cm^3/mol
L	Toluene	2.2	0.060	7.5	5.0
Ω - 6	Toluene	53	0.047	52	5.5
P1	Toluene	32	0.065	4.6	1.0
Y-52	Toluene	7.4	0.060	6.4	2.0
105-6	Toluene	2.4	0.047	6.7	1.0
P1	Benzene	63	0.079	9.0	2.0
105-6	Benzene	8.0	0.030	22.	0.8
NaX (1)	O-xylene	320	0.059	0.052	$1.0x10^4$
NaX (2)	O-xylene	340	0.029	0.054	$1.0x10^4$
NaX (3)	O-xylene	480	0.039	0.019	$1.0x10^5$
NaX (4)	O-xylene	330	0.029	0.013	$1.0x10^5$

(1) 50 μm crystal, Q = 100 cm^3/ min, data from Eic and Ruthven (1988).
(2) 50 μm crystal, Q = 140 cm^3/ min, data from Eic and Ruthven (1988).
(3) 100 μm crystal, Q = 100 cm^3/ min, data from Eic and Ruthven (1988).
(4) 100 μm crystal, Q = 160 cm^3/ min, data from Eic and Ruthven (1988).

Table 4.5. Fitted Effective Diffusivities for the Whole ID Curve in the Real Time Domain by the Linear Model.

discussed in Section 3.3.2) and 55 - 70 % for toluene and benzene, respectively. These large confidence limits result from the fact that the model is insensitive to large changes of D_e in certain K ranges, similar to the case of the ZLC model.

Table 4.5 also gives the relative deviations for each fitted curve, which are 5-7 % and 3-8 % for toluene and benzene, respectively. These values are slightly larger then those reported for the CDVC and ZLC models. This is to be expected; the whole ID spectrum, rather than only the falling portion of the spectrum, can be used with the Linear model. When only the falling portion of a spectrum was fitted using the Linear model, the relative deviations were 2-4 % and 1-2 % for toluene and benzene, respectively. The intracrystalline diffusivities predicted by fitting the falling portion of the spectra, however, are quite similar to those reported in Table 4.5.

The plots for regressed and experimental percent of mass loss vs. time for the Linear model are shown in Figs. 4.26 to 4.30. As shown in these plots, the model predictions fit the experimental data well, except sometimes in the middle stage of the process. This deviation between the fitted and experimental data may be caused by the fact that $\overline{\Psi}$, which is $\frac{(n_{max} - n)}{n_{max}}$, changes most at midddle stage of the process (which is the time span corresponding to the maximum desorption rate) and is relatively constant at early or late stages of the process.

The absolute values of the intracrystalline diffusivities, as for the CDCC model, show the right trend. The results in Table 4.5 show that benzene has a larger diffusivity than does toluene in the same zeolite, which again can be explained by the smaller critical diameter of benzene.

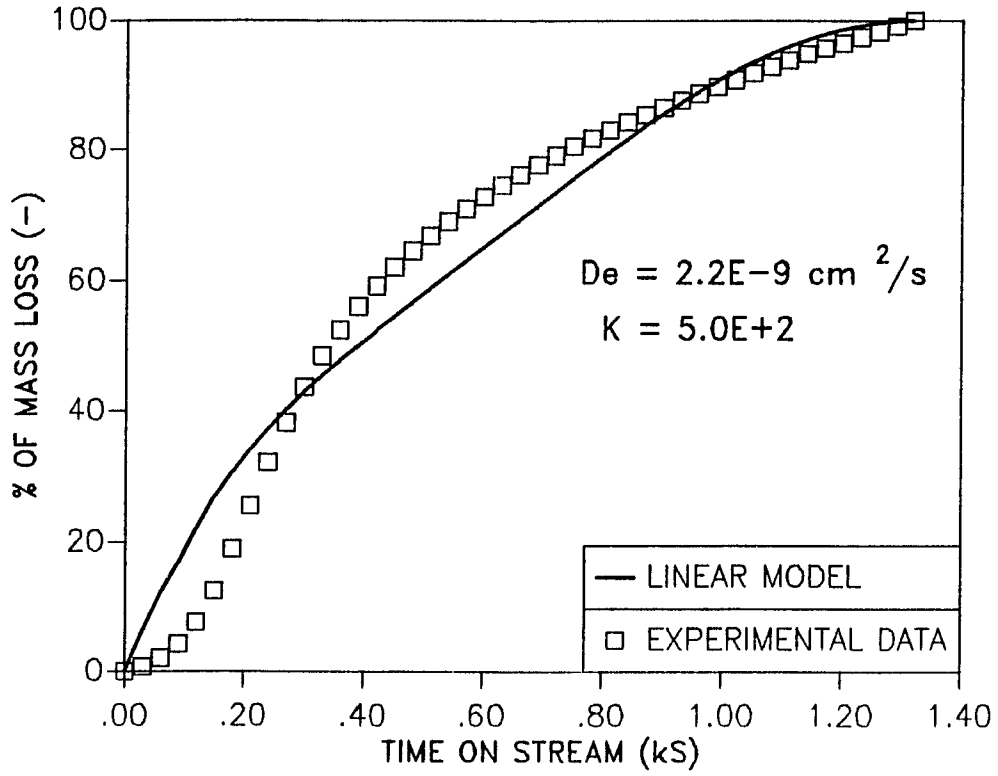

Figure 4.26, Fit of the Entire ID Spectrum for Toluene by LINAER Model, Zeolite L.

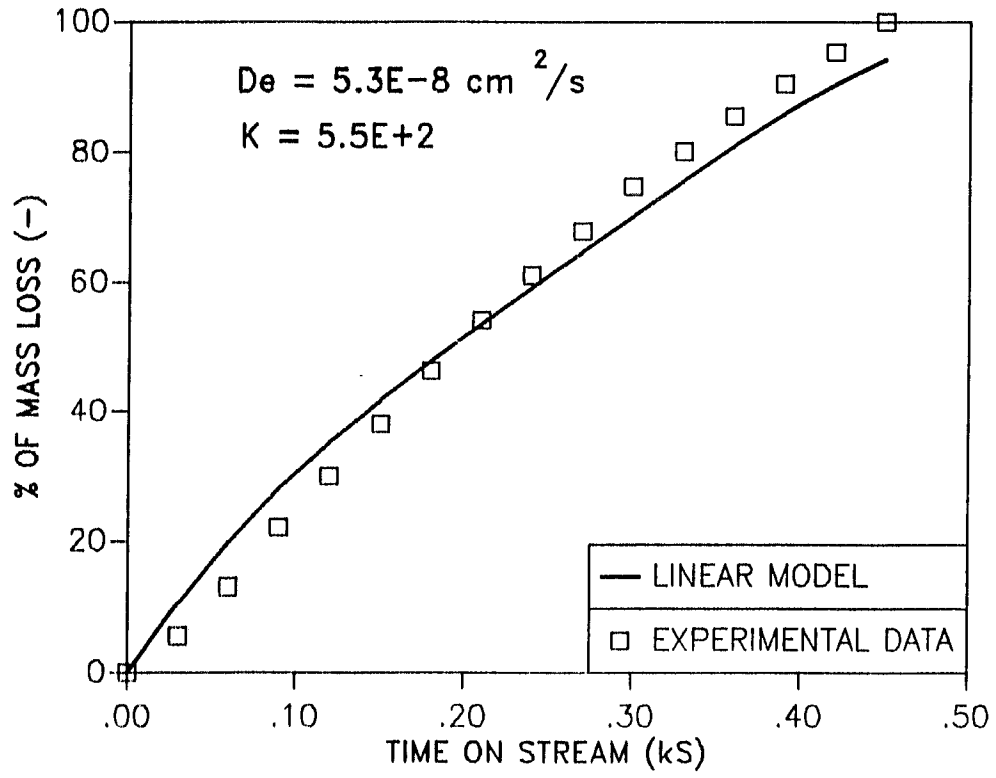

Figure 4.27, Fit of Entire ID Spectrum for Toluene by LINEAR Model, Zeolite Omega-6.

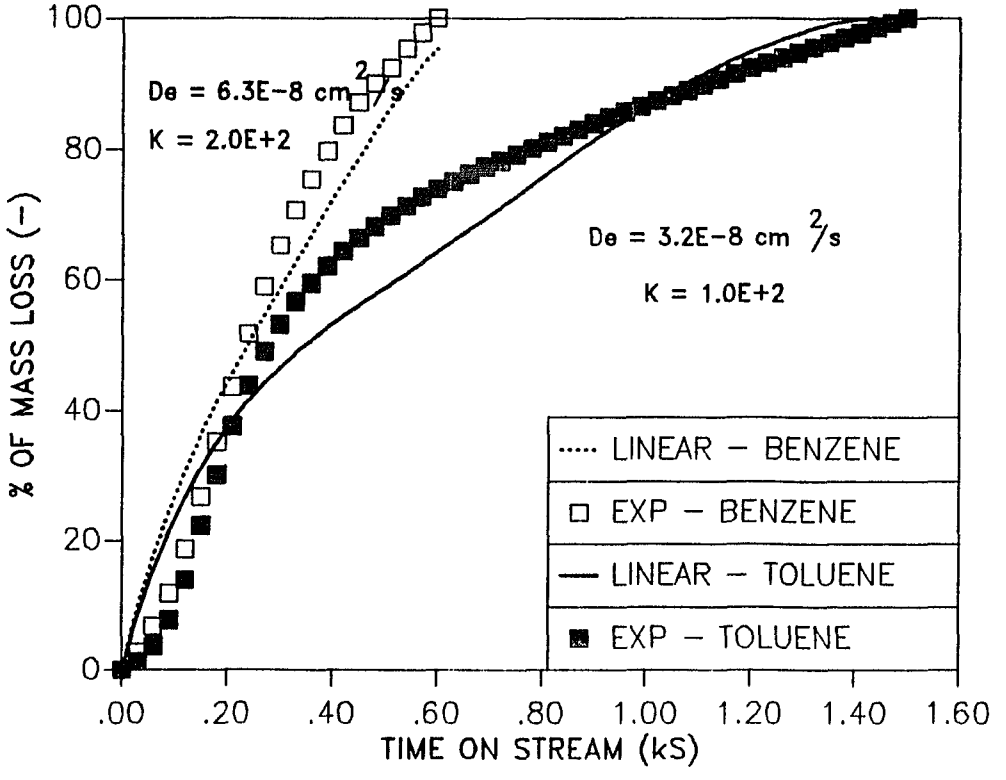

Figure 4.28, Fit of Entire ID Spectrum for Toluene or Benzene by LINEAR Model, Zeolite P1.

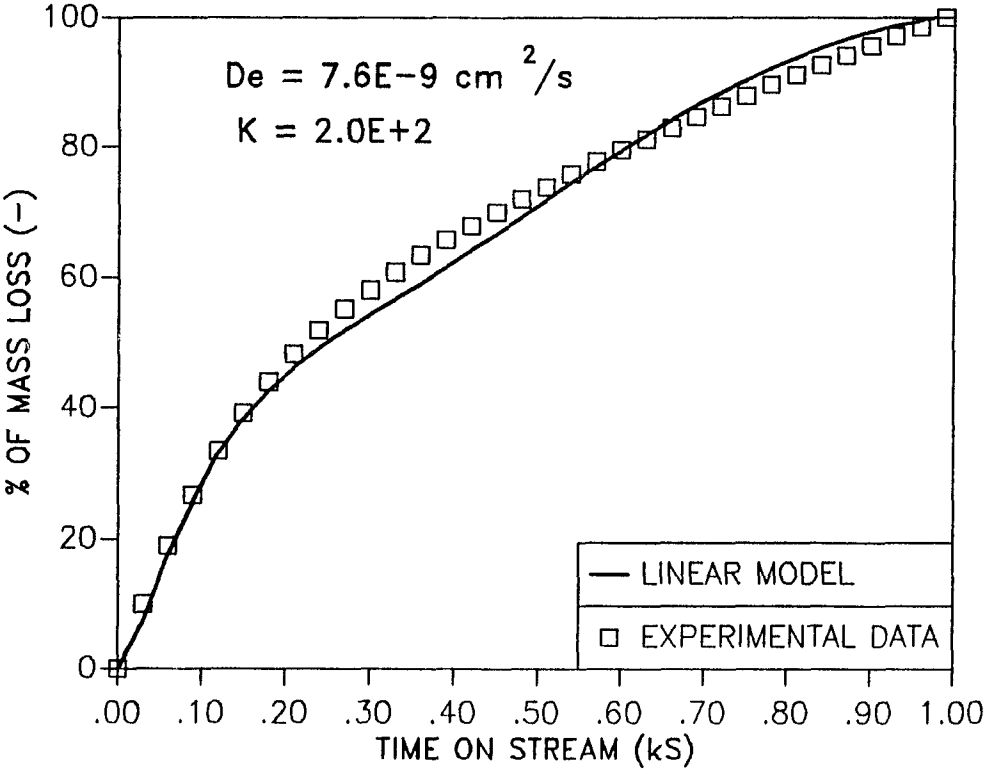

Figure 4.29, Fit of Entire ID Spectrum for Toluene by LINEAR Model, Zeolite Y-52.

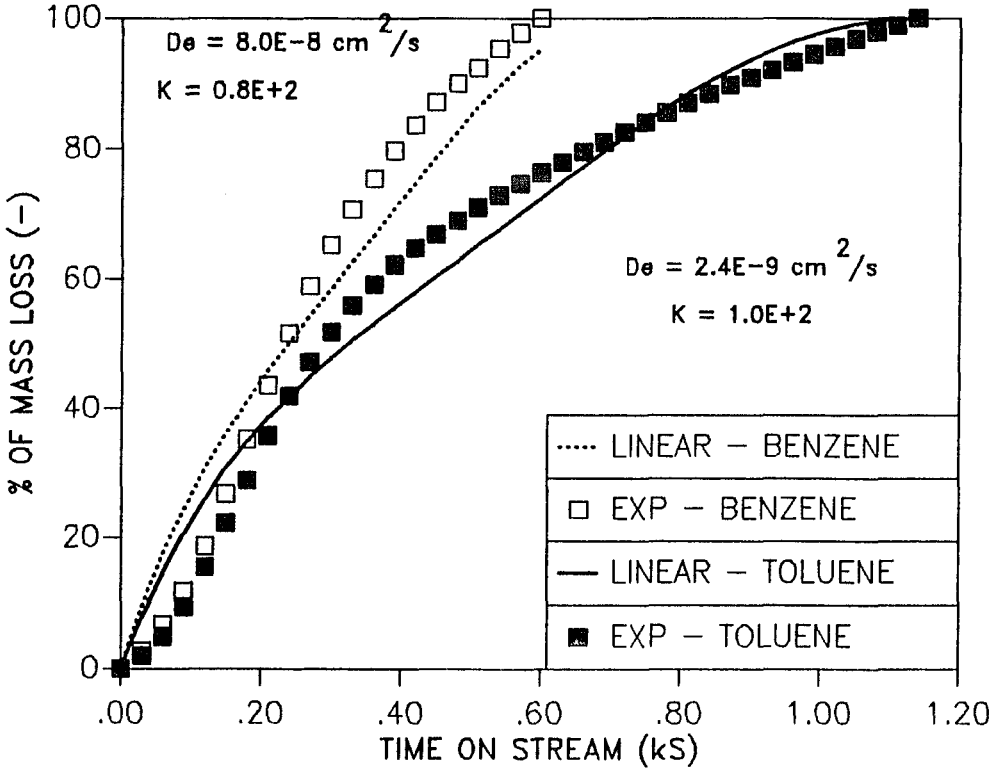

Figure 4.30, Fit of Entire ID Spectrum for Toluene or Benzene by LINEAR Model, Zeolite 105-6.

In order to further check the validity of the Linear model, the data of Eic and Ruthven (1988) (o-xylene desorbed from two NaX zeolites), at both medium and high flow rates, were also regressed. The fitting results are also listed in Table 4.5, and the corresponding percent of mass loss vs. time plots are shown in Figs. 4.31. and 4.32 for 50 μm and 100 μm NaX crystals, respectively. The regressed diffusivities for 50 and 100 μm NaX zeolites are 3.2×10^{-7} and 3.3×10^{-7} for high flow rate and 3.7×10^{-7} and 4.8×10^{-7} for medium flow rate data, respectively. These values are approximately two orders of magnitude larger than the diffusivity data reported by Eic and Ruthven and are one order of magnitude larger than those obtained by regressing all of Eic and Ruthven's data according to the CDVC and ZLC model. The larger discrepancy in diffusivities for the medium flow rate data can be explained by differences in the nature of the data as shown in Fig. 4.33. The two curves for 50 and 100 μm crystals for the high flow rate data are almost the same, and the regressed diffusivities are also the same. The relative deviation for the present fit for the medium and high flow rate data are 5.9% and 2.9% for 50 μm and 3.9% and 2.9% for 100 μm, respectively. The diffusional time constants are inversely proportional to the square of crystal radius for the haigh flow rate data, and are approximately inverse to the square of radius for the medium flow rate data. It can be concluded that the desorption technique is best used with the high flow rates.

Finally, one should note that the adsorption rate constant, k_a , used to compute τ_4 was approximated by FS, the product of the collision frequency F, and a sticking coefficient S. In the regression routine, S values of 0.1, 0.5 and 1.0 have been used to compute k_a, and it was found

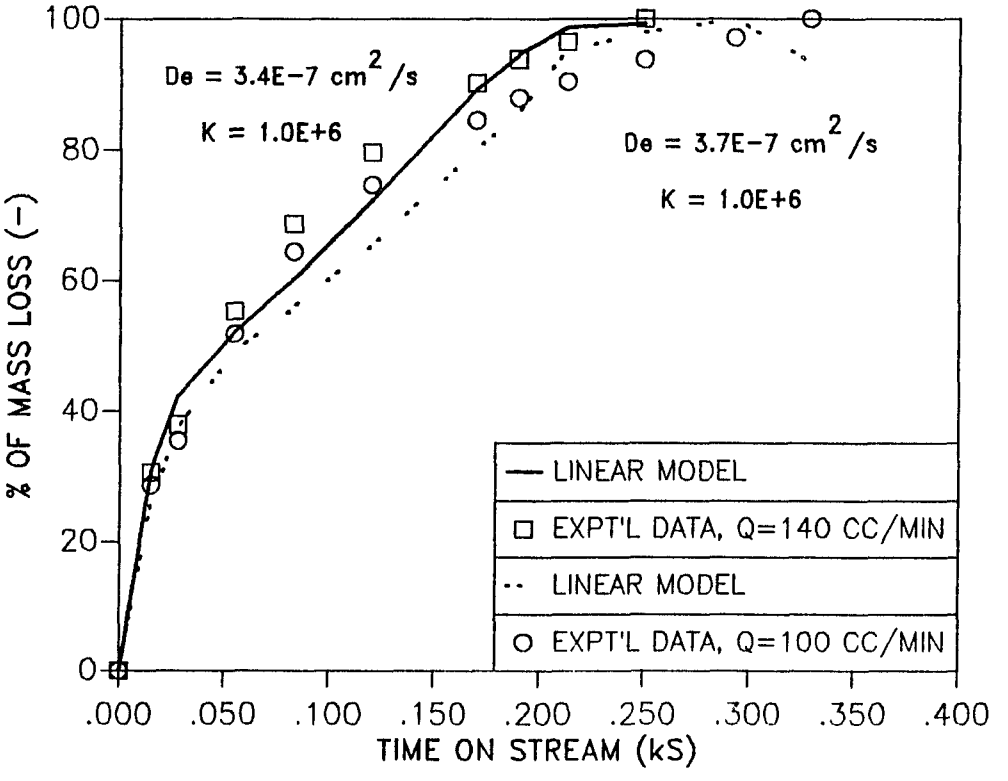

Figure 4.31, Fit Eic and Ruthven's Data for o-Xylene by LINEAR Model, 50 um NaX

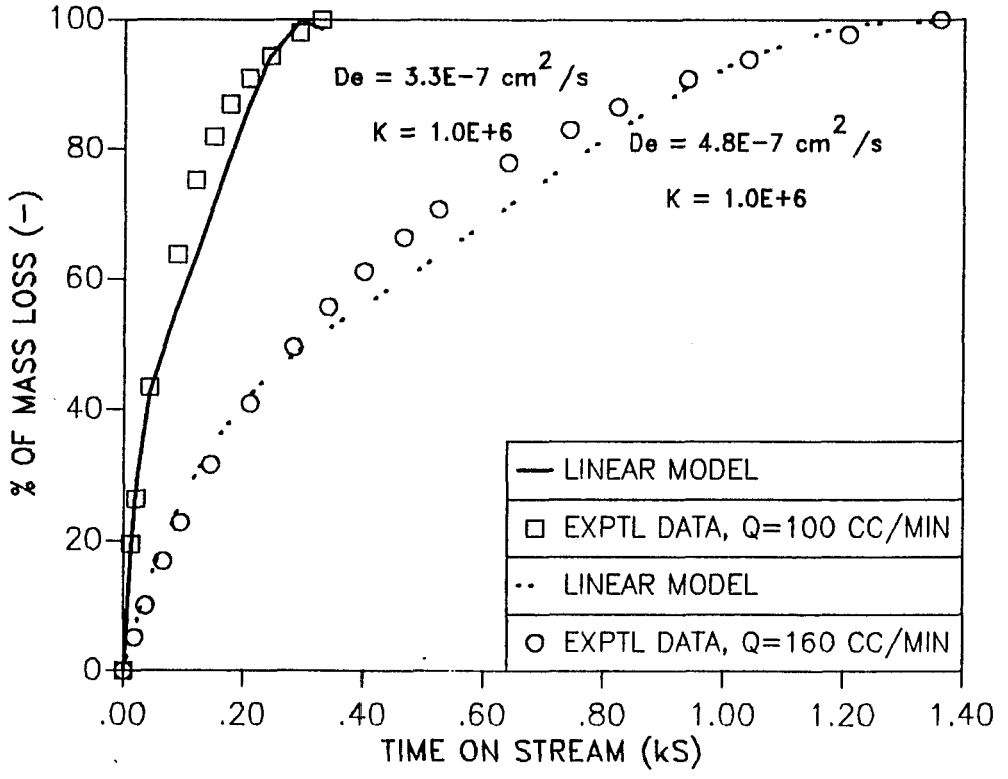

Figure 4.32, Fit Eic and Ruthven's Data for o-Xylene by LINEAR Model, 100 um NaX

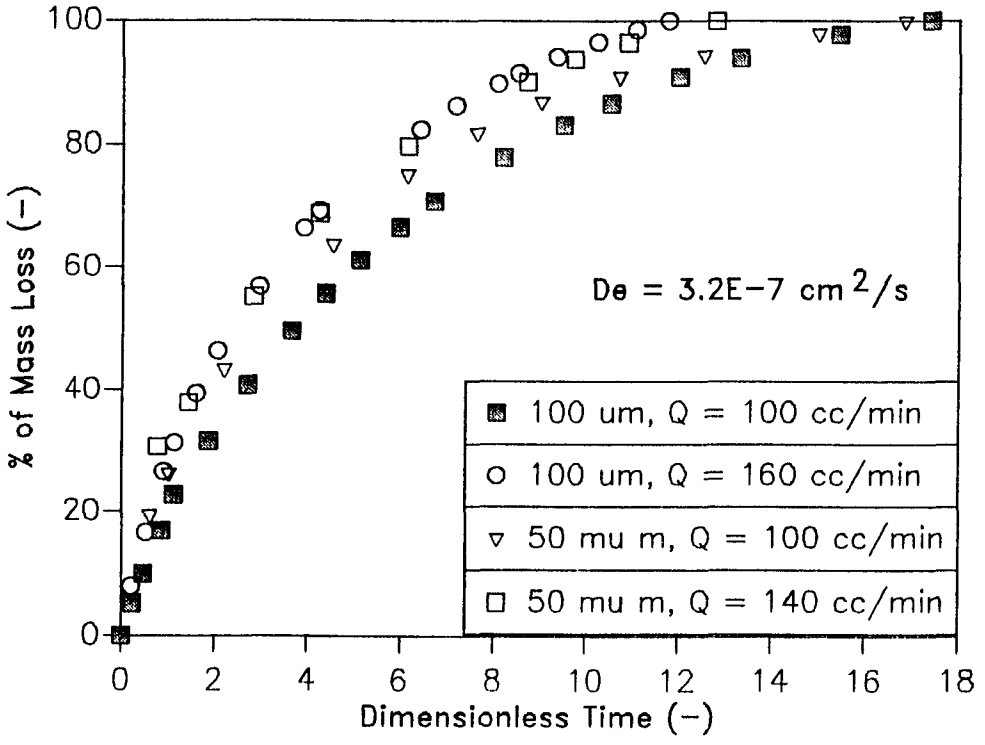

Figure 4.33, o-Xylene Desorbed from NaX.

that the regressed D_e and K values are insensitive to the variation of S. Therefore, a S value of 0.5 was used in the regression routine.

4.1.5 Comparisons of the ID Models

Before one proceeds to compare the regression results for the ID models, it is necessary to examine the basic assumptions employed in the conventional techniques (e.g., uptake rate measurements, chromatography, and tracer exchange method) used to estimate intracrystalline diffusivity and the assumptions used in various TPD systems in the literature. Then one can make comparsions between these systems and the ID models developed in this work and check the validity of each ID model.

For an uptake experiment, if the perturbation in adsorbate concentration is differential and D_e is independent of concentration, then the external surface concentration can be assumed constant or to follow Henry's law. Then the sorption system can be depicted mathematically either by the CDCC or the ZLC model and the uptake curve is given by eq. (4-10) or (4-17).

The conventional chromatography technique derives D_e from the dynamic response of a packed column to a change in sorbate concentration. The flow through a packed bed may be adquately described by an axial dispersion-plug flow model (Ruthven, 1984), and the adsorption rate can be obtained from the mass balance for an adsorbent particle. The equilibrium between the adsorbate and adsorbent is generally governed by either a linear (Henry's law) or Langmuir isotherm, and the solutions for the breakthrough curves assuming various equilibrium isotherms are available in the literature (Gary and Ruthven, 1974; Ruthven, 1984). However, the dynamic response is insensitive to D_e unless axial dispersion can be minimized.

The tracer exchange technique is a modified uptake rate experiment, and the self-diffusivity is measured by exposing the adsorbent to a change in the concentration of an isotopically labeled tracer at constant adsorbate concentration. The external surface concentration is approximately constant, therefore the system can again be described by the CDCC model and the exchange curve should follow eq. (4-10).

In conclusion, the CDCC model is widely used in describing systems with differential step changes, both in uptake rate measurement and tracer exchange. The experimental uptake and exchange curves generally agree well with eq. (4-10), if no significant readsorption effects exist in the systems under study. If the external surface concentration of adsorbent remains at equilibrium and follows a linear (Henry's law) or Langmuir isotherm, then the system can be described by models similar to the ZLC model.

In early stages of the development of TPD, diffusion effects were neglected and the desorption cell was treated as a differential bed (Cvetanovic and Amenomiya, 1967, 1972; Falconer and Schwarz, 1983); with these assumptions, the kinetics parameters associated with the adsorption process can be estimated.

Several investigators (Herz et al., 1982; Gorte, 1982; Rieck and Bell, 1984; Tronconi and Forzatti, 1986, 1987; Huang et al., 1988; Forni and Magni, 1988a; Balkenende et al., 1989) have considered both diffusion and readsorption effects during TPD experiments. The mathematical models they developed resemble the ID model, eqs. (4-3) to (4-5), except that (1) different boundary conditions were sometimes used at the external surface of the adsorbent particle; and (2) different assumptions were imposed for the adsorption and desorption processes. All the investi-

gators assumed that the desorption cell is either close to equilibrium (Herz et al., 1982; Gorte, 1982; Rieck and Bell, 1984; Tronconi and Forzatti, 1986, 1987) or that the external surface concentration of the adsorbent particle is a constant (Huang, et al., 1988; Forni and Magni, 1988a, Balkenende et al., 1989). Therefore, the TPD models used in the literature are similar to either the CDCC or ZLC models, and the solutions they obtained for the percent of mass loss are similar to eqs. (4-10) or (4-17). It is interesting to note that D_e's predicted by Forni and Magni (1988) by a model similar to the CDCC model are much smaller than those predicted by other techniques. This supports the present argument that the CDCC model is not suitable to analyze a system with significant readsorption.

The regressed diffusivities for toluene and benzene, as predicted by fitting experimental ID spectra to the four ID models, are summarized in Table 4.6. The values of D_e increased on going from the CDCC to the Linear model by one or two orders of magnitude for each model. An F-test comapring the four models showed that the extra parameter in the CDVC, ZLC and Linear models is in general statistically significant at the 95% confidence level, compared to the one parameter (CDCC) model. The results also showed that for the fitting of toluene ID spectra all three two parameter models are in general indistinguishable at 95% confidence level. However, for the fitting of benzene ID spectra, an F-test showed that the CDVC and Linear models are statistically superior to the ZLC model at the 95% confidence level, while the CDVC and Linear models are indistinguishable. Finally, for the fitting of Eic and Ruthven's (1988) data, the ZLC model is statistically superior to the Linear model at the 95% confidence level, while the CDVC and ZLC models are indistinguishable.

System(1)	CDCC $D_e \times 10^{14}$ cm^2/s	CDVC same	ZLC $D_e \times 10^{11}$ cm^2/s	LINEAR same	KINETICS same
	Whole	Falling	Falling	Falling	Whole	
L/Toluene	1.1	1.4	1.1	0.69	220	0.004 - 10.0
Ω/Toluene	8.8	10.0	0.39	2.10	5300	1.50 - 0.20
P1/Toluene	36.	37.	1.8	22.0	3200	-
Y-52/Toluene	7.4	8.8	10000.	1.0	740	0.42 - 0.0008
105-6/Toluene	2.0	2.3	5.6	0.10	240	3.3 - 0.25
P1/Benzene	55.	87.	2.9	16.0	6300	-
105-6/Benzene	3.1	3.5	0.26	1.1	800	-
NaX/o-xylene(2)	-	-	2700	3000	3700	-
NaX/o-xylene(3)	-	-	2500	2400	4800	-

(1) All data from this work at 623 K.
(2) 50 μm crystal, Eic and Ruthven (1988), 493 K.
(3) 100 μm crystal, Eic and Ruthven (1988), 493 K.

Table 4.6. Summary of Regressed Diffusivities Obtained in This Study

The above conclusion is supported by comparing the percent of mass loss vs. time plots shown in Sections 4.1.1 to 4.1.4. These figures show clearly that the CDCC model gave the worst fits to the data while the other three models gave similar fits (compare the relative deviations listed in Tables 4.3 to 4.5).

Table 4.6 also shows the trend of toluene diffusivities in the zeolite series used in this study. For all models except the CDVC, the trend can be explained in terms of the zeolites' pore geometry and chemical composition.

As listed in Table 2.1, the free apertures of the zeolite series are: L (0.71 nm), Ω (0.76 nm), Y (0.74 nm), and P1 and 105-6 (0.54 x 0.56 nm). The geometries of the pore networks were discussed in Section 1.3.3; Y, P1 and 105-6 have three-dimensional pore systems, while L and Ω have only one-dimensional pore systems. Generally, for zeolites with similar-sized free apertures, the more intersections of the pore network, the more rapid the diffusion.

The zeolites used in this study were converted to hydrogen form using conventional ion exchange techniques. The process can exchange almost 100 % of the sodium or potassium cations with ammonium cations for Ω, Y, P1 and 105-6 zeolites, but 20 % of the potassium cations of an L zeolite cannot be removed even by exhaustive ion exchange treatment (Linde fact sheet, 1977). Therefore, one should expect these unexchanged potassium cations to partially block the unidirectional channels of the L zeolite.

The final consideration is the presence of impurities in the zeolite. From X-Ray diffraction analysis of the Linde zeolites, it was found there were no significant amounts of impurities in the samples. On the contrary, the P1 zeolite may contain some amorphous material, as suggested by the

lower BET surface area listed in Table 3.1 and the slight broadening of some peaks in the X-Ray diffraction pattern shown in Fig. 3.3. This amorphous phase would undoubtedly include larger pores than those found in a purely crystalline pentasil. Therefore, one should expect a diffusivity in P1 to be larger than that in the 105-6 zeolite. But the extent of this effect is difficult to predict.

The observed order for the regressed diffusivities is P1 > Ω > Y > 105-6 > L for the CDCC model; Y > 105-6 > P1 > L > Ω for the CDVC model; P1 > Ω > Y > L > 105-6 for the ZLC model; and Ω > P1 > Y > 105-6 > L for the Linear model. Therefore, all the ID models (except CDVC) generally do show a similar order of diffusivities in a zeolite series, P1 > Ω > Y > 105-6 > L, with the order of the P1/Ω and 105-6/L pairs reversed in the Linear and ZLC models, respectively. It is evident that the residual potassium cations in the L zeolite restrict diffusion in the unidirectional channels.

It is concluded that the CDCC and CDVC models cannot physically explain the experimental spectra obtained in this study because both do not adequately take into account readsorption effects, and in addition the CDCC model does not account for variation of external surface coverage. Only the ZLC and Linear models, which consider both variation of external surface coverage and readsorption effects, can adequately correlate the ID spectra obtained in this work.

The Linear model is probably superior to the ZLC model because, first, the Linear model is suitable for analysis of systems with or without readsorption (during isothermal desorption) by adjustment of the parameter τ_4 . This was verified by its capability to fit both the spectra obtained in this work and those obtained by Eic and Ruthven. On the

contrary, the ZLC model analysis, at least as initially employed by Eic and Ruthven, cannot reproduce any experimental data (see Figs. 4.24 and 4.25). Secondly, the regressed diffusivities from the present data obtained by the Linear model are two to three orders of magnitude larger than the corresponding values obtained from the ZLC model. Hence, the diffusivities reported by the Linear model are much closer to diffusivities (Tables 4.7 and 4.8) measured by the PFG (NMR) technique. In conclusion, the ZLC technique does offer an easier method to estimate D_e than most of the conventional techniques (e.g., uptake rate measuremants and the conventional chromatography method). But the basic assumptions employed to develop the model are not justified, and it is not applicable to systems without equilibrium readsorption.

Further information that can be extracted from Tables 4.1 to 4.5 are the diffusional time constants, D_e/R^2, for the pentasils, P1 and 105-6, and NaX with different crystallite sizes. The diffusional time constants should vary inversely as the square of the crystal radius, as reported in the literature, for diffusivities determined by both sorption (Goddard and Ruthven, 1986 a; Shah et al., 1988) and tracer exchange methods (Goddard and Ruthven, 1986 b). The diffusional time constants for toluene and benzene in 105-6 and P1, as predicted by all four models, do not show the expected variation. This deviation arises from: (1) an amorphous phase exists in the P1 zeolite, which includes larger pores than those found in a purely crystalline zeolite, and the effect of these larger pores is to increase D_e for P1; (2) the existence of a rate-controlling step in addition to intracrystalline diffusion; the SiO_2/Al_2O_3 ratios are 28 and 43 for P1 and 105-6 zeolites, respectively, which indicates the two pentasils may have different adsorption capacities and different K-

values. But due to the serious interaction between D_e and K in some of these models, the regressions cannot completely distinguish different K's, and so give different D_e values as well. Therefore, the differences between the regressed diffusivities in P1 and 105-6 zeolites arise from structural and chemical factors, not from problems with the numerical analysis. This argument is supported by the fact that the ZLC data fitted to the CDVC, ZLC and Linear models do show the expected behavior of the diffusional time constants for o-xylene diffusing in two different sizes of NaX crystals, as listed in Tables. 4.3, 4.4 and 4.5; these two samples did not differ in Si/Al ratio or crystallinity, only in R.

The toluene and benzene diffusivities regressed from the Linear model are compared with the literature data listed in Tables 4.7 and 4.8. These tables only contain experimental diffusivities for X, Y and pentasil zeolites. There exist no diffusivity data for aromatics in L or Ω zeolites available in the literature. One should note that all the diffusivities (except those from Forni and Viscardi, 1986) reported in Tables 4.7 and 4.8 are at lower temperature and should be extrapolated to 623 K to make reasonable comparisons with the diffusivities obtained from Linear model. The upper and lower limits of the extrapolated D_e's are $D = D_0 \exp(\frac{-E_D}{RT})$ for an activated configurational diffusion and $D = D_0 T^{0.5}$ for Knudsen diffusion, respectively. The lower limit extrapolation increases the diffusivities by half an order of magnitude at 673 K (for a 200 - 300 K increase in temparature), while the upper limit extrapolation increases the diffusivities by one to two orders of magnitude. The regressed toluene and benzene diffusivities (Linear model) for the pentasils 105-6 and P1 are therefore similar in magnitude to the diffusivity data obtained by a Chromatographic technique at 673 K by Forni

Adsorbate	Adsorbent	P (kPa)	T (K)	D_e (cm^2/s)	Technique
ZSM-5	Toluene	101	673	3.1×10^{-9}	Chrom. (1)
ZSM-5	p-xylene	101	673	7.8×10^{-9}	Chrom. (1)
ZSM-5	p-xylene	-	303	1.0×10^{-11}	Adsorp. (2)
Y	p-xylene	101	298	5.3×10^{-13}	Adsorp. (3)
ZSM-5	p-xylene	-	313	1.9×10^{-11}	Adsorp. (4)
ZSM-11	p-xylene	-	313	2.8×10^{-11}	Adsorp. (4)
NaX	p-xylene	-	400	5.0×10^{-7}	PFG NMR (8)
NaX	p-xylene	-	400	2.5×10^{-9}	Tracer (9)
Silicalite	p-xylene	101	473	9.8×10^{-11}	Adsorp. (5)
13X	p-xylene	-	323	1.1×10^{-12}	Adsorp. (6)
NaX	Toluene	-	463	4.0×10^{-6}	PFG NMR (7)

(1) Forni and Viscardi, (1986).
(2) Post, et al., (1983).
(3) Moore and Katzer, (1972)
(4) Le van Mao et al., (1983).
(5) Wu, et al., (1983).
(6) Ragaini, et al., (1984).
(7) Karger and Ruthven (1988).
(8) Germanus, et al., (1985).
(9) Goddard and Ruthven, (1986b).

Table 4.7. Literature Intracrystalline Diffusivities for Toluene and p-Xylene

Adsorbate	Adsorbent	P (kPa)	T (K)	D_e (cm^2/s)	Technique
ZSM-5	Benzene	101	673	3.5×10^{-9}	Chrom. (1)
ZSM-5	Benzene	-	303	8.6×10^{-12}	Adsorp. (2)
ZSM-5	Benzene	101	313	2.5×10^{-10}	Adsorp. (3)
Silicalite	Benzene	101	373	5.6×10^{-11}	Adsorp. (4)
Silicalite	Benzene	-	386	5.0×10^{-10}	Tracer (5)
NaX	Benzene	-	393	1.5×10^{-7}	PFG NMR (5)
NaX	Benzene	-	423	2.0×10^{-7}	PFG NMR (5)
NaX	Benzene	-	403	4.0×10^{-8}	ZLC (6)

(1) Forni and Viscardi, (1986).
(2) Post et al. (1983).
(3) Doelle et al. (1981).
(4) Wu et al. (1983).
(5) Karger and Ruthven (1988).
(6) Eic et al. (1988).

Table 4.8. Literature Intracrystalline Diffusivities for Benzene

and Viscardi (1986). It is also evident from the Tables that the diffusivities derived from the Linear model lie between diffusivities estimated from adsorption and PFG (NMR) techniques, but the latter are one to three orders of magnitude larger for benzene and toluene. The differences in the adsorptive uptake D_e's and the present D_e 's can be explained by the temperature differences in the experiments; however, the differences with the NMR data can not be explained by any differences in experimental conditions (temperature, coverage). This is especially true since extrapolating the PFG-NMR measurements to higher temperatures magnifies the disagreement with the numbers in Table 4.6. It remains to be seen whether the remaining discrepancies in diffusivities obtained by the Linear model and by PFG NMR can be explained by any of the reasons listed in Section 1.2.2.

4.2 A Diffusion-Reaction Model for Toluene Disproportionation

The goal of this section is to estimate D_e from the diffusion controlled kinetics data of toluene disproportionation. For reaction to occur in bidisperse porous catalysts, the reactants must diffuse through the stagnant film external to the catalyst particle, then through the macropores, then adsorb on the microparticles, and finally diffuse into the microparticle to find access to the active sites. Therefore, effectiveness factors for bidisperse catalysts depend upon the rate of diffusion of reactants and products both in the macro and micropore regions as well as on the rate of reaction. A micro-macroporous diffusion-reaction model is formulated to account for the relationship between the rates of different transport processes and the rate of reaction.

4.2.1 Diffusion-Reaction Model Equations

As discussed in Section 1.4.3, for catalysts with bidisperse pore structure the microparticle can be treated as a separate aggregate, and diffusion occurs through the macropores surrounding the microparticles and in series fashion into the microparticles.

The conservation equation for a microparticle is shown in eq. (1-25). For the general case of concentration-dependent diffusivity D_μ and an unspecified intrinsic rate expression $r(C_\mu)$, eq. (1-25) has been solved for slab geometry to yield the solution in the form of eqs. (1-27) and (1-28). The observed rate of adsorption onto a microparticle is given by η_μ times $r(C_\mu{}^s)$, the "kinetics rate" evaluated at the microparticle surface.

The microparticle transport equations for the limiting reactant must be coupled to a mass balance for the limiting reactant in a macroparticle. At steady state, the transport rate of the limiting reactant into the microparticle equals the observed microparticle reaction rate. On a total particle basis this rate is eq. (1-36). The macroparticle mass balance on the limiting reactant is shown in eq. (1-38). The ε_M in eq. (1-38) is used to convert the basis from open volume to macroparticle volume. This equation is similar to eq. (1-25) and is solved similarly for slab geometry to yield:

$$\eta_M = \frac{\sqrt{2}}{LR(C_M{}^s)} \left[\int_{C_M}^{C_M{}^s} D_M(1 - \varepsilon_M)\, r(C_\mu{}^s)\, dC \right]^{0.5} \qquad (4-29)$$

where

$$L = \int_{C_M^0}^{C_M^s} \frac{D_M \, d\alpha}{\left[2\int_{C_M^0}^{\alpha} D_M(1-\varepsilon_M)\eta_\mu \, r(C_\mu^s)\, dC\right]^{0.5}} \qquad (4-30)$$

The diffusion length L in eq. (4-30) is the particle volume divided by the external surface area for a macroparticle. C_M^0 is the macroparticle centerline concentration and C_M^s the particle external surface concentration. For strong resistance to diffusion in macropores, C_M^0 is the concentration at thermodynamic equilibrium, C_M^{eq}.

The overall diffusion-reaction modulus for a system with an irreversible second-order reaction, $r(C_\mu) = kC_\mu^2$, and constant diffusivities D_μ and D_M, can be derived as:

$$\varphi = \left(\frac{1}{\eta_M}\right)_{C_M^0 = C_\mu^0 = 0}$$

$$= \left[\left(\frac{3}{2}\frac{kC_M^s}{D_M}\right)^{0.5} \frac{L}{(1-\varepsilon_M)^{0.5}}\right]\left[\left(\frac{\frac{3}{2}kC_\mu^s}{D_\mu}\right)^{0.5} 1\right]^{-0.5} \qquad (4-31)$$

$$= \varphi_M \varphi_\mu^{-0.5}$$

This formulation takes into account the bidispersity of the pore size distribution in the pellet-form zeolite catalyst, and allows for decoupling of the microparticle-macropore transport phenomena, resulting in simple individual mass transfer moduli. For the more complex kinetics (second-order reversible) and diffusivity relationships (non-constant D_M) necessary in the present work, the decoupling is much more difficult.

4.2.2 Applying the Model to Pellet-Form Zeolites

The rate constant and microparticle counterdiffusivity for the toluene disproportionation reaction can be estimated by applying the micro-macroporous diffusion-reaction model to the $k\eta$ values (computed using eq. (3-10)). The $k\eta$ values from two experiments using different catalyst sizes are sufficient to evaluate k and η (and therefore D_e) separately, provided both effectiveness factors are not so low as to be in the range where $\eta = 1/\varphi$ (Smith, 1981).

Before we can estimate intracrystalline diffusivity and rate constant from the $k\eta$'s, three problems must be addressed:

1. The intrinsic reaction kinetics must be specified.

2. The equilibrium relationship between gas-phase and a microparticle surface concentration must be specified.

3. The relationships between macropore effective diffusivities and bulk and Knudsen diffusivities, fluxes of reactants and products, and particle geometry must be specified.

In Section 1.3.2, it was concluded that when purely acidic catalysts were used for toluene disproportionation, the reaction follows approximately a second-order rate expression at low P_T. For this study, a low P_T of 0.1 bar was used for all the kinetics experiments. Therefore, the rate expression for reaction within the zeolite microparticles is taken to be

$$r(C_\mu) = kC_\mu^2 \qquad (4-32)$$

The microparticle surface concentration, $C_\mu{}^s$, must be calculated from the equilibrium isotherm; the exact equilibrium relationship depends on both the structure and chemical nature of the zeolite, but the sorption equilibrium can always be represented by the Langmuir isotherm:

$$\frac{C_\mu{}^s}{(C_\mu)_{max}} = \frac{KC_M}{1 + KC_M} \qquad (4 - 33)$$

where $(C_\mu)_{max}$ is the maximum number of molecules at $\theta = 1.0$, which can be estimated either from the maximum possible number of molecules per unit cell or the liquid density of adsorbate. The $(C_\mu)_{max}$ value used was the liquid phase density of toluene (here calculated at its boiling point of 383.6 K, 8.54×10^{-3} mol/cm^3). The $(C_\mu)_{max}$ value is not critical because altering $(C_\mu)_{max}$ only affects the ultimate value of K and not those of k and D_μ. The K-values predicted by the Linear model (Table 4.5) were used as initial guesses. The actual K-values ultimately used in the calculations were those giving realistic $C_M{}^0$ ($C_M{}^0 > C_M{}^{eq}$) and η_M ($0.01 < \eta_M < 1.0$). It should be noted that for zeolites the linear partition coefficients (κ_p) are always > 1 and therefore eq. (1-12) is not applicable.

The final problem is to find a model to relate an effective D_M to bulk and Knudsen diffusivities and pore geometry. One way to handle varying macropore sizes is to use the parallel crosslinked pore theory in its most limiting form, i.e., assume a constant macropore tortuosity, τ_M, and calculate the macropore diffusivity as follows:

$$\bar{D}_M \varepsilon_M = \int_0^{\varepsilon_M} D_M(r) d\varepsilon_M(r) / D_M{}^0 \qquad (4 - 34)$$

where the cumulative pore-size distribution data of the catalyst are required to calculate the integral.

Before applying the model it is necessary to determine if the catalyst structures satisfied the basic assumptions of the model. The most important assumption for this model is that the pore diameters should be large relative to the critical diameters of the diffusing molecules. All the macropore size distributions satisfy this assumption because the smallest macropore in each system is about 4 nm, which is approximately 7 times larger than the toluene critical diameter. It is possible to determine the dominant diffusion mechanism, bulk or Knudsen, in different regions of the measured macropore size distribution. The bulk diffusivity is independent of the pore radius and can be estimated by eq. (1-4). The relationship between Knudsen diffusivity and pore radius can be computed by eq. (1-5). At each pore size range, the diffusion mechanism with smaller diffusivity should be the dominant one. The calaulated results are given in Table 4.9, which shows that Knudsen diffusion is the controlling mechanism for the reaction mixture diffusing in the macropores of the four types of zeolite pellets. The calculated macropore diffusivities varied from roughly 1.1×10^{-3} cm^2/s in zeolite 105-6 to 7.3×10^{-3} cm^2/s in zeolite L.

Another approach to handling varying macropore sizes is to use Effective Medium Theory (EMT) with the Smooth Field Approximation (Burganos and Sotirchos, 1987; Sotirchos and Burganos, 1988). EMT assumes that all pore networks can be transformed into an effective network built with two- or three- dimensional lattices. Then the EMT for resistor networks can be used to find the effective conductance of each pore, g_e , in a uniform

network that represents approximately the same resistance to diffusion as the original network. The effective conductance can be computed from:

$$\int \frac{g(r) - g_e}{g(r) + (\frac{Z}{2} - 1) g_e} F(r)\, dr = 0 \qquad (4-35)$$

where $g_i = \frac{D_i \pi r_i^2}{l_i}$ is the condutance of the pore i, l_i is length of the pore i, Z is the coordination number (i.e. number of pores intersecting at each node), and F(r) is the probability density of pore volumes. For an effective network of pores of uniform length, a material balance at the nodes leads to:

$$\sum_i n_i \cdot \nabla C = 0 \qquad (4-36)$$

The Smooth Field Approximation (SFA) assumes that the concentration gradient in a pore can be represented by the vector projection of the macroscopic concentration gradient on the pore axis. Therefore, the Smooth Field Approximation states that:

$$\Delta C_i = l_i n_i \cdot \nabla C \qquad (4-37)$$

Then applying the SFA gives the following effective diffusivity:

$$D_e^{E-S} = \frac{\varepsilon}{\tau} \frac{\langle D(r) r^2 \rangle_e}{\langle r^2 \rangle} \qquad (4-38)$$

Using Knudsen diffuion as the controlling mechanism for diffusion in the macropore network gives

$$D_e^{E-S} = \frac{\varepsilon}{\tau} \frac{2}{3} \left(\frac{8RT}{\pi(MW)} \right)^{0.5} \frac{\langle r^3 \rangle_e}{\langle r^2 \rangle} \qquad (4-39)$$

r (nm)	Components	Overall Binary Diffusivity (cm^2/s)	Knudsen Diffusivity (cm^2/s)
For Zeolite L, Ω, and 105-6			
1.5	He-Toluene	3.7×10^{-3}	4.0×10^{-3}
2.5	He-Toluene	6.1×10^{-3}	6.7×10^{-3}
3.5	He-Toluene	8.6×10^{-3}	9.3×10^{-3}
4.5	He-Toluene	1.1×10^{-2}	1.2×10^{-2}
7.5	He-Toluene	1.8×10^{-2}	2.0×10^{-2}
15	He-Toluene	3.6×10^{-2}	4.0×10^{-2}
25	He-Toluene	5.9×10^{-2}	6.7×10^{-2}
40	He-Toluene	9.3×10^{-2}	1.1×10^{-1}
For zeolite L:			
$D_M = 7.30 \times 10^{-3}$ cm^2/s (parallel crosslinked pore model)			
$D_M = 3.32 \times 10^{-4}$ cm^2/s (EMT model with Smooth Field Approximation)			
For zeolite Ω:			
$D_M = 4.07 \times 10^{-3}$ cm^2/s (parallel crosslinked pore model)			
$D_M = 1.87 \times 10^{-4}$ cm^2/s (EMT model with Smooth Field Approximation)			
For zeolite 105-6:			
$D_M = 1.08 \times 10^{-3}$ cm^2/s (parallel crosslinked pore model)			
$D_M = 1.34 \times 10^{-4}$ cm^2/s (EMT model with Smooth Field Approximation)			
For Zeolite Y			
1.5	He-Toluene	z10	3.7×10^{-3}
2.5	He-Toluene	z11	6.2×10^{-3}
3.5	He-Toluene	z12	8.7×10^{-3}
4.5	He-Toluene	z13	1.1×10^{-2}
7.5	He-Toluene	z14	1.9×10^{-2}
15	He-Toluene	z15	3.7×10^{-2}
25	He-Toluene	z16	6.2×10^{-2}
40	He-Toluene	z17	1.0×10^{-1}
$D_M = 3.38 \times 10^{-3}$ cm^2/s (parallel crosslinked pore model)			
$D_M = 1.62 \times 10^{-4}$ cm^2/s (EMT model with Smooth Field Approximation)			

Table 4.9. Macropore Diffusivities in Zeolite Pellets at 693 K

network that represents approximately the same resistance to diffusion as the original network. The effective conductance can be computed from:

$$\int \frac{g(r) - g_e}{g(r) + (\frac{Z}{2} - 1) g_e} F(r)\, dr = 0 \qquad (4-35)$$

where $g_i = \frac{D_i \pi r_i^2}{l_i}$ is the condutance of the pore i, l_i is length of the pore i, Z is the coordination number (i.e. number of pores intersecting at each node), and F(r) is the probability density of pore volumes. For an effective network of pores of uniform length, a material balance at the nodes leads to:

$$\sum_i n_i \cdot \nabla C = 0 \qquad (4-36)$$

The Smooth Field Approximation (SFA) assumes that the concentration gradient in a pore can be represented by the vector projection of the macroscopic concentration gradient on the pore axis. Therefore, the Smooth Field Approximation states that:

$$\Delta C_i = l_i n_i \cdot \nabla C \qquad (4-37)$$

Then applying the SFA gives the following effective diffusivity:

$$D_e^{E-S} = \frac{\varepsilon}{\tau} \frac{\langle D(r) r^2 \rangle_e}{\langle r^2 \rangle} \qquad (4-38)$$

Using Knudsen diffuion as the controlling mechanism for diffusion in the macropore network gives

$$D_e^{E-S} = \frac{\varepsilon}{\tau} \frac{2}{3} \left(\frac{8RT}{\pi(MW)} \right)^{0.5} \frac{\langle r^3 \rangle_e}{\langle r^2 \rangle} \qquad (4-39)$$

where $\langle r^3 \rangle_e$ is an effective medium average and $\langle r^2 \rangle$ is an arithmatic average.

The macropore diffusivities predicted by the EMT model with the SFA, i.e. eq. (4-39), are also listed in Table 4.9. These D_M's are an order of magnitude smaller than those predicted by the parallel crosslinked pore model. The discrepancies between these two models are due to the fact that the diffusion resistances in a network are intermediate to parallel and series combinations of the individual diffusion resistances (Burganos and Sotirchos, 1987). The parallel crosslinked pore model always assumes that the resistances to mass transport in the network are combined in parallel, and the EMT model with the SFA assumes resistances ranging from purely series ($Z = 2$) to purely parallel ($Z \rightarrow \infty$) in the network. A "Z" value of 3 was used in this study, which implies the mass transport is mostly in series. Therefore, the parallel crosslinked pore and EMT models represent two extremes for transport in the macropore network, and the D_M's obtained from these two models should span the possible D_M values. The D_M's from these two models are used seperately in the following algorithm and the intracrystalline diffusivities obtained from these calculations should also represent the possible range of D_μ .

Since η is a function of kinetics and diffusional parameters, it often requires trial and error procedures to estimate k and η individually. The procedure adopted here uses two sets of $k\eta$ values (Tables 3.8 and 3.9) for powder and pellet-form zeolites. Since there are only two $k\eta$ values for each zeolite, the intracrystalline diffusivity and rate constant were calculated directly, making reasonable assumptions about K. The algorithm employed in this study is as follows:

1. Assume the rate constant, k, in units of $\frac{cm^6}{g - s - mol.}$,

2. Assume the intracrystalline diffusivity, D_μ, in $\frac{cm^2}{s}$,

3. Compute η_μ at the external surface by the collocation method discussed in Section 1.4.1 (Villadsen and Michelsen, 1978). Adjust D_μ until $(\eta_\mu)_{calc} = (\eta_\mu)_{exptl}$,

4. Using the reaction equilibrium constant and initial feed compositions, compute C_M^{eq} as an initial guess for C_M^0 ,

5. Add 16 additional equally spaced points, C_M, between C_M^s and C_M^{eq} , where

$$C_M(i) = C_M^0 + \frac{C_M^s - C_M^0}{18}(I - 1) \quad \text{for} \quad I = 1, 2, \text{-------}, 18 \qquad (4 - 40)$$

Then C_μ^s at these additional points were computed by eq. (4-33) with the values of the equilibrium constant, K, obtained from the predictions of the Linear model (Table 4.5), as well as from literature data (Barthomeuf and Ha, 1973; Ruthven and Doetsch, 1976; Forni and Viscardi, 1986),

6. Compute η_μ at these extra points by the collocation method used in step 3,

7. Solve the macropore mass balance equation, eq. (1-46), using the LSODE package for solution of simultaneous ordinary differential equations

(Hindmarsh, 1980). In order to apply LSODE to eq. (1-46), one has to convert the original equation into two first order ODE's as:

$$\frac{dY_1}{dz} = \frac{Y_2}{D_M} \qquad (4-41a)$$

$$\frac{dY_2}{dz} = R(C_M) = \eta_\mu k(C_\mu{}^s)^2(1-\varepsilon_M) \qquad (4-41b)$$

with

$$Y_1(0) = C_M{}^0 \qquad (4-41c)$$

$$Y_2(0) = 0 \qquad (4-41d)$$

where $Y_1 = C_M$ and $Y_2 = D_M \frac{dC_M}{dz}$. LSODE integrates the ODE's from $z = 0$ to $z = L$. If $(C_M{}^s)_{calc} \neq (C_M{}^s)_{exptl}$, $C_M{}^0$ is adjusted and the algorithm loops back to step 5,

8. Compute the macropore effectiveness factor, η_M, by eq. (4-29). If $(\eta_M)_{calc} \neq (\eta_M)_{exptl}$, loop back to step 1.

The parameters computed by this algorithm are listed in Tables 4.10 and 4.11. For each set of kinetics data there exists a range of K-values that could give reasonable estimates of η_M and η_μ. Using K-values larger than the upper limit listed in the tables would result in an unreasonably small η_M ($\eta_M << 0.01$), because a large K predicts a large $C_\mu{}^s$, which in turns implies a high reaction rate and large concentration gradient in the macropores. Under these conditions, the calculated $C_M{}^0$ is smaller than the corresponding $C_M{}^{eq}$, which is thermodynamically impossible. On

Catalyst	K (-)	η_M	η_μ	D_μ ($\frac{cm^2}{s}$)	k ($\frac{cm^6}{g - s - mol}$)
L	50000	0.065	0.283	7.76×10^{-13}	5.26×10^{4}
L	20000	0.217	0.946	2.98×10^{-11}	1.57×10^{4}
Ω	700000	0.0079	0.965	3.78×10^{-10}	1.70×10^{4}
Y-52	600000	0.0183	0.587	1.19×10^{-12}	7.33×10^{3}
Y-52	400000	0.0253	0.795	3.11×10^{-12}	5.30×10^{3}
105-6	600000	0.0067	0.330	2.99×10^{-13}	1.10×10^{4}
105-6	200000	0.0175	0.834	2.70×10^{-12}	4.27×10^{3}

Table 4.10. Computational Results for Toluene Disproportionation Reaction Using D_M from Parallel Crosslinked Pore Model.

Catalyst	K (-)	η_M	η_μ	D_μ ($\frac{cm^2}{s}$)	k ($\frac{cm^6}{g - s - mol}$)
L	10000	0.047	0.203	5.03×10^{-13}	7.35×10^{4}
L	5000	0.110	0.471	1.68×10^{-12}	3.10×10^{4}
Ω	1000000	0.0006	0.070	5.58×10^{-13}	2.35×10^{5}
Ω	600000	0.0008	0.102	1.47×10^{-12}	1.61×10^{5}
Y-52	200000	0.0026	0.082	5.47×10^{-14}	5.23×10^{4}
Y-52	50000	0.022	0.707	1.85×10^{-12}	6.08×10^{3}
105-6	200000	0.0045	0.217	1.70×10^{-13}	1.66×10^{4}
105-6	60000	0.0175	0.834	2.71×10^{-12}	4.27×10^{3}

Table 4.11. Computational Results for Toluene Disproportionation Reaction Using D_M from EMT Model with the SFA.

the other hand, using K-values smaller than the corresponding lower limit results in $\eta_\mu > 1$, which is unrealistic for an endothermic reaction.

The reaction rate constants obtained from this study and from the literature are listed in Table 4.12, and corresponding reaction rates are listed in Table 4.13. The rate constants obtained in this study are of the same order of magnitude as second order rate constants obtained from the literature for zeolite-catalyzed toluene disproportionation. Note that the B_2O_3/Al_2O_3 catalyst of Izumi and Shiba (1964) is not a zeolite. These results suggest that the present method can be used to estimate reaction rate constants from diffusion-controlled rate data. The validity of the method is also confirmed by the rough agreement between the initial rate data of this work and literature rate data for zeolite-catalyzed toluene disproportionation.

The rate constants listed in Table 4.12 suggest that the activities for the toluene disproportionation reaction of the zeolites used in this study follow the order L > Ω > 105-6 > Y-52 (based on the average of upper and lower bounds of the k-values listed in Table 4.12). Theoretically, the expected order of the intrinsic rates should follow the order of active site concentrations, if all the sites are uniformly active. The number of active sites for each zeolite can be estimated from the unit cell structure and Si/Al ratio, and are 8.94×10^{-4}, 4.17×10^{-3}, 2.83×10^{-3}, and 3.47×10^{-4} mol/g, for L, Ω, Y-52 and 105-6 zeolites, respectively. Therefore, the theoretical order of zeolite activities is Ω > Y-52 > L > 105-6. The discrepancy between the experimental and theoretical activity order possibly results from the uncertainty in the k-values (one-half to one order of magnitude) predicted by the diffusion-reaction model.

Catalyst	P_T (kPa)	T (K)	$kx10^{5(1)}$ $(\frac{mol}{g - s - atm^2})$	Reference
L	10.1	693	0.49 - 1.64	This study
Ω	10.1	693	0.53	This study
Y-52	10.1	673	0.16 - 0.22	This study
105-6	10.1	693	0.13 - 0.34	This study
Y-62	10.1	696	0.96	Brignac (1984)
TEA 24-2 MFI	10.1	693	0.68	Beltrame et al. (1987)
10% B_2O_3/Al_2O_3	101.0	693	$3.19x10^{-3}$	Izumi and Shiba (1964)
Ti, La-NaHY	10.1	693	3.60	Chang et al. (1987)
Cu, AlF_3 -Y	10.1	693	$3.46x10^{-2}$	Aneke et al. (1979b)

(1) From parallel crosslinked pore model.

Table 4.12. Rate Constant for Toluene Disproportionation Reaction

Kinetics Study	Catalyst	Rate $\times 10^6 \left(\frac{mol}{g-s}\right)$ (1)
This Study	L	0.089
This Study	Ω	0.044
This Study	Y-52	0.016
This Study	105-6	0.02
Brignac (1984)	Y-62	0.07
Aneke et al. (1979b)	Cu/AlF_3 - Y	0.04
Nayak and Riekert (1986)	Pentasil:Si/Al = 36	0.01
	Pentasil:Si/Al = 110	4×10^{-3}
Kaeding et al. (1981)	ZSM-5	5×10^{-3}
Wu and Leu (1983)	Cu - Mordenite (8.7 wt% Cu)	0.05
Izumi and Sliba (1964)	B_2O_3/Al_2O_3	2×10^{-4}
Chang et al. (1987)	Ti, La-NaHY	0.36

(1) All data at 698 K, P_T = 0.1 atm

Table 4.13. Reaction Rate for Toluene Disproportionation Reaction

The intracrystalline diffusivities for toluene in different zeolites as computed from the diffusion-reaction model are listed in Tables 4.10 and 4.11. The diffusivities vary from 3.8×10^{-10} to 5.4×10^{-13} cm^2/s and 2.7×10^{-12} to 5.5×10^{-14} cm^2/s, for the parallel crosslinked pore model and EMT model with SFA, respectively. Except for Ω, the EMT-SFA upper-limit estimates for D_μ are close to the comparable estimates from the parallel crosslinked pore model. These upper-limit values are close to the diffusivities predicted using the ZLC model with ID data, but are 2-3 orders of magnitude below those found using the Linear model. Comparing the D_e values listed in Tables 4.10 and 4.11 with the literature data listed in Table 4.7 shows that the intracrystalline diffusivities obtained by this kinetics approach are two to three orders of magnitude smaller than those determined by uptake rate measurements and chromatographic techniques. Furthermore, they are also at least four orders of magnitude smaller than those obtained by the PFG-NMR technique.

This observation suggests that counterdiffusion of reactants and products in the zeolite network under reaction conditions increases the effective resistance to diffusion, above that predicted from unidirectional diffusion experiments. This statement supports the findings of Kolaczkowski and Ullah (1989), who hypothesized that an "adsorption" effect reduced the D_e of the reactant (but not those of the products) below the unidirectional value by a factor of five for the dehydration of ethanol using a 13X zeolite catalyst at 623 K. However, these results are in contrast to those of Haag et al. (1982), who estimated D_e's from the kinetics of catalytic cracking of C_6 and C_9 hydrocarbons on ZSM-5 at 811 K. They derived D_e 's from kinetics data by the triangulation method as described by Smith (1981). The derived D_e's

actually exceeded the corresponding Knudsen diffusivities. They tried to explained this observation as follows: (1) the collision between molecule and pore wall is not totally elastic, hence the basic assumption imposed by the Knudsen diffusion model breaks down; and (2) fast surface diffusion enchanced the intracrystalline mass transfer. But the diffusivities derived from the kinetics data in this study are four to five orders of magnitude smaller than the corresponding Knudsen diffusivities.

Rajadhyaksha et al. (1990) have studied the counterdiffusion behavior in zeolites by Monte Carlo simulation, assuming random movement of tagged molecules in a two-dimensional array with a constant number of vacancies, a situation which is similar to an activated (configurational) counterdiffusion. They found that the mean square displacement (MSD) of the tagged molecule is a nonlinear function of concentration, with the deviation from the initial linear behavior occurring at lower values of MSD as sorbate concentration increases. Their observations imply that at high sorbate concentration (or low vacancy concentration), the molecules are constrained, having repeated encounters with the same vacancies, and the net displacement of a molecule is very low. On the contrary, for unidirectional diffusion there is a net inward flux of molecules with an equivalent outward flux of vacancies. At these conditions, repeated encounters of a molecule with the same vacancy have low probability, and the net displacement of a molecule is larger than that observed during counterdiffusion. Therefore, the net displacement during unidirectional diffusion is about three times larger than that observed during counterdiffusion. But the confirmation of these Monte Carlo results awaits further work on diffusion in zeolite catalysts under reaction conditions.

As discussed in Section 1.1, there are 2 to 3 orders of magnitude difference between the unidirectional diffusivity measured by the adsorptive uptake technique (Karger and Ruthven, 1989) and the adsorptive counterdiffusivity (Satterfield and Katzer, 1971; Satterfield et al., 1971; Moore and Katzer, 1972) for benzene and cumene in NaY and ZSM-5, respectively. But Post et al. (1983) reported that the extrapolated unidirectional diffusivities (measured by both gravimetric and chromatographic techniques) are roughly the same order of magnitude as the counterdiffusivity estimated from the diffusion-limited kinetics data for the cracking of 2,2-dimethylbutane in ZSM-5. The discrepancies between undirectional diffusivity and counterdiffusivity observed in this study are therefore in accord with those reported by Satterfield et al., but not with those estimated by Post et al.. In the former case, for the counterdiffusing molecules both critical diameters approach the intracrystalline pore diameters, and both molecules are strongly adsorbed. This is not true of the latter case (2,2-dimethylbutane cracking), which may explain the differences in the two sets of results. Therefore, it is hypothesized that counterdiffusivities are strong functions of the parameter λ (critical diameter divided by pore diameter) and the nature of molecule-surface interaction. This hypothesis would also explain the results of Kolaczkowski and Ullah (1989), which suggest that the diffusivities of larger and more strongly adsorbed molecules are those most reduced in counterdiffusion.

Finally, it must be noted that the η_M values are much smaller than the η_μ's (except for L), which implies that the major diffusion resistance is within the macropores. This conclusion is supported by computations that the macropore concentration dropped from 1.61×10^{-6} mol/cm^3 at the

external surface to roughly 1.0×10^{-8} mol/cm^3 at the centerline for all four types of zeolite pellets used in this study. Therefore, the basic assumption imposed on the diffusion-reaction model, that the reaction rate is controlled by both macro- and micropore diffusion, is only marginally satisfied, although neglect of micropore diffusion would have led to far different values of k.

In conclusion, the toluene disporportionation reactions performed in this study were generally controlled by macropore diffusion. The intracrystalline diffusivities obtained by the reaction-diffusion model are not completely reliable, but support the ZLC or Linear model results rather than the PFG-NMR results. The reaction rate constants predicted by the diffusion-reaction model are comparable with literature rate constants obtained when the reaction was not diffusion-limited, which suggests that the entire analysis has some validity.

4.2.3. Effects of Sorbate Concentrations on Measured D_e

From the above discussion, it seems necessary to probe the concentration dependence of the intracrystalline binary diffusivity (D_e) and the intracrystalline self-diffusivity (D_s). It is well known that, due to the strong electrostatic field associated with zeolite surfaces, there is no "free gas phase" inside the network of channels and cages. For this reason the correction factor to the diffusivity can be quite large at high coverage, as seen by combining Darken's equation, eq. (1-10), and the Langmuir isotherm.

$$D = D_0(1 + KC_M) \qquad (4-42)$$

The coverage is defined by dividing the micropore concentration by the maximum number of molecules in the zeolite and therefore varies between 0 and 1.

The coverage in both ID and kinetics experiments can be estimated. For the kinetics experiments, the adsorption equilibrium constant was defined by the Langmuir isotherm. Similarly, the mass action-based adsorption expression used in the Linear model reduces to the Langmuir isotherm at equilibrium. Therefore, the adsorption isotherms for both kinetics and desorption experiments are described by a Langmuir isotherm:

$$\theta = \frac{KC_M}{1 + KC_M} \qquad (4-43)$$

The theoretical relationship between a Langmuir-type K and the Henry's Law (Linear isotherm) K_L is

$$K = \frac{K_L}{(C_\mu)_{max} - C_M K_L} \qquad (4-44)$$

Most of the literature K-values (except Barthomeuf and Ha, 1973; Ruthven and Doetsch, 1976; Forni and Viscardi, 1986) are reported at lower temperatures and extrapolating to 693 K using van't Hoff's equation gives unreasonable K values ($K \simeq 0$) . Obviously there is a different mode of adsorption at high temperatures. Therefore, only the interpolated and extrapolated K's from the higher temperature literature data were used for comparsion. The K-values, after conversion to Langmuir-type K's, are roughly 1 to 10 for benzene in faujasites (Barthomeuf and Ha, 1973), and 10^4 to 10^5 for benzene and toluene in faujasites and pentasils (Ruthven and Doetsch, 1976; Forni and Viscardi, 1986).

The K-values predicted by the ZLC model (Table 4.4), which are converted to Langmuir-type K's by eq. (4-44), are roughly 10^6 , which is one to two orders of magnitude larger than any of those in the literature. The fitted equilibrium constants for the Linear model, which are Langmuir-type K's, are listed in Table 4.5. The equilibrium constants are roughly 10^2 for both toluene and benzene. These K's are three to four orders of magnitude smaller than those predicted by the ZLC model. Therefore, the K-values predicted by the Linear model for toluene lie between those reported in the literature, although with such a large spread of values it is difficult to draw comparisons. The kinetics K-values are listed in Tables 4.10 and 4.11 for toluene and are roughly 10^4 to 10^5 . These numbers are in good agreement with some of those available in the literature (Ruthven and Doetsch, 1973; Forni and Viscardi, 1986), and lie between the K-values predicted by the Linear and ZLC models.

Maximum Henry's Law K_L-values, K_{Lmax}, can also be calculated theoretically assuming C_μ can approach the liquid density of toluene at its boiling point. This is equivalent to saying that toluene cannot be packed into zeolite micropores more densely than in the liquid phase. Although it is possible that the intrazeolitic composition could be slightly larger due to specific attraction to cationic or anionic sites, the extent of this effect on the K_L -values could not be great, because adsorption in zeolites can be described excellently by liquid-phase models (Ruthven, 1984). For all the kinetics studies, a C_M value of 1.61×10^{-6} mol/cm^3 was used, which means that K_L -values larger than 5300 are suspect. The K_L values predicted by the Linear model and those from the kinetics data

are roughly 10 to 10^3 (calculated according to eq. (4-44)), and are within the limit, but the K_L values predicted from the ZLC model are suspect.

The $(C_\mu)_{max}$, Langmuir K and coverage values (calculated according to eq. (4-43)) for the ID and kinetics experiments are listed in Table 4.14. As shown in the table, the average coverages for ID experiments varied from 0.3 (except for L) to zero and the kinetics experiments have average coverages in the range of 0.008 for L, 0.009 for Ω , and 0.003 for Y, and 0.002 for 105-6 used in this study.

For most uptake rate measurements, the observed D_e is approximately independent of concentration at low sorbate concentration but increases rapidly as saturation is approached. The variation of D_e with coverage is one to two orders of magnitude using most of the literature data. The concentration-dependence of the D_e 's can be understood in terms of eq. (4-42). Usually, D_0 is independent of sorbate concentration when the size of the diffusing molecule is large relative to zeolite pore diameters. But when the size of the diffusing molecule is relatively small, D_0 is often inversely proportional to sorbate concentration (Ruthven and Doetsch, 1973; Lee et al., 1977; Goddard and Ruthven, 1978a; Ruthven, Ch. 5, 1984; Eic et al., 1988; Shah et al., 1988).

The factor D_0 is analogous to D_s, the self-diffusivity. For most of the PFG-NMR experiments, D_s also typically decreases with increased coverage (Karger et al., 1978a; Karger et al., 1980; Caro et al., 1985; Germanus et al., 1985). The observed variation of D_s is generally within an order of magnitude for the corresponding variation of coverage from 0 to unity. The most common explanation for this phenomenon is the stronger mutual hindrance between adsorbed molecules and the decrease of "free volume" at higher coverage; both of these effects tend to diminish the

Adsorbate	Adsorbent	$(C_\mu)_{max}$ mol/cm^3	K cm^3/mol	θ -
Kinetics				
L	Toluene	$8.5x10^{-3}$	$5.0x10^3 - 5.0x10^4$	0.008
Ω - 6	Toluene	$8.5x10^{-3}$	$6.0x10^5 - 7.0x10^6$	0.009
Y-52	Toluene	$8.5x10^{-3}$	$5.0x10^4 - 6.0x10^5$	0.003
105-6	Toluene	$8.5x10^{-3}$	$6.0x10^4 - 6.0x10^5$	0.002
ID				
L	Toluene	$8.5x10^{-3}$	500	0.0 - 0.58
Ω - 6	Toluene	$8,5x10^{-3}$	550	0.0 - 0.30
Y-52	Toluene	$8.5x10^{-3}$	200	0.0 - 0.30
105-6	Toluene	$8.5x10^{-3}$	100	0.0 - 0.30

Table 4.14. Langmuir Equilibrium Constant and Average Coverage for Kinetics and ID experiments

mean free jump length of the molecules, which in turn reduces D_s. This is in agreement with the Monte Carlo results cited in the previous section. Therefore the decrease in D_0 with increased coverage somewhat counteracts the effect of the correction factor in eq. (4-42), and in the Henry's Law region D_e should actually decrease somewhat with respect to coverage (Ruthven and Doetsch, 1973). At higher sorbate concentrations, the correction factor in eq. (4-42) will predominate, and then D_e should be greater than D_s. However, literature D_e's obtained from uptake rate measurements, and those obtained in this study, are generally several orders of magnitude smaller than the corresponding D_s's derived from PFG-NMR experiments, a fact which certainly cannot be explained in terms of coverage effects.

Aust et al. (1989) have used the Monte Carlo method to simulate the influence of sorbate concentration on diffusion in zeolites. They simulated steady-state diffusion in two-dimensional zeolite arrays for both diffusion under a constant concentration gradient and self-diffusion in a zeolite (molecules not allowed to move across the boundary), which are typical of kinetics and PFG-NMR experiments, respectively. For diffusion under a constant concentration gradient, they noted that D_e increases with increasing concentration, but D_e decreases when the maximum number of molecules per unit cell increases. However, after correcting D_e by Darken's equation, they found a decline in D_0 with increasing sorbate concentration (at coverage $\simeq 0.7 - 0.8$) after an initial region of almost constant D_0. These concentration dependences of D_e and D_0 are consistent with observations from uptake rate measurements, except the concentration dependence of D_0 at high sorbate concentration. The discrepancy between

the simulated and experimental concentration dependence of D_0 is probably due to neglect of sorbate-sorbent interactions in the simulations.

For D_s, Aust et al. found a very peculiar concentration dependence, with an extended plateau in the intermediate concentration range and sharp decreases at the limits of zero and unity coverage. The concentration dependence of D_s at infinite dilution is therefore uncertain, but otherwise the Monte Carlo results are in general agreement the observed concentration dependence of D_s in most of the PFG-NMR experiemtns. However, their simulation results cannot explain the large discrepancies between experimental PFG-NMR D_s and adsorptive uptake D_0 results in the literature.

The coverages in the ID experiments are higher than those in the kinetics experiments, except at very long times. Therefore, the D_e's obtained in this study do show the expected concentration dependence according to eq. (4-42), but the concentration effect can only account for at most one-half an order of magnitude difference as computed by eq. (4-42), using the liquid $(C_\mu)_{max}$ values. In conclusion, the higher D_e's derived from the Linear model desorption data may be explained by the following factors: (1) higher coverage for the desorption experiments (account for a maximum of one-half order of magnitude); (2) hindrance of movement when molecules pass each other in the zeolite windows during kinetics experiments (accounts for differences of one-half to 3 orders of magnitude from literature data); and (3) pore mouth plugging of the zeolites during catalysis. But the confirmation of these explanations awaits further work on diffusion in zeolite catalysts under reaction conditions.

CHAPTER 5

CONCLUSIONS

1. The isothermal desorption (ID) process for toluene or benzene with five different zeolites was shown to be controlled by diffusion and readsorption. The intracrystalline diffusivities (D_e) were derived by fitting the desorption curves with four models of varying complexity.

2. The Constant Diffusivity Constant Coverage (CDCC) model assumes that the external surface coverage is constant. The fitting results for ID spectra showed that the model cannot predict the experimental data, and the relative deviations are in the range of 7.5 to 15 %. The fitted curve predicted by CDCC model showed "crossover" behavior for all the systems tested because: (1) the external surface coverage is not a constant at the early stage of the process, and (2) readsorption is important, especially in the later stage of the process.

3. The Constant Diffusivity Variable Coverage (CDVC) model assumes that the external surface coverage follows an exponential decay function, similar to that of the gas phase concentration. For the falling portion of the ID spectra, the model predictions do fit the data well, although the fitted curves do not show the "crossover" behavior which was observed for the CDCC model. However, the estimated D_e for toluene

from this model is larger than that of benzene, in spite of the smaller molecule size of benzene. Therefore, this model is also not suitable for the description of ID data when significant readsorption occurs.

4. The Zero Length Chromatography (ZLC) model makes the following assumptions: (1) a sorption equilibrium exists between the gas and adsorbed phases; and (2) the cell accumulation term in the gas phase mass balance can be neglected. A two parameter, D_e and K, regression routine was used to fit the ID spectra and Eic and Ruthven's data (1988). The results showed that the estimated intracrystalline diffusivities were of 1.0×10^{-12} to 2.2×10^{-10}, 1.1×10^{-11} to 1.6×10^{-10}, and 2.4×10^{-8} to 3.0×10^{-8} for toluene, benzene and o-xylene, respectively. However, the K-values from this model do not conform to either literature data or to theoretical predictions based upon maximum zeolite coverage. It was shown that both assumptions (1) and (2) can contribute to the error.

5. The Linear model assumes that the external surface coverage follows a mass action-based adsorption expression. The system can be solved analytically in the Laplace domain, converted to the real-time domain by the Fast Fourier Transform (FFT), and fit to the experimental data by a two parameter regression routine. The results showed that the estimated intracrystalline diffusivities were 2.2×10^{-9} to 5.3×10^{-8}, 8.0×10^{-9} to 6.3×10^{-8}, and 3.2×10^{-8} to 4.8×10^{-8} for toluene, benzene and o-xylene, respectively. The observed order for toluene diffusivities is Ω> P1 > Y > 105-6 > L.

6. In conclusion, only models which take into account readsorption (either at equilibrium or not) can both fit the ID data adequately and give reasonable estimations of D_e. A nonequilibrium readsorption model is probably superior to an equilibrium readsorption model, because: (1) it can fit both the rising and falling portions of isothermal desorption curves, and (2) the D_e's predicted by such a model were always comparable to those reported in the literature by other long-time scale techniques (chromatographic, adsorptive uptake, and tracer exchange) under similar conditions. But these D_e's are still at least three orders of magnitude smaller than those predicted by the Pulse Field Gradient (NMR) technique, and the evidence gathered from this study cannot explain this discrepancy.

7. The toluene disproportionation reaction, catalyzed by a bimodal pore-size zeolite pellet, can be represented by a diffusion-reaction model that accounts for diffusion in macropores, adsorption on microparticle surfaces, diffusion in microparticles, and reaction within the microparticles.

8. The rate constants and D_e's for toluene in counterdiffusion were estimated from difffusion-limited kinetics data (both for zeolite pellets and powders) by applying the diffusion-reaction model. The estimated rate constants are comparable to the second-order intrinsic rate constants for zeolite catalysts obtained from the literature.

9. The effective binary D_e's are at least two to three orders of magnitude smaller than the unidirectional D_e's derived from the desorption

curve. The discrepancy between the two types of diffusivities can be explained by the following factors: (1) higher coverage for the desorption experiments (accounts for a maximum of one-half order of magnitude); (2) hindrance of molecular movements when they pass each other in the zeolite windows during kinetics experiments (accounts for one-half to 3 orders of magnitude from literature data); and (3) pore mouth plugging of zeolite during catalysis. Although the confirmation of these explanations awaits further work on diffusion in zeolite catalysts under reaction conditions, it was shown that the estimated counterdiffusivities do follow a trend previously noted in the literature, and the discrepancies between these counterdiffusivities and the unidirectional diffusivities can be explained in part by the above three phenomena.

NOMENCLATURE

a	activity, defined by eq. (1-10)
a	geometric constant for a particle, a=2 (sphere), =1, (cylindrical), =0 (slab)
a_v	external surface area/volume
A	pre-exponential factor
b	width of flow path
B	constant defined in eq. (1-51), $\sqrt{B} = \left(\frac{2}{n+1}\right)^{\frac{1}{2}} / \left(\frac{n+3}{4}\right)$
C	constant defined in eq. (3-1)
C	gas phase concentration
C	solute concentration
$\bar{C}$	dimensionless gas phase concentration, $(R/3)(c/n_0)$
d_p	Particle diameter
D	effective diffusivity
D_0	corrected diffusivity
$D_\times$	pre-exponential diffusivity

D_a axial dispersion coefficient

D_e effective diffusivity

D_{jk} binary diffusivity for species j and k

D_{jm} diffusivity for species j in mixture

D_K Knudsen diffusivity

D_s self-diffusivity

D_M^0 characteristic macropore diffusivity

$\bar{D}_M$ dimensionless macropore diffusivity, D_M/D_M^0

D_μ^0 characteristic micropore diffusivity

$\bar{D}_\mu$ dimensionless micropore diffusivity, D_μ/D_μ^0

E energy barrier that separate adjacant surface sites

f(r) probability density of pore volume

f(x) normalized activity distribution function

F collision frequency, $\left(\frac{RT}{2\pi M}\right)^{\frac{1}{2}}\sigma C$

F_A molar flow rate for component A

$F(\lambda)$	restriction factor
g	intensity of NMR field gradient
g_e	effective conductance
g_i	conductance of pore i
$g(C)$	function defined in eqs. (1-23), (1-34)
h, k, l	Miller Indices of reflections
$h(C)$	function defined in eq. (1-34)
I	intensity of X-Ray diffraction peak
J_i	Jacobi polynomial, defined in eq. (1-33)
k	reaction rate constant
k_{eff}	effective desorption rate constant
k_g	mass transfer coefficient
k_v	volume-based reaction rate constant
K_i	adsorption equilibrium constant for species i
l	microparticle volume/microparticle external surface area
l_i	length of pore i
L	macroparticle volume/macroparticle external surface area

L	constant defined in eq. (4-18)
M	cation in zeolite unit cellfusing species
M	molecular weight of the diffusing species
M	amount of sorbate adsorbed per weight of catalyst
M_t	total amount of adsorbate desorbed at time t
M_∞	total amount of adsorbate desorbed at infinite time
n	surface concentration
n	order of reaction
n	valence of cation in zeolite unit cell
n_i	unit vector parallel to the axis of pore i
N	desorption rate
N	number of CSTRs in the dispersion model
N_j	molar flux of reacting component j
p_i	partial pressure of species i
P	pressure
Pe	Peclet number
q	differential heat of adsorption

Q	volumetric gas flow rate
r	rate
r	spherical coordinate
r	pore radius
$\langle r^2 \rangle$	arithmatic average of pore radius
$\langle r^2(\Delta) \rangle$	mean square jump distance
$\langle r_e^3 \rangle$	effective average of pore radius
$r(C)$	rate expression, defined in eq.(1-24)
$\bar{r}$	dimensionless radius, r/R
r_1	reaction rate for primary reaction
r_2	rate of deactivation
r_D	reaction rate for toluene disproportionation
r_e	mean pore radius
r_{obs}	observed reaction rate
R	gas constant
R	catalyst particle size

R(C)	dimensionless rate experssion, $r(C)/r_s(C)$
R_b	radius of catalyst bed
Re	Reynolds number
S	Laplace variable
S	the sticking coefficient, the probability that a gas molecule striking the surface will adsorb
Sc	Schmidt number
Sh	Sherwood number
t	time on stream
t_2	diffusional time constant $\frac{D_e}{\varepsilon R^2}$
T	temperature
T_M	peak temperature
TO	number of turnover
u	superficial velocity
v	interstital gas velocity
V	volume of desorption cell
V	volume of catalyst pores

W	weight of catalyst
W_i	weight of a Jacobi polynomial
X	spatial coordinate of catalyst slab
$\bar{X}$	dimensionless coordinate in the catalyst slab, X/L
X_A	conversion of component A
Y_k	mole fraction of species k
Z	the total length of the catalyst or bed length
Z	number of water molecules in zeolite unit cell
Z	coordination number
α	BET specific surface area
α	ratio of diffusion times, $(1 - \varepsilon_M)(D_M^0/D_\mu^0)(L^2/l^2)$
α	constant used in ZLC model
α_j	stoichiometric coefficient of component j in a single reaction
β	heating rate
$\bar{\beta}$	constant defined in eq. (4-11)
γ	gyromagnetic ratio
γ	constant defined in eq (3-9)

δ	width og NMR field gradient
Δ	mean life time between two jumps in NMR measurement
ϵ	solid porosity
ζ	dimensionless coordinate in the particle, Y/L
η	effectiveness factor for solid particle
θ	dimensionless surface concentration, n/n_0
θ_1	dimensionless external surface concentration,
θ_{max}	maximum surface coverage
θ	Bragg diffraction angle
$\varkappa_p$	equilibrium partition coefficient
$\varkappa_r$	drag coefficient
λ	critical molecular diameter divided by pore diameter
ξ	dimensionless coordinate in the pellet, Z/l
ρ	apparent catalyst density
ρ_1, ρ_2	functions defined in eq. (1-32)
σ_1, σ_2	functions defined in eq. (1-31)
σ	variance

τ tortuosity factor

τ_1 cell residence time/experimental time, $\left(\frac{V}{Q}\right)\frac{D_e t}{\varepsilon R^2}$

τ_2 diffusion time/experimental time, $\left(\varepsilon\frac{R^2}{D_e}\right)\frac{D_e t}{\varepsilon R^2}$

τ_3 diffusion time/cell residence time, $\left(\frac{RQ}{D_e A_c}\right)$

τ_4 cell residence time/adsorption time, $(k_a\psi)\left(\frac{A_c}{Q}\right)$

τ_5 cell residence time/desorption time, $(k_d\frac{R}{3})\left(\frac{A_c}{Q}\right)$

φ_M pellet Thiele modulus, $[(1-\varepsilon_M)Lk_d g(C_M^s)/\varepsilon_M D_M^0]^{\frac{1}{2}}$

φ_s Thiele modulus for spherical particle,

φ_μ particle Thiele modulus, $[lk_d g(C_m^s)/C_\mu^0]^{\frac{1}{2}}$

Φ Weisz (observable) modulus, defined in eq, (1-23)

ψ dimensionless concentration

Ψ amplitude of NMR spin echo

Ψ function of$(n - n_{max})$

$\overline{\Psi}$ function of $\frac{(n - n_{max})}{n_{max}}$

Subscripts

a	adsorption
b	bulk
c	crystal
d	desorption
m	mixture
M	macropore or pellet
max	maximumre or pellet
p	particle
sat	saturation
μ	micropore or particle
∞	at time infinite

Superscripts

eq	equilibrium
s	at surface of particle
0	at center of particle

REFERENCE

1. Amelse, J.A., in Catalysis 1987; Ward, J.W. Ed., Elsevier: Amsterdam, 165 (1988).

2. Aneke, L.E.; Gerritsen, P.J.; van denBerg, P.J.; and W.A. deJong, J. Catal., 59, 26 (1979a).

3. Aneke, L.E.; Gerritsen, L.A.; Eiler, J.; and Trion, R., J. Catal., 59, 37 (1979b).

4. Aris, R., The Mathmetical Theory of Diffusion and Reaction in Permeable Catalysts, Oxford University Press, London (1975).

5. Anderson, J.R.; Foger, k.; Moler, T.; Rajadhyaksha, R.A.; and Sander, J.V.; J. Catal., 58, 114 (1979).

6. Aust, E.; Dahlke, K.; and Emig, G., J. Catal., 115, 86 (1989).

7. Baltus, R.E.; and Anderson, J.L., Chem. Eng. Sci., 38, 1959 (1983).

8. Balkenende, A.R.; Geus, J.W.; Kock, A.J.H.M.; and ven der Pas, R.J.; J. Catal., 115, 365 (1989).

9. Barrer, R.M., Adv. in Chem., 102, 1 (1971).

10. Barrer, R.M., in R.P. Townsend, Ed.; Special Publication No. 33, The Chemical Society, London, 3 (1980).

11. Barrett, E.P.; Joyner, L.G.; and Halenda, P.H., J. Amer. Soc., 73, 173 (1951).

12. Barthomeuf, D.M.; Ha, B.-K.; J. Chem. Soc., Faraday Trans. 1, 69, 2158 (1973).

13. Beltrame, P.; Beltrame, P.L.; Carniti, P.; Zuretti, G.; Leofanti, G.; Moretti, E.; and Padovan, M., Zeolites, 7, 418 (1987).

14. Benesi, H.A., J. Catal., 8, 368 (1967).

15. Bischoff, K.B., AIChE J., 11, 352 (1965).

16. Box, M.J., Computer J. 8, 42 (1965).

17. Breck, D.W. Zeolite Molecular Sieves, John Wiley & Sons, New York (1974).

18. Brignac, S.D., A Reactor Study of Nickel Loaded Zeolites, Thesis, Dept. of Chem. Eng., Louisiana State University, Baton Rouge, LA (1984).

19. Brunauer, B.; Emmet, P.H.; and Teller, E., J. Am. Chem. Soc., 60, 309 (1938).

20. Butt, J.B., Reaction Kinetics and Reactor Design, Prentice-Hall, Englewood Cliff, N.J. (1980).

21. Burganos, V.N.; Sotirchos, S.V.; AIChE J, 33, 1678 (1987).

22. Carberry, J.J., AIChE J., 8, 557 (1962).

23. Caro, J.; Bulow, M.; Schirmer, W.; Karger, J.; Heink, W.; Pfeifer, H.; and Zdanov, S.P., J. Chem. Soc., Faraday I, 81, 2541 (1985).

24. Chang, J.-R.; Shen, F.-C.; Cheng, Y.-M., and Wu., J.-C., Appl. Catal., 33, 39 (1987).

25. Chantong, A.; and Massoth, F.E., AIChE J., 29, 725 (1983).

26. Chauvin, B.; Massiani, P., Dutartre, R., Figueras, F., Fajula, F., and Des Cowzieres, T., Zeolites, 10, 174 (1990).

27. Chen, N.Y.; and Degnan, T.F., Chemical Engineering Progress , February, 32 (1988).

28. Chen, N.Y.; Kaeding, W.W.; and Dwyer, F.G., JACS, 101, 6783 (1979).

29. Churchill, S.W., AIChE J., 23, 208 (1977).

30. Choudhary; and Akoleker, D.B.; AIChE J., 116, 130 (1989).

31. Chutoransky, P. Jr; and Dwyer, F.G., Adv. Chem. Ser. No. 121, 540 (1973).

32. Corma, A.; and Cortes, A., Ind. Eng. Chem. Process Des., Dev., 19, 263 (1980).

33. Crank, J., The Mathematics of Diffusion , Oxoford Univ. Press, London, England (1975).

34. Cunningham, R.E.; and Williams, R.J.J., Diffusion in Gases and Porous Media, Plenum Press, New York (1980).

35. Cvetanovic, R.J.; and Amenomiya, Y., Advan. Catal., 17, 103 (1967).

36. Cvetanovic, R.J.; and Amenomiya, Y., Catal. Rev., 6, 21 (1972).

37. Davidova, N.; Peshev, N.; and Shopov, D., J. Catal., 58, 198 (1979).

38. Demmin, R.A.; and Gorte, R.J., J. Catal., 90, 32 (1984).

39. Derouane, E.G.; and Gabelica, Z.; J. Catal., 65, 486 (1980).

40. Doelle, H.J.; and Riekert, L., ACS Symp. Ser., 40, 401 (1977).

41. Doelle, H.J.; Neering, J., Riekert, L., and Marosi, L., J. Catal., 71, 27 (1981).

42. Dooley, K.M., Catalysis by Strong-Acid Macroporous Polymers: Sulfonic Acids and Superacids on Poly(Styrene-Divinylbenzene), Ph.D. thesis, Dept. of Chem. Eng., Univ. of Delaware, Newark, DE (1982).

43. Dooley, K.M.; Brignac, S.D.; and Price, G.L., Ind. Eng. Chem. Res., 29, 789 (1990).

44. Eatough, D.J.; Salim, S.; Izatt, R.M.; Christensen, J.J.; Analytical Chem., 46, 126 (1974).

45. Eic, M.; and Ruthven, D.M., Zeolites, 8, 40 (1988).

46. Eic, M.; Goddard, M.V., and Ruthven, D.M., Zeolites, 8, 327 (1988).

47. Evans, R.B.; Waston, G.M.; and Mason, E.A., J. Chem. Phys., 33, 2076 (1961).

48. Falconer, J.L.; and Schwartz, J.A., Catal. Rev., 25, 141 (1983).

49. Ferry, J.D., J. Gen. Physiol., 20, 95 (1936).

50. Ford, J.R., Common Los Alamos Mathematical Software Los Alamos National Laboratory, April (1984).

51. Forzatti, P.; Borghesi, M.; Pasquon, I.; and Tronoconi, E., AIChE J., 32, 87 (1986).

52. Forni, L.; and Viscardi, C.F., J. Catal., 97, 480 (1986).

53. Forni, L.; and Magni, E., J. Catal., 112, 437 (1988a).

54. Forni, L.; Magni, E.; Ortoleva, E.; Monaci, R.; and Solinas, V., J. Catal., 112, 444 (1988b).

55. Froment, G.F.; and Bischoff, K.B., Chemical Reactor Analysis and Design, John Wiley and Sons, New York (1979).

56. Gary, D.R.; and Ruthven, D.M.; Chem. Eng. Sci., 29, 571 (1974).

57. Gelbin, D.; and Fiedler, K., AIChE J., 26, 510 (1980).

58. Germanus, A., Karger, J,; Pfeifer, H.; Samulevic, N.N., and Seidal, R., Zeolites, 8, 91 (1985).

59. Gilliand, E.R.; Baddour, R.F.; Perkinson, G.P.; and Sladek, K.J., Ind. Eng. Chem. Fundam., 13, 95 (1974).

60. Goddard,M.; and Ruthven, D.M., Zeolite, 6, 283 (1986a).

61. Goddard,M.; and Ruthven, D.M., Zeolite, 6, 445 (1986b).

62. Gonzo, E.E.; and Gottifredi, J.C., Catal. Rev. Sci. Eng., 25, 119 (1983).

63. Gorte, R.J., J. Catal., 75, 164 (1982).

64. Gottifredi; J.C., Gonzo, E.E., and Quiroga, O.D., Chem. Eng. Sci., 36, 705 (1983a).

65. Gottifredi; J.C., Gonzo, E.E., and Quiroga, O.D., Chem. Eng. Sci., 36, 713 (1983b).

66. Haag, W.O.; Lago, R.M.; and Weisz, P.B., Disc. Faraday Soc., 72, 317 (1982).

67. Hanson, K.L.; Engel, A.J., AIChE J., 13, 260 (1967).

68. Hashimoto, N.; and Smith, J.M., Ind. Eng. Chem. Fundam., 13, 115 (1974).

69. Haynes, H.W., Jr., Chem. Eng. Sci., 41, 412 (1986).

70. Henri, J.P.; Chennakeshwan, B.; and Smith, J.M., AIChE J., 22, 597 (1961).

71. Herz, R.K.; Kiela, J.B.; and Marin, S.P., J. Catal., 73, 66 (1982).

72. Hindmarsh, A.C.; ACM-SIGNUM Newsletter 15, 10 (1980).

73. Hsu, J. T., and J. S. Dranoff, Comput. Chem. Eng., 11 (2), 101 (1987).

74. Huang, Y.-J.; Xue, J.; and Schwarz, J.A., AIChE J., 109, 396 (1988).

75. Hwu, F.S.; and Hightower, J.W., ACS, Philephedia Meeting, August, 26 (1984).

76. Izumi, Y; and Shiba, T., Bull. Chem. Soc. Jpn., 37, 1797 (1964).

77. Iwamura, T.; Otami, S.; and Sato, N., Bull. Japan Petro. Inst.,13, 116 (1971).

78. Jacobs, P.A.; Leeman, H.E.; and Uytterhboeven, J.B., J. Catal., 33, 31 (1974).

79. Jayaraman, V.K.; Kulkarni, B.D.; and Doraiswamy, L.K., AIChE J., 29, 251 (1983).

80. Jones, D.M.; and Griffin, G.L., J. Catal., 80, 40 (1983).

81. Kaeding, W.W.; Chu, C.; Young, L.B.; Weinstein, B.; and Butter, S.A., J. Catal., 67, 159 (1981a).

82. Kaeding, W.W.; Chu, C.; Young, L.B.; and Butter, S.A., J. Catal., 69, 392 (1981b).

83. Karger, J.; Bulow, M., Struve, P.; Kocirik, M.; and Zikanova, A., J. Chem. Soc., Faraday I, 74, 1210 (1978a).

84. Karger, J.; Bulow, M.; Lorenz, P., J. Colloid. Interface Sci., 65, 181 (1978b).

85. Karger, J.; Pfeifer, H.; Rauscher, M.; and, Walter, A., J. Chem. Soc., Faraday I, 76, 717 (1980).

86. Karger, J.; Ruthven, D.M.; Zeolites, 9, 267 (1989).

87. Kolaczkowski, S.; and Ullah, U., Chem. Engr. Sci., 44, 2843 (1989).

88. Lanewala, M.A.; and Bolton, A.P., J. Org. Chem., 34, 3107 (1969).

89. Leary, K.J.; Michales, J.N.; and Stacy, A.M., AIChE J. 34, 263 (1988).

90. Lee. J.; and Luss, D., Chem. Eng. Sci., 26, 1433 (1971).

91. Lee. L.K.; Yucel, H.; and Ruthven, D.M., ACS Symposium Series, 40, 417 (1977).

92. Lee. T.Y.; and Ma, Y.M., ACS Symp. Ser., 40, 428 (1977).

93. Lippens, B.C.; and deBoer, J.H., J. Catal., 4, 319 (1965).

94. Le Van Mao, R.; Ragaini, V.; Leofanti, G.; and Fois, R., J. Catal., 81, 418 (1983).

95. Matsumoto,H.; and Monita, M., J. Japan Petrol. Inst., 8, 572 (1967).

96. Meier, W.M.; and Olson D.N.; Altas of Zeolite Structure Types , Struc. Comm. Intl. Zeolite Assc., (1978).

97. Mingle, J.O.; and Smith, J.M., AIChE J., 7, 243 (1961).

98. Mitani, M., J. Chem. Eng. Japan, 17(4), 441 (1984).

99. Moore, R.M.; and Katzer, J.R., AIChE J., 18, 816 (1972).

100. Nayak., V.S.; and Riekert, L., Appl. Catal., 23, 403 (1986).

101. Neretnieks, I., Chem. Eng. Sci., 31, 1029 (1976).

102. Neogi, P; and Ruckenstein, E., AIChE J., 26, 787 (1980).

103. Okazaki, M.; Tamon, H.; and Toei, R., AIChE J., 26, 262 (1981).

104. Olson, D.H.; and Haag, W.O., Appl. Catal., 23, 403 (1986).

105. Ors, N.; and Dogu, T., AIChE J., 25, 723 (1979).

106. Pappenheimer, J.R., Physio. Rev., 33, 387 (1953).

107. Paludetto, R.; Storti, G.; Gamba, G.; Carra, S.; and Morbidelli, M.; Ind. Eng. Chem. Res., 26, 2250 (1987).

108. Park, S.H.; and Kim, Y.G., Chem. Eng. Sci., 39, 532 (1984).

109. Parra, C.F.; Ballievt, D.,; and Barthomeuf, D., J. Catal., 40, 52 (1975).

110. Pope, C.G.; J. Phys. Chem., 88, 6312 (1984).

111. Post, M.F.M.; Van Amstel, J.; and Kouwenhoven, H.W.; Proc. Int. Zeolite Conf. 6th, 517 (1983).

112. Poutsma, M.L., Zeolite Chemistry and Catalysis, Rabo, J.A., Ed.; ACS, Washington, 437 (1976).

113. Prasher, B.C.; and Ma, Y.H., AIChE J., 23, 303 (1977).
Gabriel, G.A.; and Ma, Y.H., AIChE J., 24, 1118 (1978).

114. Pukanic, G.W.; and Massoth, F.E., J. Catal., 28, 308 (1973).

115. Ragaini, D.M.; Fois, R.: La Van Mao, R.; and Cattanai, M.G.; Can. J. Chem. Eng., 62, 706 (1984).

116. Rajadhyaksha, R.A.; Pitale, K.K.; and Tambe, S.S., Chem. Eng. Sci., 45, 1935 (1990).

117. Renkin, E.M., J. Gen. Physiol., 38, 225 (1954).

118. Rieck, J.S.; and Bell, A.T., J. Catal., 85, 143 (1984).

119. Ruckenstein, E.; Vaidyanathan, A.S.; and Youngquist, G.R., Chem. Eng. Sci., 26, 1305 (1971).

120. Ruthven, D.M., Canda. J. Chem., 52, 3523 (1974).

121. Ruthven, D.M.; and Doetsch, I.H.; J. Chem. Soc., Faraday Trans. 1, 72, 1043 (1976).

122. Ruthven, D.M., in R.P. Townsend, Ed.; Special Publication No. 33, The Chemical Society, London, 43 (1980).

123. Ruthven, D.M., ACS Symp. Ser., 63, 345 (1983).

124. Ruthven, D.M., Principles of Adsorption and Adsorption Process , John Wiley, New York (1984).

125. Ruthven, D.M.; and Eic, M., ACS Symp. Ser., 368, 362 (1988).

126. Santacesaria, E.; Gelosa, D.; Danise, P.; and Carra, S., Ind. eng. Chem. Process des. Dev., 24, 78 (1985).

127. Satterfield, N.S., Mass Transfer in Heterogeneous Catalysis, MIT Press, Cambridge, Mass. (1970).

128. Satterfield, N.S.; Karzer, J.R.; and Vieth, W.R., Ind. Eng. Chem. Fundam., 10, 478, (1971).

129. Satterfield, N.S.; and Karzer, J.R., ACS Symp. Ser., 102, 193, (1971).

130. Satterfield, N.S.; Colton, C.K.; and Pitcher, W.H. Jr., AIChE J., 19, 628 (1973).

131. Schneider, P.; and Smith, J.M., AIChE J., 14, 762 (1968).

132. Scott, D.S.; and Dullien, F.A.L., AIChE J., 8, 113 (1962).

133. Shah, D.B.; Hayhurst, D.T.; Evanina, G.; and Guo, C.J., AIChE J., 34, 1106 (1988).

134. Shindo, Y.; Hakuta, T.; Yoshitome, H.; and Inoue, H., J. Chem. Eng. Japan, 16, 120 (1983).

135. Sing, K.S.W.; J. Chem. Eng. Japan, 16, 120 (1983).

136. Smith, J.M., Chemical Engineering Kinetics, 3rd. 2d., McGraw Hill, New York (1981).

137. Smith, R.K.; and Metzner, A.B., J. Phys. Chem., 68, 2741 (1964).

138. Sotirchos, S.V.; Burganos, V.N.; AIChE J, 34, 1106 (1988).

139. Streitwieser, A., Jr.; and Reif, L.,J. Am. Chem. Soc., 82, 5003 (1960).

140. Sudo, Y.; Misic, D.M.; and Suyuki, M., Chem. Eng. Sci., 16, 120 (1978).

141. Thakur, S.C.; Brown, L.F.; and Haller, G.L., AIChE J., 26, 355 (1980).

142. Theodorou, D.; and Wei, J., J. Catal., 83, 205 (1983).

143. Tronconi, E.; and Forzatti, P., J. Catal., 93, 197 (1985).

144. Tronconi, E.; and Forzatti, P., Chem. Eng. Sci., 41, 2541 (1986).

145. Tronconi, E.; and Forzatti, P., Chem. Eng. Sci., 42, 2779 (1987).

146. Villadsen, J.V.; and Stewart, W.E., Chem. Eng. Sci., 22, 1483 (1967).

147. Villadsen, J.V.; and Michelsen, M.L., Solution of Partial Differential Equation Models by Polynomial Approximation, Prentice-Hall, Englewood Cliffs, New Jersey, (1978).

148. von Ballmoos, R., The O^{18}-exchanged Method in Zeolite Chemistry: Synthesis, Characterization and Dealumination of High Silica Zeolites, Ph.D. thesis, Swiss Institute of Technology, Zurich, Swiss (1981).

149. von Ballmoos, R., Collection of Simulated XRD Powder Patterns for Zeolites, The Structure Commission of the International Zeolite Association, pp. 74-75 (1984).

150. Wakao, N.; and Smith, J.M., Chem. Eng. Sci., 17, 825 (1962).

151. Wakao, N.; and Smith, J.M., Ind. Eng. Chem. Fundam., 3, 123 (1964).

152. Ward, J.W.; and Hansford, R.C., J. Catal., 13, 154 (1969).

153. Wedel, S.; and Luss, D., Chem. Eng. Commun., 7, 245 (1980).

154. Weeks, T.J. Jr.; Kimak, D.G.; Bujalski, R.L.; and Balton, A.P., J. Chem. Soc., Faraday Trans. I, 72, 575 (1976).

155. Williams, J.A.; R.J. Adler; and Zolner, W.J., III, Ind. Eng. Chem. Fundam., 9 (2), 193 (1970).

156. Wu, P.; Debebe, A.; and Ma. Y.H.; Zeolites, 3, 118 (1983).

157. Yashima, T.; Otami, S.; and Sato, M., Bull. Japan Petro. Inst., 12, 106 (1970).

158. Yashima, T.; Sakaguechi, Y.; and Namba, S., Prepr. Int. Cong. Catal., 7th, A52 (1980).

159. Yasuda, Y., J. Phys. Chem., 86 1913 (1982).

160. Yasuda, Y.; and Yamamoto A., J. Catal., 93 176 (1985).

161. Young, L.B.; Butter, S.A.; and Kaeding, W.W., J. Catal., 76, 418 (1982).

APPENDIX A

Calibration for Toluene Disproportionation Reaction

A.1 Powder-Form Zeolite

The detector responses for known amounts of calibration standards were determined from the integrator and were used to prepare linear calibration plots of peak area vs. molar amount. The standards liquid mixtures were 0.2%, 2.0% and 5.0% (by volume) of benzene or xylenes in toluene.

A.1.1 GC Conditions and Column

P_{He} = 28 Psig

P_{H_2} = 40 Psig

P_{air} = 30 Psig

Helium flow rate = 36 cm^3/ min

Hydrogen flowrate = 24 cm^3/ min

Air flow rate = 300 cm^3/ min

$T_{injector}$ = 220°C

$T_{detector}$ = 220°C

Column Temperature = 75°C

The column was GP 5% SP-1200/1.75% Bentone 34, 2.4 m long and 0.318 cm o.d..

A.1.2 Product Identification

The retention times of the reactant and products on the glc column were determined relative to that of toluene. The products were then

identified by their ralative retention times. The toluene eluted from the column in 5.34 ± 0.14 min.

Compound	Relative Retention Time	# Determines
Benzene	0.43 ± 0.02	46
Toluene	1.0	46
m-xylene	2.24 ± 0.10	46
p-xylene	2.53 ± 0.09	36
o-xylene	2.91 ± 0.01	36

A.1.3 Quantitative Calibration

The detector responses of known amounts of calbration standards were determined from the integrator and used to prepare linear calibration plots of peak area vs. molar amount. The standard liquid mixtures were 0.2%, 2.0%, and 5.0% (by volume) benzene or xylenes in toluene.

Standard Liquid Mixture Results

Vol. %	Component	10^{8}x Molar Amount	10^{-5} x Response (area unit)	#Pts.
0.2	Benzene	4.501	1.64 ± 0.03	4
0.2	Xylenes	3.476	1.41 ± 0.04	4
2.0	Benzene	45.01	8.03 ± 0.85	6
2.0	Xylenes	34.76	6.88 ± 0.66	6
5.0	Benzene	112.53	25.80 ± 0.50	4
5.0	Xylenes	86.90	21.19 ± 0.26	4

From the above data, calibration factors were obtained by linear regression.

Benzene - mols = area / 2.277 X 10^{-13} - 47443

P-xylene - mols = area / 1.523 X 10^{-13} - 4797

M-xylenes - mols = area / 3.249 X 10^{-13} - 12749

O-xylenes - mols = area / 1.706 X 10^{-13} - 6543

Xylenes - mols = area / 2.409 X 10^{-13} - 22231

Since the intercepts for the linear regression results are too large to be ignored, therefore, it was decided to interpolate GC area - molar amount data.

A.2 Pellet-Form Zeolite

The detector responses for known amounts of calibration standards were determined from the integrator and were used to prepare linear calibration plots of peak area vs. molar amount. The standards liquid mixtures were 0.2%, 0.5% and 1.0% (by volume) of benzene or xylenes in toluene. The GC conditions, the column, and relative retentation times are unchanged.

A.2.1 Quantitative Calibration

The detector responses of known amounts of calbration standards were determined from the integrator and used to prepare linear calibration plots of peak area v.s. molar amount. The standard liquid mixtures was 0.2%, 0.5%, and 1.0% (by volume) benzene and xylenes, respectively in toluene.

Standard Liquid Mixture Results

Vol. %	Component	10^8x Molar Amount	10^{-5} x Response (area unit)	#Pts.
0.2	Benzene	4.501	0.67 ± 0.01	5
0.2	Xylenes	3.476	0.71 ± 0.06	5
0.5	Benzene	11.252	1.85 ± 0.07	9
0.5	Xylenes	8.690	1.74 ± 0.08	9
1.0	Benzene	22.505	2.91 ± 0.19	6
1.0	Xylenes	17.380	2.84 ± 0.17	6

From the above data, calibration factors were obtained by linear regression.

Benzene - mols = area / 8.3 X 10^{-13} - 26089

Xylenes - mols = area / 6.7 X 10^{-13} - 28268

Since the intercepts for the linear regression results are too large to be ignored, therefore, it was decided to interpolate the GC area - molar amount data.

APPENDIX B

Kinetics Results of Toluene Disproportionation Reaction

B.1 Conversion and Kinetics Data

The percentage conversion and rate of formation of a product were calculated as follows:

$$\text{Molar feed rate} = \frac{(\text{Liq. vol. feed rate})(\text{Liq vol. frac.})(\text{MW})}{\left(1. - \frac{P_{tot}}{P_{He}}\right)} \qquad (B-1)$$

$$(\text{adjusted area}) = (\text{area in product sample}) - (\text{area on feed sample}) \qquad (B-2)$$

$$\%\ \text{Con} = \frac{(\text{adjusted area})/(\text{calibration slope}) \times 100}{0.1\ \text{mol} \times 0.05\ \text{cm}^3 \frac{1\ \text{mol}}{22400\ \text{cm}^3} \frac{273\ \text{K}}{298\ \text{K}}} \qquad (B-3)$$

$$\text{Rate} = \frac{(\%\ \text{conversion}/100)\ (\text{molar feed rate})}{(\text{catalyst weight})\ (\text{Mols acid groups/weight})} \qquad (B-4)$$

B.2 Powder form zeolite

This is the kinetics results for toluene disproportionation catalyzed by powder form zeolites. The raw GC area data were converted to conversion information according to the calibration information shown in Appendix A.

B.2.1 Linde ELZ-L Zeolite

For 0.15 g of ELZ-L Zeolite, Run at Mar/25/87
He Flowrate = 36.0 cm^3/ min
Toluene Flowrate = 0.74 cm^3/hr
Reaction Temperature = 420°C

TOS (MIN)	BZ CONV%	P-XY CONV%	M-XY CONV*%	O-XY CONV%	XY CONV%
20.0	0.4590	1.4766	0.3122	0.7699	0.4276
40.0	0.4454	1.7992	0.4293	1.1223	0.5506
60.0	0.3452	1.3692	0.2778	0.7551	0.3988
80.0	0.2416	1.1849	0.2090	0.9088	0.3617
100.0	0.1921	1.0777	0.2265	1.1063	0.3799
120.0	0.1686	1.0061	0.2490	0.8932	0.3643
140.0	0.1704	1.1930	0.2229	0.8002	0.3591
160.0	0.1745	0.9512	0.1734	0.5178	0.2652
180.0	0.1481	0.7764	0.1446	0.3478	0.1983
200.0	0.1319	0.6427	0.1240	0.4837	0.1838
220.0	0.1078	0.4704	0.1139	0.4913	0.1677
240.0	0.0928	0.4327	0.1240	0.3737	0.1664
260.0	0.0850	0.4804	0.0971	0.1704	0.1356
280.0	0.0893	0.3451	0.0843	0.0519	0.1030
300.0	0.0739	0.2472	0.0696	0.0463	0.0863
320.0	0.0624	0.1886	0.0584	0.1682	0.0907
340.0	0.0498	0.1608	0.0681	0.0342	0.0758
360.0	0.0423	0.1639	0.0419	0.0299	0.0566

For 0.20 g of ELZ-L Zeolite, Run at Mar/30/87
He Flowrate = 36.0 cm^3/ min
Toluene Flowrate = 0.74 cm^3/hr
Reaction Temperature = 420°C

TOS (MIN)	BZ CONV%	P-XY CONV%	M-XY CONV*%	O-XY CONV%	XY CONV%
20.0	0.7312	1.7229	0.3045	0.6420	0.4337
40.0	0.5479	1.4411	0.4015	1.0085	0.5500
60.0	0.4164	1.4102	0.4548	1.0789	0.5797
80.0	0.3130	1.7859	0.3474	0.9118	0.4873
100.0	0.2324	1.4952	0.2858	0.7645	0.4153
120.0	0.2056	1.3098	0.2156	0.6527	0.3518
140.0	0.1775	1.1969	0.1972	0.7054	0.3351
160.0	0.1645	1.0627	0.1884	0.6162	0.3034
180.0	0.1510	0.9745	0.1721	0.5268	0.2666
200.0	0.1441	0.8294	0.1480	0.3307	0.2045
220.0	0.1300	0.7294	0.1311	0.2854	0.1825
240.0	0.1129	0.6064	0.1239	0.3000	0.1715
260.0	0.0970	0.5510	0.1102	0.1988	0.1528
280.0	0.0938	0.4779	0.0952	0.1671	0.1336
300.0	0.0761	0.2998	0.0739	0.0463	0.0923
320.0	0.0624	0.2966	0.0695	0.0417	0.0883
340.0	0.0536	0.1941	0.0524	0.0342	0.0689
360.0	0.0425	0.1657	0.0479	0.0299	0.0612

For 0.40 g of ELZ-L Zeolite, Run at Mar/06/87
He Flowrate = 36.0 cm^3/ min
Toluene Flowrate = 0.74 cm^3/hr
Reaction Temperature = 420°C

TOS (MIN)	BZ CONV%	P-XY CONV%	M-XY CONV*%	O-XY CONV%	XY CONV%
20.0	1.0412	1.6563	0.7590	1.4104	0.8596
40.0	1.0275	2.2994	1.1100	1.8241	1.1868
60.0	1.0170	1.5656	0.7185	1.4890	0.8379
80.0	1.1270	2.0139	0.9637	1.6662	1.0501
100.0	0.7080	1.4421	0.6152	1.4211	0.6989
120.0	0.6680	1.6954	0.4635	1.1277	0.5591
140.0	0.7009	1.4790	0.3968	1.0098	0.4940
160.0	0.3265	1.5285	0.4453	1.1645	0.5382
180.0	0.5373	1.3066	0.3492	0.8947	0.4430
200.0	0.5341	1.6933	0.4938	1.6223	0.6219
220.0	0.5290	1.2617	0.3131	1.1542	0.4454
240.0	0.4716	1.6225	0.4752	1.4892	0.5932
260.0	0.4607	1.4984	0.4309	1.6744	0.5771
280.0	0.5269	0.9558	0.2075	0.9316	0.3423
300.0	0.4453	1.5659	0.7012	1.6572	0.8086
320.0	0.4065	1.7757	0.5183	1.7086	0.6502
340.0	0.3570	1.4014	0.4725	1.5771	0.5802
360.0	0.3358	1.6557	0.4608	1.4559	0.5856

For 0.40 g of ELZ-L Zeolite, Run at Mar/16/87
He Flowrate = 36.0 cm^3/ min
Toluene Flowrate = 0.74 cm^3/hr
Reaction Temperature = 420°C

TOS (MIN)	BZ CONV%	P-XY CONV%	M-XY CONV*%	O-XY CONV%	XY CONV%
20.0	0.9647	1.6886	0.5975	1.6016	0.6725
40.0	0.9728	1.7143	0.8862	1.7988	0.9887
60.0	0.8185	1.5674	0.6543	2.7305	0.7595
80.0	0.6866	1.4447	0.6261	1.4066	0.7622
100.0	0.6558	1.5403	0.2137	1.4599	0.5723
120.0	0.6772	1.4219	0.5999	1.9455	0.7388
140.0	0.6386	1.9499	0.5974	1.3423	0.6713
160.0	0.6116	1.7906	0.5386	1.1994	0.6130
180.0	0.6062	1.7590	0.5277	1.2425	0.6087
200.0	0.5631	1.6890	0.5046	1.2395	0.5903
220.0	0.4451	1.6887	0.4995	1.2019	0.5840

For 0.40 g of ELZ-L Zeolite, Run at Apr/14/87
He Flowrate = 36.0 cm^3/ min
Toluene Flowrate = 0.74 cm^3/hr
Reaction Temperature = 420°C

TOS (MIN)	BZ CONV%	P-XY CONV%	M-XY CONV*%	O-XY CONV%	XY CONV%
20.0	1.3427	1.4476	0.6673	1.5123	0.7351
40.0	1.1864	2.1267	1.0177	2.0133	1.1434
60.0	1.1273	2.2047	1.0834	2.2657	1.2242
80.0	1.0384	2.2329	1.1085	2.2544	1.2392
100.0	0.9827	2.1323	1.0572	2.2283	1.1955
120.0	0.9170	2.0648	1.0308	2.1584	1.1626
140.0	0.8126	1.7900	0.8816	2.1396	1.0461
160.0	0.7314	1.7597	0.8493	1.9411	0.9967
180.0	0.6649	1.6140	0.7634	1.7167	0.9004
200.0	0.6993	1.6452	0.7778	1.7356	0.9147
220.0	0.6208	1.6160	0.7489	1.6894	0.8893
240.0	0.6427	1.5026	0.7605	1.7694	0.8913
260.0	0.4803	1.8953	0.5893	1.5836	0.7526
280.0	0.4430	1.8638	0.5789	1.4063	0.7188
300.0	0.3703	1.6931	0.5047	1.8020	0.6448
320.0	0.3563	1.6187	0.4701	1.7216	0.6126
340.0	0.3804	1.5964	0.4830	1.7013	0.6152
360.0	0.3148	1.3930	0.3861	1.6510	0.5424
380.0	0.1987	1.2860	0.3364	1.4063	0.4838
400.0	0.2070	1.1742	0.2915	1.2058	0.4314
420.0	0.1940	1.1383	0.2711	1.1434	0.4117
440.0	0.1852	1.1070	0.2494	1.0862	0.3923
460.0	0.1668	0.8760	0.2084	0.9968	0.3418
480.0	0.1515	0.8477	0.1809	0.9737	0.3090
500.0	0.1305	0.7564	0.1657	0.7596	0.2611
520.0	0.1255	0.7077	0.1570	0.6672	0.2370
540.0	0.1145	0.6475	0.1462	0.6137	0.2130
560.0	0.1084	0.6424	0.1452	0.6130	0.2112

For 0.40 g of ELZ-L Zeolite, Run at May/16/87
He Flowrate = 36.0 cm^3/ min
Toluene Flowrate = 0.74 cm^3/hr
Reaction Temperature = 420°C

TOS (MIN)	BZ CONV%	P-XY CONV%	M-XY CONV*%	O-XY CONV%	XY CONV%
20.0	1.1505	1.6936	0.7617	1.5830	1.0409
40.0	1.0641	2.4370	1.0354	2.4143	1.4609
60.0	0.9599	2.5118	1.0777	2.7305	1.5494
80.0	0.9215	2.3749	1.0388	2.7798	1.5084
100.0	0.8881	2.1325	0.9756	2.7157	1.4177
120.0	0.7783	2.0564	0.8922	2.6886	1.3421
140.0	0.7447	1.9034	0.8557	2.3745	1.2536
160.0	0.7412	1.9709	0.8741	2.3503	1.2734
180.0	0.6905	1.6655	0.7500	1.9837	1.0889
200.0	0.6765	1.7269	0.7938	2.2273	1.1603
220.0	0.5798	1.6868	0.7359	1.9924	1.0831
240.0	0.5669	1.6039	0.6983	1.8301	1.0188
260.0	0.5393	1.5362	0.6631	1.7712	0.9742
280.0	0.5133	1.4706	0.6496	1.7710	0.9545
300.0	0.4143	1.3229	0.5505	1.6572	0.8432
320.0	0.4226	1.3195	0.5436	1.4441	0.8054
340.0	0.3854	1.3197	0.5381	1.4166	0.7973
360.0	0.3643	1.2159	0.4988	1.3436	0.7422
380.0	0.3310	1.0114	0.4408	1.2352	0.6530
400.0	0.2690	1.0042	0.3880	1.1194	0.5961
420.0	0.2397	0.9417	0.3537	0.9588	0.5375
440.0	0.2048	0.8836	0.3231	0.8892	0.4961
460.0	0.1973	0.8172	0.3041	0.8819	0.4712
480.0	0.1700	0.6798	0.2387	0.7969	0.3903
500.0	0.1544	0.6650	0.2210	0.6436	0.3520
520.0	0.1393	0.5572	0.1844	0.5633	0.2900
540.0	0.1313	0.5629	0.1855	0.5435	0.2891

For 0.60 g of ELZ-L Zeolite, Run at May/06/87
He Flowrate = 36.0 cm^3/ min
Toluene Flowrate = 0.74 cm^3/hr
Reaction Temperature = 420°C

TOS (MIN)	BZ CONV%	P-XY CONV%	M-XY CONV*%	O-XY CONV%	XY CONV%
20.0	1.6646	2.7061	1.2132	2.6170	1.6592
40.0	1.5231	3.3527	1.5382	3.6579	3.3531
60.0	1.4056	3.2049	1.4899	4.0812	3.3630
80.0	1.3337	4.9658	1.4406	3.8669	3.6694
100.0	1.2571	3.0506	1.3941	3.7551	2.0095
120.0	1.3224	2.9882	1.4146	3.8140	2.0240
140.0	1.2151	2.8441	1.3119	3.6519	1.9044
160.0	1.2092	2.8857	1.3306	3.6817	1.9285
180.0	1.1652	2.7586	1.2791	3.4522	1.8385
200.0	1.1504	2.7449	1.2674	3.4345	1.8254
220.0	1.1034	2.7111	1.2424	3.3652	1.7921
240.0	1.0094	2.4829	1.1594	3.2158	1.6764
260.0	0.9005	2.4091	1.1030	3.0281	1.5969
280.0	0.9111	2.3353	1.0673	2.8820	1.5385
300.0	0.8837	2.1919	0.9938	2.6748	1.4335
320.0	0.8415	2.1821	0.9829	2.5960	1.4125
340.0	0.7758	2.1119	0.9293	2.4716	1.3449
360.0	0.7303	1.9045	0.8832	2.3150	1.2649
380.0	0.6594	1.7980	0.8112	2.2431	1.1859
400.0	0.6123	1.6765	0.7506	1.9798	1.0903
420.0	0.4224	1.2189	0.5311	1.4938	0.7888
440.0	0.4985	1.4722	0.6303	1.5324	0.9046
460.0	0.4521	1.3908	0.5904	1.5329	0.8636
480.0	0.4432	1.2314	0.5377	1.3970	0.7808
500.0	0.3675	1.1596	0.4785	1.3334	0.7174
520.0	0.3400	1.0949	0.4485	1.2152	0.6681
540.0	0.2938	0.9971	0.3959	1.0712	0.5935
560.0	0.2743	0.9648	0.3787	1.0200	0.5684
580.0	0.2520	0.9012	0.3474	0.9576	0.5267
600.0	0.2000	0.8575	0.3195	0.8672	0.4862
620.0	0.1856	0.7411	0.2746	0.6225	0.3991
640.0	0.1728	0.6850	0.2434	0.7309	0.3845
660.0	0.1631	0.6544	0.2270	0.6162	0.3506
680.0	0.1522	0.5986	0.1987	0.4990	0.3034
700.0	0.1400	0.5394	0.1816	0.4294	0.2638
720.0	0.1282	0.5241	0.1761	0.4491	0.2579

For 0.60 g of ELZ-L Zeolite, Run at May/19/87
He Flowrate = 36.0 cm^3/ min
Toluene Flowrate = 0.74 cm^3/hr
Reaction Temperature = 420°C

TOS (MIN)	BZ CONV%	P-XY CONV%	M-XY CONV*%	O-XY CONV%	XY CONV%
20.0	1.5598	1.6713	0.6892	1.5622	0.9817
40.0	1.4349	2.9823	1.2896	2.5602	1.7466
60.0	1.2793	2.9853	1.3067	2.4865	1.7485
80.0	1.2272	2.7960	1.2399	2.2520	1.6377
100.0	1.2540	2.8596	1.2688	2.3917	1.6887
120.0	1.0710	2.3847	1.2050	2.3766	1.5709
140.0	0.9952	2.2668	0.9861	2.1692	1.3640
160.0	0.9895	2.3823	1.0425	3.6817	1.3959
180.0	0.9977	4.2786	1.0673	2.0572	1.6994
200.0	1.0089	2.3168	1.0376	3.4345	1.3764
220.0	0.9900	2.3967	1.0545	3.3652	1.4045
240.0	0.9449	2.1926	1.0414	3.2158	1.3650
260.0	0.7357	1.9111	0.8994	1.9312	1.2262
280.0	0.7200	1.8240	0.8036	1.7457	1.1155
300.0	0.7223	1.7649	0.7700	1.4238	1.0335
320.0	0.6748	1.7853	0.7754	1.4983	1.0518
340.0	0.6598	1.7494	0.7598	1.4404	1.0263
360.0	0.6520	1.7021	0.7372	1.4242	1.0003
380.0	0.5692	1.5742	0.6951	1.3540	0.9400
400.0	0.4400	1.3262	0.5938	1.3037	0.8216
420.0	0.4493	1.2764	0.5276	1.1852	0.7482
440.0	0.4145	1.2584	0.5214	1.1324	0.7330
460.0	0.3898	1.2126	0.4875	0.9604	0.6755
480.0	0.3684	1.1334	0.4446	0.8833	0.6208
500.0	0.3466	1.1432	0.4599	0.9045	0.6366
520.0	0.2887	0.9676	0.4014	0.8129	0.5540
540.0	0.2008	0.8405	0.3394	0.8129	0.4899
560.0	0.1917	0.7567	0.2696	0.6846	0.4072
580.0	0.1820	0.7238	0.2517	0.5351	0.3667
600.0	0.1750	0.6981	0.2378	0.5112	0.3491
620.0	0.1566	0.6671	0.2206	0.4953	0.3296
640.0	0.1567	0.6153	0.2003	0.4555	0.3011
660.0	0.1487	0.5618	0.1887	0.4348	0.2763
680.0	0.1341	0.4590	0.1795	0.4156	0.2472
700.0	0.1137	0.4133	0.1468	0.3819	0.1979

For 0.80 g of ELZ-L Zeolite, Run at Mar/24/87
He Flowrate = 36.0 cm^3/ min
Toluene Flowrate = 0.74 cm^3/hr
Reaction Temperature = 420°C

TOS (MIN)	BZ CONV%	P-XY CONV%	M-XY CONV*%	O-XY CONV%	XY CONV%
20.0	2.0854	4.2811	1.7503	4.1397	5.5606
40.0	1.9034	4.5066	1.8876	4.2441	5.9063
60.0	1.9906	4.4229	1.8232	4.0041	5.6852
80.0	1.8233	4.3234	1.8004	4.1415	5.6610
100.0	1.7631	4.2056	1.7378	4.4508	5.6221
120.0	1.7158	3.9781	1.6359	4.2027	5.2867
140.0	1.6044	3.9989	1.7468	4.2114	5.4871
160.0	1.5550	4.1757	1.7289	4.0720	5.4658
180.0	1.5977	3.9444	1.5916	3.8896	5.0913
200.0	1.5224	3.7745	1.5347	3.5427	4.8178
220.0	1.4313	3.6482	1.9882	3.6101	4.6908
240.0	1.8662	3.2870	1.7559	3.2547	4.1660
260.0	1.7772	3.2951	1.9027	3.3702	4.3878
280.0	1.6396	3.3212	1.7969	3.1386	4.1870
300.0	1.6216	3.0744	1.6164	2.8892	3.7996
320.0	1.5426	2.9122	1.5052	2.6555	3.5299
340.0	1.3414	2.6102	1.3145	2.4220	1.4204
360.0	1.2395	2.4145	1.1839	2.3129	1.3110
380.0	1.1063	2.2610	1.1992	2.1574	1.2753
400.0	0.9748	2.2970	1.1173	2.0166	1.2181

B.2.2 Linde ELZ - Ω - 6 Zeolite

For 0.4 g of ELZ - Ω Zeolite, Run at Jul/08/87
He Flowrate = 36.0 cm^3/ min
Toluene Flowrate = 0.74 cm^3/hr
Reaction Temperature = 420°C

TOS (MIN)	BZ CONV%	P-XY CONV%	M-XY CONV*%	O-XY CONV%	XY CONV%
20.0	0.4966	0.9441	0.4370	1.0622	0.6141
40.0	0.4862	0.9745	0.4952	1.2197	0.6847
60.0	0.4466	0.8851	0.4392	1.2459	0.6345
80.0	0.3644	0.8691	0.4277	1.1451	0.6086
100.0	0.3273	0.8652	0.4075	1.1241	0.5901
120.0	0.2711	0.7194	0.3483	1.0544	0.5147
140.0	0.1981	0.6696	0.3012	0.8814	0.4469
160.0	0.1737	0.5949	0.2565	0.7833	0.3884
180.0	0.1489	0.5176	0.2122	0.6801	0.3291
200.0	0.1116	0.3616	0.1558	0.5168	0.2199
220.0	0.0882	0.2807	0.1279	0.3779	0.1721
240.0	0.0690	0.2062	0.1023	0.2828	0.1386
260.0	0.0525	0.1326	0.0619	0.0577	0.0722
280.0	0.0472	0.1317	0.0620	0.0571	0.0721
300.0	0.0302	0.0908	0.0303	0.0289	0.0394

For 0.4 g of ELZ - Ω Zeolite, Run at Jul/19/87
He Flowrate = 36.0 cm^3/ min
Toluene Flowrate = 0.74 cm^3/hr
Reaction Temperature = 420°C

TOS (MIN)	BZ CONV%	P-XY CONV%	M-XY CONV*%	O-XY CONV%	XY CONV%
20.0	0.6966	0.6252	0.2431	0.6470	0.3626
40.0	0.7854	0.7937	0.3253	0.7729	0.4665
60.0	0.6659	0.8056	0.3311	0.7943	0.4758
80.0	0.5408	0.7606	0.3100	0.7738	0.4506
100.0	0.4297	0.6750	0.2705	0.7088	0.3993
120.0	0.3349	0.5760	0.2198	0.6113	0.3329
140.0	0.2520	0.5566	0.2110	0.6223	0.3253
160.0	0.2047	0.5221	0.1971	0.6006	0.3053
180.0	0.1759	0.4623	0.1795	0.5527	0.2684
200.0	0.1578	0.4515	0.1748	0.5514	0.2610
220.0	0.1435	0.4087	0.1635	0.5220	0.2368
240.0	0.1318	0.3835	0.1535	0.4903	0.2163
260.0	0.1198	0.3578	0.1462	0.4722	0.2011
280.0	0.1088	0.3412	0.1853	0.4541	0.2422
300.0	0.1013	0.3219	0.1332	0.4287	0.1843
320.0	0.0932	0.2885	0.1248	0.3898	0.1717
340.0	0.0882	0.2695	0.1195	0.3644	0.1639
360.0	0.0845	0.2630	0.1172	0.3562	0.1610
380.0	0.0826	0.2411	0.1132	0.3289	0.1537
400.0	0.0726	0.2122	0.0950	0.2265	0.1288
420.0	0.0782	0.2120	0.1013	0.2441	0.1349

440.0	0.0819	0.2088	0.0978	0.2764	0.1351

For 0.4 g of ELZ - Ω Zeolite, Run at Jul/09/87
He Flowrate = 36.0 cm^3/ min
Toluene Flowrate = 0.74 cm^3/hr
Reaction Temperature = 420°C

TOS (MIN)	BZ CONV%	P-XY CONV%	M-XY CONV*%	O-XY CONV%	XY CONV%
20.0	0.7972	0.9317	0.5082	1.1839	0.6823
40.0	0.7547	1.0609	0.5664	1.2971	0.7610
60.0	0.6667	1.0371	0.5568	1.4032	0.7666
80.0	0.5866	1.0106	0.5397	1.3471	0.7417
100.0	0.4943	0.9512	0.5058	1.2533	0.6940
120.0	0.4005	0.8719	0.4790	1.1634	0.6490
140.0	0.3180	0.7673	0.4486	1.0922	0.6005
160.0	0.2418	0.6786	0.3589	0.9713	0.5038
180.0	0.1785	0.5494	0.3110	0.8071	0.4248
200.0	0.1484	0.4560	0.2452	0.6646	0.3415
220.0	0.1184	0.3507	0.1832	0.5183	0.2508
240.0	0.1008	0.2498	0.1442	0.3731	0.1806
260.0	0.0797	0.1878	0.1154	0.2742	0.1447
280.0	0.0609	0.1522	0.0908	0.1901	0.1137
300.0	0.0429	0.1190	0.0695	0.0565	0.0754
320.0	0.0355	0.1016	0.0560	0.0391	0.0607

For 0.4 g of ELZ - Ω Zeolite, Run at Jul/20/87
He Flowrate = 36.0 cm^3/ min
Toluene Flowrate = 0.74 cm^3/hr
Reaction Temperature = 420°C

TOS (MIN)	BZ CONV%	P-XY CONV%	M-XY CONV*%	O-XY CONV%	XY CONV%
20.0	0.2993	0.4172	0.1620	0.4307	0.2224
40.0	0.3666	0.4376	0.1611	0.4502	0.2275
60.0	0.3016	0.4200	0.1565	0.4323	0.2166
80.0	0.2034	0.3825	0.1470	0.3868	0.1957
100.0	0.1656	0.3757	0.1472	0.3853	0.1951
120.0	0.1444	0.3436	0.1439	0.3419	0.1859
140.0	0.1289	0.3189	0.1324	0.2964	0.1714
160.0	0.1142	0.2619	0.1179	0.2650	0.1531
180.0	0.1031	0.2494	0.1166	0.2671	0.1512
200.0	0.1023	0.2683	0.1176	0.2818	0.1550
220.0	0.0960	0.2807	0.1189	0.3409	0.1624
240.0	0.0902	0.2810	0.1195	0.3398	0.1627
260.0	0.0828	0.2570	0.1122	0.3094	0.1526
280.0	0.0767	0.2409	0.1070	0.2924	0.1459
300.0	0.0739	0.2371	0.1060	0.2938	0.1450
320.0	0.0690	0.2167	0.0995	0.2852	0.1378
340.0	0.0650	0.1963	0.0931	0.2621	0.1291
360.0	0.0619	0.1936	0.0915	0.2544	0.1268
380.0	0.0588	0.1827	0.0858	0.2273	0.1186

For 0.4 g of ELZ - Ω Zeolite, Run at Jul/21/87
He Flowrate = 36.0 cm^3/ min
Toluene Flowrate = 0.74 cm^3/hr
Reaction Temperature = 420°C

TOS (MIN)	BZ CONV%	P-XY CONV%	M-XY CONV*%	O-XY CONV%	XY CONV%
20.0	1.0120	0.8451	0.3312	0.8248	0.4864
40.0	0.8214	0.8843	0.3518	0.9974	0.5334
60.0	0.6048	0.8435	0.3333	0.9235	0.5027
80.0	0.4505	0.8208	0.3237	0.9247	0.4924
100.0	0.3134	0.7627	0.2958	0.9078	0.4609
120.0	0.2158	0.6729	0.2556	0.8240	0.4056
140.0	0.1701	0.5993	0.2305	0.7716	0.3684
160.0	0.1438	0.5692	0.2087	0.7343	0.3424
180.0	0.1237	0.5009	0.1855	0.6457	0.2954
200.0	0.1121	0.4755	0.1780	0.6096	0.2771
220.0	0.1021	0.4369	0.1665	0.5981	0.2560
240.0	0.0922	0.3879	0.1528	0.5513	0.2254
260.0	0.0874	0.3710	0.1472	0.5277	0.2127
280.0	0.0811	0.3188	0.1324	0.4806	0.1882
300.0	0.0758	0.2973	0.1256	0.4404	0.1777
320.0	0.0716	0.2551	0.1129	0.3918	0.1605
340.0	0.0686	0.2284	0.1050	0.3597	0.1495
360.0	0.0656	0.1994	0.0959	0.3184	0.1367
380.0	0.0633	0.1908	0.0911	0.3003	0.1302
400.0	0.0602	0.3322	0.0813	0.2641	0.1333
420.0	0.0583	0.1717	0.0809	0.2631	0.1167

For 0.6 g of ELZ - Ω Zeolite, Run at Jul/14/87
He Flowrate = 36.0 cm^3/ min
Toluene Flowrate = 0.74 cm^3/hr
Reaction Temperature = 420°C

TOS (MIN)	BZ CONV%	P-XY CONV%	M-XY CONV*%	O-XY CONV%	XY CONV%
20.0	0.5766	0.3244	0.1411	0.3449	0.1825
40.0	1.6374	0.7966	0.3280	0.6652	0.4527
60.0	1.1974	1.1473	0.5036	0.9373	0.6739
80.0	1.2926	1.3649	0.6213	1.2023	0.8321
100.0	1.1465	1.3874	0.3328	1.2846	0.6383
120.0	1.0354	1.3817	0.9627	1.2843	1.0950
140.0	0.9223	1.3658	0.6180	1.2821	0.8419
160.0	0.7990	1.3144	0.5879	1.2287	0.8042
180.0	0.6715	1.2556	0.5576	1.1803	0.7661
200.0	0.5554	1.1965	0.5256	1.1253	0.7257
220.0	0.4636	1.1199	0.4888	1.0885	0.6819
240.0	0.3574	1.0439	0.4457	1.0101	0.6274
260.0	0.2682	0.9555	0.4087	0.9502	0.5782
280.0	0.1966	0.8657	0.3676	0.8642	0.5219
300.0	0.1659	0.8003	0.3315	0.8050	0.4769
320.0	0.1397	0.7238	0.2922	0.7307	0.4256
340.0	0.1210	0.6513	0.2594	0.6938	0.3854
360.0	0.1007	0.5929	0.2293	0.6428	0.3471
380.0	0.0866	0.5365	0.1993	0.5857	0.3079
400.0	0.0748	0.4810	0.1827	0.5241	0.2706
420.0	0.0650	0.4315	0.1682	0.4877	0.2406
440.0	0.0565	0.3871	0.1535	0.4639	0.2129
460.0	0.0494	0.3460	0.1411	0.4284	0.1920

For 0.6 g of ELZ - Ω Zeolite, Run at Jul/16/87
He Flowrate = 36.0 cm^3/ min
Toluene Flowrate = 0.74 cm^3/hr
Reaction Temperature = 420°C

TOS (MIN)	BZ CONV%	P-XY CONV%	M-XY CONV*%	O-XY CONV%	XY CONV%
20.0	1.7474	0.7437	0.2983	0.7004	0.4285
40.0	1.9767	1.3060	0.5453	1.2398	0.7737
60.0	1.6791	1.5586	0.7038	1.4771	0.9626
80.0	1.4875	1.6201	0.7059	1.5514	0.9846
100.0	1.3008	1.6635	0.7230	1.6351	1.0162
120.0	1.1648	1.5827	0.6975	1.5521	0.9730
140.0	0.9899	1.5159	0.6609	1.3972	0.9130
160.0	0.8364	1.4262	0.6193	1.4655	0.8796
180.0	0.6825	1.3332	0.5779	1.3808	0.8228
200.0	0.5412	1.2349	0.5340	1.2819	0.7612
220.0	0.4158	1.0787	0.4631	1.1419	0.6651
240.0	0.3072	0.9530	0.3938	0.8771	0.5560
260.0	0.2232	0.8676	0.3552	0.8174	0.5061
280.0	0.1743	0.7422	0.2949	0.6912	0.4244
300.0	0.1433	0.6587	0.2535	0.6287	0.3724
320.0	0.1222	0.6276	0.2352	0.6305	0.3547
340.0	0.1033	0.5375	0.2295	0.5824	0.3298
360.0	0.0874	0.4595	0.1707	0.5103	0.2511
380.0	0.0693	0.3518	0.1411	0.3974	0.1897
400.0	0.0602	0.3560	0.1417	0.4145	0.1921
420.0	0.0572	0.3399	0.1353	0.3890	0.1837
440.0	0.0515	0.2997	0.1227	0.3543	0.1681
460.0	0.0456	0.2678	0.1119	0.3179	0.1542

For 0.8 g of ELZ - Ω Zeolite, Run at Jul/17/87
He Flowrate = 36.0 cm^3/ min
Toluene Flowrate = 0.74 cm^3/hr
Reaction Temperature = 420°C

TOS (MIN)	BZ CONV%	P-XY CONV%	M-XY CONV*%	O-XY CONV%	XY CONV%
20.0	1.7981	0.9140	0.3669	1.0350	0.5545
40.0	2.1375	1.3923	0.5321	1.3529	0.7942
60.0	1.9703	1.5862	0.6185	1.5146	0.9105
80.0	1.8117	1.6862	0.6652	1.5750	0.9684
100.0	1.7272	1.6697	0.6794	1.5024	0.9653
120.0	1.5088	1.4054	0.6593	1.3515	0.8883
140.0	1.4045	1.4577	0.6574	1.3088	0.8883
160.0	1.2832	1.4929	0.6673	1.3163	0.9019
180.0	1.2870	1.5197	0.7005	1.4151	0.9450
200.0	1.3520	1.6048	0.7073	1.5973	0.9903
220.0	1.2131	1.4515	0.6017	1.2959	0.8450
240.0	0.9571	1.2902	0.5387	1.1946	0.7598
260.0	0.7669	1.1521	0.4941	0.9088	0.6634
280.0	0.6318	1.1383	0.4751	1.1697	0.6871
300.0	0.5863	1.1637	0.5333	1.2171	0.7403
320.0	0.6315	1.3219	0.5627	1.2066	0.7837
340.0	0.5792	1.2772	0.5062	0.8195	0.6774
360.0	0.4991	1.2874	0.5111	1.1640	0.7346
380.0	0.4352	1.2360	0.5201	1.0627	0.7182
400.0	0.3572	1.0998	0.4921	1.0765	0.6795
420.0	0.3126	1.0604	0.4974	1.0625	0.6753
440.0	0.2614	0.9558	0.4473	0.9584	0.6075
460.0	0.2077	0.8953	0.4235	0.9131	0.5743
480.0	0.1787	0.8278	0.3870	0.8606	0.5298
500.0	0.1593	0.7950	0.3703	0.8233	0.5071
520.0	0.1413	0.7496	0.3466	0.8063	0.4805
540.0	0.1277	0.7059	0.3266	0.7812	0.4556
560.0	0.1149	0.6335	0.2870	0.6938	0.4028
580.0	0.1014	0.5112	0.2180	0.5774	0.3167
600.0	0.0860	0.4701	0.1872	0.5112	0.2724
620.0	0.0874	0.5209	0.2122	0.5595	0.3113

For 0.8 g of ELZ - Ω Zeolite, Run at Jul/18/87
He Flowrate = 36.0 cm^3/ min
Toluene Flowrate = 0.74 cm^3/hr
Reaction Temperature = 420°C

TOS (MIN)	BZ CONV%	P-XY CONV%	M-XY CONV*%	O-XY CONV%	XY CONV%
20.0	1.9634	1.4457	0.6385	1.3319	0.8763
40.0	2.2113	1.9099	0.8799	1.8186	1.1948
60.0	2.1538	2.1534	0.9159	2.0535	1.2793
80.0	1.8542	1.8784	0.8671	1.9433	1.1996
100.0	1.7676	1.7946	0.8273	1.8307	1.1412
120.0	1.6175	1.7491	0.8090	1.7801	1.1134
140.0	1.3728	1.6886	0.7815	1.7231	1.0757
160.0	1.3656	1.5874	0.7458	1.6640	1.0257
180.0	0.8893	1.5017	0.7154	1.5489	0.9734
200.0	0.6779	1.4711	0.7179	1.4548	0.9564
220.0	0.5124	1.4003	0.6217	1.3551	0.8608
240.0	0.3670	1.3065	0.5645	1.2647	0.7915
260.0	0.2459	1.1845	0.5148	1.1560	0.7208
280.0	0.1758	1.0777	0.4667	1.0636	0.6558
300.0	0.1457	1.0099	0.4374	1.0213	0.6179
320.0	0.1232	1.0263	0.4177	0.9632	0.5973
340.0	0.1021	0.8959	0.3816	0.9770	0.5536
360.0	0.0846	0.8543	0.3469	0.9312	0.5153
380.0	0.0679	0.7627	0.3079	0.8507	0.4611
400.0	0.0552	0.6810	0.2751	0.7567	0.4107
420.0	0.0459	0.6365	0.2544	0.6774	0.3771
440.0	0.0385	0.6127	0.2253	0.6131	0.3427
460.0	0.0321	0.5613	0.1924	0.5402	0.2965
480.0	0.0273	0.5156	0.1750	0.4862	0.2610
500.0	0.0234	0.4535	0.1658	0.4597	0.2368
520.0	0.0201	0.4213	0.1566	0.4369	0.2177
540.0	0.0173	0.3878	0.1427	0.3838	0.1928
560.0	0.0151	0.3190	0.1286	0.3304	0.1718
580.0	0.0136	0.2979	0.1232	0.3188	0.1650
600.0	0.0116	0.3231	0.1148	0.2872	0.1584
620.0	0.0105	0.2637	0.1082	0.2695	0.1467
640.0	0.0093	0.2236	0.1015	0.2508	0.1367

B.2.3 Linde LZ-Y-52 Zeolite

For 0.2 g of LZ-Y-52 Zeolite, Run at Mar/11/87
He Flowrate = 36.0 cm^3/ min
Toluene Flowrate = 0.74 cm^3/hr
Reaction Temperature = 400°C

TOS (MIN)	BZ CONV%	P-XY CONV%	M-XY CONV*%	O-XY CONV%	XY CONV%
20.0	0.1875	1.0918	0.1819	0.5969	0.2961
40.0	0.1821	1.0204	0.1719	0.5580	0.2734
60.0	0.1955	1.2266	0.1955	0.6851	0.3337
80.0	0.1927	1.1466	0.1834	0.5456	0.2981
100.0	0.1854	1.1510	0.1826	0.6231	0.3049
120.0	0.1876	1.1418	0.1825	0.8118	0.3221
140.0	0.1842	0.5607	0.1314	0.3323	0.1763
160.0	0.1874	1.3493	0.2453	0.8070	0.3854
180.0	0.2138	1.3134	0.2149	0.7162	0.3579
200.0	0.1962	1.1983	0.1906	0.5929	0.3162
220.0	0.1966	1.2104	0.1910	0.6767	0.3259
240.0	0.1948	1.1944	0.1902	0.8666	0.3417
260.0	0.1864	1.1220	0.2396	0.8158	0.3627
280.0	0.1992	1.3668	0.2359	0.7619	0.3778
300.0	0.2247	1.3067	0.2088	0.7086	0.3534
320.0	0.2015	1.2487	0.1954	0.6135	0.3288
340.0	0.1990	1.1877	0.1855	0.7320	0.3223
360.0	0.1905	1.0972	0.1898	0.8114	0.3271
380.0	0.1783	1.2191	0.2327	0.7909	0.3656
400.0	0.2100	1.3880	0.2313	0.7600	0.3772
420.0	0.2160	1.2760	0.1977	0.6485	0.3375
440.0	0.2081	1.2286	0.1940	0.5823	0.3221

For 0.4 g of LZ-Y-52 Zeolite, Run at Apr/29/87
He Flowrate = 36.0 cm^3/ min
Toluene Flowrate = 0.74 cm^3/hr
Reaction Temperature = 400°C

TOS (MIN)	BZ CONV%	P-XY CONV%	M-XY CONV*%	O-XY CONV%	XY CONV%
20.0	0.3024	0.8658	0.3055	0.6627	0.4463
40.0	0.3104	0.9420	0.3387	0.7774	0.4992
60.0	0.3150	1.2192	0.4620	1.0511	0.6717
80.0	0.3149	1.2169	0.4719	1.1132	0.6879
100.0	0.2757	0.9373	0.4193	1.2101	0.6225
120.0	0.2270	0.9695	0.3411	1.1617	0.5632
140.0	0.2512	1.0791	0.3834	0.7678	0.5508
160.0	0.2746	1.1072	0.4048	0.9753	0.6019
180.0	0.3098	1.1701	0.4309	1.0241	0.6377
200.0	0.3184	1.3688	0.4851	1.1429	0.7247
220.0	0.3792	0.9119	0.4744	1.2229	0.6607
240.0	0.2351	1.0474	0.3684	1.2765	0.6121
260.0	0.2612	1.0941	0.3868	0.7313	0.5500
280.0	0.2898	1.1592	0.4276	1.0015	0.6302
300.0	0.3262	1.2216	0.4546	1.0843	0.6717
320.0	0.3482	1.3677	0.5311	1.2434	0.7732
340.0	0.4091	0.9882	0.4869	1.2674	0.6879
360.0	0.2519	0.9565	0.3516	1.1461	0.5665
380.0	0.2994	1.1840	0.4477	0.8834	0.6306

For 0.4 g of LZ-Y-52 Zeolite, Run at Apr/30/87
He Flowrate = 36.0 cm^3/ min
Toluene Flowrate = 0.74 cm^3/hr
Reaction Temperature = 400°C

TOS (MIN)	BZ CONV%	P-XY CONV%	M-XY CONV*%	O-XY CONV%	XY CONV%
20.0	0.3743	0.7189	0.2833	0.6125	0.4006
40.0	0.2916	1.0838	0.4088	1.1002	0.6202
60.0	0.2899	1.1408	0.4275	1.1019	0.6426
80.0	0.2699	1.0643	0.3938	0.9403	0.5822
100.0	0.2611	1.0945	0.4025	1.0225	0.6054
120.0	0.2680	1.1474	0.4185	1.0411	0.6278
140.0	0.2762	1.1324	0.4035	1.0069	0.6095
160.0	0.3055	1.2309	0.4425	1.0453	0.6584
180.0	0.2748	1.0254	0.4153	1.0814	0.6134
200.0	0.2705	1.1278	0.4102	1.1942	0.6420
220.0	0.2794	1.1265	0.4096	1.0328	0.6170
240.0	0.2947	1.1945	0.4399	1.0292	0.6486
260.0	0.3044	1.2259	0.4509	1.0991	0.6719
280.0	0.3112	1.2990	0.4780	1.1826	0.7151
300.0	0.3355	1.3529	0.4898	1.1871	0.7324
320.0	0.3590	1.3566	0.5202	1.2361	0.7625
340.0	0.3417	1.2972	0.5279	1.3907	0.7827
360.0	0.3165	1.2490	0.4594	1.3760	0.7234
380.0	0.3420	1.3281	0.4929	1.2927	0.7470
400.0	0.3519	1.3094	0.4918	1.0894	0.7126
420.0	0.3555	1.4219	0.5369	1.2686	0.7893
440.0	0.3518	1.3403	0.4859	1.2430	0.7362
460.0	0.3868	1.4486	0.5389	1.2576	0.7931
480.0	0.3803	1.4436	0.5272	1.2702	0.7858
500.0	0.3015	1.3839	0.5145	1.4027	0.7877
520.0	0.3762	1.4176	0.5237	1.1671	0.7638
540.0	0.3914	1.4760	0.5524	1.2681	0.8086
560.0	0.3870	1.4971	0.5641	1.3652	0.8350
580.0	0.3992	1.5096	0.5588	1.4011	0.8384

For 0.4 g of LZ-Y-52 Zeolite, Run at May/01/87
He Flowrate = 36.0 cm^3/ min
Toluene Flowrate = 0.74 cm^3/hr
Reaction Temperature = 400°C

TOS (MIN)	BZ CONV%	P-XY CONV%	M-XY CONV*%	O-XY CONV%	XY CONV%
20.0	0.3743	0.7189	0.2833	0.6125	0.4006
40.0	0.2916	1.1018	0.4088	1.1002	0.6229
60.0	0.2899	1.1408	0.4275	1.1019	0.6426
80.0	0.2699	1.0643	0.3938	0.9403	0.5822
100.0	0.2611	1.0945	0.4025	1.0225	0.6054
120.0	0.2680	1.1474	0.4185	1.0411	0.6278
140.0	0.2762	1.1324	0.4035	1.0069	0.6095
160.0	0.3055	1.2309	0.4425	1.0453	0.6584
180.0	0.2748	1.0254	0.4153	1.0814	0.6134
200.0	0.2705	1.1278	0.4102	1.1942	0.6420
220.0	0.2794	1.1265	0.4096	1.0328	0.6170
240.0	0.2947	1.1945	0.4399	1.0292	0.6486
260.0	0.3044	1.2259	0.4509	1.0991	0.6719
280.0	0.3112	1.2990	0.4780	1.1826	0.7151
300.0	0.3355	1.3529	0.4898	1.1871	0.7324
320.0	0.3590	1.3566	0.5202	1.2361	0.7625
340.0	0.3417	1.2972	0.5279	1.3907	0.7827
360.0	0.3165	1.2490	0.4594	1.3760	0.7234
380.0	0.3420	1.3281	0.4929	1.2927	0.7470
400.0	0.3519	1.3094	0.4918	1.0894	0.7126
420.0	0.3555	1.4219	0.5369	1.2691	0.7894
440.0	0.3518	1.3403	0.4992	1.2430	0.7459
460.0	0.3868	1.4486	0.5389	1.2576	0.7931
480.0	0.3803	1.4436	0.5272	1.2702	0.7858
500.0	0.3015	1.3839	0.5145	1.4027	0.7877
520.0	0.3762	1.4176	0.5237	1.1671	0.7638
540.0	0.3914	1.4760	0.5524	1.2681	0.8086
560.0	0.3870	1.4971	0.5641	1.3652	0.8350
580.0	0.3992	1.5096	0.5588	1.4011	0.8384

For 0.6 g of LZ-Y-52 Zeolite, Run at May/04/87
He Flowrate = 36.0 cm^3/ min
Toluene Flowrate = 0.74 cm^3/hr
Reaction Temperature = 400°C

TOS (MIN)	BZ CONV%	P-XY CONV%	M-XY CONV*%	O-XY CONV%	XY CONV%
20.0	0.4064	0.9957	0.3667	0.8603	0.5401
40.0	0.4342	1.3371	0.5676	1.3039	0.8043
60.0	0.3998	1.1137	0.5439	1.3579	0.7618
80.0	0.3159	1.1365	0.4461	1.3819	0.6978
100.0	0.3075	1.1818	0.4513	1.3721	0.7069
120.0	0.3265	1.1502	0.4416	1.1621	0.6633
140.0	0.3196	1.1388	0.4318	1.0470	0.6371
160.0	0.3479	1.1939	0.4553	1.0742	0.6665
180.0	0.3604	1.2062	0.4592	1.2684	0.7006
200.0	0.3645	1.3130	0.5070	1.2224	0.7443
220.0	0.3943	1.3913	0.5402	1.3240	0.7955
240.0	0.4124	1.3996	0.5370	1.3148	0.7931
260.0	0.4099	1.2419	0.4682	1.1117	0.6887
280.0	0.4435	1.5200	0.5842	1.3640	0.8528
300.0	0.4582	1.5300	0.6085	1.4513	0.8852
320.0	0.5012	1.3319	0.6383	1.5124	0.8864
340.0	0.4416	1.3253	0.6302	1.5697	0.8882
360.0	0.3794	1.3976	0.6619	1.6224	0.9301
380.0	0.4555	1.3562	0.6563	1.5906	0.9150
400.0	0.3994	0.9112	0.3762	1.1696	0.5812
420.0	0.4097	1.2994	0.5124	1.5185	0.7910
440.0	0.4137	1.4445	0.5709	1.6919	0.8815
460.0	0.4253	1.3658	0.5331	1.5829	0.8257
480.0	0.4325	1.4503	0.5722	1.5200	0.8573
500.0	0.4604	1.5251	0.6019	1.5303	0.8916
520.0	0.4706	1.5604	0.6176	1.4861	0.9016
540.0	0.4737	1.4807	0.5818	1.3975	0.8503
560.0	0.4850	1.6232	0.6466	1.4821	0.9315
580.0	0.4789	1.5793	0.6268	1.4843	0.9109

For 0.6 g of LZ-Y-52 Zeolite, Run at May/05/87
He Flowrate = 36.0 cm^3/ min
Toluene Flowrate = 0.74 cm^3/hr
Reaction Temperature = 400°C

TOS (MIN)	BZ CONV%	P-XY CONV%	M-XY CONV*%	O-XY CONV%	XY CONV%
20.0	0.3851	0.9912	0.3662	0.8159	0.5324
40.0	0.3555	0.8983	0.3276	0.7118	0.4747
60.0	0.3631	1.2145	0.4691	1.0673	0.6786
80.0	0.3720	1.2706	0.4812	1.0415	0.6919
100.0	0.3637	1.2544	0.4826	1.0607	0.6934
120.0	0.3457	1.2434	0.4818	1.0685	0.6923
140.0	0.3803	1.2245	0.4680	0.9609	0.6632
160.0	0.3954	1.2906	0.4935	1.0775	0.7092
180.0	0.4190	1.3830	0.5612	1.1631	0.7852
200.0	0.3815	1.2218	0.5574	1.1983	0.7637
220.0	0.3678	1.2332	0.5322	1.1503	0.7398
240.0	0.3789	1.2611	0.5018	1.1881	0.7275
260.0	0.3771	1.2710	0.4980	1.2810	0.7404
280.0	0.3891	1.3360	0.5240	1.2638	0.7664
300.0	0.3961	1.3414	0.5298	1.2614	0.7711
320.0	0.4155	1.4526	0.5763	1.3153	0.8296
340.0	0.4382	1.4324	0.5655	1.1478	0.7934
360.0	0.4374	1.4622	0.5768	1.1344	0.8041
380.0	0.4473	1.4637	0.5789	1.1832	0.8132
400.0	0.4612	1.4841	0.5896	1.2502	0.8342
420.0	0.4782	1.5198	0.5986	1.2037	0.8390
440.0	0.4836	1.5945	0.6338	1.2941	0.8894
460.0	0.4965	1.6021	0.6378	1.2669	0.8894
480.0	0.5142	1.6641	0.6627	1.3566	0.9303
500.0	0.5257	1.6942	0.6761	1.3350	0.9413
520.0	0.5385	1.6731	0.6644	1.3407	0.9305
540.0	0.5072	1.5698	0.6178	1.2134	0.8619
560.0	0.5516	1.7446	0.6928	1.3739	0.9669
580.0	0.5783	1.7707	0.7046	1.3943	0.9824

For 0.6 g of LZ-Y-52 Zeolite, Run at May/17/87
He Flowrate = 36.0 cm^3/ min
Toluene Flowrate = 0.74 cm^3/hr
Reaction Temperature = 400°C

TOS (MIN)	BZ CONV%	P-XY CONV%	M-XY CONV*%	O-XY CONV%	XY CONV%
20.0	0.3727	1.1750	0.2444	0.8432	0.3726
40.0	0.4191	1.7656	0.4662	1.3699	0.5901
60.0	0.4553	1.8721	0.4826	1.4822	0.6190
80.0	0.4606	1.9048	0.5095	1.4872	0.6362
100.0	0.5056	1.9746	0.5462	1.5750	0.6697
120.0	0.4840	1.4846	0.6235	1.0411	0.7245
140.0	0.5127	1.4985	0.6443	1.0069	0.7529
160.0	0.5225	1.4973	0.6399	1.0453	0.7483
180.0	0.5376	1.5480	0.6875	1.0814	0.7989

For 0.8 g of LZ-Y-52 Zeolite, Run at May/07/87
He Flowrate = 36.0 cm^3/ min
Toluene Flowrate = 0.74 cm^3/hr
Reaction Temperature = 400°C

TOS (MIN)	BZ CONV%	P-XY CONV%	M-XY CONV*%	O-XY CONV%	XY CONV%
20.0	0.4156	1.6508	0.5686	1.5046	0.6450
40.0	0.4206	1.5883	0.4741	1.4827	0.5889
60.0	0.4543	1.8443	0.5713	1.5830	0.6715
80.0	0.4657	1.8072	0.5576	1.4225	0.6457
100.0	0.4871	1.4035	0.6418	1.7105	0.7351
120.0	0.5290	1.8762	0.5784	1.3923	0.6596
140.0	0.5457	1.5739	0.7238	1.5165	0.8109
160.0	0.5787	1.9763	0.7245	1.7213	0.7750
180.0	0.5324	1.4234	0.6694	1.9355	0.7735
200.0	0.5430	1.5060	0.7065	1.4016	0.8046
220.0	0.5841	1.4154	0.6438	1.5367	0.7210
240.0	0.5971	1.4045	0.6382	1.5843	0.7212
260.0	0.6479	1.6258	0.7675	1.2810	0.8480
280.0	0.7063	1.7975	0.8519	1.4253	0.9285
300.0	0.6328	1.4440	0.7194	1.8138	0.7902
320.0	0.6547	1.5987	0.7562	1.4614	0.8577
340.0	0.7072	1.6928	0.8186	1.1478	0.8924
360.0	0.7302	1.7960	0.8793	1.4562	0.9468
380.0	0.7726	1.7937	0.8744	1.4277	0.9398
400.0	0.7859	1.7773	0.8554	1.2502	0.9225
420.0	0.8245	1.8823	0.9121	1.4882	0.9800
440.0	0.8502	1.8996	0.9677	1.5278	1.0164
460.0	0.8115	1.7996	0.9898	1.6118	1.0262
480.0	0.8119	1.8666	0.9198	1.6952	1.0117
500.0	0.8493	1.8938	0.9340	1.5592	1.0030
520.0	0.8653	1.9196	0.9477	1.4856	1.0028
540.0	0.9091	2.0519	1.0264	1.6628	1.0869
560.0	0.9133	1.9968	0.9848	1.5566	1.0427
580.0	0.9799	2.1525	1.0714	1.6915	1.1277

For 0.8 g of LZ-Y-52 Zeolite, Run at May/19/87
He Flowrate = 36.0 cm^3/ min
Toluene Flowrate = 0.74 cm^3/hr
Reaction Temperature = 400°C

TOS (MIN)	BZ CONV%	P-XY CONV%	M-XY CONV*%	O-XY CONV%	XY CONV%
20.0	0.5198	1.1527	0.2753	0.9374	0.3954
40.0	0.5893	1.9841	0.6075	1.6980	0.7137
60.0	0.6152	1.4655	0.6528	1.8074	0.7585
80.0	0.6288	1.4120	0.6168	1.8340	0.7353
100.0	0.6263	1.4557	0.6446	1.4258	0.7759
120.0	0.6313	1.5319	0.7428	1.5331	0.8520
140.0	0.6287	1.6045	0.7693	1.5165	0.8731
160.0	0.6984	1.6058	0.7356	1.4248	0.8428
180.0	0.6960	1.6565	0.7611	1.4647	0.8685
200.0	0.7361	1.6528	0.7564	1.4016	0.8565
220.0	0.7421	1.6863	0.7742	1.5651	0.8938
240.0	0.7365	1.7091	0.8029	1.6843	0.9289

B.2.4 Linde ELZ-105-6 Zeolite

For 0.4 g of ELZ-105-6 Zeolite, Run at Feb/17/87
He Flowrate = 36.0 cm^3/ min
Toluene Flowrate = 0.74 cm^3/hr
Reaction Temperature = 420°C

TOS (MIN)	BZ CONV%	P-XY CONV%	M-XY CONV*%	O-XY CONV%	XY CONV%
20.0	0.0928	0.1397	0.0652	0.1532	0.0870
40.0	0.0696	0.1387	0.0725	0.1618	0.0934
60.0	0.0795	0.1270	0.0686	0.1306	0.0847
80.0	0.0726	0.1625	0.0906	0.1901	0.1136
100.0	0.0774	0.1451	0.0758	0.1695	0.0977
120.0	0.0714	0.1535	0.0830	0.1807	0.1056
140.0	0.0783	0.1554	0.0727	0.1292	0.0913
160.0	0.0864	0.1887	0.0757	0.1435	0.0999
180.0	0.0916	0.2580	0.0797	0.1609	0.1098
200.0	0.0928	0.2914	0.0866	0.1845	0.1199
220.0	0.0942	0.2661	0.0796	0.1587	0.1099
240.0	0.0993	0.3324	0.0909	0.1946	0.1265
260.0	0.0960	0.2490	0.0801	0.1628	0.1099
280.0	0.0967	0.2361	0.0822	0.1715	0.1119
300.0	0.0948	0.2318	0.0804	0.1667	0.1097
320.0	0.0910	0.2262	0.0808	0.1679	0.1099
340.0	0.0942	0.2254	0.0812	0.1673	0.1100
360.0	0.0908	0.2149	0.0793	0.1626	0.1075
380.0	0.0933	0.2265	0.0770	0.1529	0.1051
400.0	0.0928	0.2269	0.0804	0.1574	0.1082
420.0	0.0936	0.2399	0.0817	0.1646	0.1108
440.0	0.0900	0.2375	0.0806	0.1628	0.1096
460.0	0.0903	0.1886	0.0697	0.1721	0.0995
480.0	0.0842	0.3408	0.1014	0.3126	0.1417
500.0	0.0873	0.2102	0.0770	0.1476	0.1035
520.0	0.0854	0.1924	0.0735	0.1819	0.1040
540.0	0.0828	0.2225	0.0782	0.2558	0.1153
560.0	0.0816	0.1898	0.0693	0.2037	0.1033
580.0	0.0821	0.1918	0.0828	0.2610	0.1167
600.0	0.0785	0.1665	0.0840	0.1733	0.1071
620.0	0.0772	0.1993	0.1002	0.2276	0.1284
640.0	0.0865	0.2595	0.0872	0.1524	0.1142
660.0	0.1011	0.3630	0.0951	0.2301	0.1336
680.0	0.1006	0.2696	0.0856	0.1792	0.1173
700.0	0.0954	0.2058	0.0744	0.1586	0.1029
720.0	0.0953	0.2741	0.0876	0.1818	0.1193

For 0.4 g of ELZ-105-6 Zeolite, Run at Feb/25/87
He Flowrate = 36.0 cm^3/ min
Toluene Flowrate = 0.74 cm^3/hr
Reaction Temperature = 420°C

TOS (MIN)	BZ CONV%	P-XY CONV%	M-XY CONV*%	O-XY CONV%	XY CONV%
20.0	0.1067	0.1607	0.0623	0.1582	0.0884
40.0	0.1001	0.1637	0.0625	0.1582	0.0890
60.0	0.1040	0.2412	0.0948	0.3091	0.1313
80.0	0.0986	0.2657	0.1044	0.2614	0.1370
100.0	0.0972	0.2887	0.0940	0.1992	0.1271
120.0	0.1049	0.2861	0.0889	0.1979	0.1230
140.0	0.1015	0.2198	0.0792	0.1697	0.1086
160.0	0.0993	0.1991	0.0769	0.1390	0.1016
180.0	0.0863	0.1959	0.0786	0.1658	0.1061
200.0	0.1006	0.2429	0.0866	0.1897	0.1180
220.0	0.0985	0.2453	0.0872	0.1141	0.1082
240.0	0.0958	0.1950	0.0760	0.1721	0.1049
260.0	0.0948	0.2356	0.0954	0.2322	0.1272
280.0	0.0931	0.2365	0.0873	0.1929	0.1186
300.0	0.0975	0.2362	0.0812	0.1775	0.1120
320.0	0.0976	0.2164	0.0787	0.1724	0.1084
340.0	0.0919	0.2832	0.0915	0.2207	0.1262
360.0	0.0947	0.2220	0.0800	0.1683	0.1091
380.0	0.0966	0.2131	0.0789	0.1758	0.1089
400.0	0.0958	0.2297	0.0800	0.1893	0.1124
420.0	0.0958	0.2303	0.0891	0.2211	0.1217

For 0.6 g of ELZ-105-6 Zeolite, Run at Feb/18/87
He Flowrate = 36.0 cm^3/ min
Toluene Flowrate = 0.74 cm^3/hr
Reaction Temperature = 420°C

TOS (MIN)	BZ CONV%	P-XY CONV%	M-XY CONV*%	O-XY CONV%	XY CONV%
20.0	0.1626	0.3615	0.0976	0.2515	0.1366
40.0	0.1361	0.5040	0.1291	0.6535	0.1897
60.0	0.1131	0.4379	0.1395	0.5596	0.1885
80.0	0.1098	0.3996	0.1486	0.4906	0.1892
100.0	0.1042	0.5084	0.1262	0.3673	0.1717
120.0	0.1319	0.5623	0.1322	0.4132	0.1816
140.0	0.0943	0.2562	0.0830	0.1714	0.1136
160.0	0.1166	0.4815	0.1239	0.3717	0.1689
180.0	0.1172	0.4061	0.1109	0.2836	0.1505
200.0	0.1151	0.4155	0.1120	0.2223	0.1483
220.0	0.1170	0.3818	0.1056	0.2156	0.1414
240.0	0.1116	0.3743	0.1046	0.3759	0.1493
260.0	0.1062	0.3679	0.1030	0.4706	0.1532
280.0	0.1067	0.3403	0.1137	0.4536	0.1586
300.0	0.1013	0.2780	0.1238	0.3582	0.1573
320.0	0.1036	0.4706	0.1350	0.4272	0.1795
340.0	0.1259	0.5513	0.1263	0.3720	0.1743
360.0	0.1271	0.4755	0.1218	0.3486	0.1658
380.0	0.1206	0.4853	0.1235	0.3588	0.1681
400.0	0.1100	0.4079	0.1118	0.3139	0.1529
420.0	0.1091	0.3718	0.1048	0.1980	0.1392
440.0	0.1094	0.3506	0.1010	0.2063	0.1359
460.0	0.1100	0.3625	0.1026	0.3838	0.1478
480.0	0.1082	0.3563	0.1015	0.4643	0.1511
500.0	0.1069	0.3268	0.1158	0.4090	0.1568
520.0	0.1033	0.3779	0.1358	0.4140	0.1744
540.0	0.1254	0.5503	0.1255	0.3703	0.1736
560.0	0.1263	0.4639	0.1182	0.3151	0.1606
580.0	0.1211	0.4738	0.1215	0.3403	0.1649
600.0	0.1199	0.4414	0.1160	0.3153	0.1578
620.0	0.1195	0.4066	0.1101	0.2234	0.1465
640.0	0.1162	0.3730	0.1036	0.2515	0.1416
660.0	0.1127	0.3967	0.1075	0.4076	0.1544
680.0	0.1097	0.3611	0.1026	0.4613	0.1520
700.0	0.1018	0.3184	0.1233	0.3991	0.1613

For 0.6 g of ELZ-105-6 Zeolite, Run at Feb/26/87
He Flowrate = 36.0 cm^3/ min
Toluene Flowrate = 0.74 cm^3/hr
Reaction Temperature = 420°C

TOS (MIN)	BZ CONV%	P-XY CONV%	M-XY CONV*%	O-XY CONV%	XY CONV%
20.0	0.1495	0.5140	0.1338	0.4103	0.1800
40.0	0.1440	0.5098	0.1379	0.5171	0.1888
60.0	0.1435	0.6074	0.1475	0.5326	0.2031
80.0	0.1459	0.5373	0.1369	0.5346	0.1905
100.0	0.1407	0.6030	0.1467	0.5078	0.1996
120.0	0.1462	0.5325	0.1379	0.4733	0.1875
140.0	0.1420	0.5468	0.1464	0.5138	0.1968
160.0	0.1506	0.5541	0.1404	0.4548	0.1894
180.0	0.1449	0.5764	0.1538	0.5508	0.2099
200.0	0.1510	0.5935	0.1466	0.5249	0.2000
220.0	0.1451	0.5752	0.1419	0.4866	0.1935
240.0	0.1473	0.5635	0.1473	0.5610	0.2017
260.0	0.1484	0.6115	0.1495	0.5589	0.2086
280.0	0.1454	0.5934	0.1448	0.5064	0.1977
300.0	0.1484	0.5613	0.1515	0.5404	0.2047
320.0	0.1521	0.5973	0.1453	0.5320	0.1997
340.0	0.1449	0.5883	0.1455	0.4872	0.1968
360.0	0.1500	0.6290	0.1502	0.5198	0.2072
380.0	0.1493	0.5859	0.1566	0.5841	0.2175
400.0	0.1517	0.5953	0.1456	0.5716	0.2034
420.0	0.1452	0.5982	0.1463	0.4780	0.1974
440.0	0.1483	0.6106	0.1495	0.5258	0.2053
460.0	0.1512	0.5719	0.1493	0.5686	0.2056

For 0.8 g of ELZ-105-6 Zeolite, Run at Feb/19/87
He Flowrate = 36.0 cm^3/ min
Toluene Flowrate = 0.74 cm^3/hr
Reaction Temperature = 420°C

TOS (MIN)	BZ CONV%	P-XY CONV%	M-XY CONV*%	O-XY CONV%	XY CONV%
20.0	0.3829	1.0900	0.2402	0.9921	0.3770
40.0	0.3605	1.2304	0.3176	2.1324	0.6329
60.0	0.3292	1.4543	0.4488	0.5217	0.4715
80.0	0.3189	1.5205	0.3739	0.5346	0.4897
100.0	0.3002	1.1165	0.2494	0.7021	0.3562
120.0	0.2857	1.0765	0.2481	0.9752	0.3782
140.0	0.2569	1.0504	0.2377	1.0560	0.3782
160.0	0.2657	1.0009	0.4119	1.6298	0.5875
180.0	0.2527	1.1589	0.2646	2.4986	0.6524
200.0	0.2513	0.8928	0.2603	1.5338	0.4863
220.0	0.2273	1.5414	0.3236	1.5932	0.5184
240.0	0.2397	1.0094	0.2824	1.4783	0.4380
260.0	0.2354	1.0530	0.2964	1.2028	0.4226
280.0	0.2270	1.0118	0.3016	1.0589	0.4077
300.0	0.2273	1.8606	0.4845	1.6310	0.6332

For 0.8 g of ELZ-105-6 Zeolite, Run at Feb/24/87
He Flowrate = 36.0 cm^3/ min
Toluene Flowrate = 0.74 cm^3/hr
Reaction Temperature = 420°C

TOS (MIN)	BZ CONV%	P-XY CONV%	M-XY CONV*%	O-XY CONV%	XY CONV%
20.0	0.3528	0.6082	0.1475	0.2678	0.1870
40.0	0.4330	0.6511	0.1580	0.3453	0.2021
60.0	0.3528	0.6082	0.1475	0.2678	0.1870
80.0	0.2726	0.6756	0.1651	0.4759	0.2258
100.0	0.2356	0.9436	0.2345	0.9538	0.3571
120.0	0.2206	0.8362	0.1929	0.8204	0.3081
140.0	0.2188	0.9385	0.2207	0.9649	0.3507
160.0	0.2214	0.8458	0.1950	0.8380	0.3132
180.0	0.2187	0.7831	0.1775	0.6792	0.2705
200.0	0.2108	0.8241	0.1879	0.7916	0.2980
220.0	0.2051	0.8658	0.1971	0.9372	0.3273
240.0	0.1906	0.8564	0.1926	0.8504	0.3124
260.0	0.2035	0.8052	0.1876	0.8358	0.3001
280.0	0.2020	0.7997	0.1917	0.8990	0.3108
300.0	0.2275	0.9522	0.2245	0.7962	0.3376
320.0	0.2256	1.0101	0.2474	0.9540	0.3698
340.0	0.2733	0.9971	0.2769	1.0702	0.3948
360.0	0.2485	0.9966	0.2517	0.9371	0.3691
380.0	0.2262	0.9913	0.2322	0.8956	0.3547
400.0	0.2451	0.9902	0.2900	1.0280	0.3968
420.0	0.2077	0.9761	0.2473	0.9071	0.3621
440.0	0.2131	0.9211	0.2123	0.8258	0.3314
460.0	0.2530	1.0035	0.2476	0.9454	0.3684
480.0	0.2681	0.9119	0.2028	0.8114	0.3243
500.0	0.2509	0.9784	0.2580	0.9871	0.3755
520.0	0.2454	0.9886	0.2451	0.8898	0.3605
540.0	0.2424	0.9174	0.2111	0.8617	0.3339
560.0	0.2424	0.9729	0.2396	0.9164	0.3588
580.0	0.2419	0.9174	0.2251	0.8961	0.3444
600.0	0.2293	0.9110	0.2247	0.8855	0.3426
620.0	0.2396	0.8306	0.1936	0.7585	0.3025
640.0	0.2325	0.8894	0.2023	0.8222	0.3231
660.0	0.2321	0.9418	0.2198	0.8309	0.3376
680.0	0.2396	0.9824	0.2403	0.9242	0.3607
700.0	0.2390	0.9107	0.2213	0.8712	0.3394
720.0	0.2321	0.9256	0.2229	0.8611	0.3406
740.0	0.2457	0.9464	0.2251	0.8776	0.3452
760.0	0.2411	0.9580	0.2312	0.8986	0.3514
780.0	0.2286	0.9311	0.2269	0.8619	0.3432
800.0	0.2480	0.9622	0.2361	0.9587	0.3601
820.0	0.2669	1.0389	0.2586	0.8848	0.3715
840.0	0.2388	1.0052	0.2315	0.9344	0.3593
860.0	0.2799	1.0098	0.2879	1.0123	0.3960
880.0	0.2437	1.0430	0.2597	0.9001	0.3739
900.0	0.2476	0.9835	0.2433	1.0040	0.3700
920.0	0.2654	1.0270	0.2708	0.9393	0.3819
940.0	0.2427	1.0514	0.2643	0.9424	0.3810

For 0.8 g of ELZ-105-6 Zeolite, Run at Feb/28/87
He Flowrate = 36.0 cm^3/ min
Toluene Flowrate = 0.74 cm^3/hr
Reaction Temperature = 420°C

TOS (MIN)	BZ CONV%	P-XY CONV%	M-XY CONV*%	O-XY CONV%	XY CONV%
20.0	0.4712	0.7597	0.1663	0.6016	0.2470
40.0	0.4134	1.2508	0.3177	1.1590	0.4472
60.0	0.6782	1.1999	0.3007	1.1627	0.4343
80.0	0.3915	1.2861	0.3454	1.2718	0.4754
100.0	0.4021	1.2407	0.3254	1.2515	0.4591
120.0	0.4085	1.2994	0.3651	1.3186	0.4912
140.0	0.4090	1.2789	0.3784	1.2994	0.4943
160.0	0.4010	1.3546	0.4337	1.4099	0.5400
180.0	0.3882	1.3767	0.4818	1.4267	0.5682
200.0	0.3773	1.4468	0.4799	1.3940	0.5705
220.0	0.3767	1.8382	0.5496	1.5950	0.6610
240.0	0.4253	1.5472	0.4497	1.2592	0.5513
260.0	0.4644	1.5475	0.4448	1.1901	0.5421
280.0	0.4821	1.5526	0.4442	1.2296	0.5461
300.0	0.4965	1.6124	0.4655	1.2599	0.5653
320.0	0.4982	1.6050	0.4605	1.2565	0.5617
340.0	0.4938	1.5929	0.4572	1.2292	0.5563
360.0	0.4974	1.6436	0.4682	1.2739	0.5709
380.0	0.4952	1.5484	0.4326	1.3322	0.5496
400.0	0.4756	1.5316	0.4261	1.4557	0.5566

For 0.8 g of ELZ-105-6 Zeolite, Run at Apr/27/87
He Flowrate = 36.0 cm^3/ min
Toluene Flowrate = 0.74 cm^3/hr
Reaction Temperature = 420°C

TOS (MIN)	BZ CONV%	P-XY CONV%	M-XY CONV*%	O-XY CONV%	XY CONV%
20.0	0.3397	0.6835	0.3261	0.8753	0.4661
40.0	0.3076	0.8000	0.3352	0.9840	0.5067
60.0	0.3081	0.8051	0.3328	0.7312	0.4674
80.0	0.3169	0.8110	0.3358	0.8151	0.4832
100.0	0.3317	0.8649	0.3591	0.8484	0.5132
120.0	0.3712	1.0595	0.4764	1.1105	0.6672
140.0	0.2662	0.8424	0.3658	1.1248	0.5566
160.0	0.3211	0.9493	0.4034	1.0992	0.5959
180.0	0.3030	0.9233	0.3912	0.8537	0.5461
200.0	0.3275	0.9465	0.4048	0.9674	0.5766
220.0	0.3275	1.0014	0.4285	1.0404	0.6131
240.0	0.3574	1.1089	0.4615	1.1096	0.6637
260.0	0.3225	0.9091	0.4434	1.1531	0.6272
280.0	0.3123	0.9371	0.3940	1.1623	0.5969
300.0	0.3144	0.9185	0.3829	0.8174	0.5338
320.0	0.3208	1.0101	0.4314	1.0256	0.6143
340.0	0.3338	1.1208	0.4800	1.0823	0.6748

B.3 Pellet form zeolite

This is the kinetics results for toluene disproportionation catalyzed by pellet form zeolites. The raw GC area data were converted to conversion information according to the calibration information shown in Appendix A.

B.3.1 Linde ELZ-L Zeolite

For 0.20 g of ELZ-L Zeolite, Run at Dec/05/88
He Flowrate = 66.0 cm^3/ min
Toluene Flowrate = 0.49 cm^3/hr
Reaction Temperature = 420°C

TIME (MIN)	BZ CONV%	XY CONV%
20.0	0.0647	0.0000
40.0	0.0563	0.0000
60.0	0.0496	0.0000
80.0	0.0655	0.0000
100.0	0.0642	0.0000
120.0	0.0481	0.0000
140.0	0.0501	0.0000
160.0	0.0397	0.0000
180.0	0.0618	0.0000
200.0	0.0436	0.0000
220.0	0.0456	0.0000
240.0	0.0445	0.0000
260.0	0.0488	0.0000
280.0	0.0371	0.0000
300.0	0.0339	0.0000
320.0	0.0356	0.0000
340.0	0.0285	0.0000
360.0	0.0314	0.0000
380.0	0.0347	0.0000
400.0	0.0370	0.0000
420.0	0.0249	0.0000
440.0	0.0256	0.0000
460.0	0.0311	0.0000
480.0	0.0282	0.0000
500.0	0.0267	0.0000
520.0	0.0283	0.0000
540.0	0.0215	0.0000
560.0	0.0188	0.0000
580.0	0.0223	0.0000
600.0	0.0219	0.0000
620.0	0.0164	0.0000
640.0	0.0135	0.0000
660.0	0.0134	0.0000

For 0.20 g of ELZ-L Zeolite, Run at Dec/07/88
He Flowrate = 66.0 cm^3/ min
Toluene Flowrate = 0.49 cm^3/hr
Reaction Temperature = 420°C

TIME (MIN)	BZ CONV%	XY CONV%
20.0	0.0560	0.0000
40.0	0.0465	0.0000
60.0	0.0573	0.0000
80.0	0.0435	0.0000
100.0	0.0374	0.0000
120.0	0.0429	0.0000
140.0	0.0412	0.0000
160.0	0.0296	0.0000
180.0	0.0369	0.0000
200.0	0.0261	0.0000
220.0	0.0385	0.0000
240.0	0.0287	0.0000
260.0	0.0317	0.0000
280.0	0.0430	0.0000
300.0	0.0287	0.0000
320.0	0.0273	0.0000
340.0	0.0280	0.0000
360.0	0.0213	0.0000
380.0	0.0259	0.0000
400.0	0.0251	0.0000
420.0	0.0246	0.0000
440.0	0.0239	0.0000
460.0	0.0215	0.0000
480.0	0.0216	0.0000
500.0	0.0222	0.0000
520.0	0.0209	0.0000
540.0	0.0158	0.0000
560.0	0.0143	0.0000
580.0	0.0141	0.0000
600.0	0.0146	0.0000
620.0	0.0159	0.0000
640.0	0.0161	0.0000
660.0	0.0140	0.0000
680.0	0.0133	0.0000
700.0	0.0122	0.0000
720.0	0.0122	0.0000
740.0	0.0124	0.0000
760.0	0.0109	0.0000
780.0	0.0103	0.0000
800.0	0.0098	0.0000
820.0	0.0093	0.0000
840.0	0.0088	0.0000
860.0	0.0092	0.0000
880.0	0.0087	0.0000
900.0	0.0084	0.0000
920.0	0.0081	0.0000
940.0	0.0079	0.0000

For 0.20 g of ELZ-L Zeolite, Run at Dec/13/88
He Flowrate = 66.0 cm^3/ min
Toluene Flowrate = 0.49 cm^3/hr
Reaction Temperature = 420°C

TIME (MIN)	BZ CONV%	XY CONV%
20.0	0.0774	0.0000
40.0	0.0684	0.0000
60.0	0.0667	0.0000
80.0	0.0574	0.0000
100.0	0.0523	0.0000
120.0	0.0508	0.0000
140.0	0.0513	0.0000
160.0	0.0480	0.0000
180.0	0.0435	0.0000
200.0	0.0366	0.0000
220.0	0.0363	0.0000
240.0	0.0410	0.0000
260.0	0.0325	0.0000
280.0	0.0289	0.0000
300.0	0.0291	0.0000
320.0	0.0278	0.0000
340.0	0.0249	0.0000
360.0	0.0232	0.0000
380.0	0.0228	0.0000
400.0	0.0201	0.0000
420.0	0.0186	0.0000
440.0	0.0179	0.0000
460.0	0.0164	0.0000
480.0	0.0153	0.0000
500.0	0.0146	0.0000
520.0	0.0127	0.0000
540.0	0.0119	0.0000
560.0	0.0111	0.0000
580.0	0.0095	0.0000
600.0	0.0093	0.0000
620.0	0.0093	0.0000
640.0	0.0086	0.0000
660.0	0.0078	0.0000
680.0	0.0076	0.0000

For 0.20 g of ELZ-L Zeolite, Run at Nov/14/88
He Flowrate = 66.0 cm^3/ min
Toluene Flowrate = 0.74 cm^3/hr
Reaction Temperature = 420°C

TIME (MIN)	BZ CONV%	XY CONV%
20.0	0.0439	0.0000
40.0	0.0932	0.0000
60.0	0.0906	0.0000
80.0	0.0938	0.0000
100.0	0.0955	0.0000
120.0	0.0879	0.0000
140.0	0.0804	0.0000
160.0	0.0727	0.0000
180.0	0.0743	0.0000
200.0	0.0775	0.0000
220.0	0.0698	0.0000
240.0	0.0619	0.0000
260.0	0.0606	0.0000
280.0	0.0578	0.0000
300.0	0.0540	0.0000
320.0	0.0484	0.0000
340.0	0.0513	0.0000
360.0	0.0522	0.0000
380.0	0.0475	0.0000
400.0	0.0487	0.0000
420.0	0.0493	0.0000
440.0	0.0456	0.0000
460.0	0.0399	0.0000
480.0	0.0338	0.0000
500.0	0.0293	0.0000
520.0	0.0235	0.0000
540.0	0.0230	0.0000
560.0	0.0231	0.0000
580.0	0.0201	0.0000
600.0	0.0185	0.0000
620.0	0.0180	0.0000
640.0	0.0173	0.0000
660.0	0.0163	0.0000
680.0	0.0181	0.0000
700.0	0.0194	0.0000
720.0	0.0167	0.0000
740.0	0.0162	0.0000
760.0	0.0174	0.0000
780.0	0.0149	0.0000
800.0	0.0160	0.0000
820.0	0.0163	0.0000
840.0	0.0160	0.0000
860.0	0.0166	0.0000
880.0	0.0161	0.0000
900.0	0.0150	0.0000
920.0	0.0121	0.0000
940.0	0.0121	0.0000

For 0.20 g of ELZ-L Zeolite, Run at Dec/02/88
He Flowrate = 66.0 cm^3/ min
Toluene Flowrate = 0.74 cm^3/hr
Reaction Temperature = 420°C

TIME (MIN)	BZ CONV%	XY CONV%
20.0	0.1476	0.0000
40.0	0.0788	0.0000
60.0	0.0634	0.0000
80.0	0.0699	0.0000
100.0	0.0718	0.0000
120.0	0.0661	0.0000
140.0	0.0578	0.0000
160.0	0.0562	0.0000
180.0	0.0500	0.0000
200.0	0.0476	0.0000
220.0	0.0471	0.0000
240.0	0.0449	0.0000
260.0	0.0408	0.0000
280.0	0.0391	0.0000
300.0	0.0356	0.0000
320.0	0.0309	0.0000
340.0	0.0301	0.0000
360.0	0.0284	0.0000
380.0	0.0264	0.0000
400.0	0.0232	0.0000
420.0	0.0221	0.0000
440.0	0.0202	0.0000
460.0	0.0181	0.0000
480.0	0.0172	0.0000
500.0	0.0157	0.0000
520.0	0.0142	0.0000
540.0	0.0129	0.0000
560.0	0.0130	0.0000
580.0	0.0125	0.0000
600.0	0.0106	0.0000
620.0	0.0099	0.0000
640.0	0.0099	0.0000
660.0	0.0089	0.0000
680.0	0.0077	0.0000
700.0	0.0079	0.0000
720.0	0.0075	0.0000
740.0	0.0066	0.0000
760.0	0.0062	0.0000
780.0	0.0063	0.0000

For 0.20 g of ELZ-L Zeolite, Run at Jan/30/89
He Flowrate = 66.0 cm^3/ min
Toluene Flowrate = 1.00 cm^3/hr
Reaction Temperature = 420°C

TIME (MIN)	BZ CONV%	XY CONV%
20.0	0.1306	0.0000
40.0	0.2024	0.0000
60.0	0.1463	0.0000
80.0	0.1252	0.0000
100.0	0.0669	0.0000
120.0	0.0610	0.0000
140.0	0.0546	0.0000
160.0	0.0549	0.0000
180.0	0.0531	0.0000
200.0	0.0469	0.0000
220.0	0.0419	0.0000
240.0	0.0368	0.0000
260.0	0.0295	0.0000
280.0	0.0262	0.0000
300.0	0.0253	0.0000
320.0	0.0218	0.0000
340.0	0.0202	0.0000
360.0	0.0194	0.0000
380.0	0.0180	0.0000

For 0.20 g of ELZ-L Zeolite, Run at Jan/31/89
He Flowrate = 66.0 cm^3/ min
Toluene Flowrate = 1.00 cm^3/hr
Reaction Temperature = 420°C

TIME (MIN)	BZ CONV%	XY CONV%
20.0	0.1275	0.0000
40.0	0.1298	0.0000
60.0	0.0750	0.0000
80.0	0.1284	0.0000
100.0	0.0756	0.0000
120.0	0.0759	0.0000
140.0	0.0774	0.0000
160.0	0.0694	0.0000
180.0	0.0645	0.0000
200.0	0.0644	0.0000
220.0	0.0638	0.0000
240.0	0.0558	0.0000
260.0	0.0492	0.0000
280.0	0.0513	0.0000
300.0	0.0474	0.0000
320.0	0.0571	0.0000
340.0	0.0494	0.0000
360.0	0.0415	0.0000
380.0	0.0385	0.0000
400.0	0.0342	0.0000
420.0	0.0305	0.0000
440.0	0.0298	0.0000
460.0	0.0292	0.0000

B.3.2 Linde ELZ - Ω - 6 Zeolite

For 0.20 g of ELZ - Ω - 6 Zeolite, Run at Dec/15/88
He Flowrate = 66.0 cm^3/ min
Toluene Flowrate = 0.74 cm^3/hr
Reaction Temperature = 420°C

TIME (MIN)	BZ CONV%	XY CONV%
20.0	0.0311	0.0000
40.0	0.0143	0.0000
60.0	0.0086	0.0000
80.0	0.0050	0.0000

For 0.20 g of ELZ - Ω - 6 Zeolite, Run at Dec/16/88
He Flowrate = 66.0 cm^3/ min
Toluene Flowrate = 0.74 cm^3/hr
Reaction Temperature = 420°C

TIME (MIN)	BZ CONV%	XY CONV%
20.0	0.0298	0.0000
40.0	0.0194	0.0000
60.0	0.0131	0.0000
80.0	0.0081	0.0000
100.0	0.0053	0.0000
120.0	0.0040	0.0000

For 0.20 g of ELZ - Ω - 6 Zeolite, Run at Dec/21/88
He Flowrate = 66.0 cm^3/ min
Toluene Flowrate = 0.74 cm^3/hr
Reaction Temperature = 420°C

TIME (MIN)	BZ CONV%	XY CONV%
20.0	0.0444	0.0000
40.0	0.0306	0.0000
60.0	0.0198	0.0000
80.0	0.0123	0.0000
100.0	0.0081	0.0000
120.0	0.0057	0.0000

For 0.20 g of ELZ - Ω - 6 Zeolite, Run at Dec/22/88
He Flowrate = 66.0 cm^3/ min
Toluene Flowrate = 0.74 cm^3/hr
Reaction Temperature = 420°C

TIME (MIN)	BZ CONV%	XY CONV%
20.0	0.0377	0.0000
40.0	0.0278	0.0000
60.0	0.0133	0.0000
80.0	0.0112	0.0000
100.0	0.0078	0.0000
120.0	0.0054	0.0000

For 0.20 g of ELZ - Ω - 6 Zeolite, Run at Dec/23/88
He Flowrate = 66.0 cm^3/ min
Toluene Flowrate = 0.74 cm^3/hr
Reaction Temperature = 420°C

TIME (MIN)	BZ CONV%	XY CONV%
20.0	0.0352	0.0000
40.0	0.0255	0.0000
60.0	0.0156	0.0000
80.0	0.0100	0.0000
100.0	0.0070	0.0000
120.0	0.0048	0.0000

For 0.20 g of ELZ - Ω - 6 Zeolite, Run at Dec/29/88
He Flowrate = 66.0 cm^3/ min
Toluene Flowrate = 1.00 cm^3/hr
Reaction Temperature = 420°C

TIME (MIN)	BZ CONV%	XY CONV%
20.0	0.0840	0.0000
40.0	0.0305	0.0000
60.0	0.0209	0.0000
80.0	0.0124	0.0000
100.0	0.0088	0.0000
120.0	0.0062	0.0000

For 0.20 g of ELZ - Ω - 6 Zeolite, Run at Dec/30/88
He Flowrate = 66.0 cm^3/ min
Toluene Flowrate = 1.00 cm^3/hr
Reaction Temperature = 420°C

TIME (MIN)	BZ CONV%	XY CONV%
20.0	0.0422	0.0000
40.0	0.0282	0.0000
60.0	0.0173	0.0000
80.0	0.0110	0.0000
100.0	0.0074	0.0000
120.0	0.0050	0.0000
140.0	0.0045	0.0000

For 0.20 g of ELZ - Ω - 6 Zeolite, Run at Jan/04/89
He Flowrate = 66.0 cm^3/ min
Toluene Flowrate = 1.50 cm^3/hr
Reaction Temperature = 420°C

TIME (MIN)	BZ CONV%	XY CONV%
20.0	0.0448	0.0000
40.0	0.0284	0.0000
60.0	0.0188	0.0000
80.0	0.0122	0.0000
100.0	0.0086	0.0000
120.0	0.0073	0.0000
140.0	0.0053	0.0000
160.0	0.0044	0.0000

For 0.20 g of ELZ - Ω - 6 Zeolite, Run at Jan/05/89
He Flowrate = 66.0 cm^3/ min
Toluene Flowrate = 1.50 cm^3/hr
Reaction Temperature = 420°C

TIME (MIN)	BZ CONV%	XY CONV%
TIME (MIN)	BZ CONV%	XY CONV%
20.0	0.0469	0.0000
40.0	0.0264	0.0000
60.0	0.0178	0.0000
80.0	0.0128	0.0000
100.0	0.0100	0.0000
120.0	0.0083	0.0000
140.0	0.0064	0.0000
160.0	0.0046	0.0000

B.3.3 Linde LZ-Y-52 Zeolite

For 0.2 g of LZ-Y-52 Zeolite, Run at Nov/04/88
He Flowrate = 36.0 cm^3/ min
Toluene Flowrate = 0.49 cm^3/hr
Reaction Temperature = 400°C

TIME (MIN)	BZ CONV%	XY CONV%
20.0	0.0246	0.0210
40.0	0.0382	0.0242
60.0	0.0427	0.0265
80.0	0.0435	0.0300
100.0	0.0502	0.0467
120.0	0.0481	0.0475
140.0	0.0495	0.0525
160.0	0.0473	0.0482
180.0	0.0503	0.0484
200.0	0.0485	0.0534
220.0	0.0497	0.0475
240.0	0.0557	0.0494
260.0	0.0473	0.0517
280.0	0.0475	0.0533
300.0	0.0521	0.0475
320.0	0.0583	0.0512
340.0	0.0484	0.0495
360.0	0.0504	0.0522
380.0	0.0540	0.0492
400.0	0.0528	0.0496
420.0	0.0452	0.0541
440.0	0.0489	0.0494
460.0	0.0500	0.0469
480.0	0.0480	0.0507
500.0	0.0467	0.0501
520.0	0.0496	0.0478
540.0	0.0503	0.0504
560.0	0.0456	0.0545
580.0	0.0459	0.0460
600.0	0.0509	0.0464
620.0	0.0468	0.0486
640.0	0.0461	0.0491
660.0	0.0429	0.0466
680.0	0.0497	0.0388
700.0	0.0440	0.0498
720.0	0.0457	0.0463
740.0	0.0493	0.0436
760.0	0.0468	0.0481
780.0	0.0451	0.0504
800.0	0.0463	0.0429
820.0	0.0502	0.0474
840.0	0.0439	0.0488
860.0	0.0452	0.0467
880.0	0.0495	0.0431
900.0	0.0462	0.0462

920.0	0.0426	0.0477
940.0	0.0453	0.0414
960.0	0.0499	0.0432
980.0	0.0434	0.0471
1000.0	0.0418	0.0457
1020.0	0.0453	0.0401
1040.0	0.0436	0.0415
1060.0	0.0415	0.0455
1080.0	0.0416	0.0382
1100.0	0.0438	0.0279
1120.0	0.0432	0.0279
1140.0	0.0396	0.0408
1160.0	0.0421	0.0274
1180.0	0.0439	0.0273
1200.0	0.0385	0.0302
1220.0	0.0405	0.0400
1240.0	0.0401	0.0272

For 0.2 g of LZ-Y-52 Zeolite, Run at Jan/06/89
He Flowrate = 36.0 cm^3/ min
Toluene Flowrate = 0.49 cm^3/hr
Reaction Temperature = 400°C

TIME (MIN)	BZ CONV%	XY CONV%
20.0	0.0505	0.0000
40.0	0.0426	0.0000
60.0	0.0545	0.0000
80.0	0.0535	0.0000
100.0	0.0542	0.0000
120.0	0.0522	0.0000
140.0	0.0545	0.0000
160.0	0.0545	0.0000
180.0	0.0494	0.0000
200.0	0.0533	0.0000
220.0	0.0536	0.0000
240.0	0.0516	0.0000
260.0	0.0524	0.0000
280.0	0.0509	0.0000
300.0	0.0534	0.0000
320.0	0.0528	0.0000
340.0	0.0529	0.0000
360.0	0.0443	0.0000
380.0	0.0508	0.0000
400.0	0.0466	0.0000
420.0	0.0408	0.0000
440.0	0.0506	0.0000
460.0	0.0424	0.0000
480.0	0.0458	0.0000
500.0	0.0475	0.0000
520.0	0.0444	0.0000
540.0	0.0407	0.0000
560.0	0.0386	0.0000
580.0	0.0372	0.0000
600.0	0.0380	0.0000
620.0	0.0374	0.0000
640.0	0.0317	0.0000
660.0	0.0344	0.0000
680.0	0.0440	0.0000
700.0	0.0377	0.0000
720.0	0.0322	0.0000
740.0	0.0337	0.0000
760.0	0.0328	0.0000
780.0	0.0320	0.0000
800.0	0.0321	0.0000
820.0	0.0330	0.0000
840.0	0.0337	0.0000
860.0	0.0317	0.0000
880.0	0.0353	0.0000
900.0	0.0337	0.0000
920.0	0.0322	0.0000
940.0	0.0285	0.0000

For 0.2 g of LZ-Y-52 Zeolite, Run at Oct/28/88
He Flowrate = 66.0 cm^3/ min
Toluene Flowrate = 0.49 cm^3/hr
Reaction Temperature = 400°C

TIME (MIN)	BZ CONV%	XY CONV%
20.0	0.0265	0.0000
40.0	0.0349	0.0000
60.0	0.0402	0.0000
80.0	0.0443	0.0000
100.0	0.0494	0.0000
120.0	0.0520	0.0000
140.0	0.0556	0.0000
160.0	0.0578	0.0228
180.0	0.0579	0.0238
200.0	0.0572	0.0239
220.0	0.0575	0.0249
240.0	0.0570	0.0268
260.0	0.0563	0.0282
280.0	0.0546	0.0302
300.0	0.0547	0.0304
320.0	0.0503	0.0294
340.0	0.0541	0.0301
360.0	0.0596	0.0314
380.0	0.0627	0.0303
400.0	0.0654	0.0292
420.0	0.0654	0.0276
440.0	0.0586	0.0272
460.0	0.0535	0.0250
480.0	0.0549	0.0237
500.0	0.0494	0.0221
520.0	0.0513	0.0225
540.0	0.0524	0.0342
560.0	0.0540	0.0232
580.0	0.0528	0.0235
600.0	0.0502	0.0230
620.0	0.0489	0.0247
640.0	0.0470	0.0253
660.0	0.0461	0.0265
680.0	0.0455	0.0258
700.0	0.0466	0.0347
720.0	0.0471	0.0235
740.0	0.0477	0.0223
760.0	0.0468	0.0232
780.0	0.0450	0.0224
800.0	0.0432	0.0390
820.0	0.0423	0.0304
840.0	0.0399	0.0320
860.0	0.0396	0.0336
880.0	0.0386	0.0329
900.0	0.0376	0.0316
920.0	0.0386	0.0310
940.0	0.0401	0.0303

For 0.2 g of LZ-Y-52 Zeolite, Run at Oct/27/88
He Flowrate = 66.0 cm^3/ min
Toluene Flowrate = 0.74 cm^3/hr
Reaction Temperature = 400°C

TIME (MIN)	BZ CONV%	XY CONV%
20.0	0.0104	0.0000
40.0	0.0648	0.0000
60.0	0.0667	0.0000
80.0	0.0695	0.0267
100.0	0.0711	0.0328
120.0	0.0750	0.0347
140.0	0.0737	0.0471
160.0	0.0718	0.0497
180.0	0.0729	0.0412
200.0	0.0718	0.0542
220.0	0.0709	0.0541
240.0	0.0717	0.0431
260.0	0.0702	0.0564
280.0	0.0692	0.0574
300.0	0.0690	0.0575
320.0	0.0703	0.0566
340.0	0.0733	0.0558
360.0	0.0744	0.0557
380.0	0.0747	0.0546
400.0	0.0750	0.0416
420.0	0.0734	0.0407
440.0	0.0730	0.0533
460.0	0.0724	0.0519
480.0	0.0726	0.0516
500.0	0.0714	0.0390
520.0	0.0726	0.0521
540.0	0.0789	0.0537
560.0	0.0857	0.0549
580.0	0.0750	0.0537
600.0	0.0694	0.0536
620.0	0.0688	0.0552
640.0	0.0668	0.0448
660.0	0.0656	0.0576
680.0	0.0698	0.0564
700.0	0.0715	0.0550
720.0	0.0673	0.0534
740.0	0.0668	0.0404
760.0	0.0662	0.0513
780.0	0.0659	0.0390
800.0	0.0657	0.0398

For 0.2 g of LZ-Y-52 Zeolite, Run at Oct/31/88
He Flowrate = 66.0 cm^3/ min
Toluene Flowrate = 1.00 cm^3/hr
Reaction Temperature = 400°C

TIME (MIN)	BZ CONV%	XY CONV%
20.0	0.0166	0.0000
40.0	0.0572	0.0000
60.0	0.0615	0.0000
80.0	0.0651	0.0000
100.0	0.0682	0.0000
120.0	0.0644	0.0000
140.0	0.0666	0.0000
160.0	0.0677	0.0000
180.0	0.0697	0.0000
200.0	0.0721	0.0000
220.0	0.0736	0.0000
240.0	0.0710	0.0235
260.0	0.0764	0.0242
280.0	0.0939	0.0224
300.0	0.1098	0.0302
320.0	0.1855	0.0295
340.0	0.1971	0.0306
360.0	0.2010	0.0229
380.0	0.1996	0.0210
400.0	0.1936	0.0340
420.0	0.1954	0.0266
440.0	0.1982	0.0263
460.0	0.2001	0.0261
480.0	0.2028	0.0252
500.0	0.2046	0.0355
520.0	0.2057	0.0266
540.0	0.2077	0.0374
560.0	0.2094	0.0380
580.0	0.2061	0.0387
600.0	0.2040	0.0279
620.0	0.2043	0.0280
640.0	0.2046	0.0390
660.0	0.2065	0.0281
680.0	0.2029	0.0390
700.0	0.2036	0.0280
720.0	0.2032	0.0283
740.0	0.2054	0.0281
760.0	0.1982	0.0396
780.0	0.1932	0.0274
800.0	0.1884	0.0273
820.0	0.1142	0.0279
840.0	0.1126	0.0280
860.0	0.1054	0.0407
880.0	0.1000	0.0416
900.0	0.0957	0.0431

For 0.2 g of LZ-Y-52 Zeolite, Run at Nov/02/88
He Flowrate = 66.0 cm^3/ min
Toluene Flowrate = 1.00 cm^3/hr
Reaction Temperature = 400°C

TIME (MIN)	BZ CONV%	XY CONV%
20.0	0.0327	0.0000
40.0	0.0622	0.0000
60.0	0.0663	0.0000
80.0	0.0720	0.0000
100.0	0.0804	0.0000
120.0	0.0884	0.0000
140.0	0.0840	0.0000
160.0	0.0807	0.0000
180.0	0.0902	0.0000
200.0	0.0956	0.0000
220.0	0.1064	0.0000
240.0	0.1004	0.0000
260.0	0.0999	0.0000
280.0	0.1019	0.0000
300.0	0.1048	0.0000
320.0	0.1074	0.0000
340.0	0.1023	0.0293
360.0	0.0980	0.0304
380.0	0.1027	0.0297
400.0	0.1108	0.0271
420.0	0.1810	0.0251
440.0	0.1768	0.0301
460.0	0.1806	0.0324
480.0	0.1895	0.0291
500.0	0.2016	0.0201
520.0	0.2062	0.0209
540.0	0.1944	0.0305
560.0	0.2024	0.0317
580.0	0.2086	0.0294
600.0	0.2179	0.0255
620.0	0.2095	0.0296
640.0	0.2042	0.0316
660.0	0.2098	0.0310
680.0	0.2166	0.0305
700.0	0.2282	0.0286
720.0	0.2184	0.0303
740.0	0.2107	0.0310
760.0	0.2144	0.0308
780.0	0.2225	0.0293
800.0	0.2336	0.0304
820.0	0.2195	0.0286
840.0	0.2103	0.0314
860.0	0.2137	0.0315
880.0	0.2163	0.0305
900.0	0.2216	0.0214
920.0	0.2018	0.0319
940.0	0.2008	0.0237

960.0	0.2016	0.0295
980.0	0.2082	0.0288
1000.0	0.2067	0.0221
1020.0	0.1984	0.0239
1040.0	0.2041	0.0315
1060.0	0.2159	0.0224
1080.0	0.1986	0.0341
1100.0	0.2003	0.0357
1120.0	0.2079	0.0315
1140.0	0.2137	0.0333
1160.0	0.1984	0.0365
1180.0	0.2050	0.0218
1200.0	0.2158	0.0328
1220.0	0.1950	0.0341
1240.0	0.1978	0.0229
1260.0	0.2066	0.0228

B.3.4 Linde ELZ-105-6 Zeolite

For 0.2 g of ELZ-105-6 Zeolite, Run at Jan/25/89
He Flowrate = 36.0 cm^3/ min
Toluene Flowrate = 0.49 cm^3/hr
Reaction Temperature = 420°C

TIME (MIN)	BZ CONV%	XY CONV%
20.0	0.0750	0.0000
40.0	0.0676	0.0000
60.0	0.0630	0.0000
80.0	0.0584	0.0000
100.0	0.0562	0.0000
120.0	0.0536	0.0000
140.0	0.0511	0.0000
160.0	0.0489	0.0000
180.0	0.0477	0.0000
200.0	0.0462	0.0000
220.0	0.0449	0.0000
240.0	0.0433	0.0000
260.0	0.0423	0.0000
280.0	0.0399	0.0000
300.0	0.0399	0.0000
320.0	0.0376	0.0000
340.0	0.0364	0.0000
360.0	0.0324	0.0000
380.0	0.0293	0.0000
400.0	0.0252	0.0000
420.0	0.0245	0.0000
440.0	0.0248	0.0000
460.0	0.0262	0.0000
480.0	0.0214	0.0000
500.0	0.0199	0.0000
520.0	0.0190	0.0000
540.0	0.0177	0.0000
560.0	0.0168	0.0000
580.0	0.0168	0.0000
600.0	0.0161	0.0000
620.0	0.0182	0.0000
640.0	0.0139	0.0000
660.0	0.0146	0.0000

For 0.2 g of ELZ-105-6 Zeolite, Run at Feb/03/89
He Flowrate = 36.0 cm^3/ min
Toluene Flowrate = 0.49 cm^3/hr
Reaction Temperature = 420°C

TIME (MIN)	BZ CONV%	XY CONV%
20.0	0.0325	0.0000
40.0	0.0360	0.0000
60.0	0.0398	0.0000
80.0	0.0412	0.0000
100.0	0.0422	0.0000
120.0	0.0406	0.0000
140.0	0.0483	0.0000
160.0	0.0535	0.0000
180.0	0.0496	0.0000
200.0	0.0495	0.0000
220.0	0.0462	0.0000
240.0	0.0528	0.0000
260.0	0.0445	0.0000
280.0	0.0398	0.0000
300.0	0.0435	0.0000
320.0	0.0455	0.0000
340.0	0.0448	0.0000
360.0	0.0357	0.0000
380.0	0.0341	0.0000
400.0	0.0344	0.0000
420.0	0.0405	0.0000
440.0	0.0355	0.0000
460.0	0.0410	0.0000
480.0	0.0338	0.0000
500.0	0.0337	0.0000
520.0	0.0329	0.0000
540.0	0.0432	0.0000
560.0	0.0326	0.0000
580.0	0.0443	0.0000
600.0	0.0336	0.0000
620.0	0.0326	0.0000
640.0	0.0332	0.0000
660.0	0.0305	0.0000
680.0	0.0307	0.0000
700.0	0.0316	0.0000
720.0	0.0311	0.0000
740.0	0.0332	0.0000
760.0	0.0318	0.0000
780.0	0.0317	0.0000
800.0	0.0321	0.0000
820.0	0.0314	0.0000
840.0	0.0313	0.0000
860.0	0.0322	0.0000
880.0	0.0366	0.0000
900.0	0.0418	0.0000
920.0	0.0321	0.0000
940.0	0.0313	0.0000

960.0	0.0300	0.0000
980.0	0.0363	0.0000
1000.0	0.0330	0.0000
1020.0	0.0260	0.0000

For 0.2 g of ELZ-105-6 Zeolite, Run at Feb/17/89
He Flowrate = 36.0 cm^3/ min
Toluene Flowrate = 0.74 cm^3/hr
Reaction Temperature = 420°C

TIME (MIN)	BZ CONV%	XY CONV%
20.0	0.0311	0.0000
40.0	0.0321	0.0000
60.0	0.0344	0.0000
80.0	0.0398	0.0000
100.0	0.0371	0.0000
120.0	0.0393	0.0000
140.0	0.0408	0.0000
160.0	0.0424	0.0000
180.0	0.0400	0.0000
200.0	0.0411	0.0000
220.0	0.0396	0.0000
240.0	0.0430	0.0000
260.0	0.0399	0.0000
280.0	0.0420	0.0000
300.0	0.0500	0.0000
320.0	0.0516	0.0000
340.0	0.0392	0.0000
360.0	0.0373	0.0000
380.0	0.0407	0.0000
400.0	0.0426	0.0000
420.0	0.0426	0.0000
440.0	0.0432	0.0000
460.0	0.0430	0.0000

For 0.2 g of ELZ-105-6 Zeolite, Run at Mar/08/89
He Flowrate = 36.0 cm^3/ min
Toluene Flowrate = 0.74 cm^3/hr
Reaction Temperature = 420°C

TIME (MIN)	BZ CONV%	XY CONV%
20.0	0.0135	0.0000
40.0	0.0123	0.0000
60.0	0.0282	0.0000
80.0	0.0176	0.0000
100.0	0.0316	0.0000
120.0	0.0262	0.0000
140.0	0.0205	0.0000
160.0	0.0310	0.0000
180.0	0.0317	0.0000
200.0	0.0271	0.0000
220.0	0.0237	0.0000
240.0	0.0257	0.0000
260.0	0.0255	0.0000
280.0	0.0261	0.0000
300.0	0.0314	0.0000
320.0	0.0258	0.0000
340.0	0.0265	0.0000
360.0	0.0276	0.0000
380.0	0.0338	0.0000
400.0	0.0341	0.0000
420.0	0.0364	0.0000
440.0	0.0343	0.0000
460.0	0.0366	0.0000
480.0	0.0429	0.0000
500.0	0.0385	0.0000
520.0	0.0426	0.0000
540.0	0.0429	0.0000
560.0	0.0462	0.0000
580.0	0.0455	0.0000
600.0	0.0472	0.0000
620.0	0.0501	0.0000
640.0	0.0498	0.0000
660.0	0.0507	0.0000
680.0	0.0548	0.0000
700.0	0.0566	0.0000
720.0	0.0598	0.0000

For 0.2 g of ELZ-105-6 Zeolite, Run at Jan/11/89
He Flowrate = 36.0 cm^3/ min
Toluene Flowrate = 1.00 cm^3/hr
Reaction Temperature = 420°C

TIME (MIN)	BZ CONV%	XY CONV%
20.0	0.0293	0.0000
40.0	0.0306	0.0000
60.0	0.0278	0.0000
80.0	0.0314	0.0000
100.0	0.0266	0.0000
120.0	0.0305	0.0000
140.0	0.0257	0.0000
160.0	0.0276	0.0000
180.0	0.0252	0.0000
200.0	0.0262	0.0000
220.0	0.0273	0.0000
240.0	0.0284	0.0000
260.0	0.0274	0.0000
280.0	0.0403	0.0000
300.0	0.0400	0.0000
320.0	0.0365	0.0000
340.0	0.0296	0.0000
360.0	0.0382	0.0000
380.0	0.0378	0.0000
400.0	0.0432	0.0000
420.0	0.0411	0.0000
440.0	0.0529	0.0000
460.0	0.0452	0.0000
480.0	0.0442	0.0000
500.0	0.0389	0.0000
520.0	0.0445	0.0000
540.0	0.0327	0.0000
560.0	0.0362	0.0000
580.0	0.0411	0.0000
600.0	0.0439	0.0000
620.0	0.0421	0.0000
640.0	0.0401	0.0000
660.0	0.0366	0.0000
680.0	0.0439	0.0000
700.0	0.0412	0.0000
720.0	0.0466	0.0000
740.0	0.0364	0.0000
760.0	0.0390	0.0000
780.0	0.0391	0.0000
800.0	0.0436	0.0000
820.0	0.0430	0.0000
840.0	0.0448	0.0000
860.0	0.0417	0.0000
880.0	0.0417	0.0000

For 0.2 g of ELZ-105-6 Zeolite, Run at Feb/19/89
He Flowrate = 36.0 cm^3/ min
Toluene Flowrate = 1.00 cm^3/hr
Reaction Temperature = 420°C

TIME (MIN)	BZ CONV%	XY CONV%
20.0	0.0321	0.0000
40.0	0.0309	0.0000
60.0	0.0316	0.0000
80.0	0.0284	0.0000
100.0	0.0287	0.0000
120.0	0.0284	0.0000
140.0	0.0280	0.0000
160.0	0.0282	0.0000
180.0	0.0272	0.0000
200.0	0.0274	0.0000
220.0	0.0261	0.0000
240.0	0.0286	0.0000
260.0	0.0293	0.0000
280.0	0.0287	0.0000

For 0.2 g of ELZ-105-6 Zeolite, Run at Jan/31/89
He Flowrate = 36.0 cm^3/ min
Toluene Flowrate = 1.00 cm^3/hr
Reaction Temperature = 420°C

TIME (MIN)	BZ CONV%	XY CONV%
20.0	0.1306	0.0000
40.0	0.2024	0.0000
60.0	0.1463	0.0000
80.0	0.1252	0.0000
100.0	0.0703	0.0000
120.0	0.0610	0.0000
140.0	0.0546	0.0000
160.0	0.0549	0.0000
180.0	0.0531	0.0000
200.0	0.0469	0.0000
220.0	0.0419	0.0000
240.0	0.0368	0.0000
260.0	0.0295	0.0000
280.0	0.0262	0.0000
300.0	0.0253	0.0000
320.0	0.0218	0.0000
340.0	0.0202	0.0000
360.0	0.0194	0.0000
380.0	0.0180	0.0000

APPENDIX C

Computation of kη from Kinetics Data

C.1 Algorithm of Computation

The procedures to obtain kη values from raw kinetics data for toluene disproportionation are:

1. Calculated conversion vs. time data by applying the calibration results shown in Appendix I to raw GC data. Examples of conversion to benzene vs. time plots were shown in Figs. C.1 to C.4 for powder-form L, Ω, Y, and pentasil zeolites, and Figs. C.5 to C.8 for pellet-form L, Ω, Y, and pentasil zeolites, respectively.

2. Derived conversion vs. weight data by applying eq. (3-6) to conversion vs. time data obtained in step (1).

3. The number of turnovers are defined as:

$$() = \Sigma\left(\frac{\text{Mols converted / Time}}{\text{Mols Catalyst Sites}}\right) t \qquad (C-1)$$

Therefore the conversion vs. weight plots should form a single line for a catalyst with constant activity, and form several lines of decreasing slope if the catalyst was slowly deactivated. The slope of these lines equals $\frac{r_{obs}}{F_A}$ at low conversions.

4. From the derivation in Section 3.3.2, it was found that, for experiments with a deactivating catalyst, the conversion vs. weight

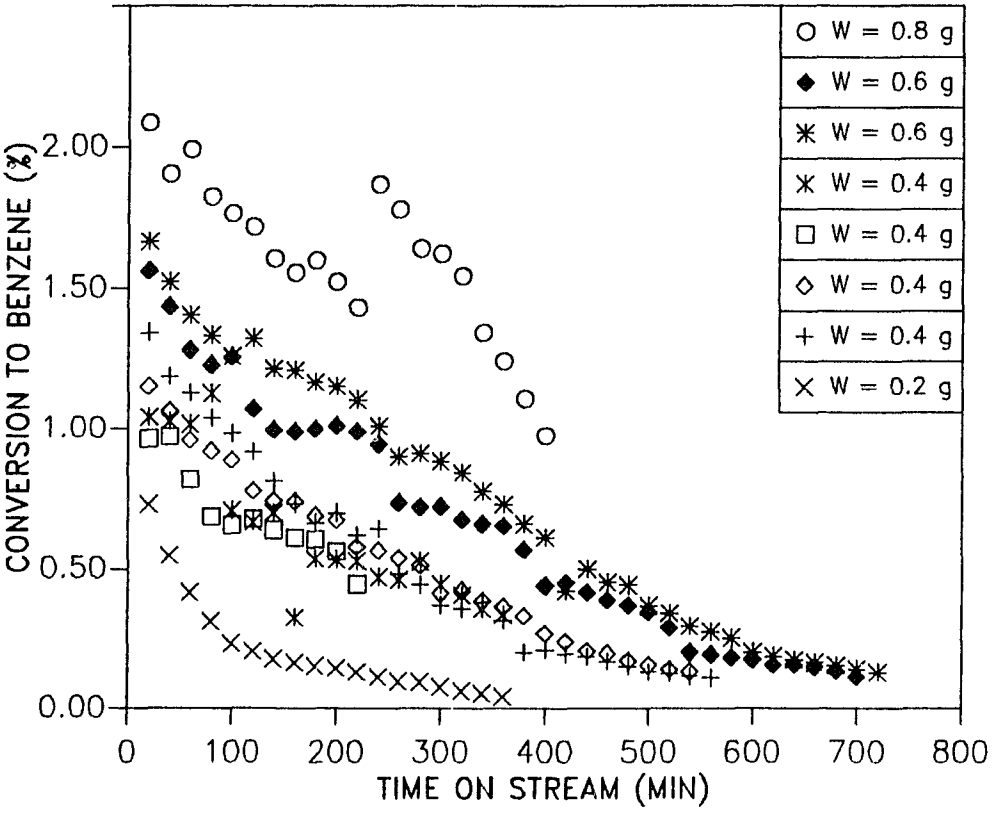

Figure C.1, Toluene Disproportionation Catalyzed by L Powder

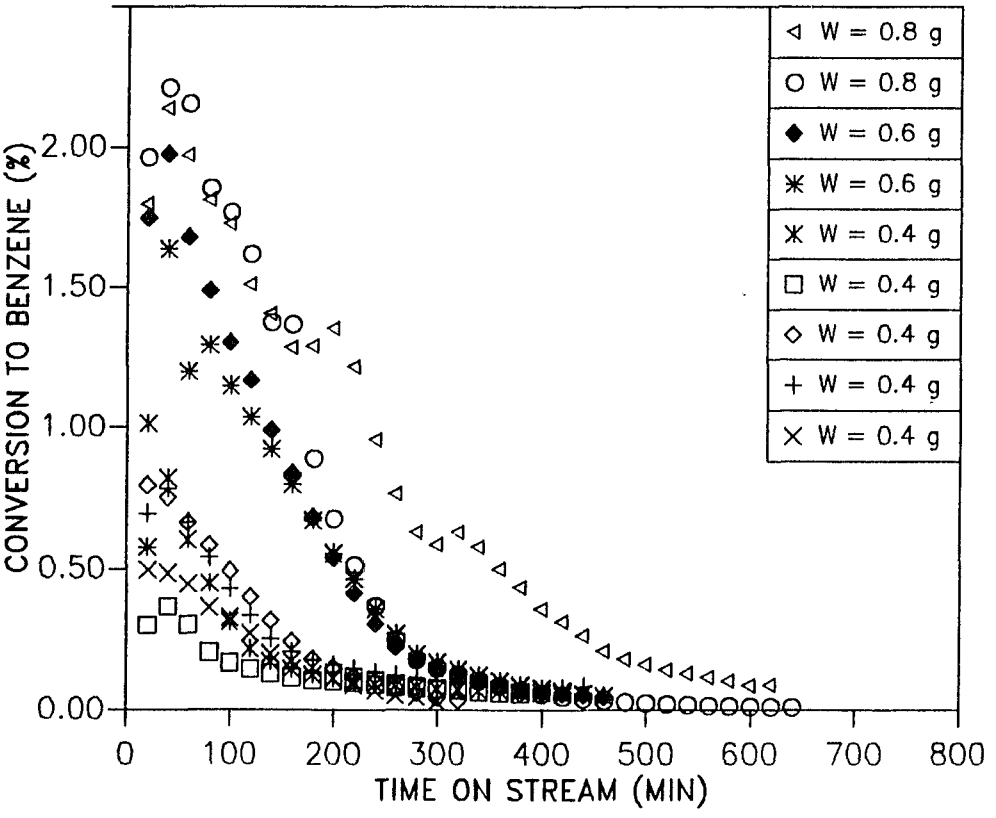

Figure C.2, Toluene Disproportionation Catalyzed by O-6 Powder

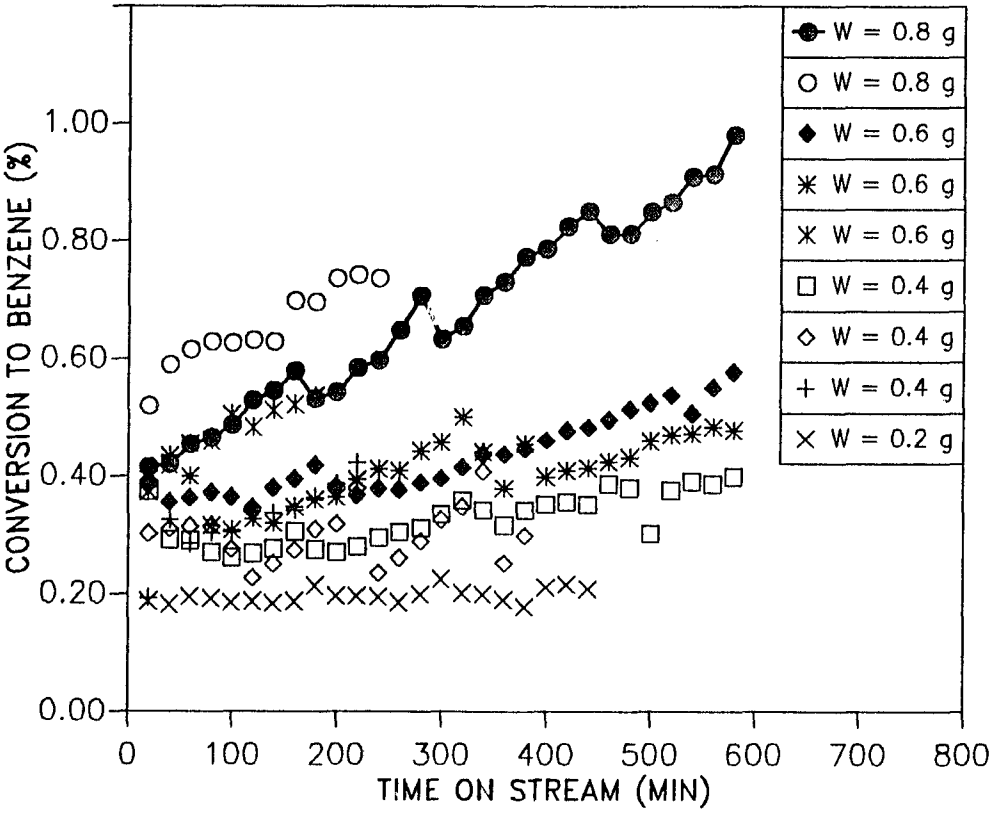

Figure C.3, Toluene Disproportionation Catalyzed by Y-52 Powder

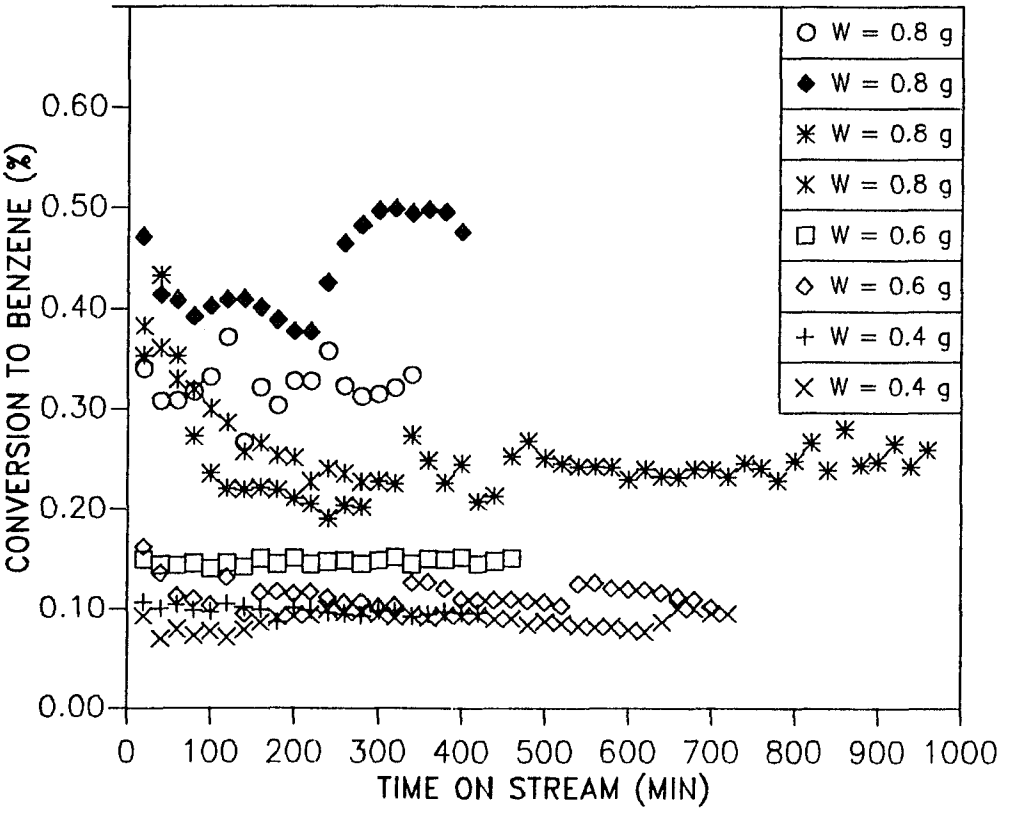

Figure C.4, Toluene Disproportionation Catalyzed by 105–6 Powder

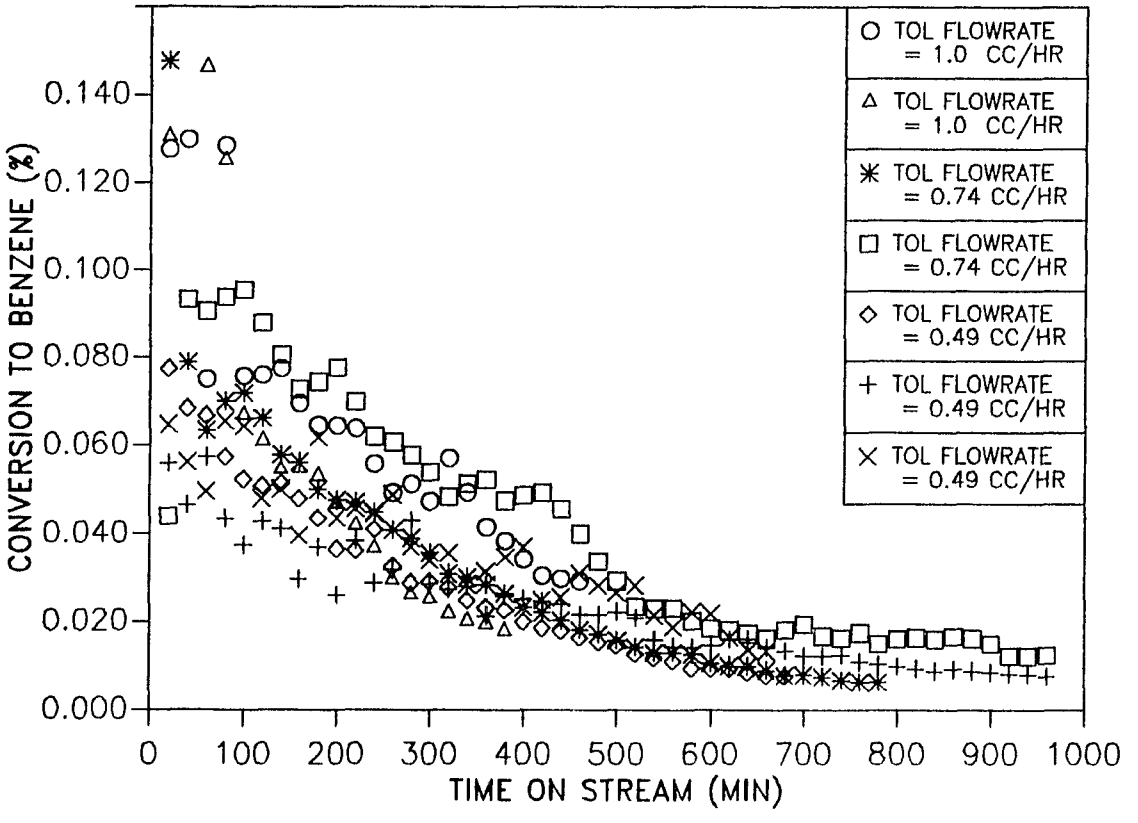

Figure C.5, Toluene Disproportionation Catalyzed by L Pellet

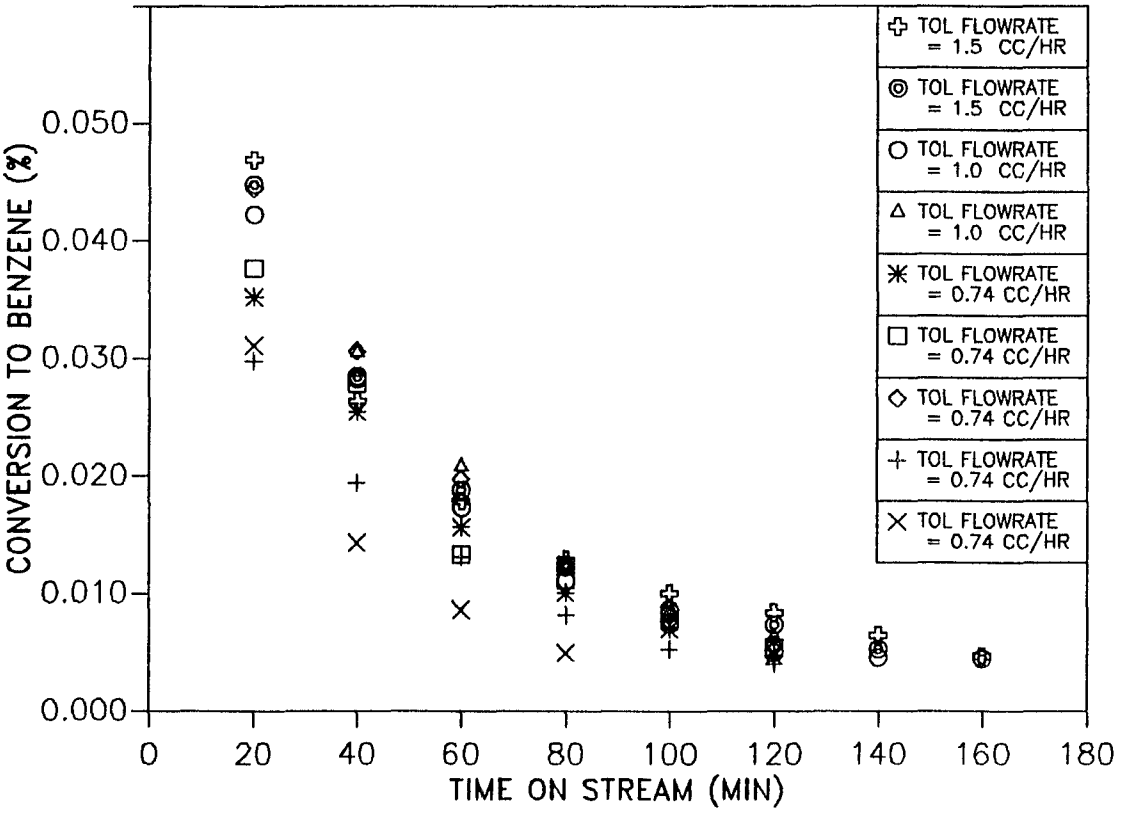

Figure C.6, Toluene Disproportionation Catalyzed by Omega Pellet

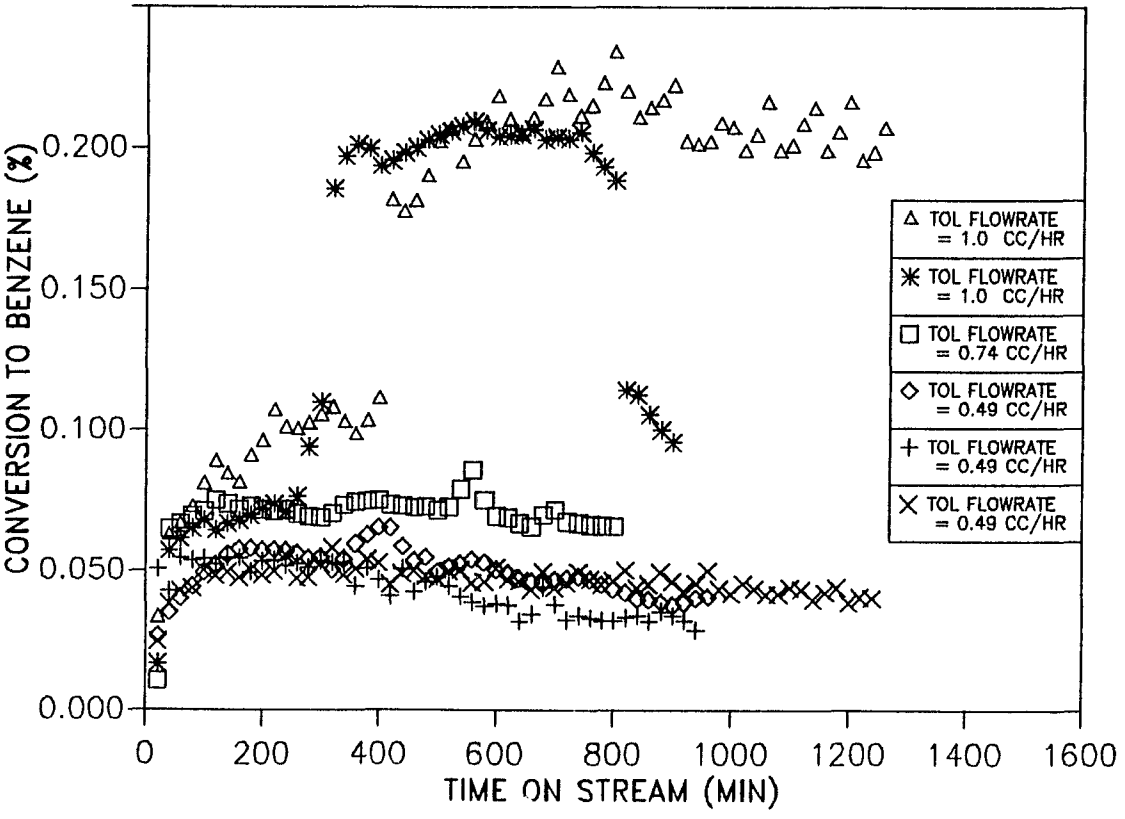

Figure C.7, Toluene Disproportionation by Y-52 Pellet

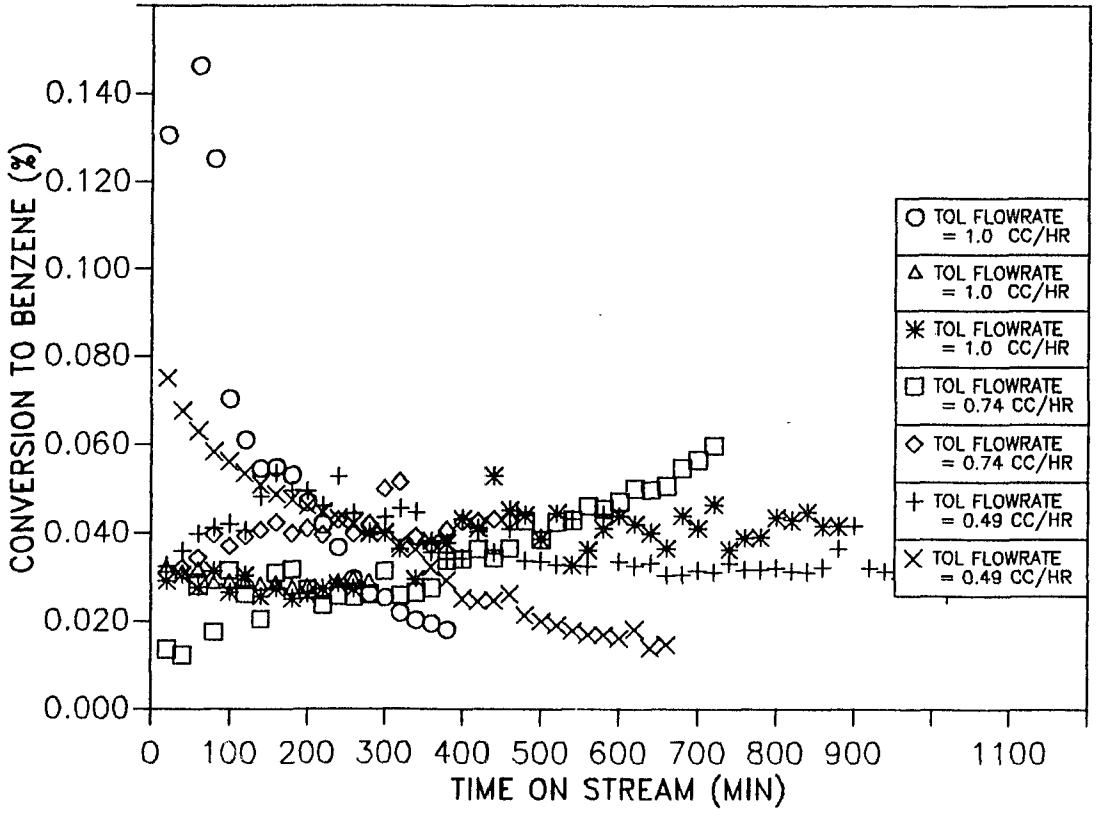

Figure C.8, Toluene Disproportionation by 105-6 Pellet

data should be compared at constant number of turnovers. The same argument is also valid for a catalyst with constant activity. Examples of this type of plot were shown in Figs. C.9 to C.12 for powder-form L, Ω, Y, and pentasil zeolites, and Figs. C.13 to C.16 for pellet-form L, Ω, Y, and pentasil zeolites, respectively.

5. From the r_{obs} data, we can compute $k\eta$ for a second order reaction by eq. (3.10). The only unknown quantity in the equation is the external surface concentration, C_s, which can be estimated from the mass transfer equaitons. The detalied computation procedures for C_s for powder- and pellet-form pentasil are shown in here as an example.

C.2 Estimation of D_s

The observed conversions for the toluene disproportionation reaction catalyzed by either powder or pellet-form zeolite catalysts were always less than 5%. Therefore, we can treat the reactor as differential. For a differential reactor, the bulk fluid composition may be approximated as the inlet composition.

C.2.1 Powder-Form Zeolites

The system properties were the following:

- Catalyst = ELZ-105-6 (Orthorhombic Pentasil)
- Temperature = 420°C = 693 K
- Total pressure = 1.1 bar
- Toluene feed rate = 0.74 cm^3/hr liquid = 1.78×10^{-4} g/s
- He flowrate = 36 cm^3/ min = 4.22×10^{-4} g/s
- Tube internal cross sectional area = 0.69 cm^2

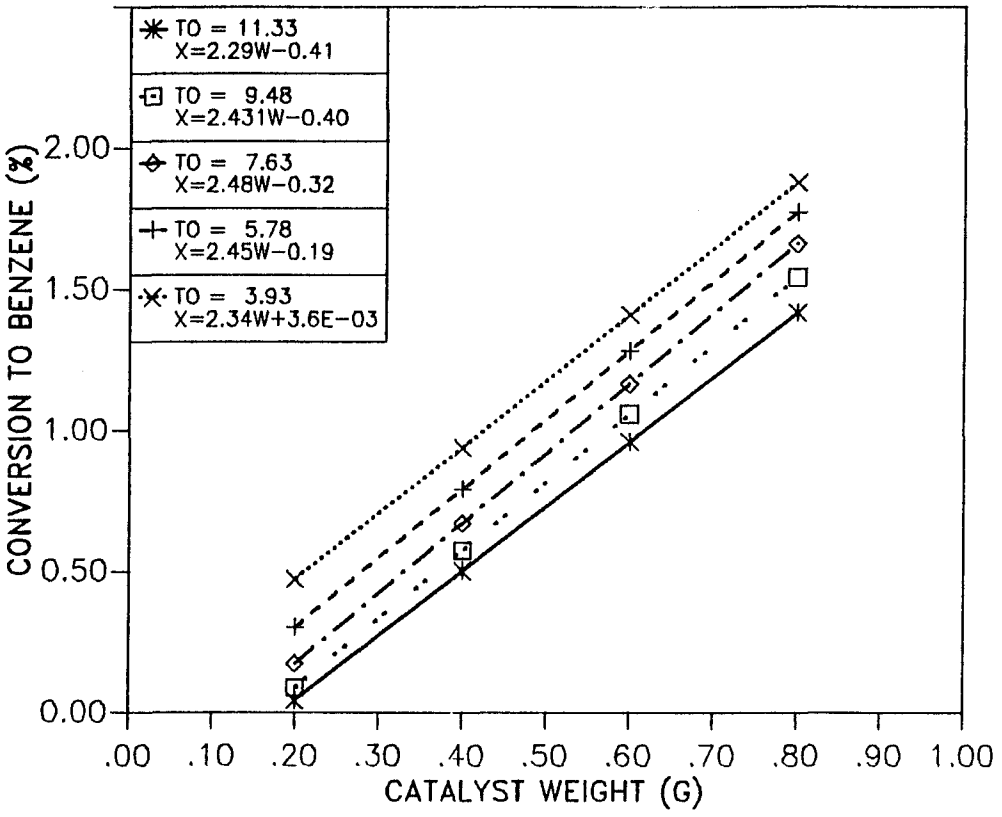

Figure C.9, Effects of Varying Space Velocities for toluene Disproportionation Catalyzed by L Powder

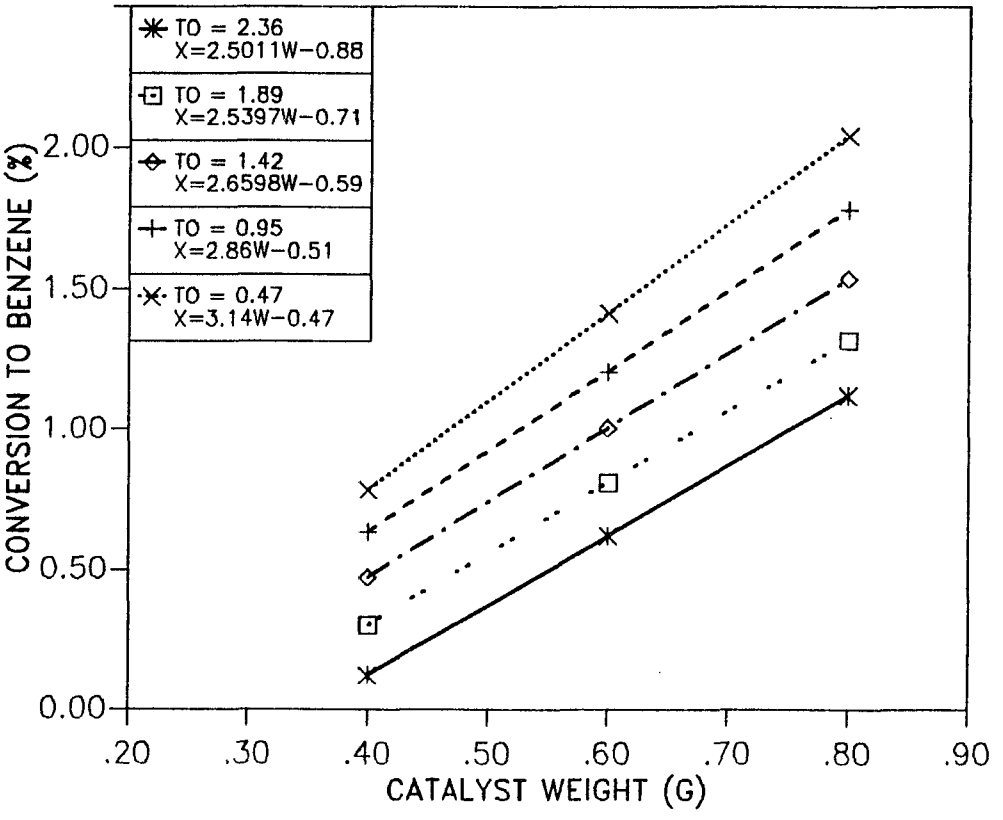

Figure C.10, Effects of Varying Space Velocities for Toluene Disproportionation Catalyzed by Omega-6 Powder

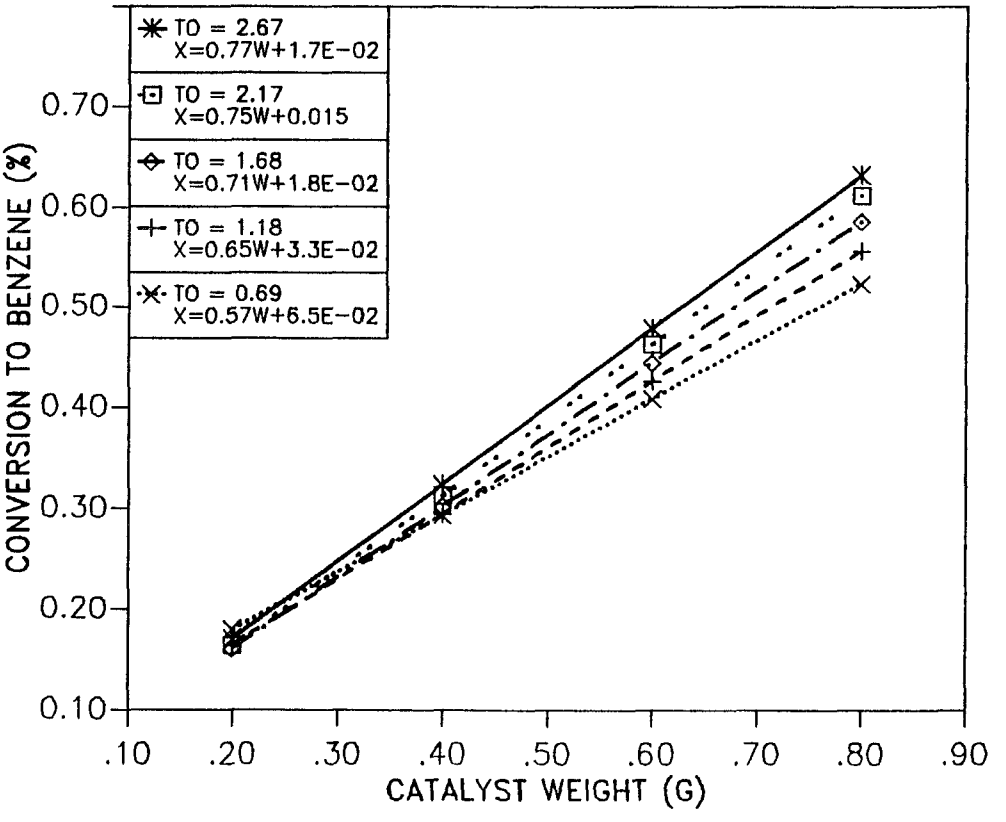

Figure C.11, Effects of Varying Space Velocities for Toluene Disproportionation Catalyzed by Y-52 Powder

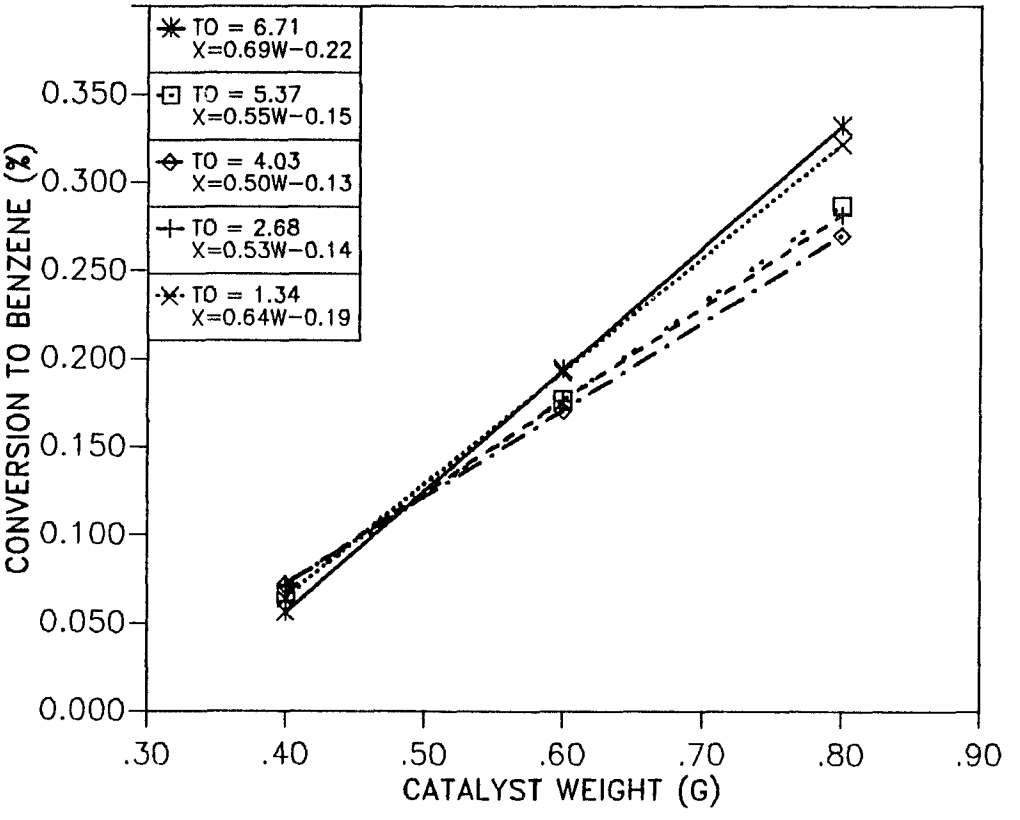

Figure C.12, Effects of Varying Space Velocities for Toluene Disproportionation Catalyzed by 105−6 Powder

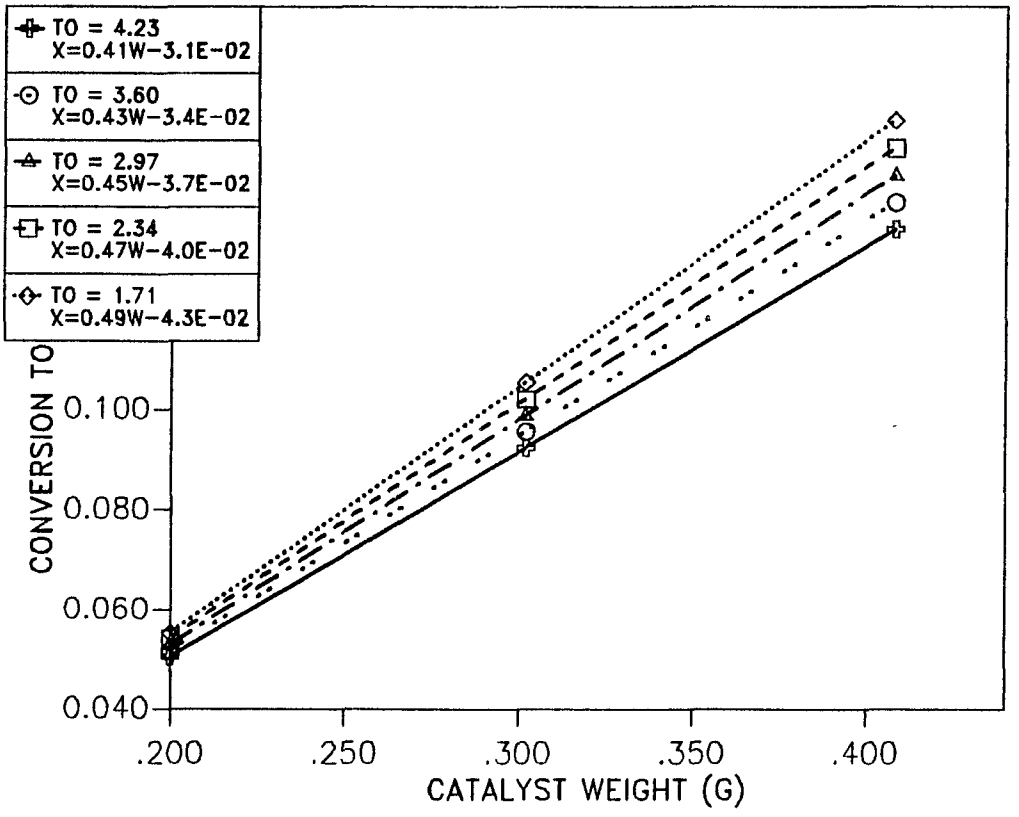

Figure C.13, Effects of Varying Space Velocities for Toluene Disproportionation by L Pellets

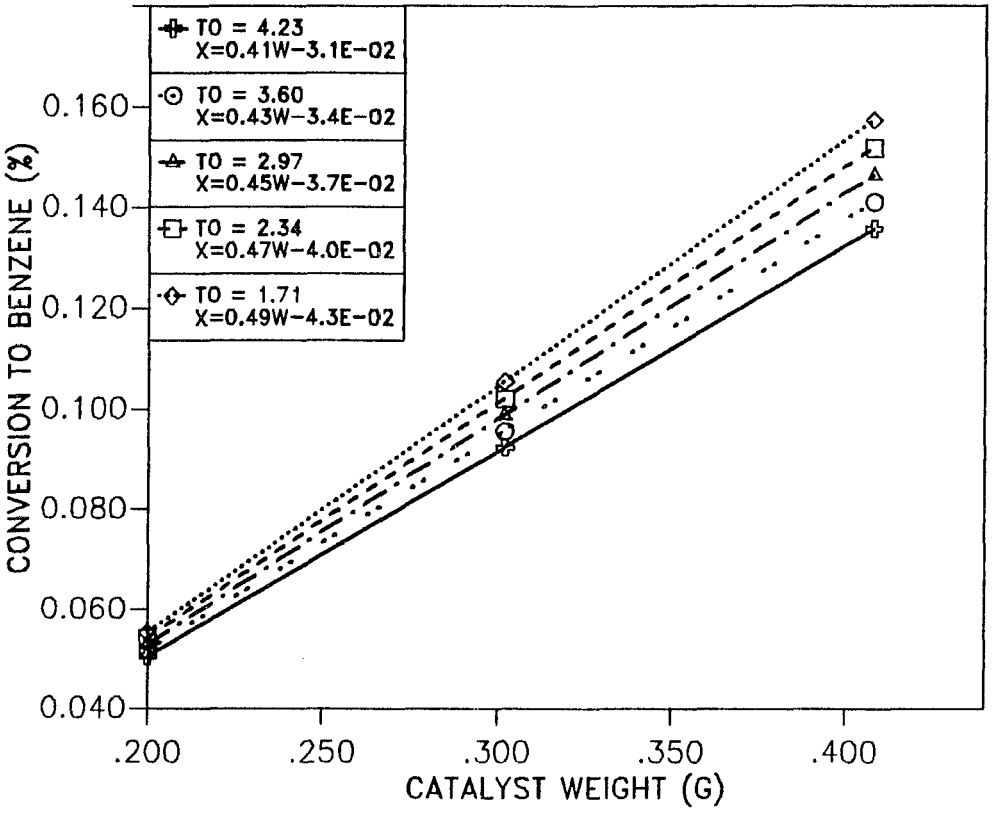

Figure C.13, Effects of Varying Space Velocities for Toluene Disproportionation by L Pellets

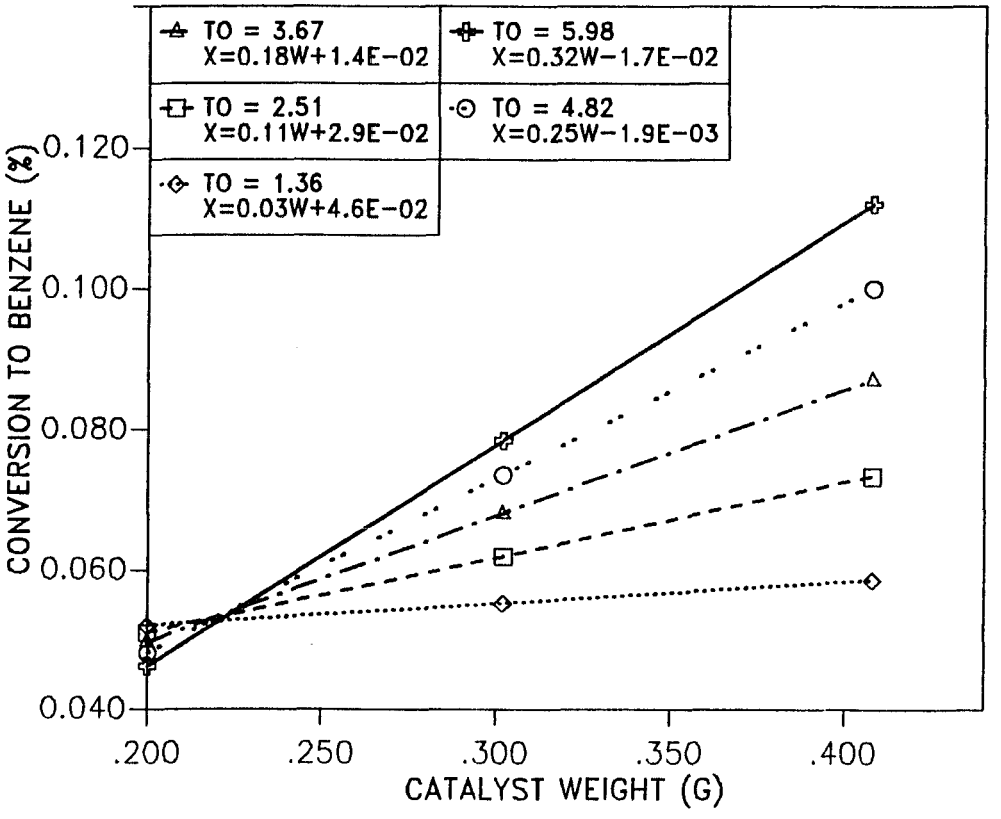

Figure C.15, Effects of Varying Space Velocities for Toluene Disproportionation by Y-52 Pellets

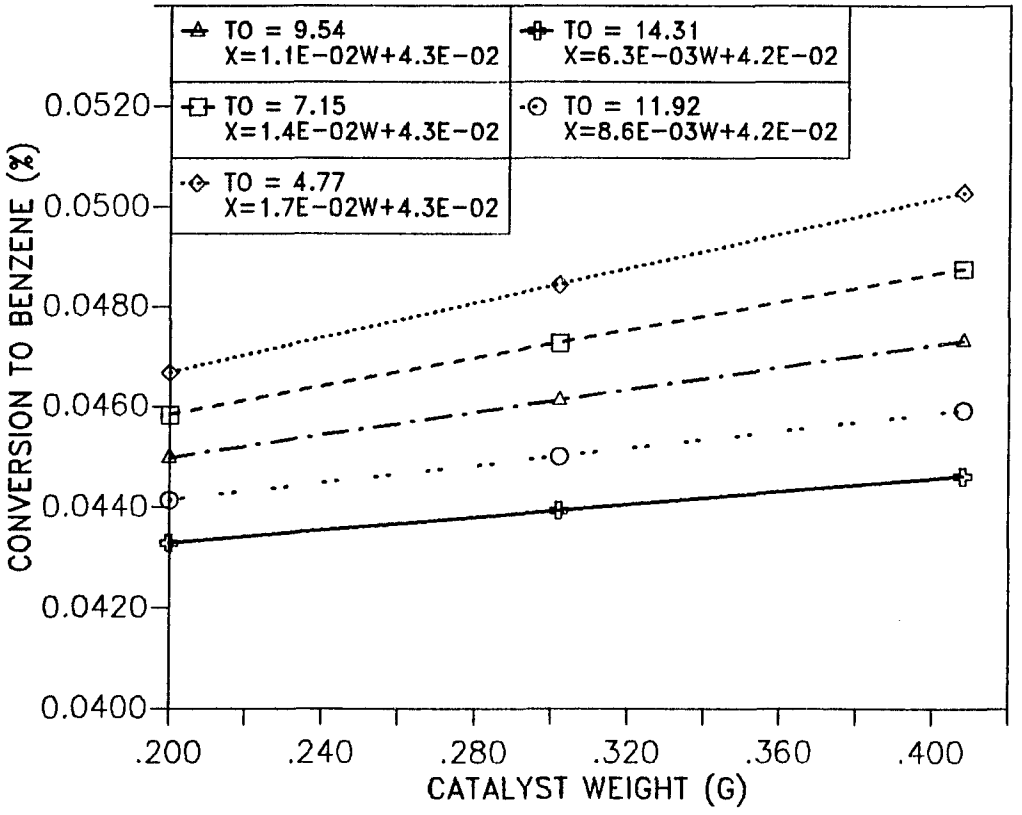

Figure C.16, Effects of Varying Space Velocities for Toluene Disproportionation by 105-6 Pellets

- Superfical mass velocity = 2.56×10^{-4} g/cm^2-s
- External surface area of catalyst = 1.89×10^{2} cm^2/g
- Viscosity of the reaction mixture = 2.95×10^{-4} g/cm-s
- Catalyst crystal density = 1.8 g/cm^3
- Catalyst bed porosity = 0.5 (estimated)
- Toluene effective binary diffusivity = 1.75×10^{-3} cm^2/s
- Average molecular weight of reaction mixture = 10.43 g/mol
- Mass density of reaction mixture = 1.83×10^{-4} g/cm^3
- Catalyst particle diameter = 7.4×10^{-3} cm

Form the above data we have:

1. Reynolds number:

$$N_{Re} = \frac{d_p G}{\mu} = 0.0064 \qquad (C-2)$$

2. Since the Reynolds number is so small, we can assume that the Sherwood number is 2.0. From the definition of Sherwood number, we have:

$$N_{Sh} = \frac{k_{c_i} d_p}{D_e} = 2.0 \qquad (C-3)$$

Therefore,

$$k_{c_i} = N_{Sh} \frac{D_e}{d_p} = 0.47 \qquad (C-4)$$

3. From the definition of mass transfer coefficient:

$$k_{c_i} = \frac{J_i}{C_{B_i} - C_{S_i}} \qquad (C-5)$$

At steady state, the rate of mass transfer equals the reaction rate. Hence,

$$\begin{aligned} N_i a_m &= \text{reaction rate/mass catalyst} \\ &= -\alpha_i r_m \end{aligned} \qquad (C-6)$$

where a_m is the external area per unit mass of catalyst, and N_i is the molar flux of species i to the external surface of the catalyst. We know that

$$N_i = k_{c_i} \frac{(C_{B_i} - C_{S_i})}{1 - y_i\left(\frac{\sum_{j=1}^{N} N_j}{N_i}\right)} \qquad (C-7)$$

Therefore,

$$\begin{aligned} (C_{B_i} - C_{S_i}) &= -\frac{\alpha_i r_m}{a_m k_{c_i}} \left(1 - y_i\left(\frac{\sum_{j=1}^{N} N_j}{N_i}\right)\right) \\ &= 2.53 \times 10^{-8}\ \text{mol/cm}^3 \end{aligned} \qquad (C-8)$$

From ideal gas law, we have

$$\begin{aligned} C_{B_i} &= \frac{y_i P}{RT} \\ &= 1.76 \times 10^{-6}\ \text{mol/cm}^3 \end{aligned} \qquad (C-9)$$

And upon calculation,

$$C_{S_i} = 1.76 \times 10^{-6}\ \text{mol/cm}^3$$

The above derivation was for the pentasil zeolite. Since all the powder-form zeolites used in this study have similar physical properties, we can assume that they all have external surface concentrations equal to the bulk concentrations.

C.2.2 Pellet-Form Zeolites

The system properties were the same as in the pervious calculation except:

- Catalyst = ELZ-105-6 (Orthorhombic Pentasil)
- Toluene feed rate = 0.49 to 1.00 cm^3/hr liquid = 1.18×10^{-4} to 2.40×10^{-4} g/s
- He flowrate = 66 cm^3/min = 9.0×10^{-4} g/s
- Superfical mass velocity = 1.59×10^{-4} to 3.24×10^{-4} g/cm^3-s
- External surface area of catalyst = 12.6 cm^2/g
- Pellet density = 0.85 g/cm^3
- Pellet porosity = 0.3 (estimated)
- Toluene effective binary diffusivity = 4.2×10^{-4} cm^2/s @ 693 K
- Average molecular weight of reaction mixture = 23.36 - 36.56 g/mol
- Mass density of reaction mixture = 4.11×10^{-4} - 6.43×10^{-4} g/cm^3

Form the above data we have:

1. Reynolds number:

$$N_{Re} = \frac{d_p G}{\mu} = 0.967 \qquad (C - 10)$$

2. Since the Reynolds number is so small, we can assume that the Sherwood number is 2.0. Computing the bulk and surface concentrations using eq. C.3-8 gives:

$$C_{B_i} = \frac{y_i P}{RT} = 1.93 \times 10^{-6} mol/cm^3 \qquad (C - 11)$$

and

$$C_{S_i} = 1.93 \times 10^{-6} \, mol/cm^3$$

C.3 Estimation of kη from Kinetics Data

Using the algorithm listed in Section C.1, and the C_S values obtained in Section C.2, we can compute the kη values for toluene disproportionation catalyzed by powder- or pellet-form zeolites.

C.3.1 Powder-Form Zeolites

(1) ELZ-105-6:

For powder-form ELZ-105-6, the conversion vs. weight data at different number of turnovers were obtained from Fig. C.12.

	Weight (g)		
	0.4	0.6	0.8
# of Turnovers			
6.7	0.092	0.136	0.35
5.4	0.092	0.133	0.303
4.0	0.092	0.131	0.29
2.7	0.091	0.129	0.311
1.3	0.091	0.126	0.367
Average	0.0916	0.131	0.324

The fitting result for the average data set is:

$$X_A = 0.00626\ W - 0.187, \qquad r^2 = 0.865$$

Therefore,

$$r_{obs} = 0.00626\ F_A$$
$$= k\eta C_S^2$$

and

$$k\eta = 3.65 \times 10^3\ cm^6/g - s - mol$$
$$= 1.10 \times 10^{-10}\ kmol/kg\text{-}s\text{-}Pka^2$$

(2) LZ-Y-52:

For powder-form LZ-Y-52, the conversion vs. weight data at different number of turnovers were obtained from Fig. C.11.

	Weight (g)			
	0.2	0.4	0.6	0.8
# of Turnovers				
2.7	0.189	0.286	0.395	0.535
2.2	0.191	0.268	0.397	0.583
1.7	0.193	0.274	0.401	0.624
1.2	0.196	0.294	0.406	0.656
0.7	0.199	0.316	0.402	0.679
Average	0.194	0.288	0.400	0.615

The fitting result for the average data set is:

$$X_A = 0.00688\ W + 0.031, \qquad r^2 = 0.959$$

Therefore,

$$r_{obs} = 0.00688\ F_A$$

$$= k\eta C_S^2$$

and

$$k\eta = 4.30 \times 10^3\ cm^6/g - s - mol$$

$$= 1.30 \times 10^{-10}\ kmol/kg\text{-}s\text{-}Pka^2$$

(3) ELZ-L:

For a slowly deactivating catalyst, such as ELZ-L, we must compare the conversion data at a constant number of turnovers. The data extracted from Fig. C.9 were:

# of Turnovers	Fitted Results	$k\,\eta \times 10^8$ kmol/kg-s-Pks^2
11.3	$X_A = 2.29\ W - 0.41$	4.30
9.5	$X_A = 2.43\ W - 0.40$	4.57
7.6	$X_A = 2.48\ W - 0.32$	4.66
5.8	$X_A = 2.45\ W - 0.19$	4.60
3.9	$X_A = 2.34\ W - 0.004$	4.40

The $k\,\eta$ values listed in the table were calculated as follows:

$$r_{obs} = \text{Average Slope} \times F_A$$
$$= k\eta C_S^2$$

Therefore,

$$r_{obs} = 0.0239\ F_A$$
$$= k\eta C_S^2$$

and

$$k\eta = 1.49 \times 10^4\ cm^6/g - s - mol$$
$$= 4.51 \times 10^{-10}\ kmol/kg\text{-}s\text{-}Pka^2$$

(4) ELZ - Ω - 6:

The catalyst ELZ - Ω - 6 also slowly deactivated. The data extracted from Fig. C.10 were:

# of Turnovers	Fitted Results	$k\,\eta \times 10^8$ kmol/kg-s-Pks^2
2.4	$X_A = 2.50\ W - 0.88$	4.70

1.9	$X_A = 2.54\ W - 0.71$	4.77
1.4	$X_A = 2.66\ W - 0.59$	5.00
0.9	$X_A = 2.86\ W - 0.51$	5.37

The k η values listed in the table were calculated as follows:

$$r_{obs} = \text{Average Slope} \times F_A$$
$$= k\eta C_S^2$$

Therefore,

$$r_{obs} = 0.0264\ F_A$$
$$= k\eta C_S^2$$

and

$$k\eta = 1.64 \times 10^4\ cm^6/g - s - mol$$
$$= 4.96 \times 10^{-10}\ kmol/kg\text{-}s\text{-}Pka^2$$

C.3.2 Pellet-Form Zeolites

(1) ELZ-105-6:

For pellet-form ELZ-105-6, the conversion vs. weight data at different numbers of turnovers were obtained from Fig. C.16.

# of Turnovers	Weight (g) 0.2	0.3	0.4
14.3	0.043	0.044	0.045
5.4	0.044	0.045	0.046
4.0	0.045	0.046	0.047
2.7	0.046	0.047	0.048
1.3	0.057	0.048	0.049
Average	0.045	0.046	0.047

The fitting result for the average data set is:

$$X_A = 0.00010\ W - 0.043, \qquad r^2 = 1.00$$

Therefore,

$$r_{obs} = 0.00010\ F_A$$
$$= k\eta C_S^2$$

and,

$$k\eta = 7.45 \times 10^{1}\ cm^6/g - s - mol$$
$$= 2.09 \times 10^{-13}\ kmol/kg\text{-}s\text{-}Pka^2$$

(2) LZ-Y-52:

For powder-form LZ-Y-52, the conversion vs. weight data at different number of turnovers were obtained from Fig. C.11.

# of Turnovers	Weight (g) 0.2	0.3	0.4
6.0	0.046	0.078	0.110
4.8	0.048	0.073	0.098
3.7	0.052	0.056	0.059
2.5	0.051	0.062	0.072
1.4	0.050	0.068	0.086
Average	0.049	0.067	0.085

The fitting result for the average data set is:

$$X_A = 0.00018\ W + 0.013, \qquad r^2 = 1.000$$

Therefore,

$$r_{obs} = 0.00018\ F_A$$

$$= k\eta C_S^2$$

Finally, we have

$$k\eta = 1.34 \times 10^2 \text{ cm}^6/\text{g - s - mol}$$

$$= 3.79 \times 10^{-13} \text{ kmol/kg-s-Pka}^2$$

(3) ELZ-L:

For a slowly deactivating catalyst, such as ELZ-L, we must compare the conversion data at a constant numbers of turnovers. The data extracted from Fig. C.9 were:

# of Turnovers	Fitted Results	$k\eta \times 10^{10}$ kmol/kg-s-Pks^2
4.2	$X_A = 0.41\ W - 0.03$	8.58
3.6	$X_A = 0.43\ W - 0.03$	9.00
3.0	$X_A = 0.45\ W - 0.04$	9.42
2.3	$X_A = 0.47\ W - 0.04$	9.84
1.7	$X_A = 0.49\ W - 0.04$	10.25

The k η values listed in the table were calculated as follows:

$$r_{obs} = \text{Average Slope} \times F_A$$

$$= k\eta C_S^2$$

Therefore,

$$r_{obs} = 0.0045\ F_A$$

$$= k\eta C_S^2$$

and

$$k\eta = 3.42 \times 10^3 \text{ cm}^6/\text{g - s - mol}$$

$$= 1.05 \times 10^{-10} \text{ kmol/kg-s-Pka}^2$$

(4) ELZ - Ω - 6:

The catalyst ELZ - Ω - 6 also slowly deactivated. The data extracted from Fig. C.10 were:

# of Turnovers	Fitted Results	$k\,\eta \times 10^{11}$ kmol/kg-s-Pks^2
0.23	$X_A = 0.019\ W - 0.039$	4.00
0.22	$X_A = 0.018\ W - 0.042$	3.79
0.21	$X_A = 0.018\ W - 0.045$	3.79
0.19	$X_A = 0.018\ W - 0.048$	3.79
0.18	$X_A = 0.018\ W - 0.051$	3.79

The k η values listed in the table were calculated as follows:

$$r_{obs} = \text{Average Slope} \times F_A$$

$$= k\eta C_S^2$$

Therefore,

$$r_{obs} = 0.001845\ F_A$$

$$= k\eta C_S^2$$

and

$$k\eta = 1.34 \times 10^2\ cm^6/g - s - mol$$

$$= 4.24 \times 10^{-12}\ kmol/kg\text{-}s\text{-}Pka^2$$

Vita

The author was born in Taipei, Taiwan, Republic of China. His parents moved to Taiwan from Mainland China in the late 50s and gave birth for both the author and his younger brother.

From the past twenty four years he spent in Taiwan, he experienced his homeland transfromed itself from a labor intensify society to a technique intensify kingdom. During the past six years, he also witness the sweeping change for the political enviroment, which pushed his country to a new democratic era. Although, there is still a long way to go, he is proud of his country and happy to see his fellow countrymen having a vivid hope for a better tomorrow.

He came to LSU from Taiwan in August, 1984 and got his master degree in 1988. During his six and half years in this Cajun country, he had his first child - Catherine from whom he observed the blossom of life.

Now being a thirtysomething fellow, he wish to feed back what he have to the society and get the best out of his life.

DOCTORAL EXAMINATION AND DISSERTATION REPORT

Candidate: Chauchyun Chang

Major Field: Chemical Engineering

Title of Dissertation: Diffusivity Estimation for Counterdiffusing Reactants in Catalytic Solids

Approved:

Kenneth M. Dooley
Major Professor and Chairman

Dean of the Graduate School

EXAMINING COMMITTEE:

F. Carl Knopf

Paul A. Russo

Geoffrey L. Price

R. F. O'Connell

David M. A. Ketzel

Date of Examination:

November 6, 1990